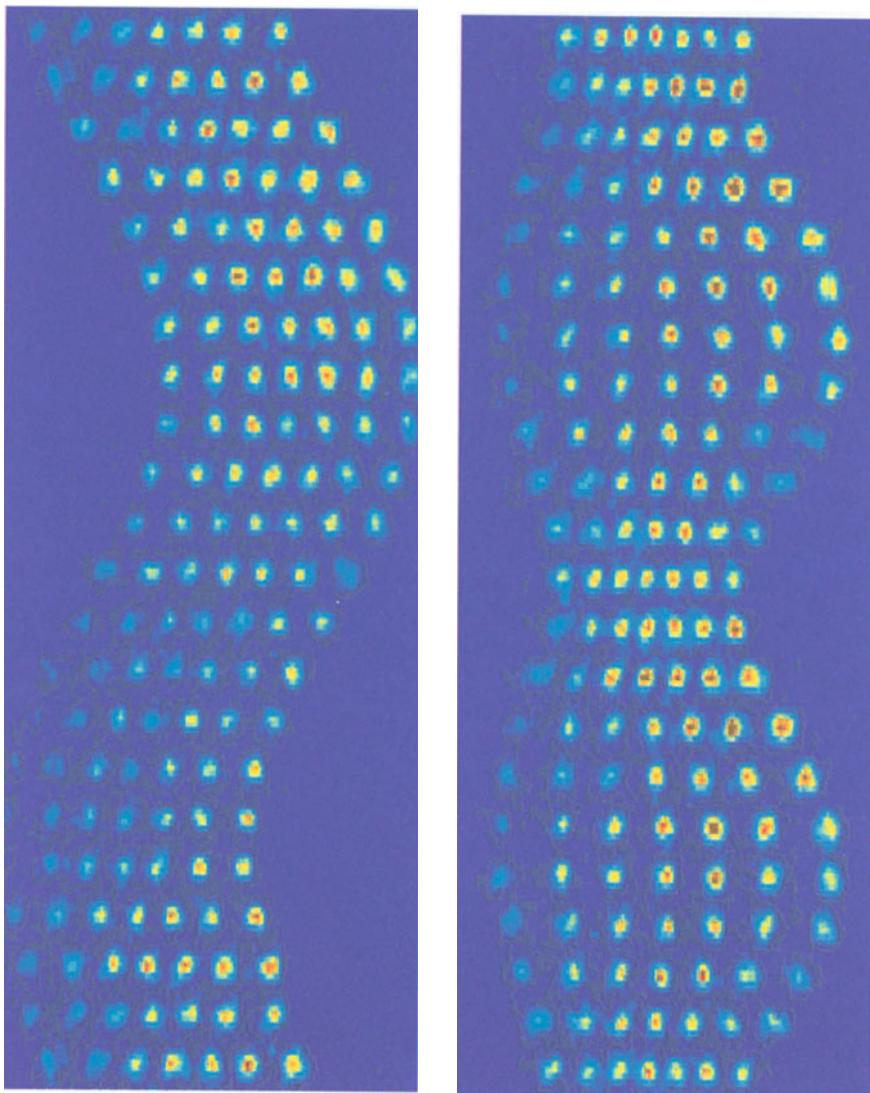


The Physics of Quantum Information

Springer-Verlag Berlin Heidelberg GmbH



<http://www.springer.de/phys/>



Experimental demonstration of the breathing mode (left) and the centre-of-mass motion (right) of a string of 7 ions which form an array of 7 qubits. The figures are compilations of a sequence of snapshots taken of the string of ions (see Chapter 5). Figures by J. Eschner, F. Schmidt-Kaler, R. Blatt, Institut für Experimentalphysik, Universität Innsbruck.

Dirk Bouwmeester
Artur Ekert
Anton Zeilinger (Eds.)

The Physics of Quantum Information

Quantum Cryptography
Quantum Teleportation
Quantum Computation

With 125 Figures



Springer

Dr. Dirk Bouwmeester

Prof. Artur Ekert

Centre for Quantum Computation
Clarendon Laboratory
University of Oxford
Parks Road
Oxford OX1 3PU
United Kingdom

Prof. Anton Zeilinger

Institut für Experimentalphysik
University of Vienna
Boltzmanngasse 5
1090 Vienna
Austria

ISBN 978-3-642-08607-6

ISBN 978-3-662-04209-0 (eBook)

DOI 10.1007/978-3-662-04209-0

Library of Congress Cataloging-in-Publication Data applied for.

Die Deutsche Bibliothek - CIP-Einheitsaufnahme

The physics of quantum information : quantum cryptography, quantum teleportation, quantum computation / Dirk Bouwmeester ... (ed.).

This work is subject to copyright. All rights are reserved, whether the whole or part of the material is concerned, specifically the rights of translation, reprinting, reuse of illustrations, recitation, broadcasting, reproduction on microfilm or in any other way, and storage in data banks. Duplication of this publication or parts thereof is permitted only under the provisions of the German Copyright Law of September 9, 1965, in its current version, and permission for use must always be obtained from Springer-Verlag Berlin Heidelberg GmbH .

Violations are liable for prosecution under the German Copyright Law.

© Springer-Verlag Berlin Heidelberg 2000

Originally published by Springer-Verlag Berlin Heidelberg New York in 2000

Softcover reprint of the hardcover 1st edition 2000

The use of general descriptive names, registered names, trademarks, etc. in this publication does not imply, even in the absence of a specific statement, that such names are exempt from the relevant protective laws and regulations and therefore free for general use.

Camera-ready by the editors using a Springe T_EX macro package.

Cover design: Erich Kirchner, Heidelberg

Printed on acid-free paper

Preface

Information is stored, transmitted and processed by physical means. Thus, the concept of information and computation can be formulated in the context of a physical theory and the study of information requires ultimately experimentation. This sentence, innocuous at first glance, leads to non-trivial consequences.

Following Moore's law, about every 18 months microprocessors double their speed and, it seems, the only way to make them significantly faster is to make them smaller. In the not too distant future they will reach the point where the logic gates are so small that they consist of only a few atoms each. Then quantum-mechanical effects will become important. Thus, if computers are to continue to become faster (and therefore smaller), new, quantum technology must replace or supplement what we have now. But it turns out that such technology can offer much more than smaller and faster microprocessors. Several recent theoretical results have shown that quantum effects may be harnessed to provide qualitatively new modes of communication and computation, in some cases much more powerful than their classical counterparts.

This new quantum technology is being born in many laboratories. The last two decades have witnessed experiments in which single quantum particles of different kinds were controlled and manipulated with an unprecedented precision. Many "gedanken" experiments, so famous in the early days of quantum mechanics, have been carried out. New experimental techniques now make it possible to store and process information encoded in individual quantum systems. As a result we have a new, fledgling field of quantum information processing that represents a highly fertile synthesis of the principles of quantum physics with those of computer and information science. Its scope ranges from providing a new perspective on fundamental issues about the nature of physical law to investigating the potential commercial exploitation by the computing and communications industries.

As part of the worldwide effort in the field, the European Commission, within the framework of the TMR (Training and Mobility of Researchers) programme, is supporting a network entitled "The Physics of Quantum Information". The chapters in this book are mainly written by various members of the network in different forms of collaboration, and they are all intended

to give a didactic introduction to essential, new areas. In addition, several sections present important achievements by researchers outside the TMR network. However, it was not our aim to write a monograph giving a complete overview of the field. Research in this field has become very active, and any comprehensive review of the field would be obsolete in a short time. The topics that are covered by this book include theoretical and experimental aspects of quantum entanglement, quantum cryptography, quantum teleportation, quantum computation, quantum algorithms, quantum-state decoherence, quantum error correction, and quantum communication.

We hope that this book will be a valuable contribution to the literature for all those who have a modest background in quantum mechanics and a genuine interest in the fascinating possibilities that it is offering us.

We are very grateful to Thomas Jennewein for the numerous figures that he drew for this book.

Oxford, Vienna, March 2000

Durk Bouwmeester

Artur Ekert

Anton Zeilinger

Contents

1. The Physics of Quantum Information:	
Basic Concepts	1
1.1 Quantum Superposition	1
1.2 Qubits	3
1.3 Single-Qubit Transformations	4
1.4 Entanglement	7
1.5 Entanglement and Quantum Indistinguishability	9
1.6 The Controlled NOT Gate	11
1.7 The EPR Argument and Bell's Inequality	12
1.8 Comments	14
2. Quantum Cryptography	15
2.1 What is Wrong with Classical Cryptography?	15
2.1.1 From SCYTALE to ENIGMA	15
2.1.2 Keys and Their Distribution	16
2.1.3 Public Keys and Quantum Cryptography	19
2.1.4 Authentication: How to Recognise Cinderella ?	21
2.2 Quantum Key Distribution	22
2.2.1 Preliminaria	22
2.2.2 Security in Non-orthogonal States: No-Cloning Theorem	22
2.2.3 Security in Entanglement	24
2.2.4 What About Noisy Quantum Channels?	25
2.2.5 Practicalities	26
2.3 Quantum Key Distribution with Single Particles	27
2.3.1 Polarised Photons	27
2.3.2 Phase Encoded Systems	31
2.4 Quantum Key Distribution with Entangled States	33
2.4.1 Transmission of the Raw Key	33
2.4.2 Security Criteria	34
2.5 Quantum Eavesdropping	36
2.5.1 Error Correction	36
2.5.2 Privacy Amplification	37
2.6 Experimental Realisations	43
2.6.1 Polarisation Encoding	43

VIII Contents

2.6.2	Phase Encoding	44
2.6.3	Entanglement-Based Quantum Cryptography	46
2.7	Concluding Remarks	47
3.	Quantum Dense Coding and Quantum Teleportation	49
3.1	Introduction	49
3.2	Quantum Dense Coding Protocol	50
3.3	Quantum Teleportation Protocol	51
3.4	Sources of Entangled Photons	53
3.4.1	Parametric Down-Conversion	53
3.4.2	Time Entanglement	54
3.4.3	Momentum Entanglement	57
3.4.4	Polarisation Entanglement	58
3.5	Bell-State Analyser	60
3.5.1	Photon Statistics at a Beamsplitter	60
3.6	Experimental Dense Coding with Qubits	62
3.7	Experimental Quantum Teleportation of Qubits	67
3.7.1	Experimental Results	69
3.7.2	Teleportation of Entanglement	72
3.7.3	Concluding Remarks and Prospects	72
3.8	A Two-Particle Scheme for Quantum Teleportation	74
3.9	Teleportation of Continuous Quantum Variables	77
3.9.1	Employing Position and Momentum Entanglement . . .	77
3.9.2	Quantum Optical Implementation	79
3.10	Entanglement Swapping: Teleportation of Entanglement	84
3.11	Applications of Entanglement Swapping	88
3.11.1	Quantum Telephone Exchange	88
3.11.2	Speeding up the Distribution of Entanglement	89
3.11.3	Correction of Amplitude Errors Developed due to Propagation	90
3.11.4	Entangled States of Increasing Numbers of Particles . .	91
4.	Concepts of Quantum Computation	93
4.1	Introduction to Quantum Computation	93
4.1.1	A New Way of Harnessing Nature	93
4.1.2	From Bits to Qubits	94
4.1.3	Quantum Algorithms	98
4.1.4	Building Quantum Computers	100
4.1.5	Deeper Implications	101
4.1.6	Concluding Remarks	103
4.2	Quantum Algorithms	104
4.2.1	Introduction	104
4.2.2	Quantum Parallel Computation	105
4.2.3	The Principle of Local Operations	107

4.2.4	Oracles and Deutsch's Algorithm	109
4.2.5	The Fourier Transform and Periodicities	114
4.2.6	Shor's Quantum Algorithm for Factorisation	119
4.2.7	Quantum Searching and NP	121
4.3	Quantum Gates and Quantum Computation with Trapped Ions	126
4.3.1	Introduction	126
4.3.2	Quantum Gates with Trapped Ions	126
4.3.3	N Cold Ions Interacting with Laser Light	128
4.3.4	Quantum Gates at Non-zero Temperature	130
5.	Experiments Leading Towards	
	Quantum Computation	133
5.1	Introduction	133
5.2	Cavity QED-Experiments: Atoms in Cavities and Trapped Ions	134
5.2.1	A Two-Level System Coupled to a Quantum Oscillator	134
5.2.2	Cavity QED with Atoms and Cavities	135
5.2.3	Resonant Coupling: Rabi Oscillations and Entangled Atoms	137
5.2.4	Dispersive Coupling: Schrödinger's Cat and Decoherence	143
5.2.5	Trapped-Ion Experiments	147
5.2.6	Choice of Ions and Doppler Cooling	148
5.2.7	Sideband Cooling	150
5.2.8	Electron Shelving and Detection of Vibrational Motion	153
5.2.9	Coherent States of Motion	154
5.2.10	Wigner Function of the One-Phonon State	157
5.2.11	Squeezed States and Schrödinger Cats with Ions	159
5.2.12	Quantum Logic with a Single Trapped ${}^9\text{Be}^+$ Ion	160
5.2.13	Comparison and Perspectives	161
5.3	Linear Ion Traps for Quantum Computation	163
5.3.1	Introduction	163
5.3.2	Ion Confinement in a Linear Paul Trap	164
5.3.3	Laser Cooling and Quantum Motion	167
5.3.4	Ion Strings and Normal Modes	169
5.3.5	Ions as Quantum Register	171
5.3.6	Single-Qubit Preparation and Manipulation	172
5.3.7	Vibrational Mode as a Quantum Data Bus	173
5.3.8	Two-Bit Gates in an Ion-Trap Quantum Computer	174
5.3.9	Readout of the Qubits	175
5.3.10	Conclusion	175
5.4	Nuclear Magnetic Resonance Experiments	177
5.4.1	Introduction	177
5.4.2	The NMR Hamiltonian	177

5.4.3	Building an NMR Quantum Computer	179
5.4.4	Deutsch's Problem	181
5.4.5	Quantum Searching and Other Algorithms	184
5.4.6	Prospects for the Future	185
5.4.7	Entanglement and Mixed States	188
5.4.8	The Next Few Years	188
6.	Quantum Networks and Multi-Particle Entanglement	191
6.1	Introduction	191
6.2	Quantum Networks I: Entangling Particles at Separate Locations	192
6.2.1	Interfacing Atoms and Photons	192
6.2.2	Model of Quantum State Transmission	193
6.2.3	Laser Pulses for Ideal Transmission	195
6.2.4	Imperfect Operations and Error Correction	197
6.3	Multi-Particle Entanglement	197
6.3.1	Greenberger–Horne–Zeilinger states	197
6.3.2	The Conflict with Local Realism	198
6.3.3	A Source for Three-Photon GHZ Entanglement	200
6.3.4	Experimental Proof of GHZ Entanglement	204
6.3.5	Experimental Test of Local Realism Versus Quantum Mechanics	206
6.4	Entanglement Quantification	210
6.4.1	Schmidt Decomposition and von Neumann Entropy	210
6.4.2	Purification Procedures	212
6.4.3	Conditions for Entanglement Measures	214
6.4.4	Two Measures of Distance Between Density Matrices	216
6.4.5	Numerics for Two Spin 1/2 Particles	217
6.4.6	Statistical Basis of Entanglement Measure	219
7.	Decoherence and Quantum Error Correction	221
7.1	Introduction	221
7.2	Decoherence	222
7.2.1	Decoherence: Entanglement Between Qubits and Environment	222
7.2.2	Collective Interaction and Scaling	224
7.2.3	Subspace Decoupled From Environment	225
7.2.4	Other Find of Couplings	225
7.3	Limits to Quantum Computation Due to Decoherence	227
7.4	Error Correction and Fault-Tolerant Computation	232
7.4.1	Symmetrisation Procedures	232
7.4.2	Classical Error Correction	234
7.4.3	General Aspects of Quantum Error Correcting Codes	236
7.4.4	The Three Qubit Code	237

7.4.5	The Quantum Hamming Bound	238
7.4.6	The Seven Qubit Code	239
7.4.7	Fault-Tolerant Computation	241
7.5	General Theory of Quantum Error Correction and Fault Tolerance	242
7.5.1	Digitisation of Noise	242
7.5.2	Error Operators, Stabiliser, and Syndrome Extraction .	243
7.5.3	Code Construction	246
7.5.4	The Physics of Noise	248
7.5.5	Fault-Tolerant Quantum Computation	250
7.6	Frequency Standards	252
8.	Entanglement Purification	261
8.1	Introduction	261
8.2	Principles of Entanglement Purification	261
8.3	Local Filtering	269
8.4	Quantum Privacy Amplification	271
8.5	Generalisation of Purification to Multi-Particle Entanglement	275
8.6	Quantum Networks II: Communication over Noisy Channels	281
8.6.1	Introduction	281
8.6.2	Ideal Communication	282
8.6.3	Correction of Transfer Errors: The Photonic Channel	283
8.6.4	Purification with Finite Means	285
8.7	Quantum Repeaters	288
References	294	
Index	311	

List of Contributors

H. Baldauf

Sect. 5.3

Max–Planck–Institut
für Quantenoptik
Hans–Kopfermann–Str. 1
85748 Garching, Germany

R. Blatt

Sects. 5.2, 5.3

Institut für Experimentalphysik
Universität Innsbruck
Technikerstrasse 25
6020 Innsbruck, Austria

S. Bose

Sect. 3.11

Centre for Quantum Computation
Clarendon Laboratory
University of Oxford
OX1 3PU Oxford, England

D. Bouwmeester

Chap. 1, Sects. 3.1–3.3, 3.5–3.10, 6.3

Centre for Quantum Computation
Clarendon Laboratory
University of Oxford
OX1 3PU Oxford, England

H.-J. Briegel

Sects. 6.2, 8.2, 8.6, 8.7

Sektion Physik
Ludwig–Maximilians–Universität
Theresienstrasse 37
80333 München, Germany

M. Brune

Sect. 5.2

Laboratoire Kastler Brossel
Département de Physique
de l’Ecole Normale Supérieure
24 rue Lhomond
75231 Paris, Cedex 05, France

J.I. Cirac

Sects. 4.3, 6.2, 8.6, 8.7

Institut für Theoretische Physik
Universität Innsbruck
Technikerstrasse 25
6020 Innsbruck, Austria

M. Daniell

Sect. 6.3

Institut für Experimentalphysik
Universität Wien
Boltzmanngasse 5
1090 Wien, Austria

D. Deutsch

Sect. 4.1

Centre for Quantum Computation
Clarendon Laboratory
University of Oxford
OX1 3PU Oxford, England

W. Dür

Sects. 8.6, 8.7

Institut für Theoretische Physik
Universität Innsbruck
Technikerstrasse 25
6020 Innsbruck, Austria

A. Ekert

Chap. 2, Sects. 4.1, 7.2, 7.6
Centre for Quantum Computation
Clarendon Laboratory
University of Oxford
OX1 3PU Oxford, England

S.J. van Enk

Sects. 6.2, 8.6
Norman Bridge Laboratory of Physics
California Institute
of Technology 12-22
Pasadena, California 91125, USA

J. Eschner

Sects. 5.2, 5.3
Institut für Experimentalphysik
Universität Innsbruck
Technikerstrasse 25
6020 Innsbruck, Austria

N. Gisin

Chap. 2, Sects. 3.4, 8.3
University of Geneva
Group of Applied Physics
20 Rue de l'Ecole de Médecine
1211 Geneva 4, Switzerland

S. Haroche

Sect. 5.2
Laboratoire Kastler Brossel
Département de Physique
de l'Ecole Normale Supérieure
24 rue Lhomond
75231 Paris, Cedex 05, France

S.F. Huelga

Sect. 7.6
Departamento de Fisica
Universidad de Oviedo
Calvo Sotelo s/n.
33007 Oviedo, Spain

B. Huttner

Chap. 2, Sect. 8.3
University of Geneva
Group of Applied Physics
20 Rue de l'Ecole de Médecine
1211 Geneva 4, Switzerland

H. Inamori

Chap. 2
Centre for Quantum Computation
Clarendon Laboratory
University of Oxford
OX1 3PU Oxford, England

J.A. Jones

Sect. 5.4
Centre for Quantum Computation
Clarendon Laboratory
University of Oxford
OX1 3PU Oxford, England

R. Jozsa

Sect. 4.2
Department of Computer Science
University of Bristol
Merchant Venturers Building
Woodland Road
BS8 1UB Bristol, England

P.L. Knight

Sects. 3.11, 6.4, 7.3, 8.5
Optics Section
Blackett Laboratory
Imperial College London
London SW7 2BZ, England

W. Lange

Sect. 5.3
Max-Planck-Institut
für Quantenoptik
Hans-Kopfermann-Str. 1
85748 Garching, Germany

D. Leibfried*Sect. 5.2*

Institut für Experimentalphysik
 Universität Innsbruck
 Technikerstrasse 25
 6020 Innsbruck, Austria

C. Macchiavello*Sects. 7.4, 7.6, 8.4*

Dipartimento di Fisica "A.Volta"
 and INFM-Unité di Pavia
 via Bassi 6
 27100 Pavia, Italy

M. Murao*Sect. 8.5*

Optics Section
 Blackett Laboratory
 Imperial College London
 London SW7 2BZ, England

H.C. Nägerl*Sects. 5.2, 5.3*

Institut für Experimentalphysik
 Universität Innsbruck
 Technikerstrasse 25
 6020 Innsbruck, Austria

G.M. Palma*Sects. 7.2, 7.4*

Dipartimento di Scienze Fisiche
 ed Astronomiche & unita'INFM
 via Archirafi 36
 90123 Palermo, Italy

J.-W. Pan*Sects. 3.7, 3.10, 6.3*

Institut für Experimentalphysik
 Universität Wien
 Boltzmanngasse 5
 1090 Wien, Austria

M.B. Plenio*Sects. 6.4, 7.3, 7.6, 8.5*

Optics Section
 Blackett Laboratory
 Imperial College London
 London SW7 2BZ, England

S. Popescu*Sect. 8.5*

5BRIMS Hewlett-Packard
 Laboratories
 Stoke Gifford
 Bristol BS12 6QZ, England

J.F. Poyatos*Sect. 4.3*

Centre for Quantum Computation
 Clarendon Laboratory
 University of Oxford
 OX1 3PU Oxford, England

J.-M. Raimond*Sect. 5.2*

Laboratoire Kastler Brossel
 Département de Physique
 de l'Ecole Normale Supérieure
 24 rue Lhomond
 75231 Paris, Cedex 05, France

J.G. Rarity*Sect. 3.4*

DERA Malvern
 St. Andrews Road, Malvern
 Worcester WR14 3PS, England
 and
 Centre for Quantum Computation
 Clarendon Laboratory
 University of Oxford
 OX1 3PU Oxford, England

F. Schmidt-Kaler

Sects. 5.2, 5.3

Institut für Experimentalphysik
Universität Innsbruck
Technikerstrasse 25
6020 Innsbruck, Austria

A. Steane

Sect. 7.5

Centre for Quantum Computation
Clarendon Laboratory
University of Oxford
OX1 3PU Oxford, England

K.-A. Suominen

Sect. 7.2

Helsinki Institute of Physics
PL 9, FIN-00014 Helsingin
Yliopisto, Finland

V. Vedral

Sects. 3.11, 6.4, 8.5

Centre for Quantum Computation
Clarendon Laboratory
University of Oxford
OX1 3PU Oxford, England

G. Weihs

Sect. 3.4

Institut für Experimentalphysik
Universität Wien
Boltzmanngasse 5
1090 Wien, Austria

H. Weinfurter

*Chap. 2, Sects. 3.1–3.3, 3.5–3.7,
3.10, 6.3*

Sektion Physik
Ludwig-Maximilians-Universität
München
Schellingstr. 4/III
80799 München, Germany

H. Walther

Sect. 5.3

Max-Planck-Institut
für Quantenoptik
Hans-Kopfermann-Str. 1
85748 Garching, Germany

A. Zeilinger

*Chap. 1, Sects. 3.1–3.3, 3.5–3.7,
3.10, 6.3*

Institut für Experimentalphysik
Universität Wien
Boltzmanngasse 5
1090 Wien, Austria

P. Zoller

Sects. 4.3, 6.2, 8.6, 8.7

Institut für Theoretische Physik
Universität Innsbruck
Technikerstrasse 25
6020 Innsbruck, Austria

1. The Physics of Quantum Information: Basic Concepts

D. Bouwmeester, A. Zeilinger

1.1 Quantum Superposition

The superposition principle plays the most central role in all considerations of quantum information, and in most of the “gedanken” experiments and even the paradoxes of quantum mechanics. Instead of studying it theoretically or defining it abstractly, we will discuss here the quintessential experiment on quantum superposition, the double-slit experiment (Fig. 1.1). According to Feynman [1], the double-slit “has in it the heart of quantum mechanics”. The essential ingredients of the experiment are a source, a double-slit assembly, and an observation screen on which we observe interference fringes. These interference fringes may easily be understood on the basis of assuming a wave property of the particles emerging from the source. It might be mentioned here that the double-slit experiment has been performed with many different kinds of particles ranging from photons [2], via electrons [3], to neutrons [4] and atoms [5]. Quantum mechanically, the state is the coherent superposition

$$|\Psi\rangle = \frac{1}{\sqrt{2}}(|\Psi_a\rangle + |\Psi_b\rangle), \quad (1.1)$$

where $|\Psi_a\rangle$ and $|\Psi_b\rangle$ describe the quantum state with only slit a or slit b open.

The interesting feature in the quantum double-slit experiment is the observation that, as confirmed by all experiments to date, the interference pattern can be collected one by one, that is, by having such a low intensity that only one particle interferes with itself. If this happens, we might be tempted to ask ourselves which of the two slits a particle “really” takes in the experiment. The answer from standard quantum mechanics is that it is not possible to make any sensible statement about the question “which slit does the particle pass through?” without using the appropriate set-up able to answer that question. In fact, if we were to perform any kind of experiment determining through which of the two slits the particle passes, we would have to somehow interact with the particle and this would lead to decoherence, that is, loss of interference. Only when there is no way of knowing, not even in principle,

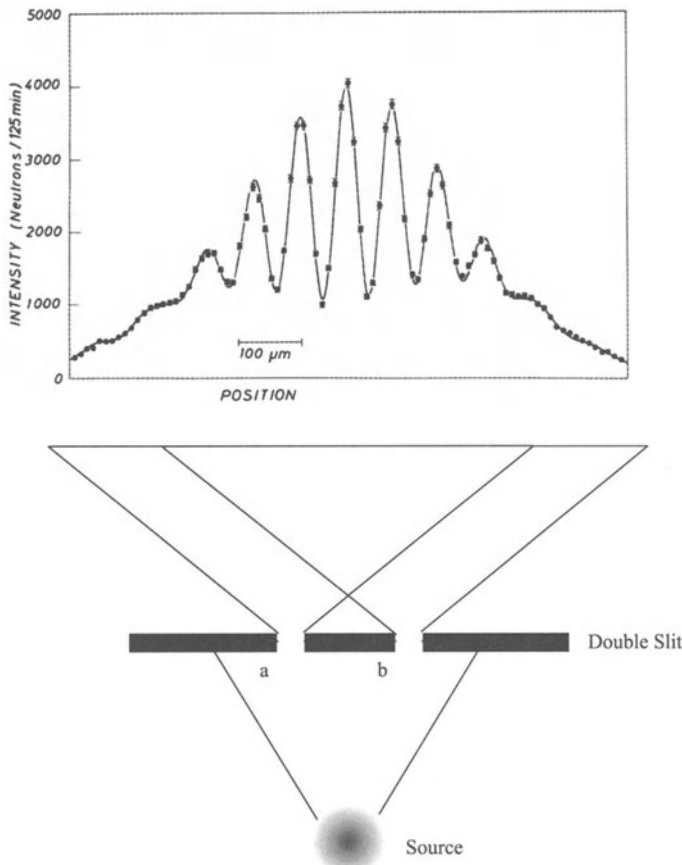


Fig. 1.1. Principle of the double-slit experiment. An interference pattern arises in an observation plane behind a double-slit assembly, even if the intensity of the source is so low that there is only one particle at a time in the apparatus. The actual interference pattern shown here is the experimental data obtained for a double-slit experiments with neutrons [4].

through which slit the particle passes, do we observe interference. As a small warning we might mention that it is not even possible to say that the particle passes through both slits at the same time, although this is a position often held. The problem here is that, on the one hand, this is a contradictory sentence because a particle is a localised entity, and, on the other hand, there is no operational meaning in such a statement. We also note that one can have partial knowledge of the slit the particle passes at the expense of partial decoherence.

1.2 Qubits

The most fundamental entity in information science is the bit. This is a system which carries two possible values, “0” and “1”. In its classical realisation the bit, which, for example could be imagined to be just a mechanical switch, is a system which is designed to have two distinguishable states; there should be a sufficiently large energy barrier between them that no spontaneous transition, which would evidently be detrimental, can occur between the two states.

The quantum analog of a bit, the *Qubit* [6], therefore also has to be a two-state system where the two states are simply called $|0\rangle$ and $|1\rangle$. Basically any quantum system which has at least two states can serve as a qubit, and there are a great variety possible, many of which have already been realised experimentally. The most essential property of quantum states when used to encode bits is the possibility of coherence and superposition, the general state being

$$|Q\rangle = \alpha|0\rangle + \beta|1\rangle, \quad (1.2)$$

with $|\alpha|^2 + |\beta|^2 = 1$. What this means is not that the value of a qubit is somewhere between “0” and “1”, but rather that the qubit is in a superposition of both states and, if we measure the qubit we will find it with probability $|\alpha|^2$ to carry the value “0” and with probability $|\beta|^2$ to carry the value “1”;

$$p(\text{“0”}) = |\alpha|^2, \quad p(\text{“1”}) = |\beta|^2. \quad (1.3)$$

While by the definition of the qubit we seem to lose certainty about its properties, it is important to know that (1.2) describes a *coherent* superposition rather than an incoherent mixture between “0” and “1”. The essential point here is that for a coherent superposition there is always a basis in which the value of the qubit is well defined, while for an incoherent mixture it is a mixture whatever way we choose to describe it. For simplicity consider the specific state

$$|Q'\rangle = \frac{1}{\sqrt{2}}(|0\rangle + |1\rangle). \quad (1.4)$$

This clearly means that with 50% probability the qubit will be found to be either in “0” or “1”. But interestingly, in a basis rotated by 45° in Hilbert space the value of the qubit is well-defined. We might simply study this by applying the proper transformation to the qubit. One of the most basic transformations in quantum information science is the so-called Hadamard transformation whose actions on a qubit are

$$H|0\rangle \rightarrow \frac{1}{\sqrt{2}}(|0\rangle + |1\rangle), \quad H|1\rangle \rightarrow \frac{1}{\sqrt{2}}(|0\rangle - |1\rangle). \quad (1.5)$$

Applying this to the qubit $|Q'\rangle$ above, results in

$$H|Q'\rangle = |0\rangle. \quad (1.6)$$

that is, a well-defined value of the qubit. This is never possible with an incoherent mixture.

1.3 Single-Qubit Transformations

Insight in some of the most basic experimental procedures in quantum information physics can be gained by investigating the action of a simple 50/50 beamsplitter. Such beamsplitters have been realised for many different types of particles, not only for photons. For a general beamsplitter, as shown in Fig. 1.2, let us investigate the case of just two incoming modes and two outgoing modes which are arranged as shown in the figure.

For a 50/50 beamsplitter, a particle incident either from above or from below has the same probability of 50% of emerging in either output beam, above or below. Then quantum unitarity, that is, the requirement that no particles are lost if the beamsplitter is non-absorbing, implies certain phase conditions on the action of the beamsplitter [7] with one free phase. A very simple way to describe the action of a beamsplitter is to fix the phase relations such that the beamsplitter is described by the Hadamard transformation of (1.5).

Let us again assume that the incident state is the general qubit

$$|Q\rangle_{in} = \alpha|0\rangle_{in} + \beta|1\rangle_{in}. \quad (1.7)$$

For a single incident particle this means that α is the probability amplitude to find the particle incident from above and β is the probability amplitude for

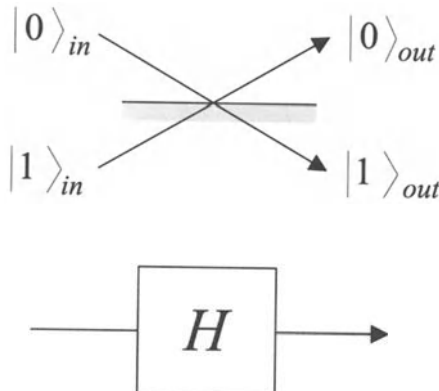


Fig. 1.2. The 50/50 beamsplitter (top) and the corresponding diagram using the Hadamard transform H (below).

finding the particle incident from below. Then the action of the beamsplitter results in the final state

$$|Q\rangle_{out} = H|Q\rangle_{in} = \frac{1}{\sqrt{2}} ((\alpha + \beta)|0\rangle_{out} + (\alpha - \beta)|1\rangle_{out}) , \quad (1.8)$$

where $(\alpha + \beta)$ is now the probability amplitude for finding the particle in the outgoing upper beam and $(\alpha - \beta)$ is the probability amplitude for finding it in the outgoing lower beam. For the specific case of either $\alpha = 0$ or $\beta = 0$, we find that the particle will be found with equal probability in either of the outgoing beams. For another specific case, $\alpha = \beta$, we find that the particle will definitely be found in the upper beam and never in the lower beam.

It is interesting and instructive to consider sequences of such beamsplitters because they realise sequences of Hadamard transformations. For two successive transformations the Mach-Zehnder interferometer (Fig. 1.3) with two identical beamsplitters results.

Furthermore, the mirrors shown only serve to redirect the beams; they are assumed to have identical action on the two beams and therefore can be omitted in the analysis. The full action of the interferometer can now simply be described as two successive Hadamard transformations acting on the general incoming state of (1.7):

$$|Q\rangle_{out} = HH|Q\rangle_{in} = |Q\rangle_{in} . \quad (1.9)$$

This results from the simple fact that double application of the Hadamard transformation of (1.5) is the identity operation. It means that the Mach-Zehnder interferometer as sketched in Fig. 1.3, with beamsplitters realising the Hadamard transformation at its output, reproduces a state identical to the input. Let us consider again the extreme case where the input consists of one beam only, that is, without loss of generality, let us assume $\alpha = 1$, the lower beam being empty. Then, according to (1.9), the particle will def-

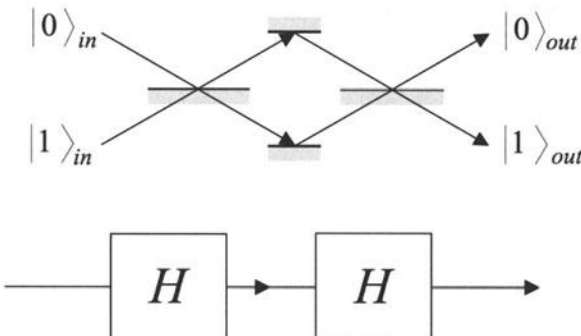


Fig. 1.3. A Mach-Zehnder interferometer (top) is a sequence of two Hadamard transformations (bottom).

initely be found in the upper output. Most interestingly, this is because between the two beamsplitters the particle would have been found (with the correct relative phase) with equal probability in both beam paths. It is the interference of the two amplitudes incident on the final beamsplitter which results in the particle ending up with certainty in one of the outgoing beams and never in the other.

In quantum information language, the output qubit of the empty Mach–Zehnder interferometer will have a definite value if the input qubit also has a definite value, and this only because between the two Hadamard transformations the value of the qubit was maximally undefined.

Another important quantum gate besides the Hadamard gate is the phase shifter, which is introduced additionally in Fig. 1.4 into the Mach–Zehnder interferometer. Its operation is simply to introduce a phase change φ to the amplitude of one of the two beams (without loss of generality we can assume this to be the upper beam because only relative phases are relevant). In our notation, the action of the phase shifter can be described by the unitary transformation

$$\Phi|0\rangle = e^{i\varphi}|0\rangle, \quad \Phi|1\rangle = |1\rangle. \quad (1.10)$$

Therefore the output qubit can be calculated by successive application of all proper transformations to the input qubit:

$$|Q\rangle_{out} = H\Phi H|Q\rangle_{in}. \quad (1.11)$$

We leave it to the reader to calculate the general expression for arbitrary input qubits. We will restrict our discussion again to the case where we have only one input namely $\alpha = 1$ and $\beta = 0$, i.e., $|Q\rangle_{in} = |0\rangle$. The final state then becomes

$$(1.12)$$

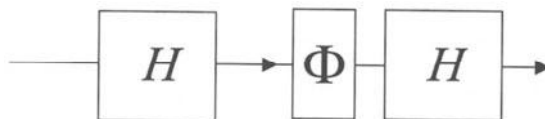
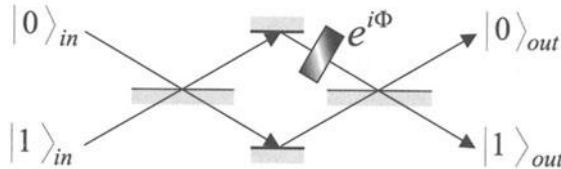


Fig. 1.4. Top: Mach–Zehnder interferometer including a phase shifter φ in one of the two beams. This completely changes the output. Bottom: The equivalent representation with Hadamard transformations and a phase shifter gate.

This has a very simple interpretation. First we observe by inspection of (1.12) that for $\varphi = 0$ the value of the qubit is definitely “0”. On the other hand, for $\varphi = \pi$ the value of the qubit is definitely “1”. This indicates that the phase shift φ is able to switch the output qubit between 0 and 1. In general, the probability that the output qubit has the value “0” is $P_0 = \cos^2(\varphi/2)$, and the probability that the qubit carries the value “1” is $P_1 = \sin^2(\varphi/2)$.

In the present section we have discussed some of the basic notions of linear transformation of qubits. We will now turn to entangled qubits.

1.4 Entanglement

Consider a source which emits a pair of particles such that one particle emerges to the left and the other one to the right (see source S in Fig. 1.5). The source is such that the particles are emitted with opposite momenta. If the particle emerging to the left, which we call particle 1, is found in the upper beam, then particle 2 travelling to the right is always found in the lower beam. Conversely, if particle 1 is found in the lower beam, then particle 2 is always found in the upper beam. In our qubit language we would say that the two particles carry different bit values. Either particle 1 carries “0” and then particle 2 definitely carries “1”, or vice versa. Quantum mechanically this is a two-particle superposition state of the form

$$\frac{1}{\sqrt{2}} (|0\rangle_1 |1\rangle_2 + e^{i\chi} |1\rangle_1 |0\rangle_2) . \quad (1.13)$$

The phase χ is just determined by the internal properties of the source and we assume for simplicity $\chi = 0$. Equation (1.13) describes what is called an entangled state [8]¹. The interesting property is that neither of the two qubits carries a definite value, but what is known from the quantum state is that as soon as one of the two qubits is subject to a measurement, the result of this measurement being completely random, the other one will immediately be found to carry the opposite value. In a nutshell this is the conundrum of quantum non-locality, since the two qubits could be separated by arbitrary distances at the time of the measurement.

A most interesting situation arises when both qubits are subject to a phase shift and to a Hadamard transformation as shown in Fig. 1.5. Then, for detection events after both Hadamard transformations, that is, for the case of the two-particle interferometer verification [10] for detections behind the beamsplitters, interesting non-local correlations result which violate Bell’s inequalities [11]. Without going into the theoretical and formal details here (for more information see Sect. 1.7), the essence of such a violation is that

¹ The word *Entanglement* is a (free) translation of the word *Verschränkung* that was introduced in 1935 by Schrödinger to characterise this special feature of composite quantum systems [9].

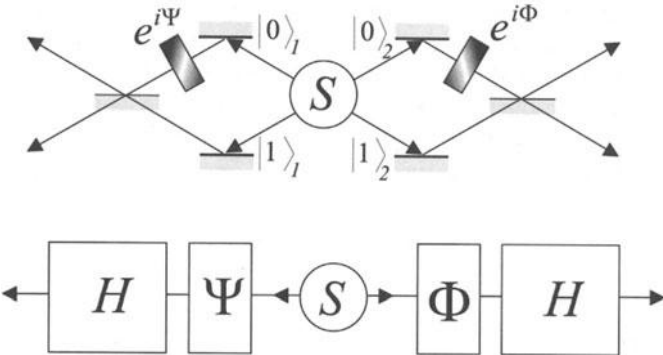


Fig. 1.5. A source emits two qubits in an entangled state. Top: A two-particle interferometer verification. Bottom: The principle in terms of one-photon gates

there is no possibility to explain the correlations between the two sides on the basis of local properties of the qubits alone. The quantum correlations between the two sides cannot be understood by assuming that the specific detector on one given side which registers the particle is not influenced by the parameter setting, that is, by the choice of the phase for the other particle. There are many ways to express precisely the meaning of Bell's inequalities, and there are many formal presentations. Some of this discussion will be presented in Sect. 1.7, and for the remainder we refer the reader to the appropriate literature (e.g., Ref. [12] and references therein).

A very interesting, and for quantum computation quite relevant generalisation follows if entanglement is studied for more than two qubits. For example, consider the simple case of entanglement between three qubits, as shown in Fig. 1.6. We assume that a source emits three particles, one into each of the apparatuses shown, in the specific superposition, a so-called Greenberger–Horne–Zeilinger (GHZ) state [13] (see also Sect. 6.3),

$$\frac{1}{\sqrt{2}}(|0\rangle_1|0\rangle_2|0\rangle_3 + |1\rangle_1|1\rangle_2|1\rangle_3). \quad (1.14)$$

This quantum state has some very peculiar properties. Again, as in two-particle entanglement, none of the three qubits carries any information on its own, none of them has a defined bit value. But, as soon as one of the three is measured, the other two will assume a well-defined value as long as the measurement is performed in the chosen 0-1 basis. This conclusion holds independent of the spatial separation between the three measurements.

Most interestingly, if one looks at the relations predicted by the GHZ state (1.14) between the three measurements after passing the phase shifters and the Hadamard transforms, a number of perfect correlations still result for certain joint settings of the three parameters [14], the interesting property now being that it is not possible to understand even the perfect correlations with a local model. This shows that quantum mechanics is at variance with

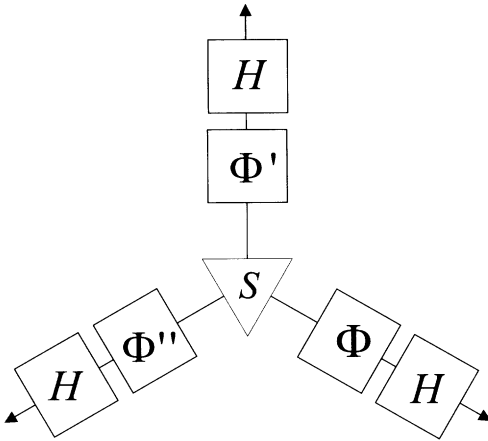


Fig. 1.6. Three-particle entanglement in a so-called GHZ state. Here we show only the representation in terms of our elementary gates, it will be straightforward for the reader to consider the physical realisation in a three-particle interferometer.

a classical local world view not only for the sector of statistical predictions of the theory but also for predictions which can be made with certainty.

1.5 Entanglement and Quantum Indistinguishability

In order to understand both the nature of entanglement and ways of producing it, one has to realise that in states of the general form (1.13) and (1.14), we have a superposition between product states. We recall from the discussion of the double-slit diffraction phenomenon (Sect. 1.1) that superposition means that there is no way to tell which of the two possibilities forming the superposition actually pertains. This rule must also be applied to the understanding of quantum entanglement. For example, in the state

$$|\Psi\rangle_{12} = \frac{1}{\sqrt{2}}(|0\rangle_1|1\rangle_2 + |1\rangle_1|0\rangle_2) \quad (1.15)$$

there is no way of telling whether qubit 1 carries the value “0” or “1”, and likewise whether qubit 2 carries the value “0” or “1”. Yet, if one qubit is measured the other one immediately assumes a well-defined quantum state. These observations lead us directly to the conditions of how to produce and observe entangled quantum states.

To produce entangled quantum states, one has various possibilities. Firstly, one can create a source which, through its physical construction, is such that the quantum states emerging already have the indistinguishability feature discussed above. This is realised, for example, by the decay of a spin-0 particle into two spin-1/2 particles under conservation of the internal

angular momentum [15]. In this case, the two spins of the emerging particles have to be opposite, and, if no further mechanisms exist which permit us to distinguish the possibilities right at the source, the emerging quantum state is

$$|\Psi\rangle_{12} = \frac{1}{\sqrt{2}}(|\uparrow\rangle_1|\downarrow\rangle_2 - |\downarrow\rangle_1|\uparrow\rangle_2), \quad (1.16)$$

where, e.g. $|\uparrow\rangle_1$ means particle 1 with spin up. The state (1.16) has the remarkable property that it is rotationally invariant, i.e., the two spins are anti-parallel along whichever direction we choose to measure.

A second possibility is that a source might actually produce quantum states of the form of the individual components in the superposition of (1.15), but the states might still be distinguishable in some way. This happens, for example, in type-II parametric down-conversion [16] (Sect. 3.4.4), where along a certain chosen direction the two emerging photon states are

$$|H\rangle_1|V\rangle_2 \text{ and } |V\rangle_1|H\rangle_2. \quad (1.17)$$

That means that either photon 1 is horizontally polarised and photon 2 is vertically polarised, or photon 1 is vertically polarised and photon 2 is horizontally polarised. Yet because of the different speeds of light for the H and V polarised photons inside the down-conversion crystal, the time correlation between the two photons is different in the two cases. Therefore, the two terms in (1.17) can be distinguished by a time measurement and no entangled state results because of this potential to distinguish the two cases. However, in this case too one can still produce entanglement by shifting the two photon-wave packets after their production relative to each other such that they become indistinguishable on the basis of their positions in time. What this means is the application of a quantum eraser technique [17] where a marker, in this case the relative time ordering, is erased such that we obtain quantum indistinguishability resulting in the state

$$|\Psi\rangle_{12} = \frac{1}{\sqrt{2}}(|H\rangle_1|V\rangle_2 + e^{i\chi}|V\rangle_1|H\rangle_2), \quad (1.18)$$

which is entangled.

A third means of producing entangled states is to project a non-entangled state onto an entangled one. We remark, for example, that an entangled state is never orthogonal to any of its components. Specifically, consider a source producing the non-entangled state

$$|0\rangle_1|1\rangle_2. \quad (1.19)$$

Suppose this state is now sent through a filter described by the projection operator

$$P = |\Psi\rangle_{12}\langle\Psi|_{12}, \quad (1.20)$$

where $|\Psi\rangle_{12}$ is the state of (1.15). Then the following entangled state results:

$$\frac{1}{2}(|0\rangle_1|1\rangle_2 + |1\rangle_1|0\rangle_2)(\langle 0|_1\langle 1|_2 + \langle 1|_1\langle 0|_2)|0\rangle_1|1\rangle_2 = \frac{1}{2}(|0\rangle_1|1\rangle_2 + |1\rangle_1|0\rangle_2); \quad (1.21)$$

it is no longer normalised to unity because the projection procedure implies a loss of qubits.

While each of the three methods discussed above can in principle be used to produce outgoing entangled states, a further possibility exists to produce entanglement upon observation of a state. In general, this means that we have an unentangled or partially entangled state of some form and the measurement procedure itself is such that it projects onto an entangled state, in much the same way as discussed just above. This procedure was used, for example, in the first experimental demonstration of GHZ entanglement of three photons (see Sect. 6.3) [18].

1.6 The Controlled NOT Gate

Thus far, we have discussed only single-qubit gates, that is, gates which involve one qubit only. Of greatest importance for quantum computation applications are two-qubit gates, where the evolution of one qubit is conditional upon the state of the other qubit. The simplest of these gates is the quantum controlled NOT gate illustrated in Fig. 1.7. The essence of the controlled NOT gate is that the value of the so-called target qubit is negated if and only if the control qubit has the logical value “1”. The logical value of the control qubit does not change. The action of the quantum controlled NOT gate can be described by the transformations

$$\begin{array}{ll} |0\rangle_c|0\rangle_t \rightarrow |0\rangle_c|0\rangle_t & |0\rangle_c|1\rangle_t \rightarrow |0\rangle_c|1\rangle_t \\ |1\rangle_c|0\rangle_t \rightarrow |1\rangle_c|1\rangle_t & |1\rangle_c|1\rangle_t \rightarrow |1\rangle_c|0\rangle_t \end{array} \quad (1.22)$$

where $|0\rangle_c$ and $|1\rangle_c$ refer to the control qubit and $|0\rangle_t$ and $|1\rangle_t$ refer to the target qubit. Together with the single-qubit transformations described in

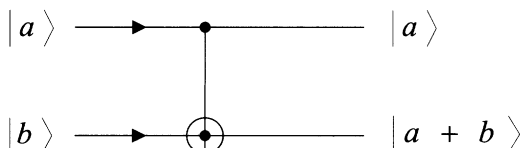


Fig. 1.7. The controlled NOT gate is a transformation involving two qubits. The value of the control qubit (the upper one in the figure) influences the lower one, whose value is flipped if the upper qubit carries “1”, and not flipped if the upper qubit carries “0”. This is equivalent to addition modulo 2.

Sect. 1.3 the quantum controlled NOT gate can be used to realise quantum computation networks. One interesting explicit application is the production of two-qubit or multi-qubit entangled states using these gates [19].

1.7 The EPR Argument and Bell's Inequality

Immediately after the discovery of modern quantum mechanics, it was realised that it contains novel, counterintuitive features, as witnessed most remarkably in the famous dialogue between Niels Bohr and Albert Einstein [20]. While Einstein initially tried to argue that quantum mechanics is inconsistent, he later reformulated his argument towards demonstrating that quantum mechanics is incomplete. In the seminal paper [21], Einstein, Podolsky and Rosen (EPR) consider quantum systems consisting of two particles such that, while neither position nor momentum of either particle is well defined, the sum of their positions, that is their centre of mass, and the difference of their momenta, that is their individual momenta in the center of mass system, are both precisely defined. It then follows that a measurement of either position or momentum performed on, say, particle 1 immediately implies a precise position or momentum, respectively, for particle 2, without interacting with that particle. Assuming that the two particles can be separated by arbitrary distances, EPR suggest that a measurement on particle 1 cannot have any actual influence on particle 2 (locality condition); thus the property of particle 2 must be independent of the measurement performed on particle 1. To them, it then follows that both position and momentum can simultaneously be well defined properties of a quantum system.

In his famous reply [22], Niels Bohr argues that the two particles in the EPR case are always parts of one quantum system and thus measurement on one particle changes the possible predictions that can be made for the whole system and therefore for the other particle.

While the EPR–Bohr discussion was considered for a long time to be merely philosophical, in 1951 David Bohm [15] introduced spin-entangled systems and in 1964 John Bell [23] showed that, for such entangled systems, measurements of correlated quantities should yield different results in the quantum mechanical case to those expected if one assumes that the properties of the system measured are present prior to, and independent of, the observation. Even though a number of experiments have now confirmed the quantum predictions [24]–[26], from a strictly logical point of view the problem is not closed yet as some loopholes in the existing experiments still make it logically possible, at least in principle, to uphold a local realist world view [27].

Let us briefly present the line of reasoning that leads to an inequality equivalent to the original Bell inequality. Consider a source emitting two qubits (Fig. 1.8) in the entangled state

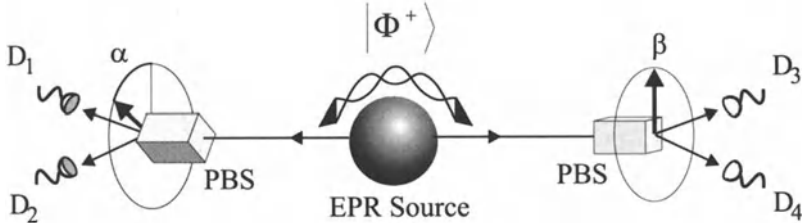


Fig. 1.8. Correlation measurements between Alice's and Bob's detection events for different choices for the detection bases (indicated by the angles α and β for the orientation of their polarising beamsplitters, PBS) lead to the violation of Bell's inequalities.

$$|\Phi^+\rangle_{12} = \frac{1}{\sqrt{2}}(|H\rangle_1|H\rangle_2 + |V\rangle_1|V\rangle_2). \quad (1.23)$$

One qubit is sent to Alice (to the left in Fig. 1.8), the other one to Bob (to the right). Alice and Bob will perform polarisation measurements using a polarising beamsplitter with two single-photon detectors in the output ports. Alice will obtain the measurement result “0” or “1”, corresponding to the detection of a qubit by detector 1 or 2 respectively, each with equal probability. This statement is valid in whatever polarisation basis she decides to perform the measurement, the actual results being completely random. Yet, if Bob chooses the same basis, he will always obtain the same result. Thus, following the first step of the EPR reasoning, Alice can predict with certainty what Bob's result will be. The second step employs the locality hypothesis, that is, the assumption that no physical influence can instantly go from Alice's apparatus to Bob's and therefore Bob's measured result should only depend on the properties of his qubit and on the apparatus he chose. Combining the two steps, John Bell investigated possible correlations for the case that Alice and Bob choose detection bases which are at oblique angles. For three arbitrary angular orientations α , β , γ , one can see [28] that the following inequality must be fulfilled:

$$N(1_\alpha, 1_\beta) \leq N(1_\alpha, 1_\gamma) + N(1_\beta, 0_\gamma), \quad (1.24)$$

where

$$N(1_\alpha, 1_\beta) = \frac{N_0}{2} \cos^2(\alpha - \beta) \quad (1.25)$$

is the quantum-mechanical prediction for the number of cases where Alice obtains “1” with her apparatus at orientation α and Bob achieves “1” with orientation β , and N_0 is the number of pairs emitted by the source. The inequality is violated by the quantum-mechanical prediction if we choose, for example, the angles $(\alpha - \beta) = (\beta - \gamma) = 30^\circ$. The violation implies that at least one of the assumptions entering Bell's inequality must be in conflict with quantum mechanics. This is usually viewed as evidence for non-locality, though that is by no means the only possible explanation.

1.8 Comments

As recently as a decade ago, the issues discussed here were mainly considered to be of a philosophical nature, though very relevant ones in our attempts to understand the world around us and our role in it. In the last few years, very much to the surprise of most of the early researchers in the field, the basic concepts of superposition and quantum entanglement have turned out to be key ingredients in novel quantum communication and quantum computation schemes. Here we have given only a condensed introduction. More details are contained in the various chapters of this book. Further information can also be found on the world wide web, for example at www.qubit.org or www.quantum.at with many links to other relevant sites.

2. Quantum Cryptography

A. Ekert, N. Gisin, B. Huttner, H. Inamori, H. Weinfurter

2.1 What is Wrong with Classical Cryptography?

2.1.1 From SCYTALE to ENIGMA

Human desire to communicate secretly is at least as old as writing itself and goes back to the beginnings of our civilisation. Methods of secret communication were developed by many ancient societies, including those of Mesopotamia, Egypt, India, and China, but details regarding the origins of cryptology¹ remain unknown [29].

We know that it was the Spartans, the most warlike of the Greeks, who pioneered military cryptography in Europe. Around 400 BC they employed a device known as the SCYTALE. The device, used for communication between military commanders, consisted of a tapered baton around which was wrapped a spiral strip of parchment or leather containing the message. Words were then written lengthwise along the baton, one letter on each revolution of the strip. When unwrapped, the letters of the message appeared scrambled and the parchment was sent on its way. The receiver wrapped the parchment around another baton of the same shape and the original message reappeared as shown in Fig. 2.1.

Julius Caesar allegedly used, in his correspondence, a simple letter substitution method. Each letter of Caesar's message was replaced by the letter that followed it alphabetically by three places. The letter A was replaced by D, the letter B by E, and so on. For example, the English word COLD after the Caesar substitution appears as FROG. This method is still called the Caesar cipher, regardless the size of the shift used for the substitution.

These two simple examples already contain the two basic methods of encryption which are still employed by cryptographers today namely *transposition* and *substitution*. In transposition (e.g. scytale) the letters of the

¹ The science of secure communication is called cryptology from Greek *kryptos* hidden and *logos* word. Cryptology embodies cryptography, the art of code-making, and cryptanalysis, the art of code-breaking.

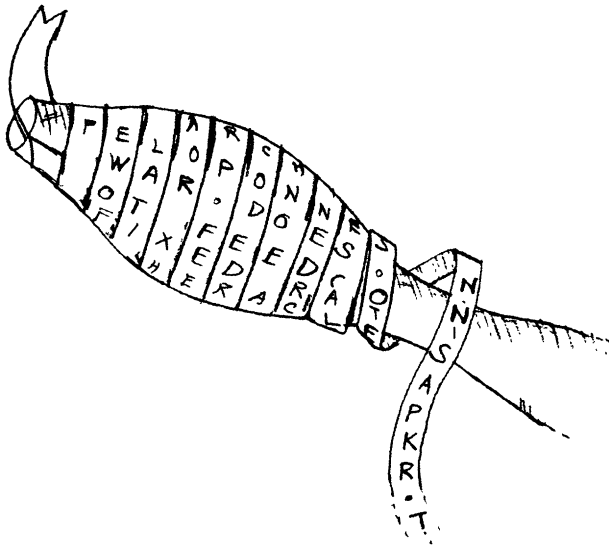


Fig. 2.1. The first cryptographic machine – a Scytale.

plaintext, the technical term for the message to be transmitted, are rearranged by a special permutation. In substitution (e.g. Caesar's cipher) the letters of the plaintext are replaced by other letters, numbers or arbitrary symbols. In general the two techniques can be combined.

Until some years ago, sophisticated cryptography was restricted primarily to the military world. Only the military had sufficient resources to produce sophisticated mechanical devices, such as the famous ENIGMA which was widely used by Germans during World War II or its American counterpart the M-209. ENIGMA ciphers were broken before the war in Poland and during the war at Bletchley Park in England. The Bletchley Park team, which included Alan Turing, had to develop the electromechanical tools to break these ciphers, which resulted in building the first digital computer called COLOSSUS. Thus modern cryptology (for an introduction see, for example, [30]–[32]) was born together with computer science. As expressed by R.L. Rivest (codiscoverer of the popular RSA public key system), cryptanalysis was “the midwife of computer science”.

2.1.2 Keys and Their Distribution

Originally the security of a cryptotext depended on the secrecy of the entire encrypting and decrypting procedures; however, today we use ciphers for which the algorithm for encrypting and decrypting could be revealed to anybody without compromising the security of a particular cryptogram. In such ciphers a set of specific parameters, called a *key*, is supplied together with

the plaintext as an input to the encrypting algorithm, and together with the cryptogram as an input to the decrypting algorithm. This can be written as

$$\hat{E}_k(P) = C, \text{ and conversely, } \hat{D}_k(C) = P, \quad (2.1)$$

where P stands for plaintext, C for cryptotext or cryptogram, k for cryptographic key, and \hat{E} and \hat{D} denote an encryption and a decryption operation respectively.

The encrypting and decrypting algorithms are publicly known; the security of the cryptogram depends entirely on the secrecy of the key, and this key must consist of a *randomly chosen*, sufficiently long string of bits. Probably the best way to explain this procedure is to have a quick look at the Vernam cipher, also known as the one-time pad pad.

If we choose a very simple digital alphabet, in which we use only capital letters and some punctuation marks, such as

A	B	C	D	E	X	Y	Z	?	,	.	
00	01	02	03	04	23	24	25	26	27	28	29

we can illustrate the secret-key encrypting procedure by the following simple example (we refer to the dietary requirements of 007): In order to obtain

S	H	A	K	E	N	N	O	T	S	T	I	R	R	E	D		
18	07	00	10	04	13	26	13	14	19	26	18	19	08	17	17	04	03
15	04	28	13	14	06	21	11	23	18	09	11	14	01	19	05	22	07
03	11	28	23	18	19	17	24	07	07	05	29	03	09	06	22	26	10

the cryptogram (sequence of digits in the bottom row) we add the plaintext numbers (the top row of digits) to the key numbers (the middle row), which are randomly selected from between 0 and 29, and take the remainder after division of the sum by 30, that is we perform addition modulo 30. For example, the first letter of the message “S” becomes a number “18” in the plaintext, then we add $18 + 15 = 33 ; 33 = 1 \times 30 + 3$, therefore we get 03 in the cryptogram. The encryption and decryption can be written as $P + k \pmod{30} = C$ and $C - k \pmod{30} = P$ respectively.

The cipher was invented in 1917 by the American AT&T engineer Gilbert Vernam. It was later shown, by Claude Shannon [33], that as long as the key is truly random, has the same length as the message, and is never reused then the one-time pad is perfectly secure. So, if we have a truly unbreakable system, what is wrong with classical cryptography?

There is a snag. It is called *key distribution*. Once the key is established, subsequent communication involves sending cryptograms over a channel, even one which is vulnerable to total passive eavesdropping (e.g. public announcement in mass-media). This stage is indeed secure. However in order to establish the key, two users, who share no secret information initially, must at

a certain stage of communication use a reliable and a very secure channel. Since the interception is a set of measurements performed by an eavesdropper on this channel, however difficult this might be from a technological point of view, *in principle* any classical key distribution can always be passively monitored, without the legitimate users being aware that any eavesdropping has taken place. This would not be such a problem if the key were established once and for all. In this case, the users may spend enough resources (such as strong safes and protection) to ensure that the key arrives safely to its addressee. But since the key has to be renewed for every message, key distribution would become prohibitively expensive. For this reason, in most applications, one does not require this absolute secrecy, but rather settles for less expensive and less secure systems.

For more mundane transmissions, the system of choice is the Data Encryption Standard (DES), which was announced in 1977, and is still in use for sensitive but non-secret information, especially for commercial transactions. This system only requires a short key, 64 bits of which 56 bits are used directly by the algorithm and 8 bits are used for error detection. It encrypts blocks of 64 bits of the plaintext. In the easiest implementation, a long plaintext is cut into blocks, and the key is then used to encrypt each of them. In more sophisticated (and safer) systems, the message is further protected by making each enciphered block depend on the previous ones. Frequent rumours that DES has been broken have never been substantiated and it seems that DES was designed using excellent criteria; given the short key length it is a very good algorithm. Further discussion of the numerous possibilities of DES are outside the scope of this review, and can be found in the literature or in the internet. As explained above, none of these are totally secure: since the same key is used many times, there is information about the plaintext in the cryptogram. The goal of the encryption methods is to hide it as well as possible. A dedicated cryptanalyst will be able to break the cipher and obtain the message, but if it takes too long the information may become obsolete. In most applications, it is recommended to use one key for only a few days, before discarding it for a new one. Of course, the problem of transmitting the key to the receiver remains, but, for all practical purposes, is made less critical, as the amount of key required is much smaller.

Thus a pretty good security is possible, but what about a perfect security? It follows from our brief discussion above that in principle we can achieve a perfect security in communication via one-time pads provided we solve the key distribution problem. The question is: can we solve the key distribution problem? The answer to this question is basically “yes”. There are two very interesting solutions, one mathematical and one physical. The mathematical one is known as *public-key cryptography* and the physical one is referred to as *quantum cryptography*.

2.1.3 Public Keys and Quantum Cryptography

Before we proceed any further let us introduce our three main characters: Alice and Bob, two individuals who want to communicate secretly, and Eve, an eavesdropper. The scenario is: Alice and Bob want to establish a secret key and Eve wants to gain at least partial information about the key.

Cryptologists have tried hard to give Alice and Bob the edge and to solve the key distribution problem. The 1970s, for example, brought a clever mathematical discovery in the shape of “public key” systems. The two main public key cryptography techniques in use today are the Diffie–Hellman key exchange protocol [34] and the RSA encryption system [35]. They were discovered in the academic community in 1976 and 1978, respectively. However, these techniques were known to the British government agencies prior to these dates, although this was not officially confirmed until recently. In fact the techniques were first discovered at CESG in the early 1970s by James Ellis, who called them “Non-Secret Encryption”. In 1973, building on Ellis’ idea, C. Cocks designed what we now call RSA, and in 1974 M. Williamson proposed what is essentially known today as the Diffie–Hellman key exchange protocol.

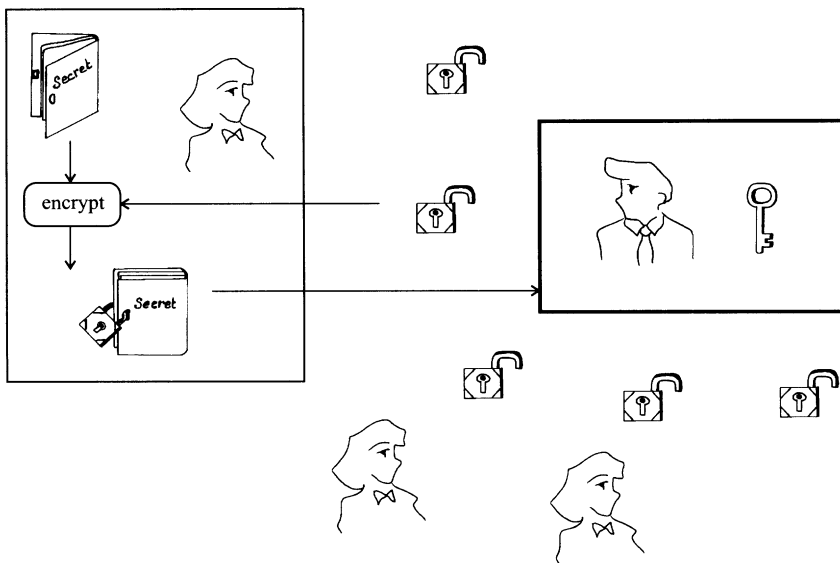


Fig. 2.2. Public key cryptosystem can be explained using the following mechanical analogy. Imagine Bob who can produce many padlocks and anybody who wants to send secret messages to Bob can receive an open padlock manufactured by Bob. An open padlock can be viewed as a public key. In particular Alice gets one too. Once the padlock is locked by Alice only Bob can open it because only Bob has the key – the private key. Thus Alice can lock any data she wants to send to Bob with this padlock. Once the data is locked, only Bob can access it thanks to his private key.

In the public-key systems users do not need to agree on a secret key before they send the message. They work on the principle of a safe with two keys, one public key to lock it, and another private one to open it. Everyone has a key to lock the safe but only one person has a key that will open it again, so anyone can put a message in the safe but only one person can take it out. Another analogy is the padlock example shown in Fig. 2.2. These systems exploit the fact that certain mathematical operations are easier to do in one direction than the other. The systems avoid the key distribution problem but unfortunately their security depends on unproven mathematical assumptions, such as the difficulty of factoring large integers. That is, it is perfectly possible to figure out the private key from the public one but it is difficult. For example, RSA – a very popular public key cryptosystem named after the three inventors, Ron Rivest, Adi Shamir, and Leonard Adleman [35] – gets its security from the difficulty of factoring large numbers. Mathematicians believe (firmly, though they have not actually proved it) that in order to factorise a number with N decimal digits, any classical computer needs a number of steps that grows exponentially with N : that is to say, adding one extra digit to the number to be factorised generally multiplies the time required by a fixed factor. Thus, as we increase the number of digits, the task rapidly becomes intractable.

This means that if and when mathematicians or computer scientists come up with fast and clever procedures for factoring large integers, the whole privacy and discretion of public-key cryptosystems could vanish overnight. Indeed, recent work in quantum computation shows that quantum computers can, at least in principle, factor much faster than classical computers [36]! This means that in one sense public key cryptosystems are already insecure: any RSA-encrypted message that is recorded today will become readable moments after the first quantum computer is switched on, and therefore RSA cannot be used for encrypting any information that will still need to be secret on that happy day. Admittedly, that day is probably decades away, but can anyone prove, or give any reliable assurance, that it is? Confidence in the slowness of technological progress is all that the security of the RSA system now rests on.

Quantum cryptography brings an entirely new way of solving the key distribution problem. What quantum computation takes away with one hand, it returns, at least partially, with the other. One of the simplest types of quantum computation — a type which is now routinely carried out in the laboratory and may soon be a commercial proposition — is quantum cryptography. It provides perfectly secure key distribution because, unlike all classical cryptography, it relies on the laws of physics rather than on ensuring that successful eavesdropping would require excessive computational effort.

Before we discuss quantum cryptography (QC) in detail let us mention briefly yet another difficulty in the business of secure communication, namely *authentication*.

2.1.4 Authentication: How to Recognise Cinderella ?

So far, we trusted the integrity of the communication channel: we allowed Eve to eavesdrop on messages exchanged between Alice and Bob, but we took for granted that Eve could not forge or modify them. That is we assumed that Alice and Bob have access to a perfect public channel, that is a channel that can be freely monitored by anybody; however, it should be impossible to modify the information sent through such a channel, e.g., a radio broadcast. This may be a risky assumption in many realistic scenarios. In some cases, a cunning Eve may interfere in the Alice–Bob communication channel by cutting it in two and impersonating Alice to Bob and vice-versa.

Under this condition, she can, for example, generate two pairs of public-private keys and give one public key to Alice and one to Bob informing Alice that she has been given Bob’s public key and informing Bob that he now has Alice’s public key. Eve keeps the corresponding private keys and from now on any subsequent communication between Alice and Bob would be under her complete control.

Likewise, a private key cryptosystem such as the one-time pad is vulnerable to tampering if the enemy knows the message being sent. Suppose an embassy is using the previously described Vernam cipher to communicate with its country. If Eve knows exactly the message being sent, such as names of some individuals, she could then intercept the encrypted message and prevent it from reaching its destination. Meanwhile, she gets the corresponding Vernam key by performing the subtraction modulo 30 of the ciphertext by the message. Afterwards she may use this key at her mercy, for interesting purposes like disinformation. This example shows that even perfectly secure cryptosystems should not be used blindly.

“Certifying” a public key or “authenticating” a message is a cryptographic technique to counter the kind of attacks described above, called man-in-the-middle or separate worlds attacks.

Once Alice and Bob truly share a secret key then convenient and efficient methods of authentication exist. However, so far there is no convenient way to certify a public key. The only reliable way to check a key’s authenticity is to meet face-to-face with its owner. Unfortunately, quantum key distribution does not provide any more convenient ways to authenticate, to counter a man-in-the-middle attack. Alice and Bob should meet at least once to exchange an authentication key².

In the following we assume that Alice and Bob do have access to a perfect public channel but we will return, very briefly though, to the authentication problem.

² In both situations, Alice and Bob can rely on a third party, a trusted arbitrator, who is in charge of certifying digital keys.

2.2 Quantum Key Distribution

Let us start our discussion of the quantum key distribution with an overview of some general principles. This will be followed by a more detailed description and experimental considerations in Sect. 2.6.

2.2.1 Preliminaria

Quantum key distribution begins with the transmission of single or entangled quanta between Alice and Bob. Eavesdropping, from a physical point of view, is based on a set of measurements performed by an eavesdropper on carriers of information, in this case on the transmitted quanta. According to the rules of quantum mechanics, in general, any measurement performed by Eve unavoidably modifies the state of the transmitted quanta and this can be discovered by Alice and Bob in a subsequent public communication³. Thus the main ingredients of the quantum key distributing system are: a quantum channel for the exchange of quanta and the so-called public channel, which is used to test whether or not the transmission through the quantum channel is distorted (see Fig. 2.3). Let us repeat that any public channel can be freely monitored by anybody; however, it should be impossible to modify the information sent through such a channel.

During the quantum transmission the key is either encoded using a prescribed set of non-orthogonal quantum states of a single particle or is obtained from a prescribed set of measurements performed on entangled particles after the transmission (in this case the key does not even exist during the transmission).

2.2.2 Security in Non-orthogonal States: No-Cloning Theorem

The idea of using non-orthogonal quantum states to encode secret information is due to Stephen Wiesner who proposed “quantum money” [37] which cannot be forged by copying. This is because one cannot clone non-orthogonal quantum states (or any unknown quantum state). To see this, consider two

³ A legitimate question here is: how can we be sure that the rules of quantum mechanics are correct? The answer is that quantum mechanics has been tested repeatedly to a very high degree of accuracy and it is the best theory we have at the moment. It does not make much sense to ask physicists to prove the laws of physics in general and of quantum mechanics in particular. Of course, no body of experimental evidence confirming quantum mechanics makes it more “correct” but one single experiment may refute the theory. The growth of our scientific knowledge is based on conjectures and refutations and most likely quantum mechanics will eventually be superseded by a new theory but it seems unlikely that this new theory will give new results in the present realm of application of quantum mechanics. Rather, new effects will be found in extreme situations as encountered, for example, in strong gravitational fields.

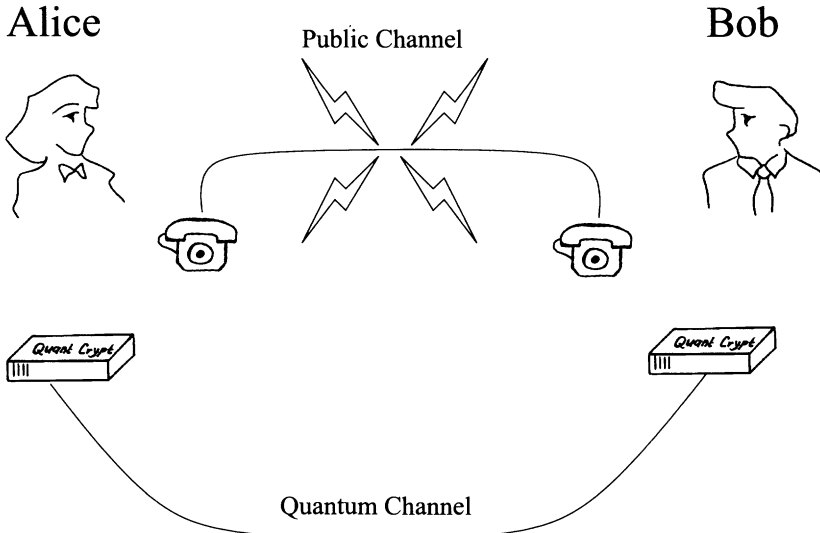


Fig. 2.3. Quantum key distribution scenario. Alice and Bob are linked by two channels, a quantum channel and a classical public channel.

normalised states $|0\rangle$ and $|1\rangle$ such that $\langle 0|1\rangle \neq 0$. Suppose there exists a cloning machine which operates as follows

$$|0\rangle|\text{blank}\rangle|\text{machine}\rangle \rightarrow |0\rangle|0\rangle|\text{machine}_0\rangle \quad (2.2)$$

$$|1\rangle|\text{blank}\rangle|\text{machine}\rangle \rightarrow |1\rangle|1\rangle|\text{machine}_1\rangle, \quad (2.3)$$

where “blank” is an initial state of a particle which after the operation becomes the clone and all the states are properly normalised. This operation must be unitary and should preserve the inner product, thus we require

$$\langle 0|1\rangle = \langle 0|1\rangle\langle 0|1\rangle\langle \text{machine}_0|\text{machine}_1\rangle, \quad (2.4)$$

which is only possible when $\langle 0|1\rangle = 0$ (the two states are orthogonal) or when $\langle 0|1\rangle = 1$ (the two states are indistinguishable and therefore cannot be used to encode two different bit values), which contradicts our initial assumption. Thus if somebody secretly prepares a random sequence of states of the type $|1\rangle|0\rangle|1\rangle|1\rangle \dots$, where $|0\rangle$ and $|1\rangle$ are chosen randomly, it is impossible to reproduce this sequence faithfully. Wiesner’s money with such unclonable quantum signatures would require storing non-orthogonal quantum states on the banknotes which is way more difficult than sending non-orthogonal quantum states from one place to another. That is why Wiesner’s idea was adapted to the key distribution. Charles Bennett and Gilles Brassard proposed to use non-orthogonal states of polarised photons to distribute cryptographic keys [38]. Any eavesdropper trying to distinguish between nonorthogonal $|0\rangle$ and $|1\rangle$ during the quantum transmission has a problem. Suppose Eve prepares her measuring device initially in a normalised state $|m\rangle$ and wants to

tell $|0\rangle$ from $|1\rangle$ without disturbing the two states, i.e., she wants to implement the following unitary operation

$$|0\rangle|m\rangle \rightarrow |0\rangle|m_0\rangle \quad (2.5)$$

$$|1\rangle|m\rangle \rightarrow |1\rangle|m_1\rangle. \quad (2.6)$$

The unitarity condition implies $\langle 0|1\rangle\langle m|m\rangle = \langle 0|1\rangle\langle m_0|m_1\rangle$, i.e., $\langle m_0|m_1\rangle = 1$, the final state of the measuring device is the same in both cases. The two states are not disturbed but Eve gained no information about the encoded bit value. A more general measurement (but still not the most general one), which disturbs the original states so that $|0\rangle \rightarrow |0'\rangle$ and $|1\rangle \rightarrow |1'\rangle$ is of the form

$$|0\rangle|m\rangle \rightarrow |0'\rangle|m_0\rangle \quad (2.7)$$

$$|1\rangle|m\rangle \rightarrow |1'\rangle|m_1\rangle. \quad (2.8)$$

The unitarity condition gives $\langle 0|1\rangle = \langle 0'|1'\rangle\langle m_0|m_1\rangle$. The minimum of $\langle m_0|m_1\rangle$, which corresponds to the situation where Eve has the best chance to distinguish the two states, is obtained for $\langle 0'|1'\rangle = 1$, i.e., the two states $|0\rangle$ and $|1\rangle$ become the same state after the interaction. Although the measurement just described is not the most general one it gives a good illustration of the trade-off between the information gained in the measurement and the disturbance of the original states. The key distribution protocol which employs this trade-off is described in detail later.

2.2.3 Security in Entanglement

The conceptual foundation for entanglement-based quantum cryptography is of a different nature and involves the Einstein–Podolsky–Rosen paradox. In 1935 Einstein together with Boris Podolsky and Nathan Rosen (EPR) published a paper in which they outlined how a “proper” fundamental theory of nature should look [21]. The EPR programme required completeness (“In a complete theory there is an element corresponding to each element of reality”), locality (“The real factual situation of the system A is independent of what is done with the system B, which is spatially separated from the former”), and defined the element of physical reality as “If, without in any way disturbing a system, we can predict with certainty the value of a physical quantity, then there exists an element of physical reality corresponding to this physical quantity”. EPR then considered a thought experiment on two entangled particles which showed that quantum states cannot in all situations be complete descriptions of physical reality. The EPR argument, as subsequently modified by David Bohm [15], goes as follows. Imagine the singlet-spin state of two spin- $\frac{1}{2}$ particles

$$|\Psi\rangle = \frac{1}{\sqrt{2}} (|\uparrow\rangle|\downarrow\rangle - |\downarrow\rangle|\uparrow\rangle), \quad (2.9)$$

where the single particle kets $|\uparrow\rangle$ and $|\downarrow\rangle$ denote spin up and spin down with respect to some chosen direction. This state is spherically symmetric and the choice of the direction does not matter. The two particles, which we label A and B, are emitted from a source and fly apart. After they are sufficiently separated so that they do not interact with each other we can predict with certainty the x component of spin of particle A by measuring the x component of spin of particle B. This is because the total spin of the two particles is zero and the spin components of the two particles must have opposite values. The measurement performed on particle B does not disturb particle A (by locality) therefore the x component of spin is an element of reality according to the EPR criterion. By the same argument and by the spherical symmetry of state $|\Psi\rangle$ the y, z, or any other spin components are also elements of reality. However, since there is no quantum state of a spin- $\frac{1}{2}$ particle in which all components of spin have definite values the quantum description of reality is not complete.

The EPR programme asked for a different description of quantum reality but until John Bell's (1964) theorem it was not clear whether such a description was possible and if so whether it would lead to different experimental predictions. Bell showed that the EPR propositions about locality, reality, and completeness are incompatible with some quantum mechanical predictions involving entangled particles [23]. The contradiction is revealed by deriving from the EPR programme an experimentally testable inequality which is violated by certain quantum mechanical predictions. In Sect. 1.7 a brief derivation of the inequality is given. Extension of Bell's original theorem by John Clauser and Michael Horne (1974) made experimental tests of the EPR programme feasible [39] and quite a few of them have been performed. The experiments have supported quantum mechanical predictions.

What does all this have to do with data security? Surprisingly, a lot! It turns out that the very trick used by Bell to test the conceptual foundations of quantum theory can protect data transmission from eavesdroppers! Perhaps it sounds less surprising when one recalls again the EPR definition of an element of reality: "If, without in any way disturbing a system, we can predict with certainty the value of a physical quantity, then there exists an element of physical reality corresponding to this physical quantity". If this particular physical quantity is used to encode binary values of a cryptographic key then all an eavesdropper wants is an element of reality corresponding to the encoding observable. This way the entanglement-based quantum cryptography made a practical use of quantum entanglement and of the Bell theorem, showing that a border between blue sky and down-to-earth research is quite blurred. The protocol is described in detail later on.

2.2.4 What About Noisy Quantum Channels?

Regardless of the type of the quantum transmission, the bottom line is: a perfect quantum channel (i.e., a channel with no noise) is secure. Any dis-

turbance in the channel is the signature that an eavesdropper tried to break into the channel. Thus noisy transmissions should be discarded. Unfortunately, quantum channels are very fragile and in practice it is impossible to avoid a certain amount of innocent noise due to interaction with the environment rather than with an eavesdropper. So, instead of discarding any noisy transmission, the legitimate users have to find a procedure to extract a secret key, even in the presence of some noise. To start with Alice and Bob have to estimate how much information may have leaked to an eavesdropper, as a function of parameters that they can measure. This amount of information could be either acceptable, tolerable, or intolerable. By tolerable we mean that by some subsequent procedures such as privacy amplification or quantum privacy amplification (see Sect. 8.4) it can be reduced to any desired acceptable level, at the expense of shortening the key. There exists, however, a threshold and if too much information has leaked to an eavesdropper no further privacy amplification is possible and the transmission should be discarded. The need for more precise security criteria was originally emphasised by Huttner and Ekert [40]; since then quantum eavesdropping has evolved into a field of its own.

If the quantum transmission over noisy channels is based on distributing entangled particles, then the quantum privacy amplification specifies the criteria of security, taking into account the most general attack an eavesdropper can mount. The quantum privacy amplification transforms partially entangled particles (due to eavesdropping or any external disturbance) into completely entangled ones and it is known when such a purification of quantum entanglement is possible. However, on the practical side, the technology required to perform quantum purification is similar to that required for the quantum computer, and is therefore not yet available.

The literature about security in single particle transmission is considerable. At the beginning, only security against so-called “incoherent attacks” – in which Eve deals with Alice’s particles individually – were discussed. But quantum mechanics allows more general and more powerful attacks, known as “coherent attacks”, in which Eve is allowed to use a quantum computer. Proofs of security against such attacks have been proposed recently. However, the more powerful the considered attacks are, the more stringent are the necessary security conditions. The same applies to the optimisation of the entire protocol, which is crucial for practical applications.

2.2.5 Practicalities

Quantum Cryptography (QC) is plagued by several other problems. The first one, which is common to most implementations, except the ones with entangled pairs of photons (Sect. 2.4), is that we still do not know how to create purely single-photon pulses. The usual source of light for QC is merely an attenuated laser. For this type of light, the number of photons in the pulse is a random variable, with a Poisson distribution. This means that some pulses

may contain no photon at all, while others contain 1, 2 or even more photons. Pulses with more than one photon per pulse should be avoided, since they may leak information to an eavesdropper. In order to make the probability of more than one photon per pulse low enough, one needs to use very weak pulses, which in turns reduces the signal to noise ratio. The value generally adopted is 0.1 photon per pulse on average (this really means that only one pulse out of 10 contains a photon), which gives a probability of more than one photon of 5×10^{-3} . This still means that 5 % of the usable pulses (with at least one photon), contain two or more photons, and could leak information to an eavesdropper. Development of a good single photon source seems technologically possible, but has not been achieved yet.

The second, more serious problem for practical applications of QC is that a quantum channel cannot be amplified without losing its quantum properties. Therefore, due to losses in the transmission, QC can operate only over limited distances. For all existing systems, which are based on infrared photons in silica fibres, the minimum loss rate is about 0.2 dB/km. So it seems that QC systems with a range of more than 100 km (with losses of 20 dB, or a transmission rate of 0.01) are not possible for the foreseeable future. Therefore, a transatlantic cable with QC secrecy remains a complete utopia for the time being.

The third problem is that QC is well adapted to point-to-point exchanges, but not so well to other types of networks. Recent proposals suggested some improvements in this direction [41], but these are still limited to one-to-a-few users. QC access for home-to-home transactions is still impractical. However, a kind of Local Area Network, with a central broadcasting station (e.g. the main branch of a bank) and a number of receivers (e.g. the local branches of the bank), is certainly conceivable.

2.3 Quantum Key Distribution with Single Particles

2.3.1 Polarised Photons

Quantum key distribution with polarised photons, as originally proposed by C.H. Bennett and G.Brassard [38, 42], employed pulses of green light in free space, over a distance of 40 cm, and we shall discuss it in some detail. This experiment was obviously not useful for actual key transmission, but represented the first experimental steps of QC. The first implementation of this particular protocol with optical fibres (over a distance of about 1 km) was done at the university of Geneva [43]. Nowadays, distances have reached the tens of kilometers range. In this section, we shall present the principles of QC with polarised photons, leaving the experimental implementations to Sect. 2.6

Let us consider pulses of polarised light, each pulse containing a single photon. We shall begin with polarisation either horizontal or vertical, denoted

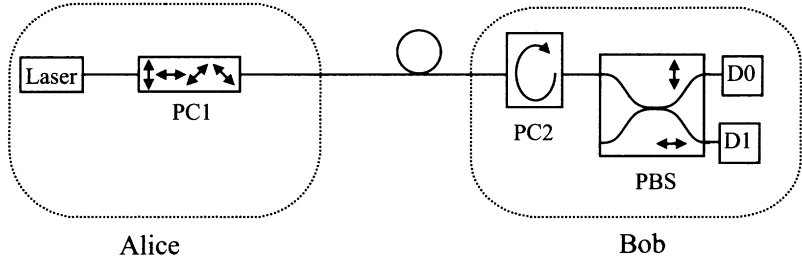


Fig. 2.4. Polarisation scheme: The sender, Alice, sends very weak pulses of polarised light to Bob. The polarisation is controlled by a Pockels cell (PC1), which enables Alice to choose between the four possible polarisations: $|\uparrow\rangle$, $|\leftrightarrow\rangle$, $|\nwarrow\rangle$, $|\swarrow\rangle$. On Bob's side, a second Pockels cell (PC2) controls the rotation of the setup: 0° corresponds to a measurement in basis \oplus , while 45° corresponds to a measurement in basis \otimes . The polarisation beamsplitter (PBS) separates the beam into two orthogonal components, which are detected by either D0 or D1 (the setup chosen corresponds to a measurement in \oplus).

in the quantum mechanical Dirac notation by $|\leftrightarrow\rangle$ and $|\uparrow\rangle$ respectively. To transmit information we need a coding system, say $|\uparrow\rangle$ codes for 0, while $|\leftrightarrow\rangle$ codes for 1. Using this system, the sender, known as Alice, can send any message to the receiver, known as Bob. For example, if Alice sends a series of pulses: $|\leftrightarrow\rangle$, $|\uparrow\rangle$, $|\leftrightarrow\rangle$, $|\leftrightarrow\rangle$, $|\uparrow\rangle$; the corresponding binary number is 10110. When she sends either $|\leftrightarrow\rangle$ or $|\uparrow\rangle$ only, we shall say that Alice sends her photons in the \oplus basis. As the required key needs to be random, Alice will send 0 or 1 with equal probability. In order to detect the message, Bob uses a Polarisation Beamsplitter (PBS) transmitting the vertical polarisation while deflecting the horizontal one. This is followed by single-photon detectors in each arm of the set-up, as shown in Fig. 2.4. Detection in detector D0 (D1) means that Alice sent a 0 (1). In this case, we shall say that Bob detects in the \oplus basis as well. As detectors are not perfect, and also due to possible losses in the transmission, both detectors will often fail to register any photon. In this case, Bob shall tell Alice that he failed to register anything, and the corresponding bit shall be discarded. Therefore, only a fraction of the original bits will be actually used, but the remaining ones should be shared by Alice and Bob. This system is thus useless for sending a given message, but it will be useful to send a cryptographic key, where the only requirements are randomness and confidentiality.

Up to this point, our setup is totally insecure. The eavesdropper, known as Eve, could also measure the pulses with a setup similar to Bob's, and re-send similar pulses to Bob. Eve would then know all the bits shared by Alice and Bob. To obtain confidentiality, Alice adds another random choice: she shall now use either the previous horizontal-vertical polarisations (the \oplus basis); or one of the two linear diagonal polarisations, with $|\nwarrow\rangle$ denoting a 0 and $|\swarrow\rangle$ denoting a 1. Here again, Alice shall send a 0 or 1 with equal probability. This corresponds to the \otimes basis. By rotating his setup by 45° ,

Table 2.1. Example of a polarisation protocol. Alice chooses at random a basis (\oplus or \otimes) and a bit value (0 or 1), and sends the corresponding polarisation state to Bob. Bob chooses also at random the reception basis, and obtains a given bit. The ensemble of these bits is the raw key. Alice and Bob then tell each other the basis used over the public channel, and keep only the bits corresponding to the same basis. This is the sifted key. They choose at random some of the remaining bits to test for Eve, then discard them. In this case, there are no errors, which indicates that the transmission is secure. The remaining bits form the shared key.

A basis	\otimes	\oplus	\oplus	\otimes	\oplus	\otimes	\otimes	\oplus	\otimes	\otimes	\oplus
A bit value	0	1	0	1	1	0	1	0	0	0	0
A sends	$ \downarrow\rangle$	$ \leftrightarrow\rangle$	$ \uparrow\rangle$	$ \nwarrow\rangle$	$ \leftrightarrow\rangle$	$ \downarrow\rangle$	$ \nwarrow\rangle$	$ \uparrow\rangle$	$ \downarrow\rangle$	$ \nwarrow\rangle$	$ \uparrow\rangle$
B basis	\otimes	\oplus	\otimes	\oplus	\oplus	\otimes	\otimes	\otimes	\oplus	\oplus	\oplus
B bit	0	1	0	0	1	0	1	1	0	1	0
Same basis?	y	y	n	n	y	y	y	n	n	n	y
A keeps	0	1			1	0	1				0
B keeps	0	1			1	0	1				0
Test Eve?	y	n			y	n	n				n
Key						0	1				0

Bob can also choose to measure in the \otimes basis. Safety is obtained thanks to a fundamental property of quantum mechanics: indeterminism. A single photon pulse prepared in the \otimes basis and measured in the \oplus basis has probability $\frac{1}{2}$ of going towards either detector, D0 or D1. And this choice is purely random: there is nothing in the photon to reveal which way it will go. So if Alice prepares a photon in, say state $|\downarrow\rangle$, and Bob (or anybody else) attempts to measure it in the \oplus basis, he may get a count in either detector, D0 or D1, with equal probability. Let us emphasise that this does not mean at all that half of the photons in a beam of $|\downarrow\rangle$ are polarised vertically and half horizontally. This would be inconsistent with the fact that, when Bob uses the \otimes basis, he always gets a 0. In fact, the system behaves as if, when it is measured, it chooses randomly which way to go.

Obviously, the above applies equally well to Eve. As Alice uses either basis at random, there is no way for Eve to decide which measurement basis to use. Whenever she uses the wrong basis, she gets a random result, which is not correlated to Alice's choice. Another important point is that Eve cannot know that she got a wrong result: a count in D0 may mean that the photon was prepared in the $|\uparrow\rangle$ state, but it may also mean that it was in the $|\downarrow\rangle$ or in the $|\nwarrow\rangle$ state, and simply "choose" to go towards D0. This is why we do need single-photon pulses: a pulse with more than one photon sent in the wrong basis may give a count in both D0 and D1, thus telling Eve that she used the wrong basis. She could then simply discard the transmission, thus avoiding creating any error. However, when she receives only one photon, Eve has no other choice but to send it on to Bob, in the state that she measured. This will unavoidably create errors in the string received by Bob. The above eavesdropping strategy, known as the intercept-resend strategy is only one of the possibilities available to Eve.

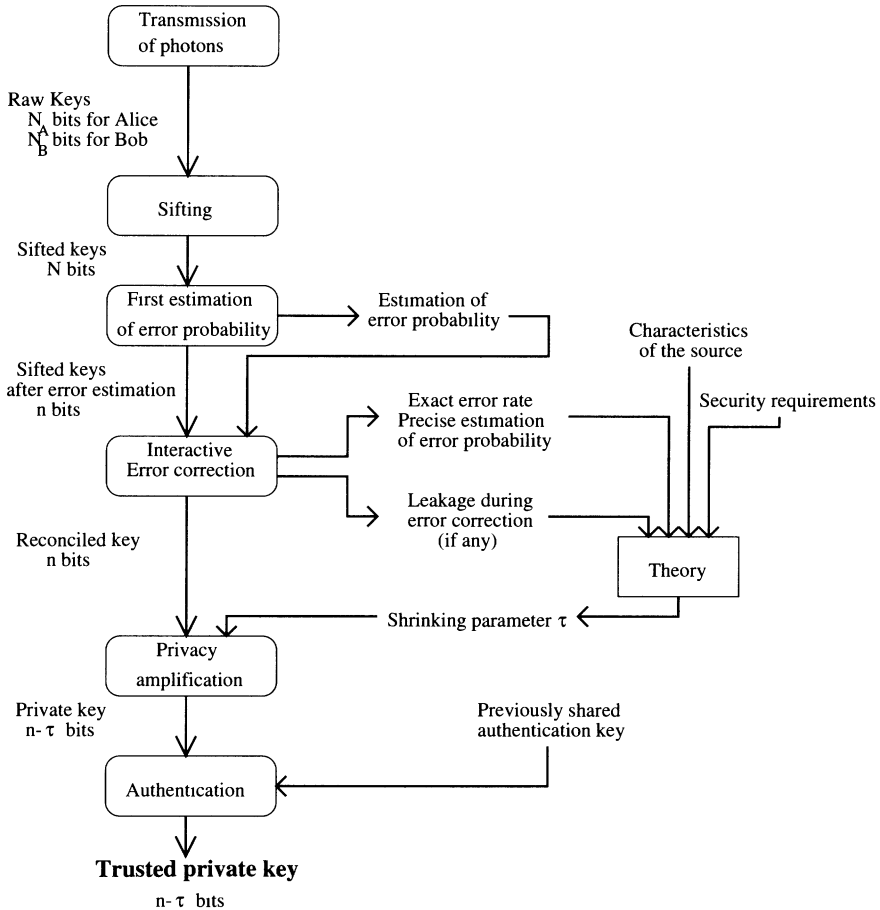


Fig. 2.5. Diagram of single-photon based quantum key distribution protocol

We now have the basic blocks for the polarisation cryptography protocol, an example of which is given in Table 2.1. The whole protocol is illustrated in Fig. 2.5 and is summarised as follows:

1. Alice chooses at random both the basis and the polarisation of her single-photon pulses, and sends them to Bob.
2. For each pulse, Bob chooses also at random which basis he will use, and measures the pulse. He either registers the count in D0 or D1, or fails to register anything, due to losses in the detection or in the transmission. The ensemble of all the received bits is the raw key.
3. Bob uses the public channel to tell Alice which photons were registered, and which basis was used. Of course, Bob does not tell the result of the measurement (count in D0 or D1). Alice answers back by telling

which basis she used. Whenever Alice and Bob used the same basis, either \oplus or \otimes , they should get perfectly correlated bits. However, due to imperfections in the setup, and to a potential eavesdropper, there will be some errors. The ensemble of these bits is the sifted key.

4. To transform their partly corrupted and maybe not entirely secret strings into a usable shared and secret key, Alice and Bob now need some processing. The processing stage is in fact common to all implementations of QC with single particles. The main steps are: to estimate the error rate of the transmission; to infer the maximum information that may have leaked to an eavesdropper; and then to correct all the errors, while reducing the information potentially available to Eve to any level required. The remaining string of bits is the secret key.

Polarisation schemes are very appealing in free space, where polarisation is conserved, but are more complicated to implement in optical fibres, due to depolarisation and randomly fluctuating birefringence. Depolarisation is not a major problem: its effects can be suppressed by means of a sufficiently coherent source. The timescale of the fluctuations of the birefringence in stable conditions is quite slow (1 hour). However, during an experiment on an installed cable, we have also observed much shorter timescales, which rendered transmission impossible. An electronic compensation system, enabling continuous tracking and correction of the polarisation is certainly possible, but requires an alignment procedure between Alice and Bob. This may make the scheme a bit too cumbersome for potential users.

2.3.2 Phase Encoded Systems

Instead of relying on polarisation, which is not easy to control in optical fibres, one can base a QC system on phase encoding. Originally the phase encoding, with optical fibres and the Mach–Zehnder interferometers, was introduced in the context of the entanglement-based quantum cryptography [44], but it can also be used with the single-particle schemes [45]. The theoretical setup is shown in Fig. 2.6. This is an extended Mach–Zehnder interferometer, with Alice on the left, and Bob on the right, with two connecting fibres. Both Alice and Bob have a phase modulator (PM) on their side to enable the coding and decoding. Let us assume for the moment that Bob does not use his PM, and that the interferometer is aligned to have a constructive interference in D0, and a destructive one on D1. If Alice uses her PM to get either 0 or π phase shift (corresponding to bit value 0 and 1), Bob will either get a count in D0 or in D1. This is the equivalent of the previous scheme with two polarisations only. To obtain confidentiality, we add the random choice of basis. Here, this means that Alice shall choose between four phase shifts: 0, π (corresponding to the \oplus basis), and $\frac{\pi}{2}$, $\frac{3\pi}{2}$ (corresponding to the \otimes basis). On his side, Bob will also choose between 0 phase shift, i.e. measuring in the \oplus basis, and

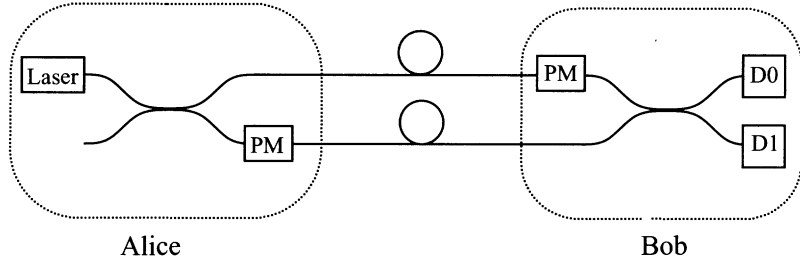


Fig. 2.6. Phase setup with an extended Mach–Zehnder interferometer. The relative choice of phase in the two phase modulators (PM) gives the interference pattern. Alice chooses between four possibilities: 0 or π corresponding to basis \oplus ; $\frac{\pi}{2}$ or $\frac{3\pi}{2}$ corresponding to basis \otimes . Bob chooses between 0 (corresponding to a measurement in basis \oplus) and $\frac{\pi}{2}$ (corresponding to \otimes). When Alice and Bob use the same basis, a count in D0 means 0, and a count in D1 means 1. When the two bases are different, there are no correlations between the bit sent by Alice and the one received by Bob.

$\frac{\pi}{2}$ phase shift, i.e. measuring in the \otimes basis. This is the equivalent to the previous polarisation scheme.

Unfortunately, keeping the phase difference in such an extended interferometer (each arm should be about 20 km long) is very difficult. Therefore a better practical setup is to collapse the interferometer, as shown in Fig. 2.7. One pulse entering Alice's side of the MZ is split into two. The two pulses propagating one after the other along the single transmission fibre are denoted by S (for short path) and L (for long path). After travelling through Bob's side of the MZ, these create three output pulses. Two of them, noted SS (for short-short) and LL (for long-long) are not relevant, as they show no interference effect. The central one however corresponds to two possible paths: SL or LS, which are indistinguishable and therefore interfere. The choice of the phase shifts by Alice and Bob gives the encoding-decoding, as in the previous paragraph. This setup is much more stable than the previous one, since

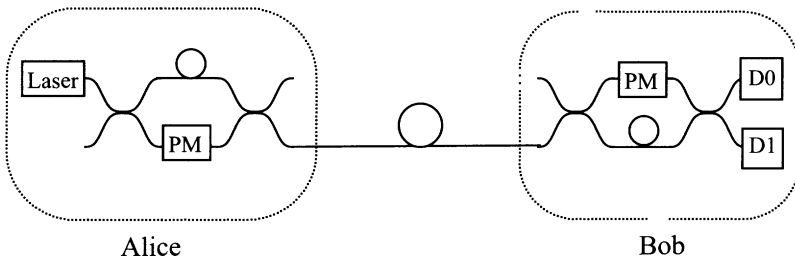


Fig. 2.7. Phase setup with a collapsed Mach–Zehnder interferometer: Instead of having the two pulses propagating through different paths, they now propagate through the same optical fibre, but with a time-delay. This increases the stability of the interferometer, but adds 3 dB of losses in Bob's setup.

the pulses actually follow the same path for most of the interferometer. The drawback is that we lose half of the signal in the two SS and LL paths.

The scheme proposed by C. Bennett [45], used only two phases for Alice. We refer the reader to the original article for a detailed explanation. The main advantage of this type of systems is that, in principle, it does not require polarisation control. In practice, however, due to some polarisation dependence in the components, it seems preferable to control the polarisation. Moreover, these schemes still need careful path length adjustment and control between the two sides of the interferometer.

2.4 Quantum Key Distribution with Entangled States

2.4.1 Transmission of the Raw Key

The key distribution is performed via a quantum channel which consists of a source that emits pairs of photons in the singlet state of polarisations:

$$|\psi\rangle = \frac{1}{\sqrt{2}} (|\uparrow\rangle|\leftrightarrow\rangle - |\leftrightarrow\rangle|\uparrow\rangle) \quad (2.10)$$

The photons fly apart along the z-axis towards the two legitimate users of the channel, Alice and Bob, who, after the photons have separated, perform measurements and register the outcome of the measurements in one of three bases, obtained by rotating the \oplus basis around the z-axis by angles $\phi_1^a = 0, \phi_2^a = \frac{1}{4}\pi, \phi_3^a = \frac{1}{8}\pi$ for Alice and by angles $\phi_1^b = 0, \phi_2^b = -\frac{1}{8}\pi, \phi_3^b = \frac{1}{8}\pi$ for Bob.

Superscripts “a” and “b” refer to Alice’s and Bob’s analysers respectively. The users choose their bases randomly and independently for each pair of the incoming particles. Each measurement yield two possible results, +1 (the photon is measured in the first polarisation state of the chosen basis) and −1 (it is measured in the other polarisation state of the chosen basis), and can potentially reveal one bit of information.

The quantity

$$E(\phi_i^a, \phi_j^b) = P_{++}(\phi_i^a, \phi_j^b) + P_{--}(\phi_i^a, \phi_j^b) - P_{+-}(\phi_i^a, \phi_j^b) - P_{-+}(\phi_i^a, \phi_j^b) \quad (2.11)$$

is the correlation coefficient of the measurements performed by Alice in the basis rotated by ϕ_i^a and by Bob in the basis rotated by ϕ_j^b . Here $P_{\pm\pm}(\phi_i^a, \phi_j^b)$ denotes the probability that the result ±1 has been obtained in the basis defined by ϕ_i^a and ±1 in the basis defined by ϕ_j^b . According to the quantum rules

$$E(\phi_i^a, \phi_j^b) = -\cos [2(\phi_i^a - \phi_j^b)]. \quad (2.12)$$

For the two pairs of bases of the same orientation (ϕ_1^a, ϕ_1^b and ϕ_3^a, ϕ_3^b) quantum mechanics predicts total anticorrelation of the results obtained by Alice and Bob: $E(\phi_1^a, \phi_1^b) = E(\phi_3^a, \phi_3^b) = -1$.

One can define the quantity S composed of the correlation coefficients for which Alice and Bob used analysers of different orientation

$$S = E(\phi_1^a, \phi_3^b) + E(\phi_1^a, \phi_2^b) + E(\phi_2^a, \phi_3^b) - E(\phi_2^a, \phi_2^b). \quad (2.13)$$

This is the same S as in the generalised Bell theorem proposed by Clauser, Horne, Shimony, and Holt, and known as the CHSH inequality [12]. Quantum mechanics requires

$$S = -2\sqrt{2}. \quad (2.14)$$

After the transmission has taken place, Alice and Bob can announce in public the orientations of the analysers they have chosen for each particular measurement and divide the measurements into two separate groups: a first group for which they used different orientation of the analysers, and a second group for which they used the same orientation of the analysers. They discard all measurements in which either or both of them failed to register a particle at all. Subsequently Alice and Bob can reveal publicly the results they obtained but within the first group of measurements only. This allows them to establish the value of S , which if the particles were not directly or indirectly “disturbed” should reproduce the result of (2.14). This assures the legitimate users that the results they obtained within the second group of measurements are anticorrelated and can be converted into a secret string of bits — the key.

An eavesdropper, Eve, cannot elicit any information from the particles while in transit from the source to the legitimate users, simply because there is no information encoded there! The information “comes into being” only after the legitimate users perform measurements and communicate in public afterwards. Eve may try to substitute her own prepared data for Alice and Bob to misguide them, but as she does not know which orientation of the analysers will be chosen for a given pair of particles there is no good strategy to escape being detected. In this case her intervention will be equivalent to introducing elements of *physical reality* to the polarisation directions and will lower S below its ‘quantum’ value. Thus the Bell theorem can indeed expose eavesdroppers.

2.4.2 Security Criteria

The best way to analyse eavesdropping in the system is to adopt the scenario that is most favourable for eavesdropping, namely where Eve herself is allowed to prepare all the pairs that Alice and Bob will subsequently use to establish a key. This way we take the most conservative view which attributes all

disturbance in the channel to eavesdropping even though most of it (if not all) may be due to an innocent environmental noise.

Let us start our analysis of eavesdropping in the spirit of the Bell theorem and consider a simple case in which Eve knows precisely which particle is in which state. Following [46] let us assume that Eve prepares each particle in the EPR pairs separately so that each individual particle in the pair has a well defined polarisation in some direction. These directions may vary from pair to pair so we can say that she prepares with probability $p(\theta_a, \theta_b)$ Alice's particle in state $|\theta_a\rangle$ and Bob's particle in state $|\theta_b\rangle$, where θ_a and θ_b are two angles measured from the vertical axis describing the polarisations. This kind of preparation gives Eve total control over the state of *individual* particles. This is the case where Eve will always have the edge and Alice and Bob should abandon establishing the key; they will learn about it by estimating $|S|$ which in this case will always be smaller than $\sqrt{2}$. To see this let us write the density operator for each pair as

$$\rho = \int_{-\pi/2}^{\pi/2} p(\theta_a, \theta_b) |\theta_a\rangle\langle\theta_a| \otimes |\theta_b\rangle\langle\theta_b| d\theta_a d\theta_b. \quad (2.15)$$

Equation (2.13) with appropriately modified correlation coefficients reads

$$\begin{aligned} S = \int_{-\pi/2}^{\pi/2} p(\theta_a, \theta_b) d\theta_a d\theta_b & \{ \cos[2(\phi_1^a - \theta_a)] \cos[2(\phi_3^b - \theta_b)] \\ & + \cos[2(\phi_1^a - \theta_a)] \cos[2(\phi_2^b - \theta_b)] \\ & + \cos[2(\phi_2^a - \theta_a)] \cos[2(\phi_3^b - \theta_b)] \\ & - \cos[2(\phi_2^a - \theta_a)] \cos[2(\phi_2^b - \theta_b)] \}, \end{aligned} \quad (2.16)$$

and leads to

$$S = \int_{-\pi/2}^{\pi/2} p(\theta_a, \theta_b) d\theta_a d\theta_b \sqrt{2} \cos[2(\theta_a - \theta_b)], \quad (2.17)$$

which implies

$$-\sqrt{2} \leq S \leq \sqrt{2}, \quad (2.18)$$

for any state preparation described by the probability distribution $p(\theta_a, \theta_b)$.

Clearly Eve can give up her perfect control of quantum states of individual particles in the pairs and entangle at least some of them. If she were to prepare all the pairs in perfectly entangled singlet states she would lose all her control and knowledge about Alice's and Bob's data who can then easily establish a secret key. This case is unrealistic because, in practice, Alice and Bob will never register $|S| = 2\sqrt{2}$. However, if Eve prepares only partially entangled pairs then it is still possible for Alice and Bob to establish the key with absolute security, provided they use a *Quantum Privacy Amplification* algorithm (QPA) [47]. The case of partially entangled pairs, $\sqrt{2} \leq |S| \leq 2\sqrt{2}$,

is the most important one and in order to claim that we have an operational key distribution scheme we have to prove that the key can be established in this particular case. Skipping technical details we will present only the main idea behind the QPA; details can be found in [47] and in Sect. 8.4.

Firstly, note that any two particles that are jointly in a pure state cannot be entangled with any third physical object. Therefore, any procedure that delivers EPR pairs in pure states must also have eliminated the entanglement between any of those pairs and any other system. The QPA scheme is based on an iterative quantum algorithm which, if performed with perfect accuracy, starting with a collection of EPR-pairs in mixed states, would discard some of them and leave the remaining ones in states converging to the pure singlet state. If (as must be the case realistically) the algorithm is performed imperfectly, the density operator of the pairs remaining after each iteration will not converge on the singlet but on a state close to it; however, the degree of entanglement with any eavesdropper will nevertheless continue to fall, and can be brought to an arbitrary low value. The QPA can be performed by Alice and Bob at distant locations by a sequence of local unitary operations and measurements which are agreed upon by communication over a public channel and could be implemented using technology that is currently being developed (c.f. [48]).

The essential element of the QPA procedure is the “entanglement purification” scheme [49] (see Chap. 8). It has been shown recently that any partially entangled states of two-state particles can be purified [50]. Thus, as long as the density operator cannot be written as a mixture of product states, i.e., is not of the form (2.15), then Alice and Bob can outsmart Eve!

2.5 Quantum Eavesdropping

The QPA procedure requires technology which is not quite available today. Therefore, let us discuss techniques which are much closer to experimental implementations. They are important because we want to build the key distribution prototypes with the current technology and we need to specify the conditions under which they are really secure. Our discussion below is of a general nature and can be applied both to the single-particle and the entanglement-based key distribution. Our description, however, for purely pedagogical reasons, assumes the single-particle scheme where Alice sends photons to Bob.

2.5.1 Error Correction

Since it is essential that Alice and Bob share an identical string of bits, they must correct the discrepancies in their sifted keys. This step, called reconciliation or error correction may use the public channel, but it should disclose

as little information as possible to Eve about the reconciled key (or use as few private bits as possible if they decide to encrypt the critical part of their public communication with a previously shared private key). The minimum number r of bits that Alice and Bob have to exchange publicly to correct their data is given by Shannon's Coding theorem [32]: In our case, in which each bit is transmitted incorrectly with an error probability ϵ independently for each bit transmitted, the theorem asserts that

$$r = n(-\epsilon \log_2 \epsilon - (1 - \epsilon) \log_2(1 - \epsilon)), \quad (2.19)$$

where n is the length of the sifted key.

Shannon's theorem has a non-constructive proof, which means that we know there exists a correction scheme disclosing only r bits of private data, but the theorem does not provide an explicit procedure. The usual linear error-correcting codes turn out to be rather inefficient in this regard. However, Brassard and Salvail [51] devised a practical interactive correction scheme that gets close to Shannon's limit. The scheme works as follows:

Alice and Bob group their bits into blocks of a given size, which has to be optimised as a function of the error rate. They exchange information about the parity of each block over the public channel. If their parities agree then they proceed to the next block. If their parities disagree, they deduce that there was an odd number of errors in the corresponding block, and search one of them recursively by cutting the block into two sub-blocks and comparing the parities of the first sub-block: if the parities agree then the second sub-block has an odd number of errors and if they do not, then the first sub-block has an odd number of errors. This procedure is continued recursively on the sub block with an odd number of errors.

After this first step, every considered block has either an even number of errors or none. Alice and Bob then shuffle the positions of their bits and repeat the same procedure with blocks of bigger size (this size being optimised as well). However, when an error is corrected, Alice and Bob might deduce that some blocks treated previously now have an odd number of errors. They choose the smallest block amongst them and correct one error recursively, as before. They proceed until every previously treated block has an even number of errors, or none.

Similar steps follow, and the interactive error correction terminates after a specified number of steps. This number is to be optimised in order to maximise the probability that no discrepancies remain and, at the same time, minimise the leakage of private data. Unlike the correction scheme used originally in [42], this correction scheme does not discard any bit from the sifted key.

2.5.2 Privacy Amplification

At this point Alice and Bob share, with high probability, an identical reconciled key. They also know the exact error rate $\bar{\epsilon}$, which gives a very good

estimation of the error probability ϵ . Alice and Bob assume that all the errors were caused by the potential eavesdropper, Eve. They also take into account the leakage during the error correction step, if any. Then they deduce τ , the number of bits by which the reconciled key has to be shortened so that Eve's information about the final key is lower than a specified value. More precisely, in most quantum key distribution protocols, given the integer τ , Alice picks randomly a $(n - \tau) \times n$ binary matrix K (a matrix whose entries are 0 or 1) and publicly transmits K to Bob (without encrypting it). The final private key is then:

$$\mathbf{k}_{\text{final}} = K \cdot \mathbf{k}_{\text{reconciled}} \pmod{2} \quad (2.20)$$

where $\mathbf{k}_{\text{reconciled}} = (k_1, k_2, \dots, k_n)$, $k_i \in \{0, 1\}$, is the reconciled key.

Implementation of privacy amplification is easy, but proving security of the entire quantum key distribution protocol is a hard theoretical task in quantum cryptography. Therefore, proofs of security have been proposed gradually, against more and more powerful attacks. Usually we divide those attacks in two categories:

1. Incoherent attacks (Fig. 2.8): In incoherent attacks, or individual particle attacks, Eve is limited to entangling a quantum probe \mathcal{P}_i with one photon at a time. She may keep \mathcal{P}_i until the entangled photon is measured by Bob and all public discussions between Alice and Bob are completed. Indeed, Alice and Bob cannot tell whether Eve measures her probes before or after Bob measures his photons. Therefore the best strategy for Eve is to wait until measurement bases are announced publicly by Alice and Bob and then cleverly measure her probes to extract as much information as possible. However, in incoherent attacks, Eve is limited to measuring her probes \mathcal{P}_i individually.

In more detail, taking into account the scenario presented in Sect. 2.3.1 and denoting by $|E\rangle_i$ the initial state of Eve's probe, the most general unitary transformation \mathcal{U} entangling \mathcal{P}_i to Alice's photon reads (in the \oplus basis):

$$|E\rangle_i |\uparrow\rangle \xrightarrow{\mathcal{U}} |E_{00}^\oplus\rangle |\uparrow\rangle + |E_{01}^\oplus\rangle |\leftrightarrow\rangle \quad (2.21)$$

$$|E\rangle_i |\leftrightarrow\rangle \xrightarrow{\mathcal{U}} |E_{10}^\oplus\rangle |\uparrow\rangle + |E_{11}^\oplus\rangle |\leftrightarrow\rangle \quad (2.22)$$

where $|E_{ij}^\oplus\rangle$ are unnormalised states of \mathcal{P}_i . Since $|E\rangle_i$ can be chosen to lie in the span of $\{|E_{ij}^\oplus\rangle\}_{i,j}$, we can assume that \mathcal{P}_i is described with a 4-dimensional Hilbert space, i.e. each probe is described by 2 qubits.

The action of \mathcal{U} , if Alice sends her photon in the \otimes basis, is derived from (2.21, 2.22) using linearity:

$$|E\rangle_i |\swarrow\rangle \xrightarrow{\mathcal{U}} |E_{00}^\otimes\rangle |\swarrow\rangle + |E_{01}^\otimes\rangle |\nwarrow\rangle \quad (2.23)$$

$$|E\rangle_i |\nwarrow\rangle \xrightarrow{\mathcal{U}} |E_{10}^\otimes\rangle |\swarrow\rangle + |E_{11}^\otimes\rangle |\nwarrow\rangle, \quad (2.24)$$

where

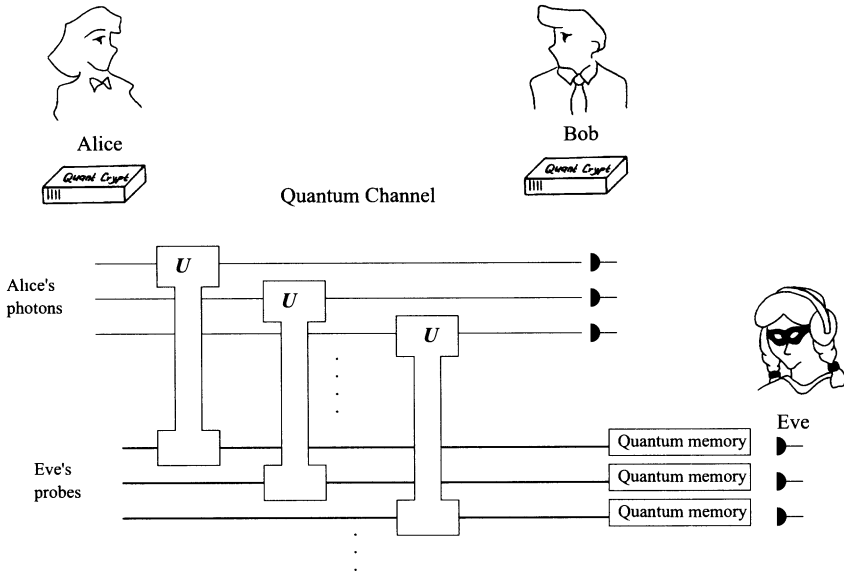


Fig. 2.8. Incoherent attacks: each photon is entangled independently to a 2-qubit probe. The probes are stored in a quantum memory until measurement bases are announced. Then each probe is measured independently.

$$|E_{00}^\otimes\rangle = \frac{|E_{00}^\oplus\rangle + |E_{10}^\oplus\rangle + |E_{01}^\oplus\rangle + |E_{11}^\oplus\rangle}{2} \quad (2.25)$$

$$|E_{01}^\otimes\rangle = \frac{|E_{00}^\oplus\rangle + |E_{10}^\oplus\rangle - |E_{01}^\oplus\rangle - |E_{11}^\oplus\rangle}{2} \quad (2.26)$$

$$|E_{10}^\otimes\rangle = \frac{|E_{00}^\oplus\rangle - |E_{10}^\oplus\rangle + |E_{01}^\oplus\rangle - |E_{11}^\oplus\rangle}{2} \quad (2.27)$$

$$|E_{11}^\otimes\rangle = \frac{|E_{00}^\oplus\rangle - |E_{10}^\oplus\rangle - |E_{01}^\oplus\rangle + |E_{11}^\oplus\rangle}{2}. \quad (2.28)$$

Eve has to choose \mathcal{U} so that:

1. the eavesdropping is discreet, i.e. for instance, the probability that Bob measures $|\leftrightarrow\rangle$ while Alice sent $|\leftrightarrow\rangle$ should be lower than the tolerated error rate. We can see that this is equivalent to requiring that the norms $\langle E_{ij}^\oplus | E_{ij}^\oplus \rangle$ and $\langle E_{ij}^\otimes | E_{ij}^\otimes \rangle$, $i \neq j$, should be small (those probabilities are usually called disturbances).
2. the eavesdropping is efficient, i.e. Eve should maximise the probability of guessing the correct bit value knowing the used basis (she learned from the public channel), and measuring her probe accordingly. For instance, suppose Eve learns that i th photon was sent in the \oplus basis. She then knows that if Alice's corresponding bit value is 0, then Eve's probe P_i should be in the mixed state:

$$\rho_0 = \text{Tr}_{\text{photon}} [(\mathcal{U}|E\rangle_i|\leftrightarrow\rangle)(\mathcal{U}|E\rangle_i|\leftrightarrow\rangle)^\dagger] \quad (2.29)$$

$$= |E_{00}^\oplus\rangle\langle E_{00}^\oplus| + |E_{01}^\oplus\rangle\langle E_{01}^\oplus|. \quad (2.30)$$

Likewise, if Alice sent her photon in the $|\leftrightarrow\rangle$ state (corresponding to the bit value 1), Eve's probe should be in the mixed state:

$$\rho_1 = \text{Tr}_{\text{photon}} [(\mathcal{U}|E\rangle_i|\leftrightarrow\rangle)(\mathcal{U}|E\rangle_i|\leftrightarrow\rangle)^\dagger] \quad (2.31)$$

$$= |E_{10}^\oplus\rangle\langle E_{10}^\oplus| + |E_{11}^\oplus\rangle\langle E_{11}^\oplus|. \quad (2.32)$$

Eve's goal is therefore to decide, as reliably as possible, whether her probe \mathcal{P}_i is in the state ρ_0 or in the state ρ_1 . It is known [52, 53] that this is achieved by performing a measurement on \mathcal{P}_i . The measured observable is determined by its eigenvectors which, in this case, coincide with the eigenvectors of $\rho_0 - \rho_1$.

The optimisation of this entanglement has been thoroughly discussed in Refs. [52]–[56] for various single-photon quantum key distribution protocols. Their results link the error probability of the quantum channel (or disturbance) to the maximum information Eve could have gained. Knowing this value (more precisely, a related value called the Renyi information) the generalised privacy amplification theorem [57] can be used to compute the shrinking parameter τ which guarantees expected confidentiality. The leakage of information is considered tolerable if τ is reasonably small compared to the size of the reconciled key.

2. Coherent attacks (Fig. 2.9): In coherent or joint attacks, Eve can entangle in any unitary manner a probe of any dimension and in any state (mixed or not) with the *whole sequence* of transmitted photons. She keeps this big probe until public discussions are over and then performs the most general measurement of her choice. The most general class of measurements is known as positive operator valued measures (POVM), for more details see for example [58].

Collective attacks (Fig. 2.10) form a subclass of the coherent attacks where Alice's photon i is entangled individually to a separate probe \mathcal{P}_i . Therefore, Eve gets the probes in the same states as in incoherent attacks. However, after public discussions are completed, Eve is allowed to carry out any POVM on all the probes considered as a single big quantum system. Note that in a collective attack, before this POVM, the individual probes \mathcal{P}_i are unentangled and independent of each other. Claims of security against coherent attacks are difficult to prove. So far, only protocols using linear error correcting codes rather than interactive error correction have been considered. Proof of the security of such protocols against collective attacks can be found in [59], and against general coherent attacks in [60].

Authentication: As we mentioned earlier, Alice and Bob should authenticate their communication in order to counter a possible man-in-the-middle

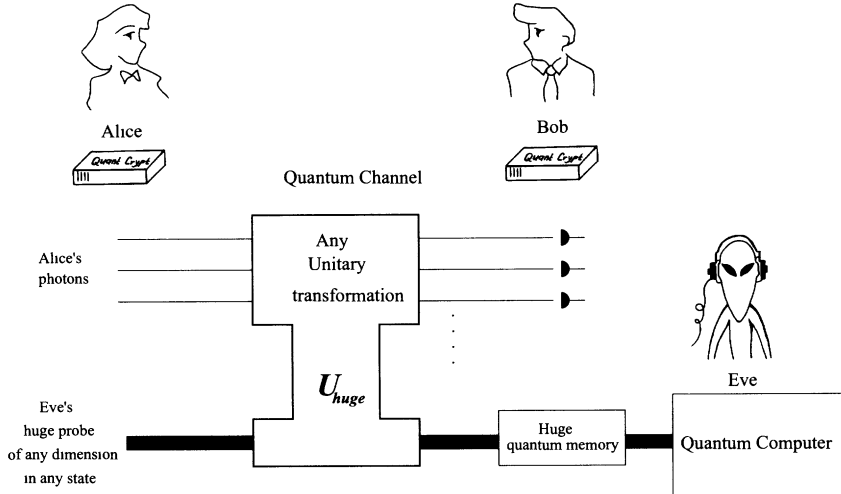


Fig. 2.9. Coherent attacks: Eve is allowed to use a probe of any dimension in any initial state and to entangle it with every photon sent by Alice in any unitary manner. This probe is stored until bases are announced.

attack. They should also ensure that they effectively share a new private key. Fortunately, there exist classical cryptographic techniques to achieve these tasks with arbitrarily high probability. We provide a concise description of an authentication algorithm and refer the reader to [61] for further details. General discussion about authentication can be found in [30].

We assumed that Alice and Bob shared an authentication key **A** which is a secret string of binary digits. This key is shorter than the new private key generated by quantum key distribution, but we assume that it is long enough for authentication purposes.

An integer t is chosen; it is a security parameter. Suppose Alice wants to authenticate the data \mathbf{M}_0 to Bob. The binary string \mathbf{M}_0 contains, for instance, predefined parts of their public discussions. The string \mathbf{M}_0 , of length m , is then broken into sub-blocks P_i of length $2s$ where $s = t + \log_2 \log_2 m$ (the last sub-block is padded with zeros if necessary). Alice and Bob take the first $2s$ bits of **A** to define a number a . The next $2s$ bits of **A** define a number b . These $4s$ bits are discarded from **A**. Then they compute, for each sub-block P_i ,

$$p'_i = ap_i + b \pmod{2^s}, \quad (2.33)$$

where p_i is the number represented by the binary string P_i .

The resulting numbers p'_i are converted into bit-streams of length s and concatenated to form \mathbf{M}_1 . The same operation is repeated (s remains unchanged) r times until the length of \mathbf{M}_r is s . The low-order t bits of \mathbf{M}_r constitute the tag T . The used part of **A** is discarded and never reused.

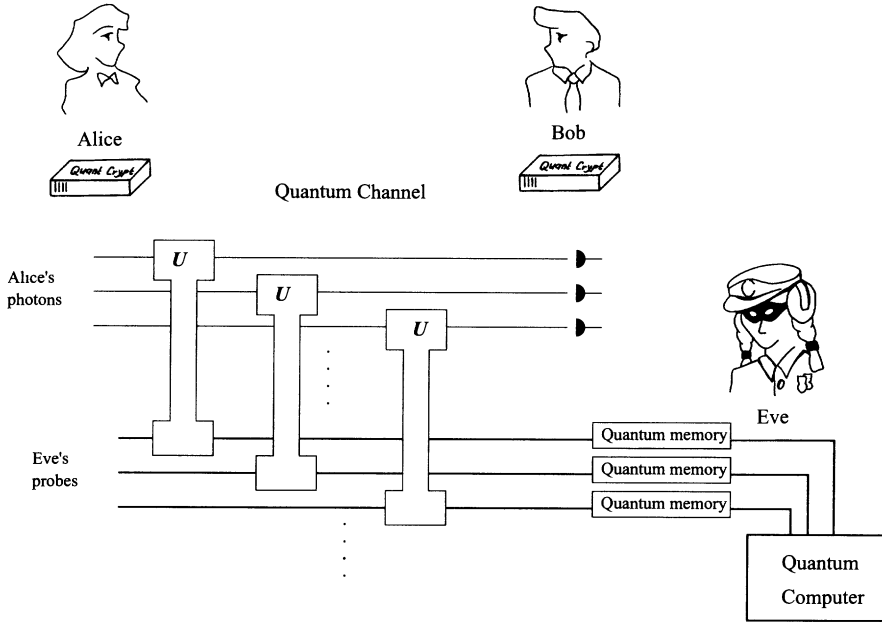


Fig. 2.10. Collective attacks: similar to incoherent attacks, but Eve is now allowed to make global generalised measurement on all probes considered as a single quantum system.

Finally the tag T is sent to Bob, who checks the authenticity of \mathbf{M}_0 by doing the same calculations and comparing their results.

The authentication in the quantum key distribution protocol could be implemented as follows. Alice authenticates predefined parts of the public communication. Bob does the same, but with other predefined parts. If this authentication succeeds, the quantum key distribution is considered to be successful and a small part of the new private key can be used as an authentication key for a next session of key distribution. This way, Alice and Bob do not need to meet again to share another authentication key. Suppose a man-in-the-middle attack was performed by Eve. Eve shares a private key with Alice, and another private key with Bob. She knows the data \mathbf{M}_0 authenticated by Alice, since Eve was impersonating Bob to Alice during the whole protocol. However, receiving T and knowing \mathbf{M}_0 , it can be shown that Eve has negligible probability of guessing the authentication key. Therefore, Eve will not be able to pass the authentication test.

2.6 Experimental Realisations

After the first proof-of-the-principle experiments by the IBM-Montreal group [42] (key distribution using polarised photons and free space propagation) and the Oxford-DERA group [44] (entangled photons, propagation in optical fibres, phase encoding) the development of quantum cryptography has continued in two distinct directions: On the one hand it aims to optimise the systems with respect to transmission length, key generation rate and quantum bit error rate (QBER), but on the other hand efforts are simultaneously made to make the systems more stable and easier to use for some potential end-user interested in secure communication, rather than in quantum mechanics and optical alignment. As shown in the previous sections, the general idea behind the various implementations is similar, except for the EPR-based schemes, differing mainly in the type of modulation or analysis used. In the following we describe some of the key developments that constitute the current state of the art in quantum cryptography.

Besides achieving a maximum of reliability for the transmitter and receiver modules of Alice and Bob, a key issue is to increase the transmission length. Generally, there are two ways: the first is to establish direct free optical path between Alice and Bob and to transmit the light through free space by using telescopes. The other approach uses optical fibres to guide the light between the two points. The choice of the transmission method more or less dictates the wavelength used. Optical fibres have very low absorption in the so-called telecom windows around 1300nm (0.35 dB/km) and around 1550nm (0.2 dB/km). However, for this regime the single photon detectors needed are not that well developed yet [62]. Free space cryptography via satellites in near earth orbits might bridge arbitrary distances and initial tests on earth indicate that such quantum cryptography transmission is in principle possible, at least for low bit rates.

2.6.1 Polarisation Encoding

The first quantum cryptography set-up used different polarisation states for the key distribution protocol. On a standard optical bench of 1m length, Alice first generated the faint light pulses with a simple light emitting diode (LED) and passed the collimated light through an interference filter ($550\pm20\text{nm}$) and a polarising filter. Using two Pockels cells, she could set one of four polarisation directions (here horizontal, vertical, left and right circular). The Pockels cell uses the change of the birefringence of certain crystals depending on some applied electrical field. Usually one needs quite high voltages, on the order of 2–4kV, to generate a rotation of the polarisation by 90° , say from horizontal to vertical. (This limits the switching rate for practical applications.) At the end of a quantum channel of 32 cm, Bob could analyse the polarisation in the basis set with his Pockels cell by detecting a photon with photomultipliers behind a Wollaston prism.

Even if, according to the authors, an eavesdropper could have broken the system by listening to the noise of the Pockels cell switches, this first demonstration experiment already has many of the appealing features of quantum cryptography. It was shown from the very beginning how simple experimental quantum cryptography can be – and should be, in order to increase the usability and acceptance for the quantum communication end-user. Moreover, an error rate of only $\sim 4.4\%$ was reached allowing one to distribute, after error correction, a key of 219 secure bits within a time of 85s.

In order to provide a larger distance between Alice and Bob, a fibre transmission line of 1 km was used in an experiment by Muller et al. [43]. However, a fibre based polarisation encoding system has to overcome several drawbacks. On the one hand, Bob’s analyser has to be kept aligned with respect to the polarisation sent by Alice; on the other hand, the polarisation of light will be changed when transported along a fibre cable. Due to the geometry of the light path, topological effects will influence the resulting polarisation at Bob’s end of the fibre [63]. Moreover, stress induced birefringence causes both fluctuations in the resulting polarisation and a reduction of the polarisation due to polarisation-mode dispersion. This necessitates the use of single mode lasers to obtain a large enough coherence time and active polarisation stabilisation between Alice and Bob. Finally, careful selection of the various optical components of the transmitter and receiver modules is necessary to minimise any intrinsic polarisation dependence.

More recently, free space systems have begun to utilise the higher stability of the polarisation encoding modules. Since atmosphere is essentially non-birefringent, one does not have to worry about the fluctuations of the relative alignment between Alice’s and Bob’s modules. Quantum cryptography over outdoor optical paths [64] mainly faces the problem of transmitting light through turbulent media and detecting single photons against a high background. Combining narrow bandwidth and spatial filtering with nanosecond timing should enable key generation with reasonable error rates. A recent experiment in Los Alamos achieved a 14% coupling efficiency over a 950m free space path length, resulting in a bit rate of 50Hz (starting with 20kHz pulse rate at Alice’s transmitter) with an error of about 1.5 [65]. This experiment shows the feasibility of establishing a secret key with a low orbit satellite, at least at night-time, with reasonable bit rate.

2.6.2 Phase Encoding

As pointed out in Sect. 2.3.2 phase encoding can be performed analogously to polarisation encoding. The extreme sensitivity to any external influences of a Mach–Zehnder set up shown in Fig. 2.6 can be overcome with the unbalanced Mach–Zehnder configuration proposed by Bennett [45]. Since the two coherent contributions are then separated by only a few nanoseconds but propagating along the same fibre, there are essentially no temperature or

stress induced fluctuations. The path length difference of Bob's unbalanced interferometer has to be the same as in Alice's interferometer and has to be kept stable on the sub-wavelength scale. However, this simply requires careful local temperature stabilisation of the two interferometers.

Phase modulators are commercially available for the two telecom wavelengths which seemingly makes the standard phase encoding scheme the best choice for fibre implementations. However, polarisation also places stringent alignment conditions on such a scheme. Of course, in the two unbalanced Mach-Zehnder interferometers the polarisation has to be controlled such that the interfering components have the same polarisation at Bob's output beamsplitter. After an initial alignment of Alice' and Bob's modules, this should be stable and cause no further trouble. A more severe problem comes from the fact that phase modulators are made of electro-optic crystals with preferred guiding only for one of the two polarisation components. In order to avoid intensity fluctuations at Bob's output, only one well defined polarisation can be sent through the modulators. This in turn again makes control of the transmitted polarisation necessary.

In their experimental realisation Townsend et al. [66] first split the incoming laser pulse ($1.3 \mu\text{m}$, 80 ps) along the two paths of Alice's unbalanced Mach-Zehnder interferometer. In one arm, the phase modulator causes one of the four possible phase shifts according to the BB84 protocol. In the other arm, the polarisation is rotated such that, at Alice's output beamsplitter, the two contributions have *orthogonal* polarisation. Bob's input beamsplitter is replaced by a polarising beamsplitter to ensure correct polarisation in the arm going to Bob's phase modulator. A polarisation controller at the end of the transmission line is set such that these two polarisation directions agree with the axes of Bob's input polarisation splitter. Although polarisation stabilisation becomes necessary again, the specifications are not so strict in such a set-up, since small deviations cause only negligible fluctuations in the final intensity. Error rates of less than 4% were achieved even for a pulse rate of 1 MHz. Further improvements with transmission over 48 km underground fibre cable were achieved by the Los Alamos group [67] with about 1% error at a pulse rate of 30 kHz.

No continuous polarisation alignment of the fibre transmission line is necessary for the so called "plug & play" system. The idea behind this is that the light pulse is emitted not at Alice's station, but by Bob, then first propagates to Alice, where it is modulated and reflected back to Bob. If the reflections in this scheme are done by *Faraday mirrors*, the polarisation of the interfering components at Bob's output are always aligned with each other.

A Faraday mirror, i.e. a 45° Faraday rotator and a back-reflecting mirror, render the back reflected light orthogonal to the light sent into the fibre, thus any polarisation changes along the transmission line or along the interferometer arms are effectively undone.

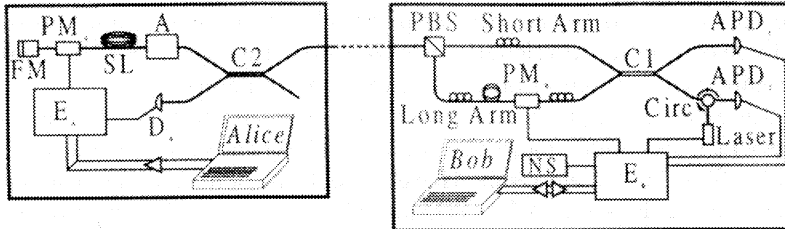


Fig. 2.11. Principle of plug&play quantum cryptography: Bob sends a light pulse through a circulator. This pulse splits at the coupler $C1$. The first half travels through the short arm. A polarisation controller is set so that this pulse is completely transmitted at the polarising beamsplitter PBS. It then propagates to Alice, where it splits again at coupler $C2$ to provide a timing signal. It then travels through Alice's equipment and is reflected back to Bob. Thanks to the Faraday mirror, the birefringence of the optical link is compensated, and the pulse comes back orthogonally polarised. It is then reflected by the PBS and takes the long arm, where Bob applies a phase shift ϕ_B with the modulator PM. The second pulse propagates through the two arms in reverse order. Alice applies to it a phase shift ϕ_A . Since both pulses travel exactly the same optical path, they reach the coupler $C1$ simultaneously with identical polarisation, giving rise to interference. A storage line SL is introduced in Alice's system to avoid problems due to Rayleigh backscattering.

The system implementing a 4-state BB84 protocol using this idea is depicted in Fig. 2.11 and in [68]. In this experiment Alice and Bob were separated by 23 km using standard telecom fibre cable as the transmission line. Without any continuous active stabilisation an error as low as 1% was achieved while a net key creation rate of 210 Hz was obtained. In all these experiments at the telecom wavelengths of 1300 nm most of the noise is due to the high dark count rate of the single photon detectors (InGaAs/InP-avalanche photo-diodes cooled to only 173 K, i.e. within the reach of Peltier cooling). Currently, clever timing and gated detection electronics help to reduce the noise level, but further improvements of the detectors will tremendously influence the subsequent applicability of quantum cryptography.

2.6.3 Entanglement-Based Quantum Cryptography

A number of new features in cryptography become possible when utilising the non-classical properties of entangled pairs of particles (see Sect. 2.4). However, with the current technology, such schemes are more difficult to realise than the single particle approaches described so far, mostly because one has to generate a high degree of entanglement. Imperfect entanglement between the photons delivered to Alice and Bob could be improved only with techniques such as entanglement purification, which are not realisable with current technology. Thus any noise in the entanglement directly determines the performance of the system. Since the first demonstration [44], the main

goal has thus been to further develop the source of entangled photon pairs. Today, parametric down-conversion is used as a source of photon pairs. Due to the low efficiency of this process broad band light has to be used to obtain a sufficient bit rate. Here a compromise has to be found in order to avoid problems when transmitting the photon pairs through dispersive optical fibre.

Most approaches use the time-energy entanglement (for details see [69, 70]). If a photon pair is produced by the process of parametric down-conversion, non-local interference can occur between the outputs of two unbalanced, but otherwise identical Mach-Zehnder or Michelson interferometers, provided the path length difference of each of the interferometers is less than the coherence time of the down-conversion pump laser. In order to discriminate between interfering and non-interfering contributions, time selection of the detection events is required. The minimum time resolution of the single photon detectors of about 300 ps makes a corresponding path length difference of about 30 cm necessary. Experiments on the EPR-Bell problem performed in Geneva demonstrate that it is possible to distribute entangled pairs along standard telecom lines and to observe a high degree of entanglement over a physical distance between the detectors of 10 km (the actual length of two optical fibres between the source and detectors was 8 km and 9 km) [71].

Polarisation entanglement can be also obtained in the process of parametric down-conversion (type II, [16]). In a recent experiment, violation of a Bell inequality was observed also for independent observers [72]. In this experiment the two observers, Alice and Bob, are separated by about 400 m (connected by 1 km optical fibre). But here all their measurements, from generating a random orientation for analysis until detection of the photon, are performed within times (~ 80 ns) much shorter than the time it takes to send information between them (~ 1300 ns). The fast electro-optic modulation system and detection electronics developed for this experiment can be directly used to perform quantum cryptography both with true single photon states as well as with a violation of a Bell inequality as an assurance of secure communication.

2.7 Concluding Remarks

Research in quantum cryptography in all its possible variations has become very active and any comprehensive review of the field would quickly be overtaken by events. Hence we have decided to provide here only some very basic knowledge, hoping that this will serve as a good starting point for entering the field. The basic message is: quantum cryptography today is a viable alternative to conventional methods of encryption and in the not-too-distant future we may have to rely on quantum mechanics rather than number theory in our confidential communication.

The reader should be warned that we have barely scratched the surface of the current activities, neglecting topics such as secure two-party computation, details of quantum authentication, detailed analysis of eavesdropping techniques and security criteria, and some alternative key distribution techniques (e.g. Vaidman and Goldenberg scheme based on sending orthogonal states in two parts). Many interesting papers on these and other related topics can be found at the Los Alamos National Laboratory e-print archive (<http://xxx.lanl.gov/archive/quant-ph>) and on other WWW servers such as <http://www.qubit.org>.

3. Quantum Dense Coding and Quantum Teleportation

3.1 Introduction

D. Bouwmeester, H. Weinfurter, A. Zeilinger

In Chap. 2 it was shown how quantum entanglement can be used to distribute secret keys. In this chapter we will address other primitives of quantum communication employing entanglement. Section 3.2 describes “Quantum Dense Coding” which is a way to transmit two bits of information through the manipulation of only one of two entangled particles, each of which individually can carry only 1 bit of information [73]. The “Quantum Teleportation” scheme as originally proposed by Bennett, Brassard, Crépeau, Jozsa, Peres, and Wootters [74] is explained in Sect. 3.3. The basic idea of quantum teleportation is to transfer the state of a quantum system to another quantum system at a distant location.

Quantum optics has proven very successful for the implementation of quantum dense coding and quantum teleportation. Two crucial ingredients for the optical implementations are the source of entangled photons, described in Sect. 3.4, and the Bell-state analyser, described in Sect. 3.5. In Sect. 3.6 the experimental demonstration of quantum dense coding is presented [75]. Section 3.7 describes the quantum teleportation experiment performed in Innsbruck [76] in which the polarisation state of a single photon is teleported using an auxiliary pair of entangled photons. Section 3.8 describes the experiment, proposed by Popescu [77] and performed in Rome [78], in which the polarisation state prepared on one of a pair of momentum entangled photons is transferred to its partner at a distant location. Section 3.9 explains the teleportation of continuous quantum variables, which was initially proposed by Vaidman [79], further elaborated upon by Braunstein and Kimble [80], and experimentally demonstrated at Caltech [81]. Each experiment has its own advantages and disadvantages and we refer to the literature for a comparison between the various methods [82]–[84].

If the initial quantum state of the teleportation protocol is part of an entangled state, the result of the teleportation process is that two systems that did not directly interact with one another become entangled. This process,

referred to as “entanglement swapping”, will be described in Sect. 3.10 and applications [85]–[87] are presented in Sect. 3.11.

3.2 Quantum Dense Coding Protocol

The scheme for quantum dense coding, theoretically proposed by Bennett and Wiesner [73], utilises entanglement between two qubits, each of which individually has two orthogonal states, $|0\rangle$ and $|1\rangle$. Classically, there are four possible polarisation combinations for a pair of such particles; 00, 01, 10, and 11. Identifying each combination with different information implies that we can encode two bits of information by manipulating *both* particles.

Quantum mechanics also allows one to encode the information in superpositions of the classical combinations. Such superpositions of states of two (or more) particles are called entangled states (see Sect. 1.4) and a convenient basis in which to represent such states for two particles, labeled 1 and 2, is formed by the maximally entangled Bell states

$$|\Psi^+\rangle_{12} = (|0\rangle_1|1\rangle_2 + |1\rangle_1|0\rangle_2)/\sqrt{2} \quad (3.1)$$

$$|\Psi^-\rangle_{12} = (|0\rangle_1|1\rangle_2 - |1\rangle_1|0\rangle_2)/\sqrt{2} \quad (3.2)$$

$$|\Phi^+\rangle_{12} = (|0\rangle_1|0\rangle_2 + |1\rangle_1|1\rangle_2)/\sqrt{2} \quad (3.3)$$

$$|\Phi^-\rangle_{12} = (|0\rangle_1|0\rangle_2 - |1\rangle_1|1\rangle_2)/\sqrt{2}. \quad (3.4)$$

Identifying each Bell state with different information we can again encode two bits of information, yet, now by manipulating only *one* of the two particles.

This is achieved in the following quantum communication scheme. Initially, Alice and Bob each obtain one particle of an entangled pair, say, in the state $|\Psi^+\rangle_{12}$ given in (3.1). Bob then performs one out of four possible unitary transformations on his particle (particle 2) alone. The four such transformations are

1. Identity operation (not changing the original two-particle state $|\Psi^+\rangle_{12}$)
2. State exchange ($|0\rangle_2 \rightarrow |1\rangle_2$ and $|1\rangle_2 \rightarrow |0\rangle_2$, changing the two-particle state to $|\Phi^+\rangle_{12}$)
3. State-dependent phase shift (differing by π for $|0\rangle_2$ and $|1\rangle_2$ and transforming to $|\Psi^-\rangle_{12}$)
4. State exchange and phase shift together (giving the state $|\Phi^-\rangle_{12}$).

Since the four manipulations result in the four orthogonal Bell states, four distinguishable messages, i.e. 2 bits of information, can be sent via Bob’s two-state particle to Alice, who finally reads the encoded information by determining the Bell state of the two-particle system. This scheme enhances the information capacity of the transmission channel to two bits compared to the classical maximum of one bit.¹

¹ While it is clear that this scheme enhances the information capacity of the transmission channel accessed by Bob to two bits, we have to notice that the channel

3.3 Quantum Teleportation Protocol

In this section we will review the quantum teleportation scheme as proposed by Bennett, Brassard, Crépeau, Jozsa, Peres, and Wootters [74]. The scheme is illustrated in the Fig. 3.1.

The idea is that Alice has particle 1 in a certain quantum state, the qubit $|\Psi\rangle_1 = \alpha|0\rangle_1 + \beta|1\rangle_1$, where $|0\rangle$ and $|1\rangle$ represent two orthogonal states with complex amplitudes α and β satisfying $|\alpha|^2 + |\beta|^2 = 1$. She wishes to transfer this quantum state to Bob but suppose she cannot deliver the particle directly to him. According to the projection postulate of quantum mechanics we know that any quantum measurement performed by Alice on her particle will destroy the quantum state at hand without revealing all the necessary information for Bob to reconstruct the quantum state. So how can she provide Bob with the quantum state? The answer is to use an ancillary pair of entangled particles 2 and 3 (EPR pair), where particle 2 is given to Alice and particle 3 is given to Bob. Let us consider the case in which the entangled pair of particles 2 and 3 shared by Alice and Bob is in the state

$$|\Psi^-\rangle_{23} = \frac{1}{\sqrt{2}}(|0\rangle_2|1\rangle_3 - |1\rangle_2|0\rangle_3). \quad (3.5)$$

The important property of this entangled state is that as soon as a measurement on one of the particles projects it onto a certain state, which can be any normalised linear superposition of $|0\rangle$ and $|1\rangle$, the other particle has to be in the orthogonal state. The specific phase relation between the two terms on the right hand side of (3.5) (here the phase difference is π , which results in the minus sign) implies that the statement of orthogonality is independent of the basis chosen for the polarisation measurement.

Although initially particles 1 and 2 are not entangled, their joint polarisation state can always be expressed as a superposition of the four maximally entangled Bell states, given by (3.1)–(3.4), since these states form a complete orthogonal basis. The total state of the 3 particles can be written as:

$$\begin{aligned} |\Psi\rangle_{123} = |\Psi\rangle_1 \otimes |\Psi\rangle_{23} = \frac{1}{2} & [|\Psi^-\rangle_{12} (-\alpha|0\rangle_3 - \beta|1\rangle_3) \\ & + |\Psi^+\rangle_{12} (-\alpha|0\rangle_3 + \beta|1\rangle_3) \\ & + |\Phi^-\rangle_{12} (\alpha|1\rangle_3 + \beta|0\rangle_3) \\ & + |\Phi^+\rangle_{12} (\alpha|1\rangle_3 - \beta|0\rangle_3)]. \end{aligned} \quad (3.6)$$

Alice now performs a Bell state measurement (BSM) on particles 1 and 2, that is, she projects her two particles onto one of the four Bell states. As a result of the measurement Bob's particle will be found in a state that is directly related to the initial state. For example, if the result of Alice's Bell state measurement is $|\Phi^-\rangle_{12}$ then particle 3 in the hands of Bob is in the

carrying the other photon transmits 0 bits of information, thus the total transmitted information does not exceed 2 bits.

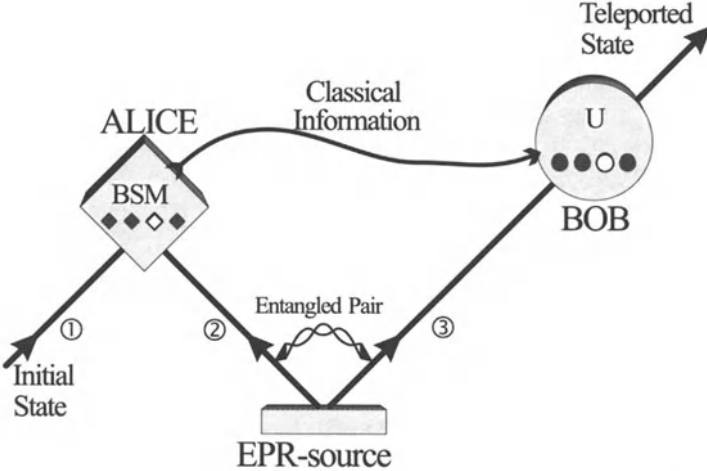


Fig. 3.1. Principle of quantum teleportation: Alice has a quantum system, particle 1, in an initial state which she wants to teleport to Bob. Alice and Bob also share an ancillary entangled pair of particles 2 and 3 emitted by an Einstein-Podolsky-Rosen(EPR) source. Alice then performs a joint Bell state measurement (BSM) on the initial particle and one of the ancillaries, projecting them also onto an entangled state. After she has sent the result of her measurement as classical information to Bob, he can perform a unitary transformation (U) on the other ancillary particle resulting in it being in the state of the original particle. In the case of quantum teleportation of a qubit, Alice makes a projection measurement onto four orthogonal entangled states (the Bell states) that form a complete basis. Sending the outcome of her measurement, i.e. two bits of classical information, to Bob will enable Bob to reconstruct the initial qubit.

state $\alpha|1\rangle_3 + \beta|0\rangle_3$. All that Alice has to do is to inform Bob via a classical communication channel on her measurement result and Bob can perform the appropriate unitary transformation (U) on particle 3 in order to obtain the initial state of particle 1. This completes the teleportation protocol.

Note that, during the teleportation procedure, the values of α and β remain unknown. By her Bell state measurement Alice does not obtain any information whatsoever about the teleported state. All that is achieved by the Bell state measurement is a transfer of the quantum state. Note also that during the Bell state measurement particle 1 loses its initial quantum state because it becomes entangled with particle 2. Therefore the state $|\Psi\rangle_1$ is destroyed on Alice's side during teleportation, thus obeying the no-cloning theorem of quantum mechanics [88]. Furthermore, the initial state of particle 1 can be completely unknown not only to Alice but to anyone. It could even be quantum mechanically completely undefined at the time the Bell state measurement takes place. This is the case when, as already remarked by Bennett et al. [74], particle 1 itself is a member of an entangled pair and therefore has no well-defined properties on its own. This ultimately leads to entanglement swapping which will be discussed in Sect. 3.10 [85, 87].

The experimental implementation of quantum teleportation or of quantum dense coding and entanglement swapping requires the generation of entangled particles and the construction of a Bell state analyser. The following two sections describe experimental techniques in quantum optics by which entangled photons and a (partial) Bell state analyser can be realised.

3.4 Sources of Entangled Photons

N. Gisin, J.G. Rarity, G. Weihs

There exist several sources of entangled quantum systems. A source of entangled atoms based on cavity quantum electrodynamics will be described in Sect. 5.2.3. Entangled ions have been prepared in electromagnetic Paul traps, see Sect. 5.2.11. Controlled entanglement between nuclear spins within a single molecule can be achieved by the technique of nuclear magnetic resonance and is presented in Sect. 5.3. Sources of entanglement in solid state physics are also being studied; however, it is still too early to see whether controlled entanglement in solid state physics is realisable. Here we will describe the sources of entanglement using quantum optics, which have been proven to be most successful, up to now, in generating high-quality entanglement.

In quantum optics there are two classes in which entanglement can be established (for a general view on creating entanglement see Sect. 1.5). One class is characterised by entanglement between single photons and will be described in this section. The other way is to establish entanglement between the quadrature components (i.e. the in- and out-of-phase electric-field components with respect to a local oscillator) of light beams or between two orthogonal polarisation components of light beams (see Sect. 3.9.2).

3.4.1 Parametric Down-Conversion

Nonlinear optical processes have been utilised for many experiments in quantum optics. Nonlinear optics is the part of classical electrodynamics which deals with strong fields that are scattered inelastically in various media. Inelastic scattering in the optical domain means that not only the direction but also the frequency of light is being changed by the interaction with the material, which is described by its electromagnetic susceptibility. During such interactions in most cases new fields are created. A power expansion of the susceptibility gives the lowest order nonlinear processes; three-wave-mixing (parametric interactions) and four-wave-mixing. The individual components P_i of the electromagnetic polarisation \mathbf{P} inside a material are given by

$$P_i = \chi_{ij}^{(1)} E_j + \chi_{ijk}^{(2)} E_j E_k + \chi_{ijkl}^{(3)} E_j E_k E_l + \dots, \quad (3.7)$$

where the E_i are the components of the electric field.

In order to be able to observe nonlinear interactions from an interaction volume that is large compared to the wavelengths involved, we have to consider contributions from the whole volume. Interference between these contributions leads to the so-called phase-matching relations, which are relations between the wavevectors of the respective electromagnetic fields.

If we look at these processes from a quantum electrodynamical viewpoint, we find that there are not only the stimulated but also the spontaneous processes just as in the interactions of the electromagnetic field with an atom. The spontaneous creation of photons in nonlinear interactions was first investigated theoretically by Klyshko [89] and experimentally by Burnham and Weinberg [90]. A special case of such a process is spontaneous parametric down-conversion, a $\chi^{(2)}$ -nonlinear process, in which only one of the fields is initially excited with a frequency ω_p . Due to the nonlinear interaction and this pump field, photons will be created spontaneously in the other two fields at frequencies ω_1 and ω_2 . As energy is conserved in the interaction we will find that

$$\omega_1 + \omega_2 = \omega_p. \quad (3.8)$$

Together with the phase-matching condition

$$\mathbf{k}_1 + \mathbf{k}_2 = \mathbf{k}_p, \quad (3.9)$$

this leads to various solutions of the interaction dynamics, depending on the material used and on the frequencies that are being observed. The rate of conversion is governed by the modulus of the corresponding components of $\chi^{(2)}$ and is in general very low. If, for example, we pump a material with a high nonlinearity (e.g. potassium di-deuterium phosphate, β -barium borate) with 100 mW (UV), we can observe of the order of 10^{10} photons per second of converted light from a small (a few mm long) piece of crystal. Symmetry considerations tell us further that $\chi^{(2)}$ -nonlinearities are only possessed by materials which are non-centrosymmetric, a property that belongs only to certain crystals.

In parametric down-conversion in the visible range of the spectrum, we distinguish two possible phase-matching schemes. “Type-I” phase-matching is the case where the two down-conversion photons have parallel polarisations whereas in “type-II” phase-matching they have orthogonal polarisations in the basis distinguished by the crystal orientation. It is the simultaneous production of the two photons in the conversion process and the phase-matching relations, together with proper spatial and temporal selection of the observed light, which are responsible for the creation and observation of entanglement.

3.4.2 Time Entanglement

There are various properties of photon pairs emerging from a down-conversion process that can be correlated. In type-I and type-II down-conversion we can

observe what is sometimes called time entanglement, which only relies on the fact that the two photons in a pair are created simultaneously and that they satisfy the energy conservation rule stated above. This latter criterion means that the emission time of any pair is uncertain within the coherence time of the pump laser. The simultaneity criterion arises because the individual photons of the pair are broadband (nanometre bandwidth) with coherence times of order 100 fs. This kind of entanglement has been used for so-called two-photon Franson–interferometry (see Fig. 3.2), where both photons pass separate unbalanced Mach–Zehnder interferometers [91]. The two interferometers are constructed in the same way and such that the coherence length of an individual photon is shorter than the path-length difference. As a result no interference can be seen in the direct count rates of detectors at the outputs of the interferometers. If, however, we look at the coincidences in the outputs of the two interferometers, we will observe oscillations of the coincidence count rates as we vary the phases between the arms of the interferometers. The state within the interferometers can be represented by

$$|\Psi\rangle = \frac{1}{2} \left[|S\rangle_1 |S\rangle_2 + e^{i(\phi_1 + \phi_2)} |L\rangle_1 |L\rangle_2 + e^{i\phi_2} |S\rangle_1 |L\rangle_2 + e^{i\phi_1} |L\rangle_1 |S\rangle_2 \right], \quad (3.10)$$

where the subscripts 1 and 2 refer to the photon moving to the left and to the right respectively in Fig. 3.2. State (3.10) is in fact a product state. However only long–long (L-L) and short–short (S-S) detections are truly coincident at the detectors and other events can be discarded by suitable coincidence gating. Initial experiments [91] did not use this time gating and were limited to maximum interference visibility of 50%. Later experiments using narrow coincidence gates to post-select only the entangled state show interference visibilities greater than 90% [92].

An interesting elaboration of time-entanglement should be mentioned. One can replace the cw pump laser by a pulsed laser followed by an unbalanced interferometer with pulses shorter than the arm length difference of the interferometer [93], see Fig. 3.3. Thus, if a pump photon is split into a

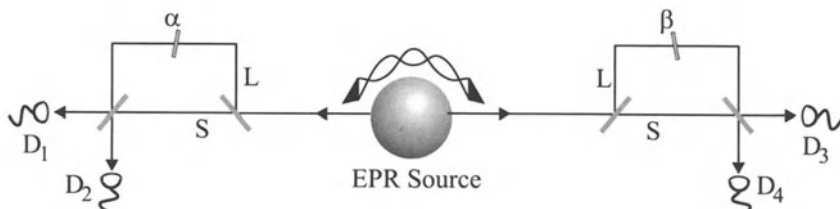


Fig. 3.2. Schematic of a Franson–type experiment testing the interference of time-entangled photon pairs by measuring them with two remote unbalanced Mach–Zehnder-interferometers. The phase of each interferometer can be changed by a phase shifter in the long (L) paths.

twin-photon inside the crystal after the first interferometer, the time of creation of the latter is undefined. More precisely, the unbalanced interferometer transforms the state of the pump photon in a superposition $\alpha|\text{short}\rangle_{\text{pump}} + \beta|\text{long}\rangle_{\text{pump}}$ and the down-conversion process in the crystal transforms this state into

$$\alpha|\text{short}\rangle_s \otimes |\text{short}\rangle_i + \beta|\text{long}\rangle_s \otimes |\text{long}\rangle_i. \quad (3.11)$$

Contrary to time entangled photons produced with a cw pump laser, the coherence of the pulsed pump laser is of no importance, as the necessary coherence is built by the unbalanced interferometer. In other words, the uncertainty of the pump photon's arrival time at the crystal (within the coherence length of the pump laser) is replaced by the two sharp values corresponding to $|\text{short}\rangle$ and $|\text{long}\rangle$ which form the basis of our qubit space. Hence, any standard laser diode, for instance, can be used as pump. Moreover, the basic states can be distinguished by their time of arrival, without any optical

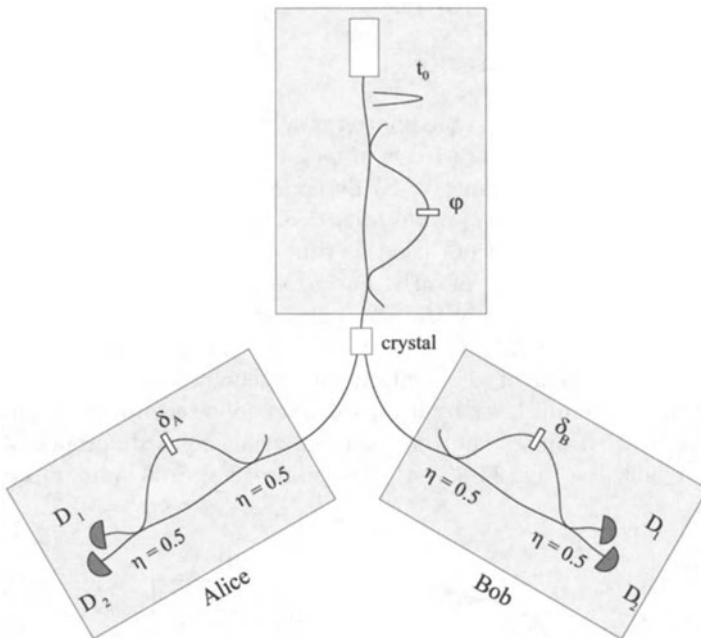


Fig. 3.3. Schematic of the pulsed time-entangled twin-photon source and a possible application for quantum cryptography. The twin-photons created by a pump photon passing through the short and the long arm of the first interferometer are coherent. Alice and Bob detect photons at 3 different times (relative to the emission time): short, medium, long. Short and long counts are 100% correlated. Medium counts correspond to the complementary basis, $|\text{short}\rangle \pm |\text{long}\rangle$, and are also perfectly correlated (assuming $\varphi + \delta_A + \delta_B = 0$). Note that no random generator is necessary, nor any active optical element.

circuit. By varying the coupling ratio and phase of the unbalanced interferometer, all 2-qubit entangled states can be produced. Hence all of the 2-qubit quantum communication protocols can be implemented.

3.4.3 Momentum Entanglement

Another kind of entanglement that is present in non-collinear down-conversion is momentum entanglement. This is induced by the phase-matching relation which governs the emission of different wavelengths into different directions. Using apertures A (see Fig. 3.4) two individual mode pairs (directions) from the emission of a down-conversion source are selected [94]. The selection is such that each pair consists of one photon with colour a (slightly above half of the pump frequency) and one photon with colour b (slightly below half of the pump frequency). The pairs are emitted into either modes a_1, b_1 or modes a_2, b_1 as shown in Fig. 3.4. Before the beam-splitter we thus have the state

$$|\Psi\rangle = \frac{1}{\sqrt{2}} [e^{i\phi_b} |a\rangle_1 |b\rangle_2 + e^{i\phi_a} |a\rangle_2 |b\rangle_1], \quad (3.12)$$

which is entangled although the modes at this stage are clearly distinguishable. The entanglement manifests itself when the a -modes and b -modes are recombined in a beam-splitter. From behind the beamsplitter upper and lower paths cannot be distinguished leading to interference. The 50/50 beam-splitter transforms the incoming fields through

$$|in\rangle_1 \rightarrow \frac{1}{\sqrt{2}} [|out\rangle_3 + i|out\rangle_4], \quad (3.13)$$

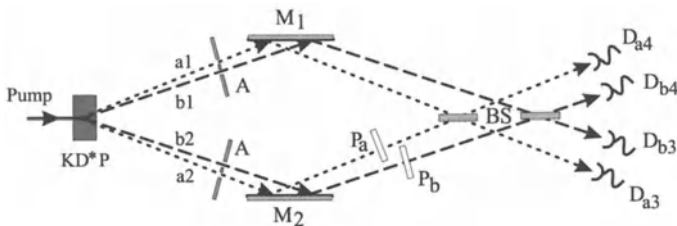


Fig. 3.4. Schematic of the Rarity–Tapster experiment on momentum entanglement from a type-I down-conversion source. Two correlated pairs of modes are selected from the emission spectrum of a type-I down-conversion source using two double apertures A. The different wavelengths are recombined on two beam-splitters BS. The detectors D_{a3} , D_{b3} , D_{a4} , and D_{b4} are used to measure the outputs from the beam-splitters.

$$|in\rangle_2 \rightarrow \frac{1}{\sqrt{2}} [|out\rangle_4 + i|out\rangle_3].$$

The state before the detectors is thus

$$\begin{aligned} |\Psi\rangle = \frac{1}{2} & [(e^{i\phi_a} - e^{i\phi_b})|a\rangle_4|b\rangle_3 + (e^{i\phi_b} - e^{i\phi_a})|a\rangle_3|b\rangle_4 \\ & + i(e^{i\phi_a} + e^{i\phi_b})|a\rangle_4|b\rangle_4 + i(e^{i\phi_a} + e^{i\phi_b})|a\rangle_3|b\rangle_3]. \end{aligned} \quad (3.14)$$

The four terms now show the probability amplitudes for coincident detections in each of the four possible detector pairs. Taking the modulus square of these amplitudes provides the probability of coincident detections between the a - and b -detectors which varies cosinusoidally on changing interferometer phase difference $\phi = \phi_a - \phi_b$. First order interference effects between the combined a - and b -modes are not seen because there is no phase conservation for individual photons of each pair. The phase conservation in parametric down-conversion arises in the energy conservation stated above; it is the sum of the phases in the a - and b -modes that are locked to that of the pump beam.

The a -mode (b -mode) interferometer measures a ‘phase’ between the two possible emissions in a basis fixed by the offset phase ϕ_a (ϕ_b). The 100% correlation (anticorrelation) in the binary measurement of this phase whenever $\phi = \phi_a - \phi_b = 0$ ($\pi/2$) confirms the non-local nature of the effect. This result cannot be reproduced if there is a local realistic phase (satisfying the sum phase condition above) associated with each photon pair as it leaves the crystal. In the experiment [94] an interference visibility of 82% was measured, beyond the maximum predicted for any local realistic model of the experiment. However the interference visibility is low compared to polarisation based entanglement experiments due to the difficulties of alignment and overlap of the four beams.

3.4.4 Polarisation Entanglement

More recently a new type of down-conversion source was found, which relies on non-collinear type-II phase matching [16]. At certain angles between the pump-beam and the optic axis of the conversion crystal the phase-matching conditions will be such that the photons are emitted along cones, which do not have a common axis, as is illustrated in Fig. 3.5 and Fig. 3.6. One of the cones is ordinarily polarised the other one extraordinarily. These cones will in general intersect along two directions. If we now remember that in type-II down-conversion the two photons in a pair are always polarised orthogonally, we will find that along the two directions of intersection the emitted light is unpolarised, because we cannot distinguish whether a certain photon belongs to one or the other cone. This is not yet exactly true, because in the birefringent crystal the ordinary and extraordinary photons will propagate at different velocities and so we could at least in principle distinguish the two cases by the order of their detection times. It is, however possible to compensate for that “walkoff”, by inserting identical crystals of half the thickness

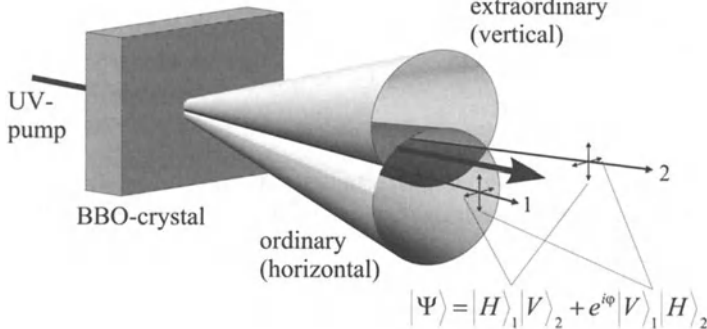


Fig. 3.5. Non-collinear type-II down-conversion can produce two tilted cones of light of a certain wavelength. At same time other wavelengths are emitted, but in order to observe polarisation entanglement only we cut out a certain wavelength using narrow-band optical filters.

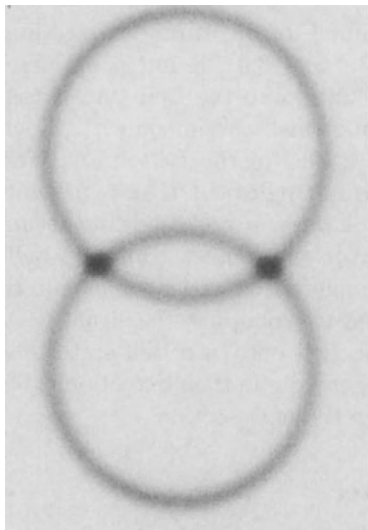


Fig. 3.6. Type-II down-conversion light as seen through a narrow-band filter. The two rings are the ordinary and extraordinary cones of light rays. Along the intersecting directions we observe unpolarised light.

rotated by 90° in each of the two beams. This procedure completely erases any such information and we have a true polarisation-entangled state which can be described by

$$|\Psi\rangle = \frac{1}{\sqrt{2}} [|V\rangle_1 |H\rangle_2 + e^{i\varphi} |H\rangle_1 |V\rangle_2]. \quad (3.15)$$

Furthermore we can use these compensator crystals to change the phase φ between the two components of the entangled state. If we use an additional

half-wave plate in one of the two beams we can also produce the other two of the four Bell-states.

$$|\Phi^\pm\rangle = \frac{1}{\sqrt{2}} [|V\rangle_1 |V\rangle_2 \pm |H\rangle_1 |H\rangle_2]. \quad (3.16)$$

Again in order to see the interference effects the state is studied in a basis where the vertical and horizontal polarisations cannot be distinguished. This can be done simply by mixing the states in a polariser rotated to 45°.

3.5 Bell-State Analyser

D. Bouwmeester, H. Weinfurter, A. Zeilinger

Formally speaking, a Bell-state analysis, required for quantum dense coding and for quantum teleportation (see Sects. 3.2 and 3.3), is not a problem. All you have to do is project any incoming state onto the Bell state basis, (3.1)–(3.4), and you will find out by repeating this experiment with which probability the original state can be found in one of the Bell states. The Bell states depend, of course, on the type of entanglement that is present. In the case of entanglement between the polarisation and the momentum degree of freedom of a single photon, the projection onto a complete Bell-state basis is possible (see Sect. 3.8) with simple linear optical elements. In the case of polarisation entanglement between two photons, the situation is more complicated and, so far, only the projection onto two Bell states has been achieved, leaving the other two states degenerate in their detection. This partial Bell-state analysis will be explained in the next section.

3.5.1 Photon Statistics at a Beamsplitter

The partial Bell-state analysis of polarisation entanglement exploits the statistics of two qubits at a beamsplitter. The basic principle of that Bell-state analyser rests on the observation that of the four Bell states (3.1)–(3.4) only one state is antisymmetric under exchange of the two particles. This is the $|\Psi^-\rangle_{12}$ state (3.2), which clearly changes sign upon exchange of labels 1 and 2. The other three states are symmetric. We thus observe that the qubit obeys fermionic symmetry in the case of $|\Psi^-\rangle_{12}$ and bosonic symmetry in case of the other three states. Thus far we have not specified whether the particles carrying the qubits are bosons or fermions. In fact, the four Bell states could equally well be those of fermions or those of bosons. This is because the states written in (3.1)–(3.4) are not the complete states of the particles but describe only the internal (two-level) state of the particles. The total state can be obtained by adding the spatial state of the particles which

could also be symmetric or antisymmetric. Then, in the case of bosons, the spatial part of the wave function has to be antisymmetric for the $|\Psi^-\rangle_{12}$ state and symmetric for the other three, while for fermions this has to be just the reverse.

Let us first consider two photons, which are bosons, and assume that the Bell states above describe the polarisation of the photons, that is, an internal degree of freedom. Then, clearly, the total state of the two photons has to be symmetric. For the case of the two particles incident symmetrically onto a beamsplitter, i.e., one entering from each input mode $|a\rangle$ and $|b\rangle$, the possible external (spatial) states are

$$|\Psi_A\rangle_{12} = \frac{1}{\sqrt{2}}(|a\rangle_1|b\rangle_2 - |b\rangle_1|a\rangle_2) \quad (3.17)$$

$$|\Psi_S\rangle_{12} = \frac{1}{\sqrt{2}}(|a\rangle_1|b\rangle_2 + |b\rangle_1|a\rangle_2), \quad (3.18)$$

where $|\Psi_A\rangle_{12}$ and $|\Psi_S\rangle_{12}$ are antisymmetric and symmetric, respectively. Because of the requirement of symmetry, the total two-photon states are

$$|\Psi^+\rangle|\Psi_S\rangle, \quad |\Psi^-\rangle|\Psi_A\rangle, \quad |\Phi^+\rangle|\Psi_S\rangle, \text{ and } |\Phi^-\rangle|\Psi_S\rangle. \quad (3.19)$$

We note that only the state antisymmetric in external variables is also antisymmetric in internal variables. It is this state which also emerges from the beamsplitter in an external antisymmetric state. This can easily be found by assuming that the beamsplitter does not influence the internal state and by applying the beamsplitter operator (Hadamard transformation) on the external (spatial) state. Using

$$H|a\rangle = \frac{1}{\sqrt{2}}(|c\rangle + |d\rangle) \quad (3.20)$$

$$H|b\rangle = \frac{1}{\sqrt{2}}(|c\rangle - |d\rangle) \quad (3.21)$$

it can now easily be seen that

$$H|\Psi_A\rangle_{12} = \frac{1}{\sqrt{2}}(|c\rangle_1|d\rangle_2 - |d\rangle_1|c\rangle_2) = |\Psi_A\rangle_{12}. \quad (3.22)$$

Therefore the spatially antisymmetric state is an eigenstate of the beamsplitter operator [95, 96]. In contrast, in all three cases of the symmetric external state $|\Psi_S\rangle$, the two photons emerge together in one of the two outputs of the beamsplitter. It is therefore evident that the state $|\Psi^-\rangle$ can be clearly discriminated from all the other states. It is the only one of the four Bell states which leads to coincidences between detectors placed on each side after a beamsplitter [97]–[99]. How can we then identify the other three states? It turns out that distinction between $|\Psi^+\rangle$ on the one hand and $|\Phi^+\rangle$ and $|\Phi^-\rangle$ on the other hand can be based on the fact that only in $|\Psi^+\rangle$ do the two photons have different polarisation while in the other two they have the same

polarisation. Thus performing polarisation measurements and observing the photons on the same side of the beamsplitter distinguishes the state $|\Psi^+\rangle$ from the states $|\Phi^+\rangle$ and $|\Phi^-\rangle$. It should be remarked that a simple generalisation of this procedure implies that any two orthogonal maximally entangled states can be distinguished from each other in the same way, because by local unitary transformations one can perform rotations in the two-dimensional Hilbert space.

Consider now the same experiment with fermions [100] where again the Bell states describe the internal states, for example if the two qubits are entangled in spin, we find that the four possible states now are

$$|\Psi^+\rangle|\Psi_A\rangle, \quad |\Psi^-\rangle|\Psi_S\rangle, \quad |\Phi^+\rangle|\Psi_A\rangle, \text{ and } |\Phi^-\rangle|\Psi_A\rangle. \quad (3.23)$$

because of the antisymmetry requirement of the total state. For fermions, therefore, only one of the states is spatially symmetric, the other three are spatially anti-symmetric. Thus in only one of the cases, namely for $|\Psi^-\rangle$, will both fermions emerge together from the beamsplitter. In the other three cases they will emerge from different sides. Yet, remarkably, it is again this state which can immediately be distinguished from the other three because of its distinct symmetry properties.

3.6 Experimental Dense Coding with Qubits

A quantum-optical demonstration of the quantum dense coding scheme [75], described in Sect. 3.2, requires three distinct parts (Fig. 3.7): the EPR-source generating entangled photons, Bob's station for encoding the messages by a unitary transformation of his particle, and Alice's Bell-state analyser to read the signal sent by Bob. The polarisation-entangled photons can be produced by type-II parametric down-conversion (Sect. 3.4.4). A UV-beam ($\lambda = 351$ nm) from an argon-ion laser is down-converted into pairs of photons ($\lambda = 702$ nm) with orthogonal polarisation.

The entangled state $|\Psi^+\rangle$ is obtained after compensation of birefringence in the BBO crystal along two distinct emission directions (carefully selected by 2 mm irises, 1.5 m away from the crystal). One beam was first directed to Bob's encoding station, the other directly to Alice's Bell-state analyser; in the alignment procedure an optical trombone was employed to equalise the path lengths to well within the coherence length of the down-converted photons ($\ell_c \approx 100 \mu\text{m}$), in order to enable Alice to perform a (partial) Bell-state analysis.

For polarisation encoding, the necessary transformations of Bob's particle were performed using a half-wave retardation plate for changing the polarisation and a quarter-wave plate to generate the polarisation dependent phase

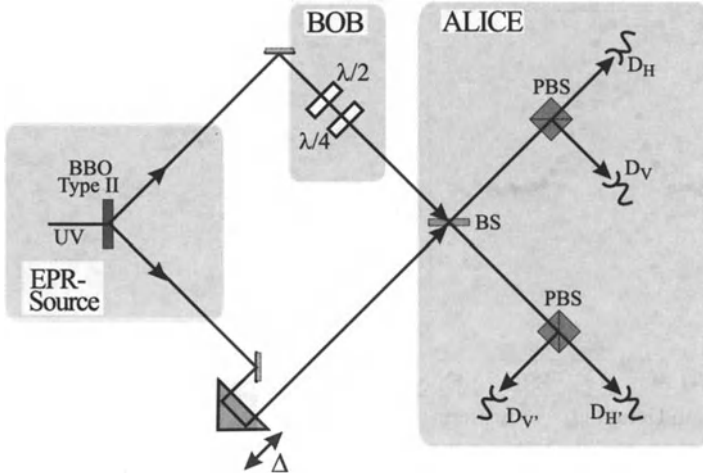


Fig. 3.7. Experimental set-up for quantum dense coding [75].

shift². The beam manipulated in this way in Bob's encoding station was then combined with the other beam at Alice's Bell-state analyser. It consisted of a single beamsplitter followed by two-channel polarisers in each of its outputs and proper coincidence analysis between four single photon detectors.

Since only the state $|\Psi^-\rangle$ has an antisymmetric spatial part, only this state will be registered by coincidence detection between the different outputs of the beamsplitter (i.e. coincidence between detectors D_H and $D_{V'}$ or between $D_{H'}$ and D_V). For the remaining three states both photons exit into the same output port of the beamsplitter. The state $|\Psi^+\rangle$ can easily be distinguished from the other two due to the different polarisations of the two photons, giving, behind the two-channel polariser, a coincidence between detectors D_H and D_V or between $D_{H'}$ and $D_{V'}$. The two states $|\Phi^+\rangle$ and $|\Phi^-\rangle$ both result in a two-photon state being absorbed by a single detector and thus cannot

Table 3.1. Overview of possible manipulations and detection events of the quantum dense coding experiment with correlated photons.

Bob's setting		State sent	Alice's registration events
$\lambda/2$	$\lambda/4$		
0°	0°	$ \Psi^+\rangle$	coinc. between D_H and D_V or $D_{H'}$ and $D_{V'}$
0°	90°	$ \Psi^-\rangle$	coinc. between D_H and $D_{V'}$ or $D_{H'}$ and D_V
45°	0°	$ \Phi^+\rangle$	2 photons in either D_H , D_V , $D_{H'}$ or $D_{V'}$
45°	90°	$ \Phi^-\rangle$	2 photons in either D_H , D_V , $D_{H'}$ or $D_{V'}$

² The component polarised along the axis of the quarter-wave plate is advanced only by $\pi/2$ relative to the other. Reorienting the optical axis from vertical to horizontal causes a net phase change of π between $|H\rangle$ and $|V\rangle$.

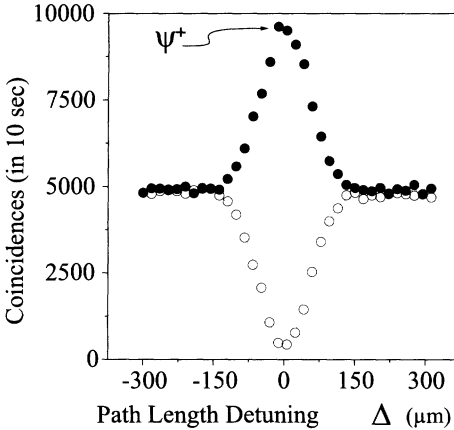


Fig. 3.8. Coincidence rates C_{HV} (●) and $C_{HV'}$ (○) as functions of the path length difference Δ when the state $|\Psi^+\rangle$ is transmitted. For perfect tuning ($\Delta = 0$) constructive interference occurs for C_{HV} , allowing identification of the state sent.

be distinguished. Table 3.1 gives an overview of the different manipulations and detection probabilities of Bob's encoder and Alice's receiver.

The experiments were performed by first setting the output state of the source such that the state $|\Psi^+\rangle$ left Bob's encoder when both retardation plates are set to vertical orientation; the other Bell-states could then be generated with the respective settings (Table 3.1). To characterize the interference observable at Alice's Bell-state analyser, we varied the path length difference Δ of the two beams with the optical trombone. For $\Delta \gg \ell_c$ no interference occurs and one obtains classical statistics for the coincidence count rates at the detectors. For optimal path-length tuning ($\Delta = 0$), interference enables one to read the encoded information.

Figures 3.8 and 3.9 show the dependence of the coincidence rates C_{HV} (●) and $C_{HV'}$ (○) on the path length difference for $|\Psi^+\rangle$ and $|\Psi^-\rangle$, respectively (the rates $C_{H'V'}$ and $C_{H'V}$ display analogous behaviour; we use the notation C_{AB} for the coincidence rate between detectors D_A and D_B). At $\Delta = 0$, C_{HV} reaches its maximum for $|\Psi^+\rangle$ (Fig. 3.8) and vanishes (aside from noise) for $|\Psi^-\rangle$ (Fig. 3.10). $C_{HV'}$ displays the opposite dependence and clearly signifies $|\Psi^-\rangle$. The results of these measurements imply that if both photons are detected, we can identify the state $|\Psi^+\rangle$ with a reliability of 95%, and the state $|\Psi^-\rangle$ with 93%.

When using Si-avalanche diodes in the Geiger-mode for single photon detection, a modification of the Bell-state analyser is necessary, since then one also has to register the two photons leaving the Bell-state analyser for the states $|\Phi^+\rangle$ or $|\Phi^-\rangle$ via a coincidence detection.³

³ A special identification of the two-photon state is necessary: Si-avalanche photodiodes give the same output pulse for one or more photons, thus only a coin-

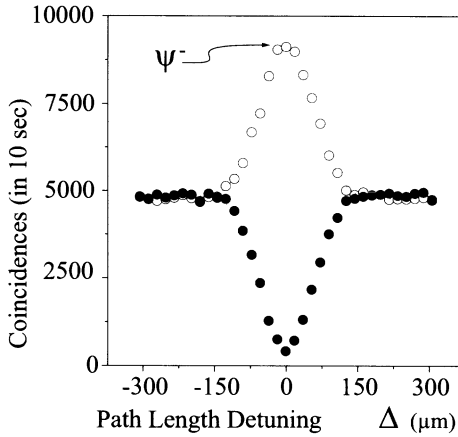


Fig. 3.9. Coincidence rates C_{HV} (●) and $C_{HV'}$ (○) depending on the path length difference Δ , for transmission of the state $|\Psi^-\rangle$. The constructive interference for the rate $C_{HV'}$ enables one to read the information associated with that state.

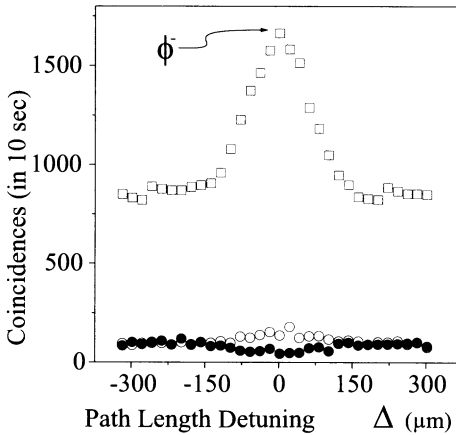


Fig. 3.10. Coincidence rates $C_{H\bar{H}}$ (□), C_{HV} (●), and $C_{HV'}$ (○) as functions of the path length detuning Δ . The maximum in the rate $C_{H\bar{H}}$ signifies the transmission of a third state $|\Phi^-\rangle$ encoded in a two-state particle. $C_{H\bar{H}}$ is smaller by a factor of 4 compared to the rates of Figures 3.8 and 3.9 due to a further reduced registration probability of $|\Phi^-\rangle$, see text.

One possibility is to avoid interference for these states completely by introducing polarisation-dependent delays $\gg \ell_c$ before Alice's beamsplitter, e.g., using thick quartz plates, retarding $|H\rangle$ in one beam and $|V\rangle$ in the other. Another approach is to split the incoming two-photon state at an additional

cidence detection allows the registration of the two-photon state. Special photomultipliers can distinguish between one- and two-photon absorption, but are too inefficient at present.

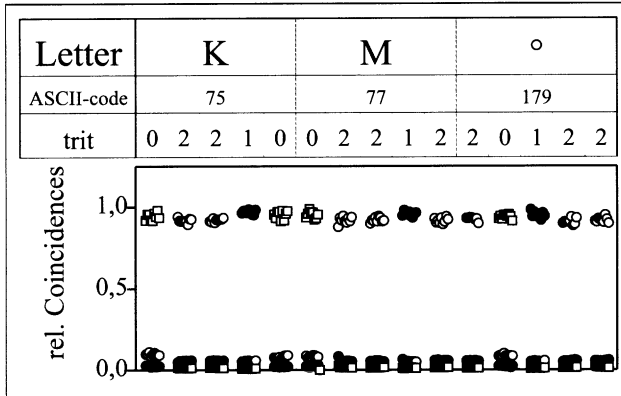


Fig. 3.11. “1.58 bit per photon” quantum dense coding : The ASCII-codes for the letters “KM \circ ” (i.e. 75, 77, 179) are encoded in 15 trits (with “0” \equiv $|\Phi^-\rangle \hat{=} \square$, “1” \equiv $|\Psi^+\rangle \hat{=} \bullet$, “2” \equiv $|\Psi^-\rangle \hat{=} \circ$) instead of the 24 bits usually necessary. The data for each type of encoded state are normalised to the maximum coincidence rate for that state.

beamsplitter and to detect it (with 50% likelihood) by a coincidence count between detectors in each output. For the purpose of this proof-of-principle demonstration, we put such a configuration only in place of detector D_H . Figure 3.10 shows the increase of the coincidence rate $C_{H\bar{H}}(\square)$ at path length difference $\Delta = 0$, with the rates C_{HV} and $C_{HV'}$ at the background level, when Bob sends the state $|\Phi^-\rangle$.

Note, however, that for both methods half of the time both photons still are absorbed by one detector; therefore, and since we inserted only one such configuration, the maximum rate for $C_{H\bar{H}}$ is about a quarter of that of C_{HV} or $C_{HV'}$ in Figs. 3.8 and 3.9.

Since we now can distinguish the three different messages, the stage is set for the quantum dense coding transmission. Figure 3.11 shows the various coincidence rates (normalised to the respective maximum rate of the transmitted state) when sending the ASCII codes of “KM \circ ” (i.e. codes 75, 77, 179) in only 15 trits instead of 24 classical bits. From this measurement one also obtains a signal-to-noise ratio by comparing the rates signifying the actual state with the sum of the two other registered rates. The ratios for the transmission of the three states varied due to the different visibilities of the respective interferences and were $S/N_{|\Psi^+\rangle} = 14.8$, $S/N_{|\Psi^-\rangle} = 13.0$, and $S/N_{|\Phi^-\rangle} = 8.5$.

3.7 Experimental Quantum Teleportation of Qubits

D. Bouwmeester, J.-W. Pan, H. Weinfurter, A. Zeilinger

In this section an experimental demonstration of quantum teleportation of qubits, encoded in the polarisation state of single photons, will be given [76]. During teleportation, an initial photon which carries the polarisation that is to be transferred and one of a pair of entangled photons are subjected to a measurement such that the second photon of the entangled pair acquires the polarisation of the initial photon. Figure 3.12 is a schematic drawing of the experimental setup. As explained in Sect. 3.3, an experimental realisation of quantum teleportation necessitates both creation and measurement of entangled states, indicated in Fig. 3.12 by the Einstein–Podolski–Rosen (EPR) source and the Bell-state measurement (BSM) respectively. The EPR source of polarisation entangled photons was described in Sect. 3.4 and the $|\Psi^-\rangle_{12}$ Bell-state analyser was described in Sect. 3.5.

The experimental realisation of the quantum teleportation of a qubit presented in this section is restricted to use the $|\Psi^-\rangle_{12}$ Bell-state projection only.⁴ The unitary transformation that Bob has to perform when Alice measures photon 1 and 2 in $|\Psi^-\rangle_{12}$ is simply the identity transformation, i.e. Bob should detect a photon in the same state as photon 1.

To avoid photons 1 and 2, which are created independently, being distinguished by their arrival times at the detectors, which would eliminate the possibility of performing the Bell-state measurement, the following technique is used. Photon 2, together with its entangled partner photon 3, is produced by pulsed parametric down-conversion. The pump pulse, generated by a frequency-doubled mode-locked titanium-sapphire laser, is 200 fs long. The pulse is reflected back through the crystal (see Fig. 3.12) to create a second pair of photons, photons 1 and 4. Photon 4 is used as a trigger to indicate the presence of photon 1. Photons 1 and 2 are now located within 200 fs long pulses, which can be tuned by a variable delay such that maximal spatial overlap of the photons at the detectors is obtained. However, this does not yet guarantee indistinguishability upon detection since the entangled down-converted photons typically have a coherence length corresponding to about a 50 fs long wavepacket, which is shorter than the pulses from the pump laser. Therefore, coincidence detection of photons 1 and 2 with their partners 3 and 4 with a time resolution better than 50 fs could identify which photons were created together. To achieve indistinguishability upon detection, the photon wavepackets should be stretched to a length substantially longer than that of the pump pulse. In the experiment this was done by placing 4 nm narrow interference filters in front of the detectors. These filter out pho-

⁴ It is possible to extend the Bell-state analyser into an analyser that can uniquely identify both the $|\Psi^-\rangle_{12}$ state and the $|\Psi^+\rangle_{12}$ (see Sect. 3.5).

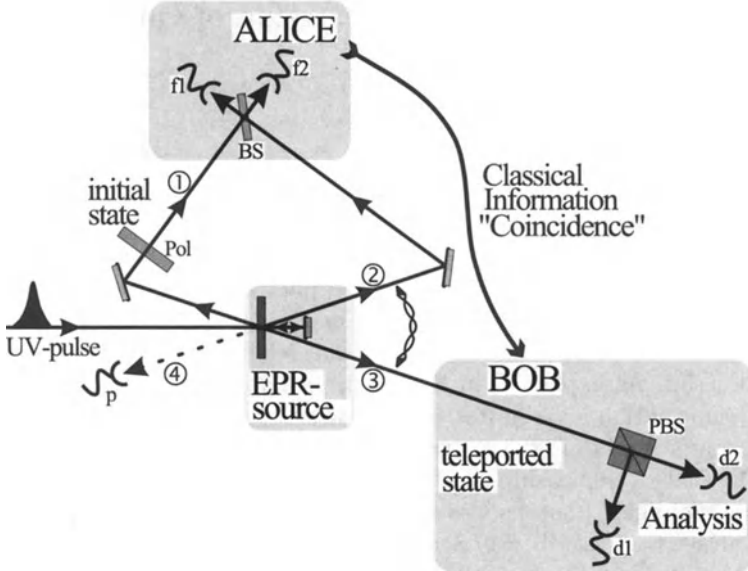


Fig. 3.12. Schematic drawing of the experimental setup for quantum teleportation of a qubit. A pulse of ultraviolet (UV) light passing through a nonlinear crystal creates the ancillary pair of entangled photons 2 and 3. After retroflection during its second passage through the crystal, the ultraviolet pulse can create another pair of photons, one of which will be prepared in the initial state of photon 1 to be teleported, the other one serving as a trigger indicating that a photon to be teleported is underway. Alice then looks for coincidences after a beamsplitter (BS) where the initial photon and one of the ancillaries are superposed. Bob, after receiving the classical information that Alice obtained a coincidence count in detectors f1 and f2 identifying the $|\Psi^-\rangle_{12}$ Bell-state, knows that his photon 3 is in the initial state of photon 1 which he then can check using polarisation analysis with the polarising beamsplitter (PBS) and the detectors d1 and d2. The detector P provides the information that photon 1 is underway.

ton wavepackets with a time duration of the order of 500 fs, which yields a maximum indistinguishability of photons 1 and 2 of about 85% [101].

All the important experimental components of the teleportation setup have now been discussed. This brings us to the question of how to prove experimentally that an unknown quantum state can be teleported with the above setup? For this, one has to show that teleportation works for a set of known non-orthogonal states. The test for non-orthogonal states is necessary to demonstrate the crucial role of quantum entanglement in the teleportation scheme.⁵

⁵ The reason for this is essentially the same as the reason why non-orthogonal states are used in constructing Bell's inequality (see Sect. 1.7 and references therein).

3.7.1 Experimental Results

In the first experiment photon 1, which has encoded the initial qubit, is prepared with a linear polarisation at 45° . Teleportation should work as soon as photons 1 and 2 are detected in the $|\Psi^-\rangle_{12}$ state. This implies that if a coincidence between detectors f1 and f2 (Fig. 3.12) is recorded, i.e. photons 1 and 2 are projected onto the $|\Psi_1^-\rangle$ state, then photon 3 should be polarised at 45° (to within an irrelevant overall minus sign, see (3.6)). The polarisation of photon 3 is analysed by passing it through a polarising beamsplitter selecting $+45^\circ$ and -45° polarisation. To demonstrate teleportation, only detector d2 at the $+45^\circ$ output of the polarising beamsplitter should detect a photon once f1 and f2 record a coincidence detection. Detector d1 at the -45° output of the polarising beamsplitter should not detect a photon. Therefore, recording a three-fold coincidence d2f1f2 ($+45^\circ$ analysis) together with the absence of a three-fold coincidence d1f1f2 (-45° analysis) is a proof that the polarisation of photon 1, which represents the initial qubit, has been transferred to photon 3.

To meet the condition of indistinguishability of photons 1 and 2 (see previous subsection), the arrival time of photon 2 is varied by changing the delay between the first and second down-conversion by translating the retroflection mirror (see Fig. 3.12). Within the region of temporal overlap of photons 1 and 2 at the detectors the teleportation should occur.

Outside the region of teleportation photons 1 and 2 will each go to either f1 or to f2 independently of one another. The probability of obtaining a coincidence between f1 and f2 is therefore 50%. This is twice as high as the probability inside the region of teleportation since only the $|\Psi^-\rangle$ component of the two-photon state entering the beamsplitter will give a coincidence recording. Since photon 2 is part of an entangled state it does not have a well-defined polarisation on its own, and the joint state of photons 1 and 2 is an equal superposition of all four Bell states, irrespective of the state of photon 1. Photon 3 should also have no well-defined polarisation because it is entangled with photon 2. Therefore, d1 and d2 both have a 50% chance of receiving photon 3. This simple argument yields a 25% probability both for the -45° analysis (d1f1f2 coincidences) and for the $+45^\circ$ analysis (d2f1f2 coincidences) outside the region of teleportation.

Figure 3.13 summarises the predictions as a function of the delay. Successful teleportation of the $+45^\circ$ polarisation state is then characterized by a decrease to zero in the -45° analysis, see Fig. 3.13a, and by a constant value for the $+45^\circ$ analysis, see Fig. 3.13b. Note that the above arguments are conditional upon the detection of a trigger photon by detector p (see Fig. 3.12).

The experimental results for teleportation of photons polarised at $+45^\circ$ are shown in the first panel of Fig. 3.14. Figure 3.14a and 3.14b should be compared with the theoretical predictions shown in Fig. 3.13.

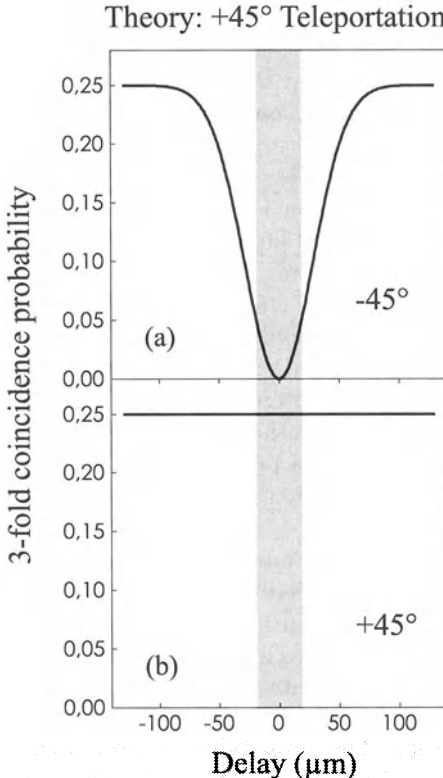


Fig. 3.13. Theoretical prediction for the three-fold coincidence probability between the two Bell-state detectors (f_1, f_2) and one of the detectors analysing the teleported state. The signature of teleportation of a photon polarisation state at $+45^\circ$ is a dip to zero at zero delay in the three-fold coincidence rate with the detector analysing -45° ($d_1f_1f_2$) (a) and a constant value for the detector analysis $+45^\circ$ ($d_2f_1f_2$) (b). The shaded area indicates the region of teleportation.

The strong decrease in the -45° analysis, and the constant signal for the $+45^\circ$ analysis, indicate that photon 3 is polarised along the direction of photon 1, consistent with the quantum teleportation protocol. Note again that a four-fold coincidence detection has been used where the fourth photon is a trigger that indicates the presence of photon 1.

To rule out any classical explanation for the experimental results, a four-fold coincidence measurement for the case of teleportation of the $+90^\circ$ polarisation states, that is, for a state non-orthogonal to the $+45^\circ$ state, has been performed. The experimental results are shown in Fig. 3.14c and 3.14d. Visibilities of $70\% \pm 3\%$ are obtained for the dips in the orthogonal polarisation states.

From Fig. 3.14 one can directly obtain the measured fidelity of teleportation of a qubit encoded in the polarisation of a single-photon state. The

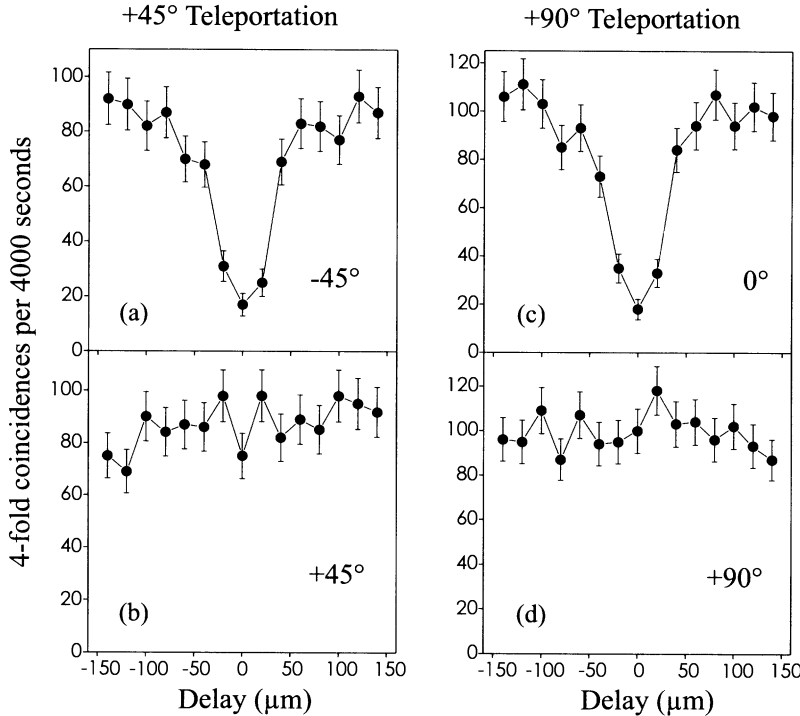


Fig. 3.14. Experimental demonstration of the teleportation of qubits: Measured coincidence rates $d1f1f2$ (-45°) and $d2f1f2$ ($+45^\circ$) in the case where the photon state to be teleported is polarised at $+45^\circ$ (a) and (b) or at $+90^\circ$ (c) and (d), and conditional upon the detection of the trigger photon by detector p. The four-fold coincidence rates are plotted as a function of the delay (in μm) between the arrival of photons 1 and 2 at Alice's beamsplitter (see Fig. 3.12). These data, in conjunction with Fig. 3.13, confirm teleportation for an arbitrary qubit state.

fidelity is defined as the overlap of the input qubit with the teleported qubit and is plotted in Fig. 3.15. In the experiment, the detection of the teleported photons played the double role of filtering out the experimental runs in which there is a single input qubit present and of measuring the fidelity of the teleportation procedure. With respect to the filtering, note that two detection events at Alice's Bell-state analyser could have been due to two pairs of photons both created during the return passage of the pump pulse. Then no photon will be observed by Bob [83], but two photons will travel towards detector p. This situation can be identified and therefore eliminated by using a detector p that can discriminate between a one-photon and a two-photon impact [102].

Whether or not such a modified detection is used, the measured fidelity will be the same [84] and is primarily determined by the degree of indistinguishability of the photons detected in Alice's Bell-state analyser. The

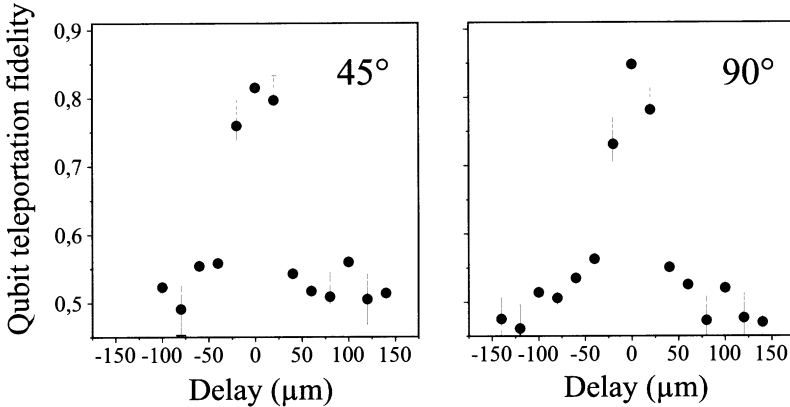


Fig. 3.15. Fidelity of teleportation of a qubit encoded in the polarisation of a single-photon state: The overlap of the input qubit with the teleported qubit has been determined via a four-fold coincidence technique to be as high as 80%.

amount of indistinguishability is directly related to the ratio of the bandwidth of the pump pulse and the interference filters. The larger this ratio the higher the fidelity but the lower the countrates.

3.7.2 Teleportation of Entanglement

Instead of using the fourth photon in the experiment described above as a mere trigger to indicate that photon 1 is underway, one can explore the fact that photon 1 and 4 can also be produced in an entangled state, say in the $|\Psi^-\rangle_{14}$ state, as illustrated in Fig. 3.16.

The state of photon 1 is therefore completely undetermined and all the information is stored in joint properties of photons 1 and 4. If photon 1 is now subjected to quantum teleportation as described in the previous section, photon 3 obtains the properties of photon 1 and therefore becomes entangled with photon 4 (see Fig. 3.16). Interestingly, photon 4 and photon 3 originate from different sources and never interacted directly with one another, yet they form an entangled pair after the quantum teleportation procedure. The experimental verification of this process of transferring entanglement [86], known as entanglement swapping, and several possible applications [85, 87] will be described in Sects. 3.10 and 3.11.

3.7.3 Concluding Remarks and Prospects

Pairs of polarisation entangled photons and two-photon interferometric methods have been used to transfer one qubit encoded in the polarisation state of one photon onto another one. Teleportation has also been addressed in other

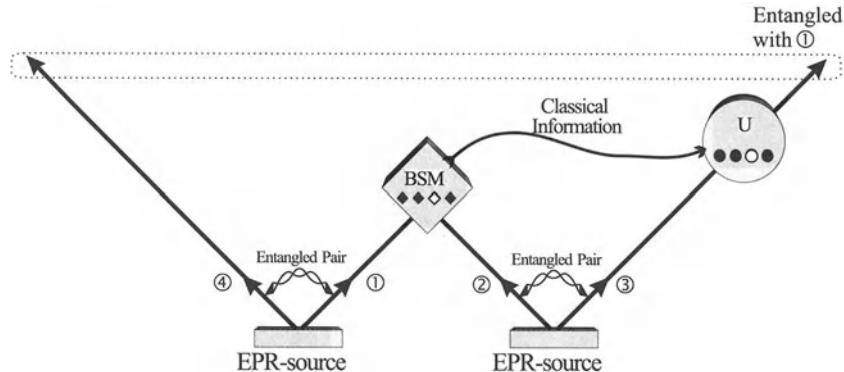


Fig. 3.16. Principle of entanglement swapping: Two EPR sources produce two pairs of entangled photons, pair 1-4 and pair 2-3. Two photons, one from each pair (photons 1 and 2) are subjected to a Bell-state measurement(BSM). This results in projecting the other two outgoing photons 3 and 4 onto an entangled state.

optical systems, which will be discussed in the following two sections. However, quantum teleportation is by no means restricted to optical experiments. In addition to pairs of entangled photons one can employ entangled atoms [103], and one can, in principle, entangle photons with atoms or phonons with ions, and so on. Then teleportation would allow the transfer of the state of, for example, fast-decohering, short-lived particles onto some more stable systems. This opens up the possibility of quantum memories, where the information of incoming photons is stored on trapped ions/atoms, carefully shielded from the environment.

Furthermore, with entanglement purification [49] (see Chap. 8), a scheme for improving the quality of entanglement when it has been degraded by decoherence during storage or transmission of the particles over noisy channels, it becomes possible to send the quantum state of a particle to some place, even if the available quantum channels are of limited quality and thus sending the particle itself might destroy the fragile quantum state. If the distance over which one wants to send the quantum state through a noisy quantum channel becomes too long, the fidelity of transmission becomes too low for the application of the standard purification method. In this situation the quantum repeater method allows one to divide the quantum channel into shorter segments that are purified separately and then connected by entanglement swapping [104] (Sect. 8.7). The feasibility of preserving quantum states in a hostile environment will have great advantages in the realm of quantum communication and quantum computation.

3.8 A Two-Particle Scheme for Quantum Teleportation

D. Bouwmeester

The teleportation scheme, as described in Sect. 3.3, presents two new concepts. First, it shows how entanglement can be used as part of a quantum communication channel. Second, it shows that the information associated with the state of a quantum particle can be physically decomposed into, and reconstructed from a classical component and a genuine quantum one. Alone, neither of these two components contain any information whatsoever about the quantum state; put together, they determine it completely.

In the previous section these concepts were demonstrated using three- and four-photon experiments. A limitation of these experiments was that Alice could not perform a full Bell-state measurement, which reduced the efficiency of the quantum state teleportation. A full Bell-state measurement would imply a controlled interaction between two photons, which is extremely difficult to implement in practice. The scheme described here, which was proposed by S. Popescu [77] and experimentally realised in Rome [78], avoids this problem but does place restrictions on the quantum states that can be transferred.

The original teleportation scheme involves three particles. Two of the particles, one sent to Alice and one sent to Bob are in an entangled state (singlet) and constitute the “non-local communication channel”. The third particle is initially in the state Ψ which Alice has to transmit. One might imagine that the particle was prepared in this state by a third party, the Preparer, or that Alice acquired it herself directly from nature. The scheme considered here involves only two particles, namely the ones which form the non-local channel. The Preparer has to help Alice by encoding Ψ directly into her member of the singlet pair instead of encoding it into a third particle. To this end, the Preparer uses some other degree of freedom of Alice’s particle, different from the degree of freedom by which it is entangled with Bob’s particle. This doesn’t change the problem facing Alice – Alice cannot find out what Ψ is. So if she were limited to the use of classical channels she couldn’t help Bob prepare his particle in the state Ψ . However, by using the nonlocal quantum channel she is able to accomplish the task, transferring the quantum state to Bob.

In this two-particle scheme Alice’s actions are simpler than in the three-particle scheme, since to make different degrees of freedom of the same particle interact is often easier than to make two different particles interact.

We will describe the two-particle protocol for quantum teleportation by going step by step through the optical experimental setup proposed in Ref. [77]. The first step is to produce two photons entangled in their direction of propagation, i.e. entangled in momentum, but each with a well-defined

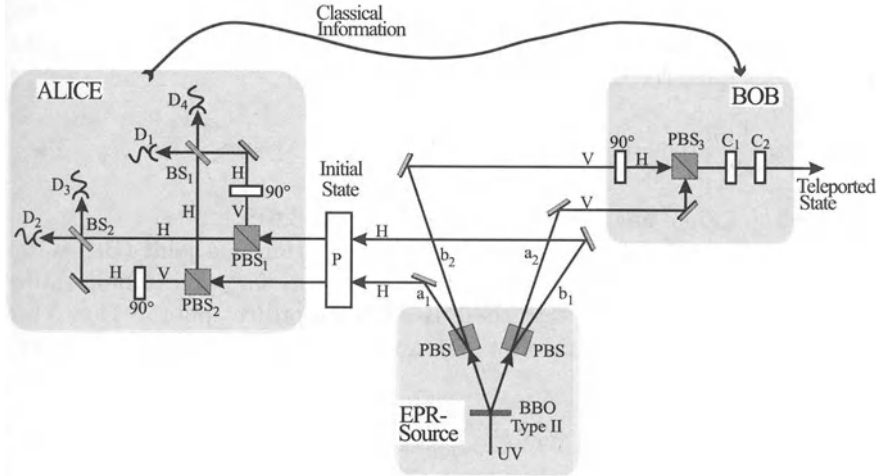


Fig. 3.17. Experimental scheme for the two-particle protocol for quantum teleportation. The setup consists of a type-II (BBO) down-conversion source for polarisation entangled photons, polarising beamsplitters (PBS), 50/50 beamsplitters (PB), single-photon detectors (D), 90° polarisation rotation plates, the Preparer (P) of the initial quantum state, and polarisation transformers (C).

polarisation. The box representing the EPR source in Fig. 3.17 shows how this can be achieved [78]. Using type-II parametric down-conversion, one first creates the polarisation entangled state

$$|\Psi^+\rangle = \frac{1}{\sqrt{2}} (|H\rangle_1 |V\rangle_2 + |V\rangle_1 |H\rangle_2), \quad (3.24)$$

where 1 and 2 label the two output directions of the correlated photons. Following this, both photons are passed through polarising beam splitters which deflect/transmit horizontal/vertical photons. This transfers the polarisation entanglement into momentum entanglement resulting in the state

$$\frac{1}{\sqrt{2}} (|a_1\rangle |a_2\rangle + |b_1\rangle |b_2\rangle) |H\rangle_1 |V\rangle_2. \quad (3.25)$$

Labels 1 and 2 now indicate the double channels that lead to Alice and Bob respectively. Photons with label 1 are necessarily H polarised and photons with label 2 necessarily V polarised. The momentum entangled photons form the nonlocal transmission channel.

On the way to Alice photon 1 is intercepted by the Preparer P who changes the polarisation from H to an arbitrary quantum superposition

$$|\Psi\rangle_1 = \alpha |H\rangle_1 + \beta |V\rangle_1. \quad (3.26)$$

The Prepare affects the polarisation in both paths a_1 and b_1 in the same way. The state $|\Psi\rangle_1$ is the quantum state that Alice wants to transmit to

Bob. Note that it is crucial that both the spatial and polarisation degrees of freedom of the quantum particles are being used.⁶ The total state $|\Phi\rangle$ of the two photons after the preparation is

$$|\Phi\rangle = \frac{1}{\sqrt{2}} (|a_1\rangle|a_2\rangle + |b_1\rangle|b_2\rangle) |\Psi\rangle_1|V\rangle_2, \quad (3.27)$$

which is the formal analogue of the state Ψ_{123} in (3.6).

The next step in the protocol is that Alice performs a joint (Bell-state) measurement on the initial state $|\Psi\rangle_1$ and on her part of the momentum entangled state. Assuming that there is a way to project photon 1 onto the four Bell states for its polarisation and momentum, we obtain the equivalent of (3.6):

$$\begin{aligned} |\Phi\rangle = \frac{1}{2} & [(|a_1\rangle|V\rangle_1 + |b_1\rangle|H\rangle_1)(\beta|a_2\rangle + \alpha|b_2\rangle)|V\rangle_2 \\ & + (|a_1\rangle|V\rangle_1 - |b_1\rangle|H\rangle_1)(\beta|a_2\rangle - \alpha|b_2\rangle)|V\rangle_2 \\ & + (|a_1\rangle|H\rangle_1 + |b_1\rangle|V\rangle_1)(\alpha|a_2\rangle + \beta|b_2\rangle)|V\rangle_2 \\ & + (|a_1\rangle|H\rangle_1 - |b_1\rangle|V\rangle_1)(\alpha|a_2\rangle - \beta|b_2\rangle)|V\rangle_2]. \end{aligned} \quad (3.28)$$

The first part of each term corresponds to a Bell state for photon 1 and the second part to the corresponding state of photon 2. In contrast to the case of the three-particle protocol, the projection of particle 1 onto the Bell-state basis does not pose a serious problem, and can be achieved with almost 100% efficiency. For the projection we have to entangle the polarisation and directional properties of photon 1. This can be done by using polarising beamsplitters in paths a_1 and b_1 , and by combining the V component coming from a_1 ($|a_1\rangle|V\rangle_1$) with the H component coming from b_1 ($|b_1\rangle|H\rangle_1$), and vice versa. The combination, sensitive to the relative phase, is obtained by rotating the photons to the same polarisation and letting them interfere on a normal beamsplitter. A photon detection by D_1 , D_2 , D_3 , or D_4 now corresponds directly to a projection onto one of the four Bell states.

The final step of the protocol is that Alice informs Bob which detector registered a photon. With this information Bob can reproduce the initial polarisation state as follows. He first transforms the momentum superposition of photon 2 (see (3.28)) into the same superposition in polarisation by simply using a 90° rotation plate in paths b_2 (or a_2) and a polarising beamsplitter to combine the paths. After this, he just switches two optical elements on or off, depending on the information obtained from Alice, to interchange H and V and to provide a relative phase shift of π between H and V . This transforms the polarisation state of photon 2 into the polarisation state prepared on photon 1, and thus completes the transmission.

⁶ M. Zukowski proposed to use both the spatial and polarisation degrees of freedom of particles for generating “three-particle” GHZ entanglement using only two particles [105].

An advantage of the present scheme is that it uses a full Bell-state measurement and only two particles in demonstrating two basic concepts of teleportation: it proves that quantum information can be decomposed into the classical and the genuine quantum part, and it displays the nonlocal transmission. Furthermore it has a high efficiency compared to the three-particle scheme described in the previous section.

A drawback of the scheme is that it does not allow Alice to teleport the state of an outside particle. Therefore it requires the Preparer's help: the initial polarisation state given to Alice has to be prepared on a particle which is momentum entangled with the one given to Bob. Also the state Ψ has to be pure, implying that it cannot be part of an entangled state.

We refer to Ref. [78] for details about the experimental realisation of the setup described above and for the experimental data confirming the transfer of the quantum state from Alice to Bob.

Acknowledgement: We are very grateful to S. Popescu for his help in preparing this section.

3.9 Teleportation of Continuous Quantum Variables

D. Bouwmeester

3.9.1 Employing Position and Momentum Entanglement

In this section we outline the basic idea of another scheme for quantum teleportation, proposed by L. Vaidman [79], further elaborated on by Braunstein and Kimble [80], and experimentally realised at Caltech [81]. This scheme uses position and momentum entanglement instead of polarisation entanglement. The result of this quantum teleportation scheme is that the position and momentum (defining the external state) of a quantum system are transferred to a distant quantum system, in contrast to the schemes discussed in Sects. 3.7 and 3.8 where the internal state (polarisation) was transferred. An important difference between position and momentum compared to polarisation is their representation in terms of superpositions of certain basis states. Position and momentum both require an infinite number of basis states since, to any two different positions or momenta there correspond two different eigenstates which are orthogonal (position eigenstates and momentum eigenstates form an infinite-dimensional Hilbert space). The polarisation of a particle can however be expressed as the superposition of only two basis states (polarisation has a two-dimensional Hilbert space).

Consider the case in which Alice has a quantum particle with a certain position x_1 and momentum p_1 (see Fig. 3.18), and she wishes to send this

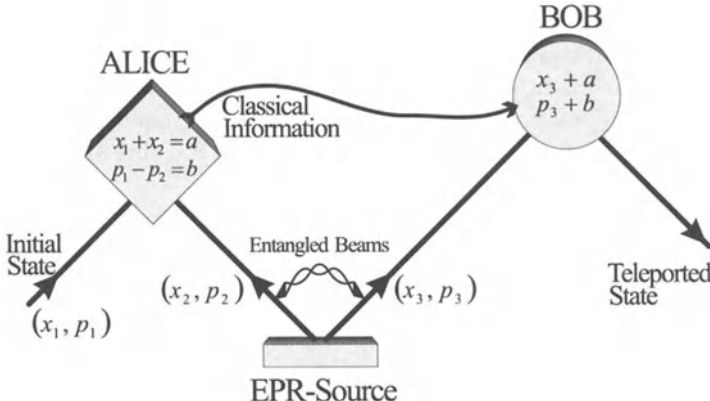


Fig. 3.18. Schematic drawing of quantum teleportation of continuous variables.

quantum information to Bob who is at a distant location. Due to the Heisenberg uncertainty relation between x and p , which follows from the fact that the operators for position and momentum do not commute, $[\hat{x}, \hat{p}] = i\hbar$, Alice cannot measure both x_1 and p_1 with arbitrary precision. Therefore, quantum mechanics forbids Alice to obtain the information she wishes to transfer. The way out of this dilemma is conceptually the same as the protocol described in Sect. 3.3. In the same manner an auxiliary pair of entangled particles, produced by the EPR source in Fig. 3.18, has to be distributed between Alice and Bob. However, the auxiliary particles should now be entangled in their position and momentum. Let us consider the case in which the entanglement of particles 2 and 3 is described by the conditions:

$$x_2 + x_3 = 0, \text{ and } p_2 - p_3 = 0. \quad (3.29)$$

The properties of the individual particles, x_2 , x_3 , p_2 , and p_3 are completely undetermined by (3.29). Instead, their joint properties are defined. Note that, although the operators \hat{x} and \hat{p} do not commute for each particle, the operators for $(x_2 + x_3)$ and $(p_2 - p_3)$ do commute as a result of the relative minus sign between the addition of the positions and the addition of momenta. Therefore, for the entangled state the joint properties, $(x_2 + x_3)$ and $(p_2 - p_3)$, can both be measured with an arbitrary accuracy.

The next step in the protocol is that Alice performs the equivalent of a Bell-state measurement on particles 1 and 2. That is, the state of particles 1 and 2 is projected onto an entangled state. In the case of teleportation of the internal (polarisation) state of a particle, there are only 4 possible outcomes for the Bell-state measurement since the polarisation entanglement between two particles, each individually with a two-dimensional Hilbert space, can be represented as a superposition of 4 basis states. In the present case the measurement by Alice yields

$$x_1 + x_2 = a, \text{ and } p_1 - p_2 = b, \quad (3.30)$$

where a and b are two real numbers which both have a continuous range of possible values. This indicates that the measurement of the sum of positions and the difference in momenta of the two particles requires the projection onto an (∞) -dim Hilbert space.

As a result of the initial entanglement (3.29) and of Alice's measurement (3.30), the information obtained about the quantum state in the hands of Bob is

$$x_3 = x_1 - a, \text{ and } p_3 = p_1 - b. \quad (3.31)$$

To complete the quantum teleportation protocol, all Alice has to do is to send Bob via a classical channel the results of her measurements, i.e. the measured values a and b , and then Bob just displaces the position and momentum of his particle by a and b , respectively. The final result is that Bob has particle 3 in the initial quantum state of particle 1.

3.9.2 Quantum Optical Implementation

The experimental implementation of quantum teleportation of continuous quantum variables has been performed at Caltech, California [81]. This implementation does not use the position x and momentum p of particles but uses light beams that can be characterized by parameters obeying the same commutation relations as \hat{x} and \hat{p} . The analogy is based on the fact that a single (transversal) mode of the quantized radiation field can be characterized by a quantum harmonic oscillator [106]–[109].

The classical harmonic oscillator of mass m , frequency ω , displacement x , and momentum p is described by the Hamiltonian

$$H = \frac{p^2}{2m} + \frac{m}{2}\omega^2 x^2. \quad (3.32)$$

To obtain the quantum-mechanical Hamiltonian, x and p should be interpreted as operators ($x \rightarrow \hat{x}$, and $p \rightarrow \hat{p} = i\hbar\partial/\partial x$) which obey the commutation relation $[\hat{x}, \hat{p}] = i\hbar$. If we define

$$\hat{x} = \sqrt{\frac{\hbar}{2m\omega}} (\hat{a}^\dagger + \hat{a}), \quad (3.33)$$

$$\hat{p} = i\sqrt{\frac{\hbar m\omega}{2}} (\hat{a}^\dagger - \hat{a}), \quad (3.34)$$

then the Hamiltonian for the quantized harmonic oscillator takes the natural form

$$\hat{H} = \hbar\omega \left(\hat{a}^\dagger \hat{a} + \frac{1}{2} \right). \quad (3.35)$$

The most important relations for \hat{a} and \hat{a}^\dagger are

$$\hat{a}|n\rangle = \sqrt{n}|n-1\rangle, \quad \hat{a}|0\rangle = 0, \quad (3.36)$$

$$\hat{a}^\dagger|n\rangle = \sqrt{n+1}|n+1\rangle, \quad (3.37)$$

$$[\hat{a}, \hat{a}^\dagger] = 1, \quad [\hat{a}, \hat{a}] = [\hat{a}^\dagger, \hat{a}^\dagger] = 0, \quad (3.38)$$

$$\hat{a}^\dagger\hat{a} = \hat{N}, \quad (3.39)$$

with $|n\rangle$ the n th-excited state of the quantum harmonic oscillator and \hat{N} the number operator. According to (3.36) and (3.37), \hat{a} and \hat{a}^\dagger can be interpreted as the annihilation (lowering) and creation (raising) operators for the harmonic oscillator.

A single transversal mode (frequency ω) of the quantized radiation field can be expressed in terms of the operators \hat{a} and \hat{a}^\dagger . In its most basic form, i.e. including all prefactors into a single constant E_0 and considering one polarisation direction, the electric field vector operator at a fixed position is given by

$$\hat{\tilde{E}}(t) = E_0 (\hat{a}e^{-i\omega t} - \hat{a}^\dagger e^{+i\omega t}), \quad (3.40)$$

where \hat{a}^\dagger and \hat{a} are now interpreted as the photon-creation and photon-annihilation operators. In analogy to the harmonic oscillator, we can define operators \hat{X} and \hat{P} via

$$\hat{X} = (\hat{a}^\dagger + \hat{a}), \quad (3.41)$$

$$\hat{P} = i(\hat{a}^\dagger - \hat{a}). \quad (3.42)$$

The electric field operator can now be expressed in terms of \hat{X} and \hat{P} as

$$\hat{\tilde{E}}(t) = E_0 \left(\hat{X} \cos(\omega t) + \hat{P} \sin(\omega t) \right). \quad (3.43)$$

The eigenvalues of \hat{X} and \hat{P} , referred to as the quadrature field amplitudes, can be interpreted as the amplitudes of the in- and out-of-phase components of the electric field (with respect to a local oscillator). From the commutation relation $[\hat{X}, \hat{P}] = 2i$ it follows that $\Delta X \Delta P = 1$ ($(\Delta A)^2 = \langle A^2 \rangle - \langle A \rangle^2$), which means that the in- and out-of-phase amplitudes cannot be simultaneously measured with arbitrary accuracy, in close analogy to the position x and momentum p of a quantum particle. Hence we have now established the mapping of x and p for a particle to X and P for a single-mode light field.

The next step towards an implementation of the quantum teleportation scheme with continuous parameters is to construct entangled light fields. To achieve this we need to introduce the notion of squeezed light [108]. It is instructive to visualise the quantum state of a single-mode light field in the X, Y plane. The vacuum state is represented by disc 1 around the origin in Fig. 3.19. Disc 2 in Fig. 3.19 represents a “coherent field” which is defined as a displaced vacuum field.

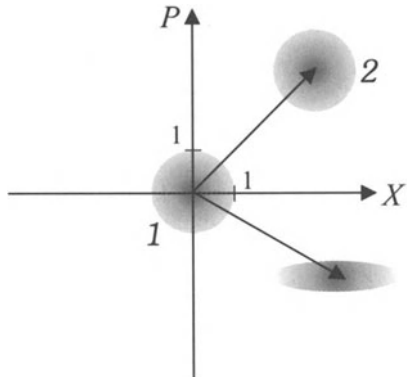


Fig. 3.19. Representation of single-mode light fields in the X (in-phase amplitude) and P (out-of-phase amplitude) plane. Disc 1, around the origin, indicates the symmetric minimum-uncertainty vacuum state. Disc 2 represents a coherent state which is defined as a displaced vacuum state. The ellipse represents a squeezed state (squeezed in the P direction).

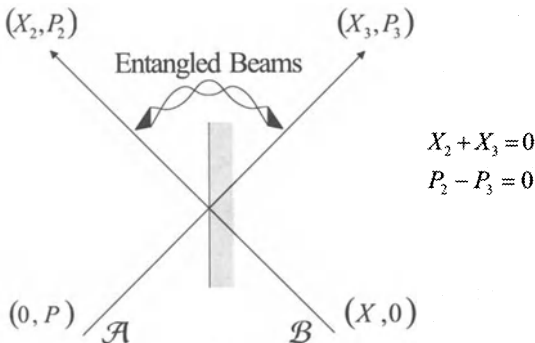


Fig. 3.20. Production of entangled light fields. Two light fields, \mathcal{A} and \mathcal{B} , maximally squeezed in X and Y , entering a 50/50 beamsplitter produce at the output of the beamsplitter a pair of entangled light beams.

The discs indicate the minimum uncertainty in the values for X and P . The uncertainty is symmetric in X and P , however this symmetry is not necessary in order to fulfill the relation $\Delta X \Delta P = 1$. The ellipse in Fig. 3.19 represents a squeezed state for which $(\Delta Y)^2 < 1$ and necessarily $(\Delta X)^2 > 1$.

Consider now the case of two light fields \mathcal{A} and \mathcal{B} maximally squeezed in X and Y , respectively, and let these beams enter the two input ports of a 50/50 beamsplitter as illustrated in Fig. 3.20. Behind the beamsplitter the fields labeled with 2 and 3 are characterized by the relations

$$X_2 + X_3 = 0, \text{ and } P_2 - P_3 = 0, \quad (3.44)$$

which specify precisely the desired entangled state [81]. (For polarisation entangled light fields see Refs. [110]–[112].)

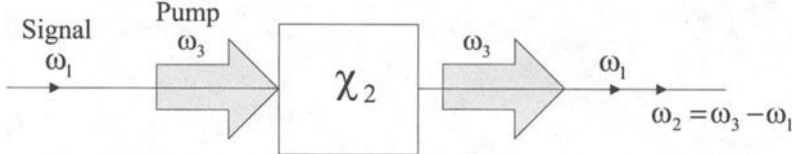


Fig. 3.21. Parametric amplification. An incoming signal field with frequency ω_1 is combined inside a nonlinear crystal (χ_2 material) with a strong pump field with frequency ω_3 . As a result of the nonlinear interaction, the signal field will be amplified and a third field will be created with the frequency $\omega_2 = \omega_3 - \omega_1$.

The production of squeezed states, as required for the generation of entangled light fields, is based on parametric amplification inside a nonlinear crystal [107, 112, 113]. An incoming signal field with frequency ω_1 will be combined inside a nonlinear crystal with a strong pump field with frequency ω_3 (see Fig. 3.21). As a result of the nonlinear interaction, the signal field will be amplified and a third field will be created with the frequency $\omega_2 = \omega_3 - \omega_1$. We consider the simplest case involving only one polarisation direction, assuming collinear phase matching, that is all fields propagate in the same direction, and taking the degenerate case of $\omega_1 = \omega_2 \equiv \omega$ and $\omega_3 = 2\omega$.

The evolution of the radiation field with frequency ω , interacting inside the crystal with the strong field at frequency 2ω , is described by the following Hamiltonian,

$$\hat{H} = \hbar\omega \left(\hat{a}^\dagger \hat{a} + \frac{1}{2} \right) + S \cos(2\omega t) (\hat{a}^\dagger - \hat{a})^2. \quad (3.45)$$

The second term on the right-hand side of (3.45) describes the interaction between the pump field, which is described classically, and the two fields at degenerate frequency ω . S is the coupling strength which depends on the nonlinearity inside the crystal and on the pump intensity. The principle of energy conservation reduces this interaction term to

$$S ((\hat{a})^2 e^{i2\omega t} - (\hat{a}^\dagger)^2 e^{-i2\omega t}). \quad (3.46)$$

The time evolution of the radiation field operator (we work in the Heisenberg representation in which the operators evolve as a function of time) is determined by the evolution equations for \hat{a} and \hat{a}^\dagger :

$$\frac{d\hat{a}}{dt} = -\frac{i}{\hbar} [\hat{a}, \hat{H}] = -i\omega\hat{a} - iS\hat{a}^\dagger e^{-i2\omega t}, \quad (3.47)$$

$$\frac{d\hat{a}^\dagger}{dt} = -\frac{i}{\hbar} [\hat{a}^\dagger, \hat{H}] = i\omega\hat{a}^\dagger + iS\hat{a} e^{+i2\omega t}. \quad (3.48)$$

This set of coupled equations decouples if we use the operators \hat{X} and \hat{P} as defined in (3.41) and (3.42). The evolution equations for the quadrature field-amplitude operators are simply

$$\frac{d\hat{X}}{dt} = S\hat{X}, \quad \frac{d\hat{P}}{dt} = -S\hat{P}, \quad (3.49)$$

which have the solutions

$$\hat{X}(t) = \hat{X}(0)e^{St}, \quad \hat{P}(t) = \hat{P}(0)e^{-St}. \quad (3.50)$$

As a function of the interaction time, t , the in-phase amplitude operator \hat{X} grows exponentially whereas the out-of-phase amplitude operator \hat{P} decreases exponentially. Degenerate parametric amplification thus acts as a phase-sensitive amplifier, providing gain to in-phase ($\varphi = 0 \text{mod}\pi$) signals and damping to out-of-phase ($\varphi = (\pi/2)\text{mod}\pi$) signals. In other words, the parametric amplification of a signal will squeeze the P component of the light field.

To enhance the interaction time, and hence the amount of squeezing, the nonlinear crystal is usually placed inside an optical cavity which is resonant with ω . Such a device is called an optical parametric oscillator (OPO). The cavity losses are kept slightly larger than the parametric amplification to prevent laser operation and hence the build up of very high intensity light fields which would introduce saturation effects (mixing of higher order nonlinearities) inside the crystal. In the experiment reported in Ref. [81] there was no external field at frequency ω injected in the OPO, so that only the vacuum is amplified.

Having described the production of EPR light fields using two squeezed light fields and a beamsplitter, we now turn to the problem of performing a Bell-state-like measurement. Whereas the Bell-state analyser for polarisation entangled states posed experimental problems, see Sect. 3.5, here the projection onto an entangled state is straightforward. Mixing the initial beam, characterized by (X_1, P_1) , with one beam coming from the EPR source, represented by (X_2, P_2) , onto a 50/50 beamsplitter, yields in the two output ports beams characterized by

$$(X_C, P_C) = (X_1 - X_2, P_1 - P_2), \text{ and } (X_D, P_D) = (X_1 + X_2, P_1 + P_2). \quad (3.51)$$

Using the balanced homodyne detection method (see e.g. Ref. [107]), Alice can now measure the X component of beam \mathcal{D} and the P component of \mathcal{C} , providing her with the values $a = X_1 + X_2$, and $b = P_1 - P_2$, respectively, as required for the quantum teleportation protocol. The balanced homodyne detection method is based on mixing of the signal field with a local oscillator on a 50/50 beamsplitter and the recording of the difference in the photocurrent (proportional to the field intensity) between two detectors in the output arms of the beamsplitter. The difference in measured intensity as a function of the phase φ of the local oscillator is given by [107]

$$I(\varphi) = C(X \sin \varphi + P \cos \varphi), \quad (3.52)$$

where C is an overall constant depending on the intensity of the local oscillator and on the properties of the detectors. Tuning the phase φ of the local oscillator, one can measure any superposition of the quadrature components.

Following the quantum teleportation scheme, Alice sends to Bob the measured values a and b and Bob has to displace the light field at his side accordingly. Bob can achieve the displacement experimentally by reflecting his light field from a partially reflecting mirror (say 99% reflection and 1% transmission) and adding through the mirror a field that has been phase and amplitude modulated according to the values a and b . In principle, Bob ends up with an almost perfect replica of the light field that was initially in the hands of Alice.

The actual experiment, reported in Ref. [81], requires several sophisticated experimental techniques, such as the generation of highly squeezed states and the precise alignment in positions and phases of the light fields. Imperfections in these techniques limited the quality, defined here as the measured overlap of the input state at Alice and the teleported state at Bob, to 0.58 ± 0.02 . This quality is, however, higher than the limit of 0.5 which can be obtained (under the assumption that the output state falls in the class of coherent states) by only classical communication between Alice and Bob.

Acknowledgement: We are very grateful to H.J. Kimble and E.S. Polzik for their useful comments on this section.

3.10 Entanglement Swapping: Teleportation of Entanglement

D. Bouwmeester, J.-W. Pan, H. Weinfurter, A. Zeilinger

Entanglement can be realised by having two entangled particles emerge from a common source [94, 114] (Sect. 3.4), or by allowing two particles to interact with each other [103, 115] (Sects. 4.3, 5.2.4 and 5.2.11). Yet, another possibility to obtain entanglement is to make use of a projection of the state of two particles onto an entangled state. This projection measurement does not necessarily require a direct interaction between the two particles: When each of the particles is entangled with one other partner particle, an appropriate measurement, for example, a Bell-state measurement, of the partner particles will automatically collapse the state of the remaining two particles into an entangled state. This striking application of the projection postulate is referred to as entanglement swapping [74, 85, 87].

Consider two EPR sources, each simultaneously emitting a pair of entangled particles (Fig. 3.22). In anticipation of the experiments described below, we assume that these are polarisation entangled photons in the state

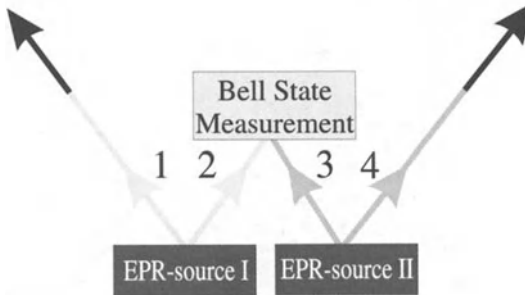


Fig. 3.22. Principle of entanglement swapping. Two EPR sources produce two pairs of entangled photons, pair 1-2 and pair 3-4. One photon from each pair (photons 2 and 3) is subjected to a Bell-state measurement. This results in a projection the other two outgoing photons, 1 and 4, onto an entangled state. Change of shading of the lines indicates the change in the set of possible predictions that can be made.

$$|\Psi\rangle_{1234} = \frac{1}{2} (|H\rangle_1 |V\rangle_2 - |V\rangle_1 |H\rangle_2) (|H\rangle_3 |V\rangle_4 - |V\rangle_3 |H\rangle_4). \quad (3.53)$$

The total state describes the fact that photons 1 and 2 (3 and 4) are entangled in an antisymmetric polarisation state. Yet, the state of pair 1-2 is factorisable from the state of pair 3-4, that is, there is no entanglement of either of the photons 1 or 2 with either of the photons 3 or 4.

We now perform a joint Bell-state measurement on photons 2 and 3, that is, photons 2 and 3 are projected onto one of the four Bell states (see Sect. 3.5). This measurement also projects photons 1 and 4 onto a Bell state, one that depends on the result of the Bell-state measurement for photons 2 and 3. Close inspection shows that for the initial state given in (3.53) the emerging state of photons 1 and 4 will be identical to the one onto which photons 2 and 3 are projected. This is a consequence of the fact that the state of (3.53) can be rewritten as

$$\begin{aligned} |\Psi\rangle_{1234} = \frac{1}{2} (& | \Psi^+ \rangle_{14} | \Psi^+ \rangle_{23} - | \Psi^- \rangle_{14} | \Psi^- \rangle_{23} \\ & - | \Phi^+ \rangle_{14} | \Phi^+ \rangle_{23} + | \Phi^- \rangle_{14} | \Phi^- \rangle_{23}). \end{aligned} \quad (3.54)$$

In all cases photons 1 and 4 emerge entangled, despite the fact that they never interacted in the past. After projection of particles 2 and 3 one knows about the entanglement between particles 1 and 4.

As already noted in Sect. 3.7.2, entanglement swapping can also be viewed as the teleportation of an entangled state, and the experimental setup (Fig. 3.23) used for its demonstration is similar to the teleportation setup shown in Fig. 3.12. We refer to Sect. 3.7 for a description of the common features of the setups. The essential difference between the two experiments is that in the teleportation scheme for single qubits (Fig. 3.12) photon 4 played the role of a trigger, indicating the presence of photon 1, whereas here (Fig. 3.23) the entanglement between each pair of photons is fully utilised.

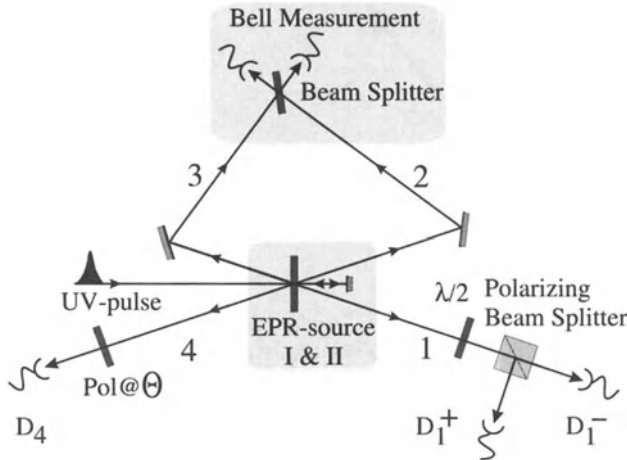


Fig. 3.23. Experimental setup. A UV pulse passing through a nonlinear crystal creates pair 1-2 of entangled photons. Photon 2 is directed to the beamsplitter. After reflection, during its second passage through the crystal the UV pulse creates a second pair 3-4 of entangled photons. Photon 3 will also be directed to the beamsplitter. When photons 2 and 3 yield a coincidence click at the two detectors behind the beamsplitter they are projected into the $|\Psi^-\rangle_{23}$ state. As a consequence of this Bell-state measurement the two remaining photons 1 and 4 will also be projected into an entangled state. To analyse their entanglement one looks at coincidences between detectors D_1^+ and D_4 , and between detectors D_1^- and D_4 , for different polarisation angles Θ . By rotating the $\lambda/2$ plate in front of the polarising beam-splitter one can analyse photon 1 in any linear polarisation basis. Note that, since the detection of coincidences between detectors D_1^+ and D_4 , and D_1^- and D_4 are conditional on the detection of the Ψ^- state, one looks at 4-fold coincidences.

Entanglement swapping can be seen as teleportation either of the state of photon 2 over to photon 4 or the state of photon 3 over to photon 1. Those viewpoints are completely equivalent. The remarkable feature of the scheme is that the state actually teleported is a photon state which is not well defined. As is well known, the state of a particle which is maximally entangled to another has to be described by a maximally mixed density matrix. Therefore, what is teleported in such a situation is not the quantum state of the photon but just the way in which it was entangled with another photon.

According to the entanglement swapping scheme, upon projection of photons 2 and 3 onto the $|\Psi^-\rangle_{23}$ state, photons 1 and 4 should be projected onto the $|\Psi^-\rangle_{14}$ state. To verify that this entangled state is obtained we have to analyse the polarisation correlations between photons 1 and 4 conditional on coincidences between the detectors of the Bell-state analyser. If photons 1 and 4 are in the $|\Psi^-\rangle_{14}$ state their polarisations should be orthogonal upon measurement in any polarisation basis. Using a $\lambda/2$ retardation plate at 22.5° and two detectors (D_1^+ and D_1^-) behind a polarising beam splitter, one can analyse the polarisation of photon 1 along the $+45^\circ$ axis (D_1^+) and the -45°

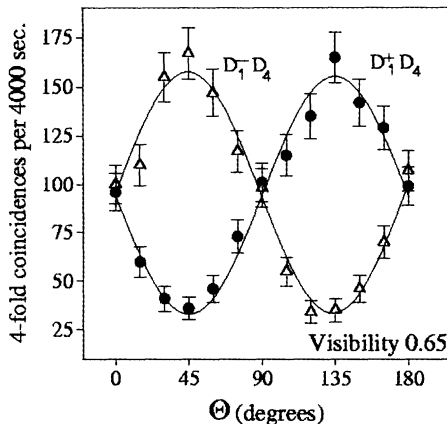


Fig. 3.24. Entanglement verification. Four-fold coincidences, resulting from two-fold coincidences $D1^+D4$ and $D1^-D4$ conditional on the two-fold coincidences at the Bell-state measurement, when varying the polariser angle Θ . The two complementary sine curves with a visibility of 0.65 ± 0.02 demonstrate that photons 1 and 4 are polarisation entangled.

axis ($D1^-$). Photon 4 is analysed by detector D4 at the variable polarisation direction Θ .

If entanglement swapping occurs, then the two-fold coincidences between $D1^+$ and D4, and between $D1^-$ and D4, conditional on the $|\Psi^-\rangle_{23}$ detection, should show two sine curves as a function of Θ which are 90° out of phase. The $D1^+D4$ curve should, in principle, go to zero for $\Theta = 45^\circ$ whereas the $D1^-D4$ curve should show a maximum at this position. Figure 3.24 shows the experimental results for the coincidences between $D1^+$ and D4, and between $D1^-$ and D4, given that photons 2 and 3 have been registered by the two detectors in the Bell-state analyser.

Note that this method requires four-fold coincidences. The result clearly demonstrates the expected sine curves, complementary for the two detectors ($D1^+$ and $D1^-$), registering photon 1 along orthogonal polarisations. By additional measurements it was verified that the sine curves are independent (up to the corresponding shift in Θ) of the detection basis of photon 1, that is, independent of the rotation angle of the $\lambda/2$ retardation plate. The observed visibility of 0.65 clearly surpasses the 0.5 limit of a classical wave theory. Note that this result is a realisation of quantum teleportation in a clear quantum situation, since entanglement between two particles that did not share a common origin nor interacted with one another in the past is the very result of the procedure. In the following section several applications of entanglement swapping will be presented.

3.11 Applications of Entanglement Swapping

S. Bose, V. Vedral and P.L. Knight

Entanglement swapping can be used for a number of practical purposes: constructing a *quantum telephone exchange*, to *speed up* the distribution of entangled particles between two parties, in a sort of *series purification* and for the *construction of entangled states involving higher number of particles* [87]. We describe these applications in some detail below.

3.11.1 Quantum Telephone Exchange

Suppose there are N users in a communication network. To begin with, each user of the network needs to share entangled pairs of particles (in a Bell state) with a central exchange. Consider Fig. 3.25 : A, B, C and D are users who share the Bell pairs (1,2), (3,4), (5,6) and (7,8) respectively with a central exchange O. Now suppose that A, B and C wish to share a GHZ triplet. Then a measurement which projects particles 2, 3 and 5 to GHZ states will have to be performed at O. Immediately, particles 1, 4 and 6 belonging to A, B and C respectively will be reduced to a GHZ state. In a similar manner one can entangle particles belonging to any N users of the network and create a N -particle cat state.

The main advantages of using this technique for establishing entanglement over the simple generation of N -particle entangled states at a source and their subsequent distribution are as follows.

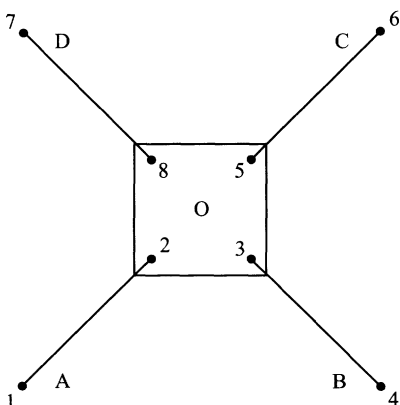


Fig. 3.25. The configuration used for the distribution of entanglement. Initially users A,B,C and D share Bell pairs with the central exchange O. Subsequently, a local measurement at O is sufficient to entangle particles belonging to any subset of users chosen from A, B, C and D .

(A) Firstly, each user can at first purify a large number of partially decohered Bell pairs shared with the central exchange to obtain a smaller number of pure shared Bell pairs. These can then be used as the starting point for the generation of any types of multiparticle cat states of the particles possessed by the users. The problems of decoherence during propagation of the particles can thus be avoided (at least in principle). Also the necessity of having to purify N -particle cat states can be totally avoided. Purification of singlets followed by our scheme will generate N -particle cats in their purest form.

(B) Secondly, our method allows a certain degree of freedom to entangle particles belonging to any set of users only if the necessity arises. It may not be known in advance exactly which set of users will need to share an N -particle cat state. To arrange for all possibilities in an a priori fashion would require selecting all possible combinations of users and distributing particles in multiparticle entangled states among them. That is very uneconomical. On the other hand, generating entangled N -tuplets at the time of need and supplying them to the users who wish to communicate is definitely time consuming.

Biham, Huttner and Mor [116] have developed a similar scheme of cryptographic network with exchanges using a time reversed EPR scheme for setting up the connections.

3.11.2 Speeding up the Distribution of Entanglement

We now explain how standard entanglement swapping helps to save a significant amount of time when one wants to supply two distant users with a pair of atoms or electrons (or any particle possessing mass) in a Bell state from some central source. The trick is to place several Bell-state-producing and Bell-state-measuring substations in the route between them. Consider Fig. 3.26a: A and B are two users separated by a distance L ; O, which is situated midway between A and B is a source of Bell pairs. The time needed for the particles to reach A and B is at least $t_1 = L/2v$ where $v < c$ (the speed of light) is the speed of the particles. Now consider Fig. 3.26b in which two Bell pair producing stations C and D are introduced halfway between AO and BO, respectively, and O is now just a Bell state measuring station. At $t = 0$, both C and D send off Bell pairs (1,2) and (3,4) respectively. 2 and 3 arrive at O, 1 reaches A and 4 reaches B. They all arrive at their destinations exactly at $t = L/4v$. At this instant a Bell state measurement is performed on particles 2 and 3 at O. This measurement immediately reduces the particles 1 and 4 reaching A and B respectively, to a Bell state. If the time of measurement is denoted by t_m , then the time needed to supply a Bell pair to A and B with the two extra substations C and D on the path is $t_2 = L/4v + t_m$. It is evident that t_2 is less than t_1 if $t_m < L/4v$. Of course, to this time one must add the time needed to classically communicate between the station O and the users A and B the particular Bell state to which particles 1 and 4 are projected. So for photons in Bell states, this procedure does not really

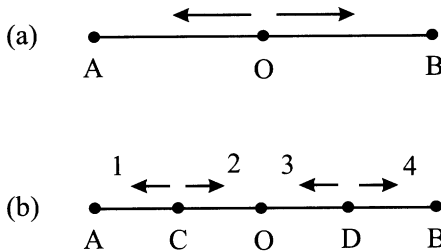


Fig. 3.26. A method of increasing the speed of distributing an entangled pair of particles (with nonzero mass) between two distant users A and B is illustrated. Extra Bell-state-generating substations C and D are inserted between A and B and a Bell-state projection is performed at O to speed up the distribution of a Bell pair between A and B.

save any time. But for particles possessing mass, this is definitely one way to reduce the time needed to supply two distant users with a Bell pair. In this way one can reduce the time needed to supply two distant users with a Bell pair even further by including more and more Bell pair producing and measuring substations on the way.

3.11.3 Correction of Amplitude Errors Developed due to Propagation

We would like to show that entanglement swapping can be used, with some probability which we quantify, to correct amplitude errors that might develop in maximally entangled states during propagation. Assume that in Fig. 3.26b, the Bell pairs emitted from C and D acquire amplitude errors and become less entangled states of the type

$$|\Psi\rangle = \cos\theta|01\rangle + \sin\theta|10\rangle. \quad (3.55)$$

Thus, the combined state of the two entangled pairs, when particles 2 and 3 reach O is given by,

$$\begin{aligned} |\Phi\rangle = & \cos^2\theta|0101\rangle + \sin\theta\cos\theta(|1001\rangle \\ & + |0110\rangle) + \sin^2\theta|1010\rangle. \end{aligned} \quad (3.56)$$

If a Bell state measurement is now performed on particles 2 and 3 that reach O, then the probability of them being projected onto the Bell states $|00\rangle + |11\rangle$ or $|00\rangle - |11\rangle$ is $\sin^2 2\theta/2$, while the probability of them being projected onto any of the other two Bell states is $(1 + \cos^2 2\theta)/2$. In the first case (i.e when 2 and 3 get projected to $|00\rangle + |11\rangle$ or $|00\rangle - |11\rangle$), the distant particles 1 and 4 are projected onto the Bell states $|00\rangle + |11\rangle$ or $|00\rangle - |11\rangle$. In this way in spite of amplitude errors due to propagation of the particles, A and B may finally share a Bell state. Of course in case of the other two outcomes of the state of particles 2 and 3, particles 1 and

4 go to states even less entangled than that of (3.55). That is why we can consider entanglement swapping suitable for correction of amplitude errors only probabilistically. The probability of success in this case ($\sin^2 2\theta/2$), is lower than the probability of failure ($(1 + \cos^2 2\theta)/2$). However, from the outcome of the Bell-state measurement, one knows when the correction has been successful. This may be regarded as a kind of purification in series, in contrast to the standard purifications [47, 117] (see Sect. 8.2) which occur in parallel. It can be shown that there is a measure of entanglement which is conserved in this type of purification process [118] (see also Sect. 6.4 for measures of entanglement).

3.11.4 Entangled States of Increasing Numbers of Particles

Entangled states involving higher numbers of particles can be generated from entangled states involving lower numbers of particles by employing our scheme. The basic ingredients which we need are GHZ (three particle maximally entangled) states and a Bell state measuring device. Let us describe how to proceed from an N -particle maximally entangled state to an $N + 1$ -particle maximally entangled state. One has to take one particle from the N -particle maximally entangled state and another particle from a GHZ state and perform a Bell state measurement on these two particles. The result will be to put these two particles in a Bell state and the remaining $N + 1$ particles in a maximally entangled state. Symbolically, the way to proceed from an N -particle maximally entangled state to a $N + 1$ -particle maximally entangled state is given by

$$|E(N)\rangle \otimes |E(3)\rangle \xrightarrow{\text{Bell State Meas.}} |E(N+1)\rangle \otimes |E(2)\rangle.$$

An example of proceeding from a 4 particle maximally entangled state to a 5 particle maximally entangled state by the above procedure is shown in Fig.3.27.

As far as the question of generating the GHZ state, which is a basic ingredient, is concerned, one can perhaps use the method suggested by Zeilinger et al. [119] (see also Sect. 6.3.4 for the generation of three-photon entanglement) Alternatively, one can generate GHZ states using our method by starting from three Bell pairs and performing a GHZ state measurement, taking one particle from each pair. An explicit scheme, for producing 3-particle GHZ states from 3 entangled pairs was suggested earlier by Zukowski et al. [101].

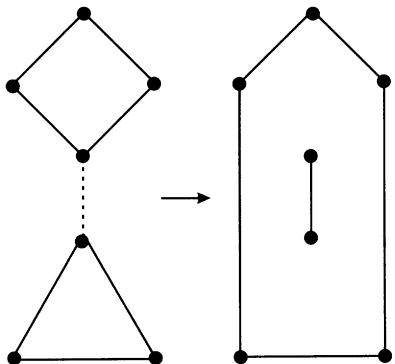


Fig. 3.27. Building of a 5 particle entangled state from a 4 particle entangled state using a GHZ state and a Bell state measurement

4. Concepts of Quantum Computation

There are many ways and levels of explaining quantum computation. This chapter is intended to reflect this fact. It is composed of the three self-contained sections. The first one gives a very basic introduction to the subject stressing the fundamental issues and avoiding mathematical formalism. Many may find this level of explanation adequate for their purposes. Those who want to become familiar with details are encouraged to proceed to the second section. It takes the reader from the very first quantum algorithms, through the discussion of computational complexity, to more advanced topics, such as quantum factoring. Last but not least, the third section provides a proposal for converting esoteric theoretical ideas into working devices. Chapter 5 presents experimental achievements to date and continuing efforts to make further progress in quantum computation.

4.1 Introduction to Quantum Computation

D. Deutsch and A. Ekert

4.1.1 A New Way of Harnessing Nature

Many milestones in the history of technology have involved the discovery of new ways of harnessing nature — exploiting various physical resources such as materials, forces, and sources of energy. In the twentieth century *information* was added to this list when the invention of computers allowed complex information processing to be performed outside human brains. The history of computer technology has itself involved a sequence of changes from one type of physical realisation to another — from gears to relays to valves to transistors, integrated circuits and so on. Today's advanced lithographic techniques can etch logic gates and wires less than a micron across onto the surfaces of silicon chips. Soon they will yield even smaller components, until

we reach the point where logic gates are so small that they consist of only a few atoms each.

On the scale of human perception and above, classical (non-quantum) laws of physics are good phenomenological approximations, but on the atomic scale the laws of quantum mechanics become dominant, and they have quite a different character. If computers are to continue to become faster (and therefore smaller), new, *quantum* technology must replace or supplement what we have now, but it turns out that such technology can offer much more than smaller and faster microprocessors. It can support entirely new modes of computation, with new quantum algorithms that do not have classical analogues. And more: the quantum theory of computation plays an even more fundamental role in the scheme of things than its classical predecessor did, so that anyone seeking a fundamental understanding of either physics or information processing must incorporate its new insights into their world view.

4.1.2 From Bits to Qubits

What makes quantum computers so different from their classical counterparts? Let us take a closer look at the basic unit of information: the *bit*. Although bits and qubits have already been explained in Chap.1, we have decided, for the completeness and consistency of this exposition, to mention them again.

From a physical point of view a bit is a two-state system: it can be prepared in one of two distinguishable states representing two logical values — no or yes, false or true, or simply 0 or 1. For example, in digital computers, the voltage between the plates of a capacitor can represent a bit of information: a charge on the capacitor denotes 1 and the absence of charge denotes 0. One bit of information can also be encoded using, for instance, two different polarisations of light or two different electronic states of an atom. Now, quantum mechanics tells us that if a bit can exist in either of two distinguishable states, it can also exist in *coherent superpositions* of them. These are further states, which in general have no classical analogues, in which the atom represents *both* values, 0 and 1, simultaneously. To get used to the idea that a physical quantity can have two values at once, it is helpful to consider the experiment in Fig. 4.1.

A half-silvered mirror is one that reflects half the light that impinges upon it, while allowing the remaining half to pass through unaffected. Let us aim a single photon at such a mirror, as in Fig. 4.1. What happens? One thing we know is that the photon doesn't split in two: we can place photodetectors wherever we like in the apparatus, fire in a photon, and verify that if any of the photodetectors registers a hit, none of the others do. In particular, if we place a photodetector behind the mirror in each of the two possible exit beams, the photon is detected with equal probability at either detector. So does the photon leave the first mirror in one of the two possible directions, at random? It does not! It may seem obvious that at the very least, the photon

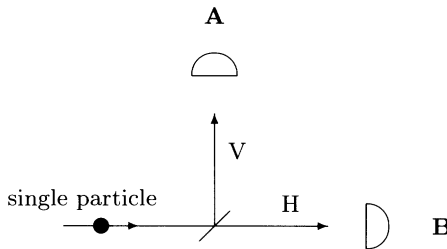


Fig. 4.1. A half-silvered mirror reflects half the light that impinges upon it. But a single photon doesn't split: when we send a photon towards such a mirror it is detected, with equal probability, either at detector A or B. This does not, however, mean that the photon leaves the mirror in either the horizontal (H) or the vertical (V) direction at random. In fact the photon takes both paths at once! This can be demonstrated with the help of a slightly more complicated experiment shown in Fig. 4.2.

is *either* in the transmitted beam H *or* in the reflected beam V during any one run of this experiment. But that is not so either. In fact the photon takes both paths at once, as can be demonstrated with the help of the apparatus shown in Fig. 4.2. Two normal mirrors are placed so that both paths intersect at a second half-silvered mirror. With this setup we can observe the astonishing, purely quantum phenomenon of *single-particle interference*.

Suppose that a particular photon followed the horizontal path marked H in Fig. 4.2 after striking the mirror. Then (by comparison with Fig. 4.1) we should find that the two detectors registered hits with equal probability.

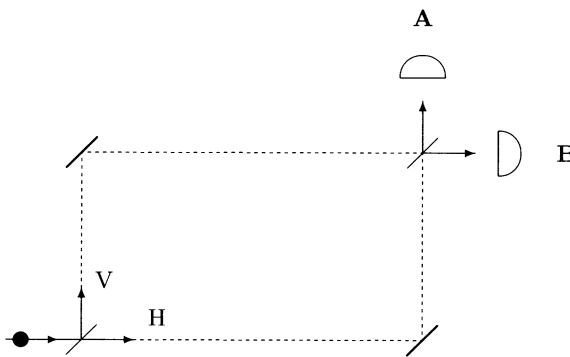


Fig. 4.2. Single-particle interference. A photon which enters the interferometer always strikes detector A and never detector B. Any explanation which assumes that the photon takes exactly one path through the interferometer — either H or V — leads to the conclusion that detectors A and B should on average each fire on half the occasions when the experiment is performed. But experiment shows otherwise.

Exactly the same would be observed if the photon were on the vertical path V. Hence if it were really the case that the photon takes exactly one path through the apparatus — no matter which one — detectors A and B would on average each fire on half the occasions when the experiment is performed. However, that is not what happens. It turns out that in the arrangement shown, the photon *always* strikes detector A and *never* detector B.

The inescapable conclusion is that the photon must, in some sense, have travelled both routes at once — for if either of the two paths is blocked by an absorbing screen, it immediately becomes equally probable that A or B is struck. In other words, blocking off either of the paths illuminates B; with both paths open, the photon somehow receives information that prevents it from reaching B, information that travels along the other path at the speed of light, bouncing off the mirror, exactly as a photon would. This property of quantum interference — that there seem to be invisible counterparts affecting the motion of particles that we detect — applies not only to photons but to all particles and all physical systems. Thus quantum theory describes an enormously larger reality than the universe we observe around us. It turns out that this reality has the approximate structure of multiple variants of that universe, co-existing and affecting each other only through interference phenomena — but for the purposes of this article, all we need of this “parallel universes” ontology is the fact that what we see as a single particle is actually only one tiny aspect of a tremendously complex entity, the rest of which we cannot detect directly. Quantum computation is all about making the invisible aspects of the particle — its counterparts in other universes — work for us.

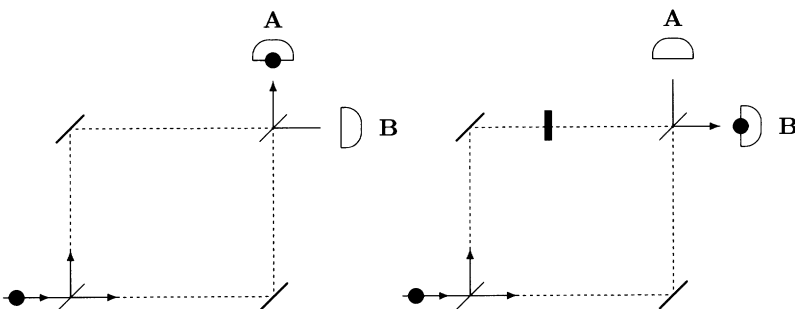


Fig. 4.3. A sliver of glass inserted into one of the two paths in the interferometer can redirect photons from one detector to another. All photons that enter the left interferometer strike detector A. In the right interferometer, the interference is modified by the presence of the sliver of glass on the vertical path, and as a result all photons end up in detector B. Thus something that has happened on only one of the paths has, with certainty, changed the final outcome of the experiment. This effect is especially useful in quantum computation.

One effect that is especially useful in quantum computation can be demonstrated if we delay the photon on one of the paths H or V. This can be done by inserting a sliver of glass into that path, as illustrated in Fig. 4.3. Since the interference between the photon and its invisible counterpart depends on their exact arrival times, we can, for instance, choose the thickness of the glass, and hence the delay time, in such a way that the photon will certainly (i.e. in all universes) emerge at detector B instead of detector A. Thus something that has happened on only one of the paths (and hence in only one of the universes) has affected both of them. We shall return to this point below.

Just as the photon can be in a coherent superposition of being on the path H and on the path V, any quantum bit, or *qubit*, can be prepared in a superposition of its two logical states 0 and 1. That is the sense in which a qubit can store both 0 and 1 simultaneously, in arbitrary proportions. But note that just as the photon, if measured, will be detected on only one of the two paths, likewise if the qubit is measured, only one of the two numbers it holds will be detected, at random: not a very useful property in itself.

But now let us push the idea of superpositions of numbers a little further. Consider a register composed of three physical bits. A classical 3-bit register can store exactly one of eight different numbers i.e the register can be in one of the eight possible configurations 000, 001, 010, ..., 111, representing the numbers 0 to 7. But a quantum register composed of three qubits can simultaneously store up to eight numbers in a quantum superposition. It is quite remarkable that eight different numbers can be physically present in the same register; but it should be no more surprising than the numbers 0 and 1 both being present in the same qubit. If we add more qubits to the register its capacity for storing quantum information increases exponentially: four qubits can store 16 different numbers at once, and in general L qubits can store up to 2^L numbers at once. A 250-qubit register — essentially made of 250 atoms, say — would be capable of holding more numbers simultaneously than there are atoms in the known universe. (If anything, this *understates* the amount of quantum information that they hold, for in general, the elements of a superposition are present in continuously variable proportions, each with its own phase angle as well.) Even so, if we measure the register's contents, we will see only one of those numbers. However, now we can start doing some non-trivial quantum computation, for once the register is prepared in a superposition of many different numbers, we can perform mathematical operations on all of them at once.

For example, if the qubits are atoms then suitably tuned laser pulses affect their electronic states and cause initial superpositions of encoded numbers to evolve into different superpositions. During such an evolution each number in the superposition is affected, so we are performing a massive parallel computation. Thus a quantum computer can in a single computational step perform the same mathematical operation on, say, 2^L different input numbers, and the result will be a superposition of all the corresponding outputs. In order

to accomplish the same task any classical computer has to repeat the computation 2^L times, or has to use 2^L different processors working in parallel. In this way a quantum computer offers an enormous gain in the use of computational resources such as time and memory — though only in certain types of computation.

4.1.3 Quantum Algorithms

What types? As we have said, ordinary information storage is not one of them, for although the computer now holds all the outcomes of 2^L computations, the laws of physics only allow us to see one of them. However, just as the single answer “A” in the experiment of Fig. 4.2 depends on information that travelled along each of two paths, quantum interference now allows us to obtain a single, final result that depends logically on all 2^L of the intermediate results.

This is how a remarkable quantum algorithm recently discovered by Lov Grover of AT&T’s Bell Laboratories in New Jersey [120] achieves the mind-boggling feat of searching an unsorted list of N items in only \sqrt{N} or so steps. Consider, for example, searching for a specific telephone number in a directory containing a million entries, stored in the computer’s memory in alphabetical order of names. It is easily proved (and obvious) that no classical algorithm can improve on the brute-force method of simply scanning the entries one by one until the given number is found, which will, on average, require 500,000 memory accesses. A quantum computer can examine all the entries simultaneously, in the time of a single access. However, if it is merely programmed to print out the result at that point, there is no improvement over the classical algorithm: only one of the million computational paths (i.e. one in a million universes) would have checked the entry we are looking for, so there would be a probability of only one in a million that we would obtain that information if we measured the computer’s state. But if we leave that quantum information in the computer, unmeasured, a further quantum operation can cause that information to affect other paths, just as in the simple interference experiment described above. In this way the information about the desired entry is spread, through quantum interference, to more universes. It turns out that if this interference-generating operation is repeated about 1000 times, (in general, \sqrt{N} times) the information about which entry contains the desired number will be accessible to measurement with probability 0.5 — i.e. it will have spread to more than half the universes. Therefore repeating the entire algorithm a few more times will find the desired entry with a probability overwhelmingly close to 1.

In addition to finding the entry with a given property, variations on Grover’s search algorithm can also find the largest or smallest value in a list, or the modal value, and so on, so it is a very versatile searching tool. However, in practice, searching a physical database is unlikely to become a major application of Grover’s algorithm — at least so long as classical

memory remains cheaper than quantum memory. For since the operation of transferring a database from classical to quantum memory (bits to qubits) would itself require $O(N)$ steps, Grover's algorithm would improve search times by at best a constant factor, which could also be achieved by classical parallel processing. Where Grover's algorithm would really come into its own is in *algorithmic* searches — that is, searches of lists that are not stored in memory but are themselves generated on the fly by a computer program. For instance, a chess-playing quantum computer could use it to investigate a trillion possible continuations from a given position in roughly the number of steps that a classical computer (using blind “brute-force” searching) would need to investigate a mere million. Despite the greater scope for “tree-pruning” in classical chess-playing algorithms, this is likely to provide a very significant improvement.

As Gilles Brassard of the Université de Montréal has recently pointed out [121], another important application of Grover's algorithm will be in cryptanalysis, to attack classical cryptographic schemes such as DES (the Data Encryption Standard, see Chap. 2 on quantum cryptography). Cracking DES essentially requires a search among $2^{56} = 7 \times 10^{16}$ possible keys. If these can be checked at a rate of, say, one million keys per second, a classical computer would need over a thousand years to discover the correct key while a quantum computer using Grover's algorithm would do it in less than four minutes!

By some strange coincidence, several of the superior features of quantum computers have applications in cryptography. One of them is Grover's algorithm. Another is the quantum algorithm discovered in 1994 by Peter Shor, also of AT&T's Bell Laboratories in New Jersey, for factorising large integers efficiently [36]. Here the difference in performance between the quantum and classical algorithms is even more spectacular. Mathematicians believe (firmly, though they have not actually proved it) that in order to factorise a number with N decimal digits, any classical computer needs a number of steps that grows exponentially with N : that is to say, adding one extra digit to the number to be factorised generally *multiplies* the time required by a fixed factor (see Sect. 4.2). Thus, as we increase the number of digits, the task rapidly becomes intractable. The largest number that has been factorised as a mathematical challenge, i.e. a number whose factors were secretly chosen by mathematicians in order to present a challenge to other mathematicians, had 129 digits. No one can even conceive of how one might factorise, say, thousand-digit numbers by classical means; the computation would take many times as long the estimated age of the universe. In contrast, quantum computers could factor thousand-digit numbers in a fraction of a second — and the execution time would grow only as the cube of the number of digits.

Now, the intractability of factorisation underpins the security of what are currently the most trusted methods of encryption, in particular of the RSA (Rivest, Shamir and Adleman) system, which is often used to protect

electronic bank accounts [122] (for details see Chap. 2). Once a quantum factorisation engine (a special-purpose quantum computer for factorising large numbers) is built, all such cryptographic systems will become insecure.

The potential power of quantum phenomena to perform computations was first adumbrated in a talk given by Richard Feynman at the First Conference on the Physics of Computation, held at MIT in 1981. He observed that it appeared to be impossible in general to simulate the evolution of a quantum system on a classical computer in an efficient way [123]. The computer simulation of quantum evolution typically involves an exponential slowdown in time, compared with the natural evolution, essentially because the amount of classical information required to describe the evolving quantum state is exponentially larger than that required to describe the corresponding classical system with a similar accuracy. (To predict interference effects, one has to describe all the system's exponentially many counterparts in parallel universes.) However, instead of viewing this intractability as an obstacle, Feynman regarded it as an opportunity. He pointed out that if it requires that much computation to work out what will happen in a multi-particle interference experiment, then the very act of setting up such an experiment and measuring the outcome is equivalent to performing a complex computation.

Quantum computation has already been used, in simple cases, to predict the behaviour of quantum systems. At some point in the foreseeable future, they will take on a new and irreplaceable role in the structure of science, for the ability of science to make predictions will then depend on quantum computation.

The foundations of the quantum theory of computation (which must now be regarded as *the* theory of computation — Turing's classical theory being only an approximation) were laid down in 1985 when David Deutsch of the University of Oxford published a crucial theoretical paper in which he described a *universal quantum computer* [124]. Since then, the hunt has been on for interesting things for quantum computers to do, and at the same time, for the scientific and technological advances that could allow us to build quantum computers.

4.1.4 Building Quantum Computers

In principle we know how to build a quantum computer; we start with simple quantum logic gates (see Chap. 1) and connect them up into quantum networks.

A quantum logic gate, like a classical gate, is a very simple computing device that performs one elementary quantum operation, usually on two qubits, in a given time [125]. Of course, quantum logic gates differ from their classical counterparts in that they can create, and perform operations, on quantum superpositions. However as the number of quantum gates in a network increases, we quickly run into some serious practical problems. The more interacting qubits are involved, the harder it tends to be to engineer the interaction that

would display the quantum interference. Apart from the technical difficulties of working at single-atom and single-photon scales, one of the most important problems is that of preventing the surrounding environment from being affected by the interactions that generate quantum superpositions. The more components there are, the more likely it is that quantum information will spread outside the quantum computer and be lost into the environment, thus spoiling the computation. This process is called *decoherence* and is discussed in detail in Chap. 7. Thus our task is to engineer sub-microscopic systems in which qubits affect each other but not the environment.

Some physicists are pessimistic about the prospects of substantial further progress in quantum computer technology. They believe that decoherence will in practice never be reduced to the point where more than a few consecutive quantum computational steps can be performed. (This, incidentally, would already allow for some very useful devices — see Table 4.1 below.) Other, more optimistic researchers believe that practical quantum computers will appear in a matter of years rather than decades. We tend towards the optimistic end of the scale, partly because theory tells us that there is now no *fundamental* obstacle in the way and that quantum error correction and fault tolerant computation (see Chap. 7) are possible, partly thanks to the astonishing talents and problem-solving abilities of the experimental physicists now working on this project, and partly because optimism makes things happen.

However, the problems will not be solved in one fell swoop. The current challenge is not to build a fully-fledged universal quantum computer right away, but rather to move from the experiments in which we merely observe quantum phenomena to experiments in which we can control those phenomena in the necessary ways. Simple quantum logic gates involving two qubits are being realised in laboratories in Europe and U.S.A. The next decade should bring control over several qubits and, without any doubt, we shall already begin to benefit from our new way of harnessing nature. It is known, for instance, that simple quantum networks can offer better frequency standards [126] (see Sect. 7.6). Some possible milestones in the development of quantum computer technology are shown in Table 4.1.

4.1.5 Deeper Implications

When the physics of computation was first investigated systematically in the 1970s, the main fear was that quantum-mechanical effects might place fundamental bounds on the accuracy with which physical objects could realise the properties of bits, logic gates, the composition of operations, and so on, which appear in the abstract and mathematically sophisticated theory of computation. Thus it was feared that the power and elegance of that theory, its deep concepts such as computational universality, its deep results such as Turing's halting theorem, and the more modern theory of complexity, might

Table 4.1. Milestones in the development of quantum computer technology

Type of hardware	No. of qubits needed	No. of steps before decoherence	Status
Quantum Cryptography	1	1	implemented
Entanglement based quantum cryptography	2	1	demonstrated
Quantum C-NOT gate	2	1	demonstrated
Composition of gates	2	2	demonstrated
Deutsch's algorithm	2	3	demonstrated
Channel capacity doubling	2	2	imminent
Teleportation	3	2	demonstrated
Entanglement swapping	4	1	demonstrated
Repeating station for quantum cryptography	a few	a few	theory still incomplete
Quantum simulations	a few	a few	simple demos
Grover's algorithm with toy data	3+	6+	demonstrated with NMR
Ultra-precise frequency standards	a few	a few	foreseeable
Entanglement purification	a few	a few	foreseeable
Shor's algorithm with toy data ...	16+ ... hundreds	hundreds + ... hundreds	
Quantum factoring engine	thousands	thousands	
Universal quantum computer	+	+	

all be mere figments of pure mathematics, not really relevant to anything in nature.

Those fears have not only been proved groundless by the research we have been describing, but also, in each case, the underlying aspiration has been wonderfully vindicated to an extent that no one even dreamed of just twenty years ago. As we have explained, quantum mechanics, far from placing limits on what classical computations can be performed in nature, permits them all, and in addition provides whole new modes of computation, including algorithms that perform tasks (such as perfectly secure public-key cryptography) that no classical computer can perform at all. As far as the elegance of the theory goes, researchers in the field have now become accustomed to the fact that the real theory of computation hangs together better, and fits in far more naturally with fundamental theories in other fields, than its classical approximation could ever have been expected to. Even at the simplest level, the very word “quantum” means the same as the word “bit” — an elementary chunk — and this reflects the fact that fully classical physical systems, being subject to the generic instability known as “chaos”, would not support digital computation at all (so even Turing machines, the theoretical prototype of all classical computers, were secretly quantum-mechanical all along!). The Church–Turing hypothesis in the classical theory (that all “natural” models of computation are essentially equivalent to each other), was never proved. Its

analogue in the quantum theory of computation (the Turing Principle, that the universal quantum computer can simulate the behaviour of any finite physical system) was straightforwardly proved in Deutsch's 1985 paper [124]. A stronger result (also conjectured but never proved in the classical case), namely that such simulations can always be performed in a time that is at most a polynomial function of the time taken for the physical evolution, has since been proved in the quantum case.

Among the many ramifications of quantum computation for apparently distant fields of study are its implications for both the philosophy and the practice of mathematical proof. Performing any computation that provides a definite output is tantamount to *proving* that the observed output is one of the possible results of the given computation. Since we can describe the computer's operations mathematically, we can always translate such a proof into the proof of some mathematical theorem. This was the case classically too, but in the absence of interference effects it is always possible to note down the steps of the computation, and thereby produce a proof that satisfies the classical definition: a sequence of propositions each of which is either an axiom or follows from earlier propositions in the sequence by the standard rules of inference. Now we must leave that definition behind. Henceforward, a proof must be regarded as a process — the computation itself, not a record of all its steps — for we must accept that in future, quantum computers will prove theorems by methods that neither a human brain nor any other arbiter will ever be able to check step-by-step, since if the “sequence of propositions” corresponding to such a proof were printed out, the paper would fill the observable universe many times over. A more comprehensive discussion of the deeper implications of quantum computation can be found in [127].

4.1.6 Concluding Remarks

Experimental and theoretical research in quantum computation is now attracting increasing attention from both academic researchers and industry worldwide. The idea that nature can be controlled and manipulated at the quantum level is a powerful stimulus to the imagination of physicists and engineers. There is almost daily progress in developing ever more promising technologies for realising quantum computation and new quantum algorithms with various advantages over their classical counterparts. There is potential here for truly revolutionary innovation.

This contribution is a revised version of the introductory paper on quantum computation which originally appeared in the March 1998 issue of the Physics World [128].

4.2 Quantum Algorithms

R. Jozsa

4.2.1 Introduction

A quantum algorithm is any physical process which utilises characteristically quantum effects to perform useful computational tasks. It is convenient to formalise the description of these quantum computational processes in terms of a model which closely parallels the formalism of classical computation. In essence, the memory bits of the computer are qubits rather than bits and the elementary operations are unitary transformations, each operating on a fixed finite number of qubits, rather than the Boolean operations of classical computation. It may be argued [124] that a model of this type suffices to describe any general quantum physical process. Any computer is required to operate by “finite means” i.e. it is equipped only with the possibility of applying any operation of some finite fixed set of basic unitary operations. Any other unitary operation that we may need in an algorithm must be built (or rather approximated to sufficient accuracy) out of these basic building blocks by concatenating their action on selected qubits. It may be shown [129, 130] that various quite small collections of unitary operations (so-called “universal sets” of operations) suffice to approximate any unitary operation on any number of qubits to arbitrary accuracy.

One of the most useful and significant consequences of this formalism is that it provides a way of assessing the complexity of a computational task (again by paralleling concepts from classical computational complexity theory). We will be particularly concerned with the time complexity, i.e. assessing the number of elementary operations required to complete a computational task as a function of the size of the input.

If two computers A and B are equipped with different (universal) sets of basic operations then the time complexity of any computational task will in general be different. However, B may first program each of A 's basic operations in terms of its own set and hence run any program which is written in terms of A 's set of operations. Let k be the maximum number of steps that B requires to mimic any one of A 's basic operations. Then the time complexity on B for any computational task will be at most k times the time complexity relative to A , i.e. a change in the set of basic operations results in at most a constant slowdown (independent of input size) for any computational task. In computational complexity theory we are generally not interested in the exact number of steps in a computation but rather, only in the characteristic rate of growth of the number of steps with increasing input size. Indeed we generally only ask whether the number of steps is bounded by a polynomial

function of the input size (giving so-called polynomial-time algorithms or efficient algorithms) or whether it grows exponentially (or super-polynomially) with input size. According to the above remarks this distinction will be independent of the choice of computer and it is an intrinsic property of the computational task itself.

In the study of quantum algorithms it is of paramount interest to find polynomial-time algorithms for problems where no classical polynomial-time algorithm is known, i.e. we wish to demonstrate that quantum effects may give rise to an exponential speedup in running time over classical information processing. We will describe various situations in which this occurs – the algorithms of Deutsch, Simon and Shor. We will also describe the quantum searching algorithm of Grover which provides a square root speedup over any classical algorithm, rather than an exponential speedup. This is still of considerable practical interest and Grover’s algorithm also has much theoretical interest because of its relation to the classical complexity class called NP [131, 132].

We will see in Chap. 5 that the prospective implementation of any extended quantum algorithm currently presents a very considerable experimental challenge. However the existence of interesting quantum algorithms, merely at the level of theoretical constructs, is of great value in itself as it points to new essential differences between the fundamental structure classical physics compared to quantum physics. From our point of view of information processing, time evolution in quantum physics is seen to be intrinsically more complex than classical time evolution, in a way that can be quantified using the conceptual framework of computational complexity theory.

The essential quantum mechanical effects giving rise to the computational speedup in the quantum algorithms listed above, may be traced to various properties of quantum *entanglement*. We begin by discussing two such effects which feature predominantly; we refer to them as “quantum parallel computation” (Sect. 4.2.2) and “the principle of local operations” (Sect. 4.2.3).

4.2.2 Quantum Parallel Computation

Consider a function $f : A \rightarrow B$ where A and B are finite sets. Typically A and B may be the collection of all 2^n n -bit strings (for some n), as in the algorithms of Deutsch and Simon, or \mathcal{Z}_N , the set of integers mod N (for some N) as in Shor’s algorithm. In our applications A and B will also be Abelian groups. Let \mathcal{H}_A (respectively \mathcal{H}_B) be a Hilbert space with an orthonormal basis labelled by the elements of A (respectively B). In the context of quantum computation the computation of f corresponds to a unitary evolution U_f which is customarily taken as an operation on $\mathcal{H}_A \otimes \mathcal{H}_B$ transforming $|a\rangle|b\rangle$ into $|a\rangle|b \oplus f(a)\rangle$ (c.f. Fig. 4.4). Here \oplus denotes the Abelian group operation in B .

\mathcal{H}_A is the state space of the input register and \mathcal{H}_B is the state space of the output register. The input $|a\rangle$ is carried through to ensure that U_f is

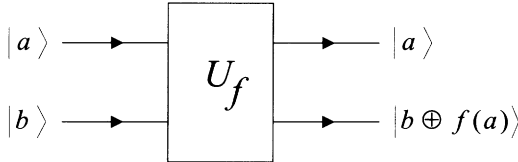


Fig. 4.4. Quantum gate picture of the unitary transformation U_f corresponding to the evaluation of the function f . The upper and lower lines represent the input and output registers respectively.

unitary for every possible f . If b is initially set to 0 then $f(a)$ may be read directly from the output register by a standard measurement in the given basis.

Suppose now that the input register is set up as a superposition of values, say the equal superposition $\sum_{a \in A} |a\rangle$ (where we have omitted the normalisation factor). Then applying U_f with $b = 0$ we get, by the linearity of quantum evolution, the output superposition $\sum |a\rangle |f(a)\rangle$ (c.f. Fig. 4.5).

By running U_f just *once* we have computed *all* values of f in superposition. This is the process of quantum parallel computation, introduced by Deutsch in [124]. Note that the output state $\sum |a\rangle |f(a)\rangle$ is generally an entangled state of the input and output registers. Indeed the phenomenon of superposition is a feature also of *classical* linear systems and any effect depending on superposition alone can readily be implemented in a classical system. However the phenomenon of quantum entanglement has no classical analogue and its fundamental role in quantum computation has been emphasised and elaborated in [133, 134].

Let $B = \{0, 1\}$ denote the additive group of integers mod 2 and denote by \mathcal{B} the Hilbert space of one qubit i.e. a two dimensional Hilbert space equipped with a standard basis denoted by $\{|0\rangle, |1\rangle\}$. \mathcal{B}^n will denote the 2^n -dimensional Hilbert space $\mathcal{B} \otimes \dots \otimes \mathcal{B}$ of n qubits with a basis $\{|x\rangle : x \in B^n\}$ labelled by all n -bit strings. Let H denote the fundamental one-qubit unitary operation

$$H = \frac{1}{\sqrt{2}} \begin{pmatrix} 1 & 1 \\ 1 & -1 \end{pmatrix}. \quad (4.1)$$

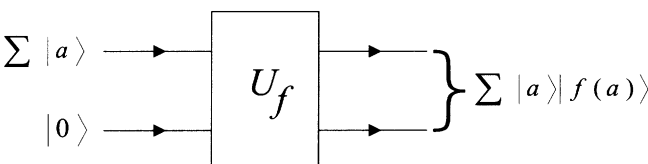


Fig. 4.5. Quantum parallel computation.

Thus

$$H|0\rangle = \frac{1}{\sqrt{2}}(|0\rangle + |1\rangle) \text{ and } H|1\rangle = \frac{1}{\sqrt{2}}(|0\rangle - |1\rangle). \quad (4.2)$$

Consider a function $f : B^n \rightarrow B$. As an example of computation by quantum parallelism, we may set up a superposition of all input values and compute all values of f in superposition as follows:

- (i) Start with the standard state $|0\rangle \dots |0\rangle$ of n (input) qubits and apply H separately to each qubit. This will result in the state:

$$\frac{1}{2^{n/2}}(|0\rangle + |1\rangle) \dots (|0\rangle + |1\rangle) = \frac{1}{2^{n/2}} \sum_{x \in B^n} |x\rangle. \quad (4.3)$$

- (ii) Adjoin a further single (output) qubit in state $|0\rangle$ and apply U_f giving the state:

$$|f\rangle = \frac{1}{2^{n/2}} \sum_{x \in B^n} |x\rangle |f(x)\rangle. \quad (4.4)$$

Note that (i) requires only $O(n)$ operations, which is polynomial in n , yet it leads to a superposition of *exponentially* many values of f in (4.4).

Quantum entanglement also plays another important role in the representation of superpositions. If we wish to build a general superposition of 2^n modes classically, we would need a *single* system capable of supporting each mode, e.g. 2^n modes of vibration of a vibrating string. These modes will correspond to higher and higher levels of some physical resource, e.g. energy in the vibrating string, and a general superposition of 2^n modes would then require an exponential (in n) amount of the physical resource to represent it. In contrast, in quantum theory, we can represent a superposition of 2^n states using n 2-level systems – *because of the phenomenon of entanglement*. A general such superposition now requires only a *linear* amount of physical resources to represent it, since at most each of the n systems needs to be separately excited. Hence, although superposition occurs in classical systems, the phenomenon of quantum entanglement leads to an exponential saving of physical resources needed to represent large superpositions.

4.2.3 The Principle of Local Operations

In all computation, be it classical or quantum, the information which is being processed is embodied in the identity of the physical state of (part of) the computer. Let us compare the description of the identity of a state of n classical bits with its quantum analogue, a state of n qubits. Although n bits can be in any one of exponentially many states, each state can be fully described by giving just n bits of information. In contrast, a general (entangled) state of n qubits may involve exponentially many superposition components which

need to be listed. In this sense a quantum system can embody exponentially more information than its classical counterpart. This is not a consequence of the fact that quantum amplitudes can take a continuous range of values – it persists even if we limit amplitudes to some simple basic set of numbers. For example the $(n + 1)$ -qubit state $|f\rangle$ in (4.4) embodies the information of all the exponentially many zero/one values of the function f . Note that the information needed to describe an unentangled (product) state of n qubits grows only linearly with n , being n times the information needed to describe a single qubit state.

The formalism of quantum mechanics allows the vast information content of a quantum state to be efficiently processed, at a rate that cannot be matched in real time by any classical means. This remarkable feature of quantum theory was first noted by Feynman in [123]. Suppose that we have a physical system of n qubits in some entangled state $|\psi\rangle$ and we apply a 1-qubit operation U to the first qubit. This would count as one step in a quantum computation (or rather a constant number of steps independent of n , if U needs to be fabricated from other basic operations provided by the computer). Consider now the classical computation corresponding to this processing of information in the state. $|\psi\rangle$ may be described in components (relative to the product basis of the n qubits) by $a_{i_1 \dots i_n}$ where each subscript is 0 or 1, and U is represented by a 2×2 unitary matrix U_i^j . The application of U corresponds to the matrix multiplication

$$a_{i_1 \dots i_n}^{(\text{new})} = \sum_j U_{i_1}^j a_{j i_2 \dots i_n}. \quad (4.5)$$

Thus the 2×2 matrix multiplication needs to be performed 2^{n-1} times, once for each possible value of the string $i_2 \dots i_n$, requiring a computing effort which grows *exponentially* with n . On a quantum computer, because of entanglement, this 2^{n-1} repetition is unnecessary. This is our “principle of local operations”: a single local unitary operation on a subsystem of a large entangled system processes the embodied information by an amount which would generally require an exponential effort to represent in classical computational terms.

In the sense noted above, n qubits have an exponentially larger capacity to represent information than n classical bits. However the potentially vast information embodied in a quantum state has a further remarkable feature – most of it is *inaccessible* to being read by any possible means! Indeed quantum measurement theory places severe restrictions on the amount of information that we can obtain about the identity of a given unknown quantum state. This intrinsic inaccessibility of the information may be quantified [135, 136] in terms of Shannon’s information theory [137]. In the case of a general state of n qubits, with its $O(2^n)$ information content, it turns out that at most n classical bits of information about its identity may be extracted from a single copy of the state by any physical means whatsoever. This coincides with the maximum information capacity of n classical bits.

The full (largely inaccessible) information content of a given unknown quantum state is called quantum information. Natural quantum physical evolution may be thought of as the processing of quantum information. Thus the viewpoint of computational complexity reveals a new bizarre distinction between classical and quantum physics: to perform natural quantum physical evolution, Nature must process vast amounts of information at a rate that cannot be matched in real time by any classical means, yet at the same time, most of this processed information is kept hidden from us! However it is important to point out that the inherent inaccessibility of quantum information does *not* cancel out the possibility of exploiting this massive information processing capability for useful computational purposes. Indeed, small amounts of information may be extracted about the overall identity of the final state which would still require an exponential effort to obtain by classical means. The technique of quantum parallel computation described above, provides an example: the full quantum information of the state $|f\rangle$ in (4.4) incorporates the information of all the individual function values $f(x)$ but this is not accessible to any measurement. However certain global properties of the collection of all the function values *may* be determined by suitable measurements on $|f\rangle$ which are not diagonal in the standard basis $\{|x\rangle|y\rangle\}$. For example, if f is a periodic function, we may determine the value of the period which falls far short of characterising the individual function values but would generally still require an exponential number of function evaluations to obtain reliably by classical means. This will be a key fact in the workings of Shor's efficient quantum factoring algorithm (Sect. 4.2.6).

Having discussed some basic computational benefits of quantum theory in general terms we will now describe the workings of various fundamental quantum algorithms.

4.2.4 Oracles and Deutsch's Algorithm

Deutsch's algorithm [124, 138] was the first explicit example of a computational task which could be performed exponentially faster using quantum effects than by any classical means. It was subsequently improved in [139] and we will describe here its most up-to-date form.

Consider first the four possible one-bit functions $f : B \rightarrow B$. We have two constant functions:

$$\begin{array}{ll} f(0) = 0 & f(0) = 1 \\ f(1) = 0 & f(1) = 1 \end{array} \quad \text{or} \quad \quad (4.6)$$

and two “balanced” functions (balanced in the sense that the output values 0 and 1 occur equally often):

$$\begin{array}{ll} f(0) = 0 & f(0) = 1 \\ f(1) = 1 & f(1) = 0 \end{array} . \quad (4.7)$$

Suppose now that we are given a “black box” or “oracle” which computes an (unknown) one of these functions. The oracle may be pictured as a sealed box (c.f. Fig. 4.4) providing the value of the function for any given input value (or input superposition as in Fig. 4.5). Alternatively we may think of the oracle as a computer subroutine which we may run but whose text or internal workings we are not allowed to examine. (Later we will give a discussion of the significance of this limitation on our access to the evaluation of f .) Our problem is to determine whether the function computed by the oracle is balanced or constant.

In the context of classical computation we clearly need to query the oracle twice to solve the problem with certainty. Indeed if we know only one value of the function (i.e. either $f(0)$ or $f(1)$) then we have no information at all about whether the function is balanced or constant! We will now show that on a quantum computer the problem may be solved with certainty with just one query to the oracle.

We exploit the possibility of quantum parallel computation (as described above) but with an extra twist – of first setting the output register to $\frac{1}{\sqrt{2}}(|0\rangle - |1\rangle)$. The quantum computation runs as follows. Starting from the standard state $|0\rangle|0\rangle$ of the input and output registers we apply the NOT operation to the output and then H to both registers giving

$$\begin{aligned} |0\rangle|0\rangle &\rightarrow |0\rangle|1\rangle \rightarrow \left(\frac{|0\rangle+|1\rangle}{\sqrt{2}}\right)\left(\frac{|0\rangle-|1\rangle}{\sqrt{2}}\right) \\ &= \frac{1}{\sqrt{2}} \sum_{x \in B} |x\rangle \left(\frac{|0\rangle-|1\rangle}{\sqrt{2}}\right). \end{aligned} \quad (4.8)$$

Next we present this state to the oracle, i.e. we apply U_f . Recalling that U_f transforms $|x\rangle|y\rangle$ into $|x\rangle|y \oplus f(x)\rangle$ we see that

$$U_f : |x\rangle(|0\rangle - |1\rangle) \longrightarrow \begin{cases} |x\rangle(|0\rangle - |1\rangle) & \text{if } f(x) = 0 \\ -|x\rangle(|0\rangle - |1\rangle) & \text{if } f(x) = 1 \end{cases}.$$

Thus

$$U_f : \frac{1}{\sqrt{2}} \sum_{x \in B} |x\rangle \left(\frac{|0\rangle - |1\rangle}{\sqrt{2}}\right) \longrightarrow \left(\frac{1}{\sqrt{2}} \sum_{x \in B} (-1)^{f(x)} |x\rangle\right) \left(\frac{|0\rangle - |1\rangle}{\sqrt{2}}\right). \quad (4.9)$$

Throughout this process the output register has remained in state $\frac{1}{\sqrt{2}}(|0\rangle - |1\rangle)$. The input register is left in state $\frac{1}{\sqrt{2}} \sum_{x \in B} (-1)^{f(x)} |x\rangle$. If f is a constant function we get $\pm \frac{1}{\sqrt{2}}(|0\rangle + |1\rangle)$ and if f is balanced we get $\pm \frac{1}{\sqrt{2}}(|0\rangle - |1\rangle)$. Now it is easy to verify directly that H is its own inverse, i.e. that $HH = I$. Thus finally applying H to the input register (and noting (4.2)) the state of this register will be $\pm |0\rangle$ if f was constant and $\pm |1\rangle$ if f was balanced. These may be reliably distinguished by a measurement in the standard basis, thus distinguishing balanced from constant functions with certainty after just one

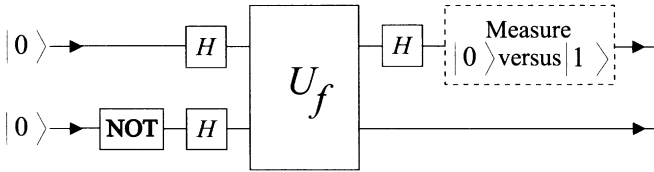


Fig. 4.6. Deutsch's algorithm for 1-bit functions. A measured value of 0 (respectively 1) signals that f is constant (respectively balanced).

query to the oracle. The overall sequence of operations is summarised in the network diagram shown in Fig. 4.6.

The above distinction between one and two calls to the oracle has no direct significance for formal complexity considerations but we may readily generalise the idea of the above process to a situation which *does* exhibit an *exponential* separation between the classical and quantum solutions.

Instead of having functions from one bit to one bit suppose we are given an oracle which computes some function from n bits to one bit:

$$f : B^n \rightarrow B$$

(and we also know the value of n). It is promised that the function is either constant (i.e. the 2^n values are either all 0 or all 1) or balanced, where balanced means that exactly half (i.e. 2^{n-1}) of the values are 0 and half are 1. Note that for $n > 1$ a general function from n bits to 1 bit is neither balanced nor constant but there are a large number of possible balanced functions. Our problem is again to determine (with certainty) whether f is balanced or constant. The case of $n = 1$ is precisely the problem considered previously.

In a classical scenario, if we query the oracle 2^{n-1} times to obtain 2^{n-1} values of f , in any way whatever with later queries possibly depending on the outcome of earlier ones, then we will still not be able to solve the problem in *every* case. Indeed suppose that the 2^{n-1} values come out to be all the same (which is always possible although very unlikely if the function is really balanced). Then regardless of the choice of input arguments there will always be a constant and a balanced function which is consistent with the totality of the information gained. Hence any classical solution to the problem must query the oracle more than 2^{n-1} times i.e. at least an exponential (in n) number of times. In fact it is easy to see that $2^{n-1} + 1$ queries will always suffice. In a quantum scenario the problem may be solved with certainty in every case with just *one* call to the oracle. The method is a straightforward generalisation of the one bit case.

We start with a row of n (input) qubits and one (output) qubit all in standard state $|0\rangle$. We apply H to each of the input qubits. As given in (4.3) this results in an equal superposition of all inputs in the first n qubits. We prepare the last (output) qubit in state $\frac{1}{\sqrt{2}}(|0\rangle - |1\rangle)$ exactly as previously.

Next we offer the resulting $n + 1$ qubit state to the oracle. This is formally the same as (4.9) except that now x ranges over B^n rather than just B . After processing by the oracle the first n qubits will be in state

$$|\xi_f\rangle = \frac{1}{\sqrt{2^n}} \sum_{x \in 2^n} (-1)^{f(x)} |x\rangle. \quad (4.10)$$

(In passing we note here that in the original 1992 version of the Deutsch algorithm [138] the output register was initialised in state $|0\rangle$ and two calls to the oracle were needed to produce the state $|\xi_f\rangle$). Now if f was a constant function then $|\xi_f\rangle$ will be just an equal superposition of all the $|x\rangle$'s with an overall plus or minus sign whereas if f was a balanced function then $|\xi_f\rangle$ will be an equally weighted superposition with exactly half of the $|x\rangle$'s having minus signs. Thus these two possibilities are orthogonal and so there exists a suitable measurement on $|\xi_f\rangle$ which will distinguish balanced from constant functions with certainty.

We need to describe explicitly how this measurement can be performed. In any quantum algorithm we cannot assume that any measurement can be performed by fiat as one step of computation (just as we cannot assume the application of complicated unitary operations as one step). To assess the complexity of any measurement we assume that the only possible measurement available to us is an elementary $|0\rangle$ versus $|1\rangle$ measurement of any one qubit in the computational basis and this counts as one step. Any general measurement may be reduced to a sequence of these standard measurements by first unitarily rotating the eigenbasis of the measurement into the computational basis and then successively reading the bits. The complexity of the measurement is then measured by the number of steps required to implement this unitary rotation plus the number of qubits that need to be read.

In our case the measurement that distinguishes balanced from constant $|\xi_f\rangle$'s may be implemented simply as follows. Recalling that H is its own inverse (i.e. $HH = I$) and that H applied to each qubit of $|0\rangle|0\rangle\dots|0\rangle$ results in an equal superposition of all $|x\rangle$'s (c.f. (4.3)), it follows that if H is again applied to each qubit of this equal superposition then the resulting state will be $|0\rangle|0\rangle\dots|0\rangle$. Hence we apply H to each qubit of $|\xi_f\rangle$ (involving n steps). If f was constant then the resulting state is $\pm|0\rangle|0\rangle\dots|0\rangle$. If f was balanced then the resulting state will be orthogonal to this i.e. a superposition of $|x\rangle$'s with $x \neq 00\dots 0$. Thus we read each of the n qubits to see if they are all 0 or not (a further n steps) which completes the measurement. Overall, Deutsch's quantum algorithm requires $O(n)$ steps (including one call to the oracle) to distinguish balanced from constant functions with certainty whereas any classical algorithm requires $O(2^n)$ steps to achieve the same task.

Deutsch's algorithm is a so-called “oracle result” or “relativised” separation result (relative to an oracle). It does not provide an *absolute* exponential separation between quantum and classical computation but gives this sepa-

ration only if we make some further (plausible but unproven) computational assumptions related to the fact that we are forbidden access to the internal workings of the oracle. In effect we have assumed that, if we are given a program which computes f , there is no mechanical way of using the syntax of a general such program to determine whether f is constant or balanced, more quickly than by just running the program a sufficient number of times. Of course, a constant function for example, may have a very short program which may be recognised immediately as computing a constant function but an adversary may also provide a very complicated disguised program which still computes a constant function, and this may be very hard to see by reading the syntax. Although this assumption is very plausible it remains unproven as it is very difficult to analyse algorithms which operate on the syntax of a program as input! We remark that if an *absolute* exponential separation between classical and quantum computation could be proved it would resolve some long standing fundamental open questions in classical complexity theory (e.g. it would imply that $P \neq PSPACE$; see [131] for a definition of these terms). Thus it is likely to be very difficult to formally prove that quantum computation is exponentially more powerful than classical computation.

Another significant feature of Deutsch's algorithm is that if the algorithm is not required to work perfectly, i.e. if we tolerate some (arbitrarily small) error in the answer, then the displayed exponential separation between classical and quantum computation collapses. Indeed given any $\epsilon > 0$ there is a classical (probabilistic) algorithm running for a *constant* number of steps (independent of $n!$), which will distinguish balanced from constant functions, providing an answer that is correct with probability $(1 - \epsilon)$ for any given choice of f . This algorithm runs simply as follows. We evaluate f on some K *randomly* chosen inputs. If the answers are all the same then f is deemed to be constant. Otherwise it is deemed to be balanced. A little thought shows that the answer 'balanced' is always correct and the answer 'constant' will be correct with probability of error less than $1/2^K$. Thus for any given $\epsilon > 0$ we choose K large enough to have $\frac{1}{2^K} < \epsilon$. Note that K is independent of n so the K evaluations count as a constant number of steps in the algorithm.

It is only in the limiting case of $\epsilon = 0$ that the exponential separation between quantum and classical computation occurs. One may argue that this limiting situation is actually unphysical because any computer, being a physical device, can never be perfectly isolated from its environment. Thus it always has some (generally very small) probability of functioning incorrectly, e.g. a memory bit may be flipped by a cosmic ray at any time. Hence it is of great interest to exhibit a computational task whose computational complexity separates quantum from classical computation by an exponential amount even if a small error in the result is tolerated. The first such example was given by Bernstein and Vazirani [140]. Using a recursive construction they described a computational task involving an oracle which could be solved on a quantum computer in polynomial time but which required $O(n^{\log n})$

time on a classical computer. Then Simon [141] described a simpler oracle problem which could be solved in $O(n^2)$ time on a quantum computer but required fully exponential time (i.e. $O(2^n)$ time) on a classical computer. The apotheosis of this line of development was the algorithm of Shor [36] for factorisation which also eliminated the dependence on an oracle. Shor's algorithm provides a method for factorising an integer N in a number of steps which is polynomial (less than cubic) in the number of digits ($\log N$) of N and returns a correct result with probability $1 - \epsilon$ for any prescribed $\epsilon > 0$. Despite a great deal of effort for some hundreds of years (by eminent mathematicians such as Gauss, Legendre, Fermat and others) there is no known *classical* probabilistic polynomial time algorithm for this problem. Unlike the algorithms of Deutsch and Simon, Shor's algorithm does not involve an oracle. However this does not provide a proof of an absolute exponential benefit of quantum computation over classical computation because there is also no known *proof* that a classical polynomial time factoring algorithm does not exist (only an immense wealth of unsuccessful attempts at constructing such an algorithm!).

4.2.5 The Fourier Transform and Periodicities

Shor's quantum factoring algorithm and Simon's algorithm will depend in an essential way on a quantum computer's remarkable ability to efficiently determine the periodicity of a given periodic function. We illustrate the ideas involved with the following basic example. Suppose that we have a black box which computes a function $f : \mathcal{Z}_N \rightarrow \mathcal{Z}$ that is guaranteed to be periodic with some period r :

$$f(x + r) = f(x) \quad \text{for all } x. \quad (4.11)$$

Recall that \mathcal{Z}_N denotes the group of integers modulo N and addition here is modulo N . We also assume that f does not take the same value twice within any single period. Note that (4.11) can hold only if r divides N exactly.

Our aim is to determine r . Classically (in the absence of any further information about f) we can merely try different values of x in the black box hoping for two equal results which will then give information about r . Generally we will require $O(N)$ random tries to hit two equal values with high probability. Using quantum effects we will be able to find r using only $O((\log N)^2)$ steps, which represents an exponential speedup over any classical algorithm.

We begin by using quantum parallel computation to compute all values of f in equal superposition, resulting in the state

$$|f\rangle = \frac{1}{\sqrt{N}} \sum_{x=0}^{N-1} |x\rangle |f(x)\rangle. \quad (4.12)$$

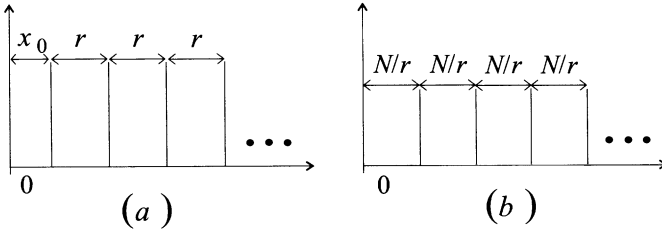


Fig. 4.7. Graphical representation of the periodic amplitudes of (a) the state $|\psi\rangle$ and (b) its Fourier transform. In passing to $\mathcal{F}|\psi\rangle$ the periodicity r has been inverted to N/r and the random shift x_0 has been eliminated.

Although this state embodies the periodicity of f it is not immediately clear how to extract the information of r ! If we measure the value in the second register, giving a value y_0 say, then the state of the first register will be reduced to an equal superposition of all those $|x\rangle$'s such that $f(x) = y_0$. If x_0 is the least such x and $N = Kr$ then we will obtain in the first register the periodic state

$$|\psi\rangle = \frac{1}{\sqrt{K}} \sum_{k=0}^{K-1} |x_0 + kr\rangle. \quad (4.13)$$

It is important to note here that $0 \leq x_0 \leq r-1$ has been generated at random, corresponding to having seen any value y_0 of f with equal probability. So if we now measure the value in this register, the overall result is merely to produce a number between 0 and $N - 1$ uniformly at random, giving no information at all about the value of r !

The resolution of this difficulty is to use the Fourier transform which, even for classical data, is known to be able to pick out periodic patterns in a set of data regardless of how the whole pattern is shifted. The discrete Fourier transform \mathcal{F} for integers modulo N is the N by N unitary matrix with entries

$$\mathcal{F}_{ab} = \frac{1}{\sqrt{N}} e^{2\pi i \frac{ab}{N}}. \quad (4.14)$$

If we apply this unitary transform to the state $|\psi\rangle$ above then we obtain [144]

$$\mathcal{F}|\psi\rangle = \frac{1}{\sqrt{r}} \sum_{j=0}^{r-1} e^{2\pi i \frac{x_0 j}{r}} \left| j \frac{N}{r} \right\rangle. \quad (4.15)$$

The important point to note here is that the random shift x_0 no longer appears in the ket labels (see Fig. 4.7).

If we now read the label we will obtain a value c say, which is necessarily a multiple of N/r , i.e. $c = \lambda N/r$. Thus we can write

$$\frac{c}{N} = \frac{\lambda}{r}, \quad (4.16)$$

where c and N are known numbers and and $0 \leq \lambda \leq r - 1$ has been chosen uniformly at random by the measurement (as all amplitudes in $\mathcal{F}|\psi\rangle$ have equal size.) Now if the randomly chosen λ is fortuitously coprime to r (i.e. λ and r have no common factors) we can determine r by cancelling c/N down to an irreducible fraction. What is the probability that a randomly chosen r actually *is* coprime to r ? According to the prime number theorem (c.f. [142, 143] and appendix A of [144]), the number of prime numbers less than or equal to r goes as $r/\log r$ for large r . Thus the probability that our randomly chosen λ is coprime to r is at least $1/\log r$ which exceeds $1/\log N$. Hence if we repeat the above procedure $O(\log N)$ times we can succeed in determining r with any prescribed probability $1 - \epsilon$ as close to 1 as desired.

We noted above that we want our quantum algorithm for determining r to run in time $\text{poly}(\log N)$, i.e. in a number of steps which is polynomial in $\log N$ rather than N itself, to achieve an exponential speed up over any known classical algorithm for determining periodicity. We showed above that $O(\log N)$ repetitions suffice to determine r but there is still a significant gap in our argument: the Fourier transform \mathcal{F} that we used is a large non-trivial unitary operation, of size $N \times N$, and we cannot *ab initio* just assume that it can be implemented using only $\text{poly}(\log N)$ basic computational operations. Indeed it may be shown that any $d \times d$ unitary operation may be implemented on a quantum computer (equipped with any universal set of operations) in $O(d^2)$ steps [124, 144]. This is also the number of steps needed for the classical computation of multiplying a $d \times d$ matrix into a d dimensional column vector. For our use of \mathcal{F} this bound of $O(N^2)$ does not suffice. Fortunately the Fourier transform has extra special properties which enable it to be implemented in $O((\log N)^2)$ steps. These properties stem from the classical theory of the fast Fourier transform (FFT) [145] which shows how to reduce the $O(N^2)$ steps of classical matrix multiplication to $O(N \log N)$ steps. If the same ideas are implemented in a quantum setting then the principle of local operations may be seen [134, 144] to reduce the number of steps to $O((\log N)^2)$ giving our desired implementation. Having made this important point we will omit the considerable technical details of the FFT construction and its implementation in a quantum setting. These details are elaborated in [134] to which we refer the interested reader. Note also that according to (4.14) we have

$$\mathcal{F}|0\rangle = \frac{1}{\sqrt{n}} \sum_{x=0}^{N-1} |x\rangle , \quad (4.17)$$

so that once we have an efficient implementation of \mathcal{F} we will be able to efficiently produce the uniform large superposition necessary to get $|f\rangle$ in (4.12).

In summary, the quantum algorithm for determining the periodicity of a given function f , with N inputs, begins with an application of quantum parallel computation to compute all values of f in superposition using $O(\log N)$ steps. The the Fourier transform is applied to pick out the periodic struc-

ture of the resulting state. The principle of local operations applied to the quantum implementation of the FFT algorithm guarantees that the Fourier transform may be implemented in $\text{poly}(\log N)$ steps. An analogous classical computation would require $O(N)$ invocations of f to compute a column vector of all the function values and then $O(N \log N)$ steps to perform the FFT. Thus the quantum algorithm represents an exponential speedup.

It is interesting to observe that the concept of periodicity and the construction of the Fourier transform may be extended to apply to *any* finite group G . Our discussion above pertains simply to the special case of the additive group of integers modulo N . The generalised viewpoint provides considerable insight into the workings of the Fourier transform. We will now briefly outline some of the essential ideas involved, restricting attention to the case of finite Abelian groups. (The remainder of this section may be omitted, if desired, without any loss of continuity with the following sections.)

Let G be any finite Abelian group. Let $f : G \rightarrow X$ be a function on the group (taking values in some set X) and consider

$$K = \{k \in G : f(k + g) = f(g) \text{ for all } g \in G\}. \quad (4.18)$$

(Note that we write the group operation in additive notation). K is necessarily a subgroup of G called the stabiliser or symmetry group of f . It characterises the periodicity of f with respect to the group operation of G . In our previous example G was \mathbb{Z}_N and K was the cyclic subgroup of all multiples of r . Given a device that computes f , our aim is to determine K . More precisely we wish to determine K in time $O(\text{poly}(\log |G|))$ where $|G|$ is the size of the group and the evaluation of f on an input counts as one computational step. (Note that we may easily determine K in time $O(\text{poly}(|G|))$ by simply evaluating and examining all the values of f). We begin as in our example by constructing the state

$$|f\rangle = \frac{1}{\sqrt{|G|}} \sum_{g \in G} |g\rangle |f(g)\rangle \quad (4.19)$$

and read the second register. Assuming that f is suitably non-degenerate – in the sense that $f(g_1) = f(g_2)$ iff $g_1 - g_2 \in K$, i.e. that f is one-to-one within each period – we will obtain in the first register

$$|\psi(g_0)\rangle = \frac{1}{\sqrt{|K|}} \sum_{k \in K} |g_0 + k\rangle, \quad (4.20)$$

corresponding to seeing $f(g_0)$ in the second register and g_0 has been chosen at random. In (4.20) we have an equal superposition of labels corresponding to a randomly chosen coset of K in G . Now G is the disjoint union of all the cosets so that if we read the label in (4.20) we will see a random element of a random coset, i.e. a label chosen equiprobably from all of G , yielding no information at all about K .

The general construction of a “Fourier transform on G ” will provide a way of eliminating g_0 from the labels (just as in our example) and the resulting state will then provide direct information about K . Let \mathcal{H} be a Hilbert space with a basis $\{|g\rangle : g \in G\}$ labelled by the elements of G . Each group element $g_1 \in G$ gives rise to a unitary “shifting” operator $U(g_1)$ on \mathcal{H} defined by

$$U(g_1)|g\rangle = |g + g_1\rangle \quad \text{for all } g. \quad (4.21)$$

Note that the state in (4.20) may be written as a g_0 -shifted state:

$$\sum_{k \in K} |g_0 + k\rangle = U(g_0) \left(\sum_{k \in K} |k\rangle \right). \quad (4.22)$$

Our basic idea now is to introduce into \mathcal{H} a new basis $\{|\chi_g\rangle : g \in G\}$ of special states which are *shift-invariant* in the sense that

$$U(g_1)|\chi_{g_2}\rangle = e^{i\phi(g_1, g_2)} |\chi_{g_2}\rangle \quad \text{for all } g_1, g_2, \quad (4.23)$$

i.e. the $|\chi_g\rangle$ ’s are the common eigenstates of all the shifting operations $U(g)$. Note that the $U(g)$ ’s all commute so such a basis of common eigenstates is guaranteed to exist. Then according to (4.22) if we view $|\psi(g_0)\rangle$ in the new basis then $\sum_{k \in K} |k\rangle$ and $\sum_{k \in K} |g_0 + k\rangle$ will contain the same pattern of labels, determined by the subgroup K only. Reading the label in the new basis will then directly provide information about the constituent elements of K .

The Fourier transform \mathcal{F} on G is defined to simply be the unitary transformation which takes the shift-invariant basis back to the standard basis:

$$\mathcal{F}|\chi_g\rangle = |g\rangle \quad \text{for all } g. \quad (4.24)$$

Hence to read $|\psi(g_0)\rangle$ in the new basis we just apply \mathcal{F} and read in the standard basis.

To give an explicit construction of \mathcal{F} it suffices to give the states $|\chi_g\rangle$ written as components in the standard basis. There is a standard way of calculating these components based on constructions from group representation theory. We omit the details here but the interested reader will find an introduction in [134] and [146]. For the group \mathcal{Z}_N we get

$$|\chi_k\rangle = \frac{1}{\sqrt{N}} \sum_{j=0}^{N-1} e^{2\pi i \frac{jk}{N}} |j\rangle \quad (4.25)$$

leading to the Fourier transform formula given in (4.14).

The above group-theoretic framework serves to generalise and extend the applicability of the quantum algorithm for periodicity determination. For example, Simon’s quantum algorithm [134, 141, 146, 147] turns out to be just a periodicity determination on the group $(\mathcal{Z}_2)^n$, the group of all n -bit

strings with componentwise addition modulo 2. Simon considered the following problem: suppose that we have a black box which computes a function f from n -bit strings to n -bit strings. It is also promised that the function is “two-to-one” in the sense that there is a fixed n -bit string ξ such that

$$f(x + \xi) = f(x) \quad \text{for all } n\text{-bit strings } x. \quad (4.26)$$

Our problem is to determine ξ .

To see that this is just a generalised periodicity determination, note that in the group $(\mathbb{Z}_2)^n$ of n -bit strings, every element satisfies $x + x = 0$. Hence (4.26) states just that f is periodic on the group with periodicity subgroup $K = \{0, \xi\}$. Thus to determine ξ we construct the Fourier transform on the group of n -bit strings and apply the standard algorithm above. The relevant Hilbert space \mathcal{H} with a basis labelled by n -bit strings is just a row of n qubits. Using the general constructions of group representation theory, the Fourier transform may be seen [134] to be the application of H (from (4.1)) to each of the n qubits. The quantum algorithm determines ξ in $O(n^2)$ steps whereas it may be argued [141] that any classical algorithm must evaluate f at least $O(2^n)$ times. A full description of the algorithm may be found in [141, 146, 147].

The Fourier transform formalism has emerged as the most important ingredient in the quantum algorithms discovered so far. Some interesting further developments of it, including the extension to non-Abelian groups, may be found in [148, 149].

4.2.6 Shor’s Quantum Algorithm for Factorisation

The most celebrated quantum algorithm devised to date is Shor’s efficient algorithm for factorisation [36, 144, 146]. Given a number N we wish to determine a number k (not equal to 1 or N) which divides N exactly. In this section we will outline how this problem may be reduced to a problem of periodicity determination for a suitable periodic function f . Then the quantum algorithm described in the preceding section will achieve the factorisation of N in $\text{poly}(\log N)$ time, i.e. polynomial in the number of digits of N .

We note first that there is no known classical algorithm which will factorise any given N in a time polynomial in the number of digits of N . For example the most naive factoring algorithm involves test-dividing N by each number from 1 to \sqrt{N} (as any composite N must have a factor in this range). This requires at least \sqrt{N} steps (at least one step for each trial factor) and $\sqrt{N} = 2^{\frac{1}{2} \log N}$ is exponential in $\log N$. In fact using all the ingenuity of modern mathematics, the fastest known classical factoring algorithm runs in a time of order $\exp((\log N)^{\frac{1}{3}} (\log \log N)^{\frac{2}{3}})$.

To reduce the problem of factoring N to a problem of periodicity we will need to use some basic results from number theory. These are further described in the appendix of [144] and complete expositions may be found

in most standard texts on number theory such as [142, 143]. We begin by selecting a number $a < N$ at random. Using Euclid's algorithm, we compute in $\text{poly}(\log N)$ time, the highest common factor of a and N . If this is larger than 1, we will have found a factor of N and we are finished! However it is overwhelmingly likely that a randomly chosen a will be coprime to N . The prime number theorem (mentioned in the last section) implies that this probability will be exceed $1/\log N$ for large N . If a is coprime to N , then Euler's theorem of number theory guarantees that there is a power of a which has remainder 1 when divided by N . Let r be the smallest such power:

$$a^r \equiv 1 \pmod{N} \quad \text{and } r \text{ is the least such power.} \quad (4.27)$$

(If a is not coprime to N , then no power of a has remainder 1). r is called the *order* of a modulo N . Next we show that the information of r can provide a factor of N .

Suppose that we have a method for determining r (see below) and suppose further that r comes out to be an *even* number. Then we can rewrite (4.27) as $a^r - 1 \equiv 0 \pmod{N}$ and factorise as a difference of squares:

$$(a^{r/2} - 1)(a^{r/2} + 1) \equiv 0 \pmod{N}. \quad (4.28)$$

Let $\alpha = a^{r/2} - 1$ and $\beta = a^{r/2} + 1$. Then N exactly divides the product $\alpha\beta$. If neither α nor β is a multiple of N then N must divide partly into α and partly into β . Thus computing the highest common factor of N with α and β (again using Euclid's algorithm) will generate a non-trivial factor of N .

As an example take $N = 15$ and choose the coprime number $a = 7$. By computing the powers of 7 modulo 15 we find that $7^4 \equiv 1 \pmod{15}$, i.e. the order of 7 modulo 15 is 4. Thus 15 must exactly divide the product $(7^{4/2} - 1)(7^{4/2} + 1) = (48)(50)$. Computing the highest common factor of 15 with 50 and 48 gives 5 and 3 respectively, which are indeed nontrivial factors of 15.

Our method will give a factor of N provided that r comes out to be even and that neither of $(a^{r/2} \pm 1)$ are exact multiples of N . To guarantee that these conditions occur often enough (for randomly chosen a 's) we have

Theorem: Let N be odd and suppose that $a < N$ coprime to N is chosen at random. Let r be the order of a modulo N . Then the probability that r is even and $a^{r/2} \pm 1$ are not exact multiples of N is always $\geq \frac{1}{2}$. \square
The (somewhat lengthy) proof of this theorem may be found in appendix B of [144], to which we refer the reader for details.

Overall, our method will produce a factor of N with probability at least half in every case. This success probability may be amplified as close as desired to 1, since K repetitions of the procedure (with K constant independent of N) will succeed in factorising N with probability exceeding $1 - \frac{1}{2^K}$.

All steps in the procedure, such as applying Euclid's algorithm and the arithmetic manipulation of numbers, can be done in $\text{poly}(\log N)$ time. The

only remaining outstanding ingredient is a method for determining r in $\text{poly}(\log N)$ time. Consider the exponential function:

$$f(x) = a^x \bmod N. \quad (4.29)$$

Now (4.27) says precisely that f is periodic with period r , i.e. that $f(x+r) = f(x)$. Thus we use the quantum algorithm for periodicity determination, described in the previous section, to find r . To apply the algorithm as stated, we need to restrict the scope of x values in (4.29) to a *finite* range $0 \leq x \leq q$ for some q . If q is not an exact multiple of (the unknown) r , i.e. $q = Ar + t$ for some $0 < t < r$, then the resulting function will not be exactly periodic – the single final period over the last t values will be incomplete. However if q is chosen large enough, giving sufficiently many intact periods of f , then the single corrupted period will have negligible effect on the use of the $q \times q$ Fourier transform to determine r , as we might intuitively expect. In fact it may be shown that if q is chosen to have size $O(N^2)$ then we get a reliable efficient determination of r . For the technical analysis of this imperfect periodicity (involving the theory of continued fractions) we refer the reader to [36, 144]. q is also generally chosen to be a power of 2 which fits in particularly well with the formalism of *fast* Fourier transforms (c.f. [134, 145]).

4.2.7 Quantum Searching and NP

Suppose that we have a database consisting of an unsorted unstructured list of N records and at most one of the records satisfies a given property of interest. We want to locate the special record. Any classical method which locates the record with some constant probability (independent of N) will require $O(N)$ steps. Indeed elementary probability theory shows that if we examine k of the records then we have probability k/N of finding the special record. This probability tends to 0 with increasing N unless k is at least of order N . Grover's quantum searching algorithm [120, 150] solves the problem with only $O(\sqrt{N})$ steps. Thus quantum effects can provide a square root speedup in this problem which should be contrasted to the much greater exponential speedup exhibited by the previously discussed quantum algorithms. In Grover's algorithm we will require the ability to examine different records in superposition just as our previous algorithms evaluated functions on superpositions of input values.

The assumption of unstructuredness of the database is very important for the result. For example if the database consisted of N random numbers which are *sorted* in ascending order then we would need only $O(\log N)$ steps classically (using a standard bisection method) to locate any given one of the numbers. Similarly any prior known structure of the database might be exploited to reduce the search time. The unstructuredness assumption is analogous to our previous use of oracles (or black boxes) whose internal structure we were unable to access. In fact the database searching problem

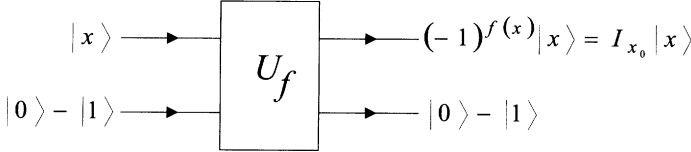


Fig. 4.8. The construction of I_{x_0} from U_f . Here f is the oracle which marks x_0 .

may be more accurately re-phrased in terms of an oracle as follows: we are given a black box which computes a function of N inputs, with output values 0 or 1. Furthermore it is promised that $f(x) = 1$ for exactly one input value x_0 (all other values of f being 0). Our task is to find x_0 .

We will now outline Grover's quantum searching algorithm for finding x_0 in $O(\sqrt{N})$ steps. (The following technical details may be omitted if preferred at first reading, without essential loss of continuity, noting the features of the algorithm already described above.) As in our discussion of Deutsch's algorithm and quantum parallel computation, we will assume that the oracle is given as a unitary transformation U_f which transforms $|x\rangle|j\rangle$ into $|x\rangle|j \oplus f(x)\rangle$. Here $1 \leq x \leq N$, $j = 0$ or 1 and \oplus is addition modulo 2. It will also be convenient to restrict attention to the case where $N = 2^n$ i.e. N is a power of 2 so that f is a function from n bits to one bit. Let \mathcal{B}^n be the Hilbert space of n qubits (i.e. the input register) with a standard basis $\{|x\rangle\}$ labelled by all n -bit strings x . The original form of Grover's algorithm is based on two unitary operations I_{x_0} and D , each acting on \mathcal{B}^n . I_{x_0} is the operation which merely inverts the amplitude of $|x_0\rangle$:

$$I_{x_0}|x\rangle = \begin{cases} |x\rangle & \text{if } x \neq x_0 \\ -|x\rangle & \text{if } x = x_0 \end{cases}. \quad (4.30)$$

This is easily constructed from U_f by first setting its output register (the last of $n + 1$ qubits) to $\frac{1}{\sqrt{2}}(|0\rangle - |1\rangle)$ just as we did in Deutsch's algorithm. The action of U_f then effects I_{x_0} on the input register while leaving the output register in state $\frac{1}{\sqrt{2}}(|0\rangle - |1\rangle)$ (see Fig. 4.8).

The operator D is defined as follows. Let H_n be the application of H (c.f. (4.1)) to each of the n qubits and let I_0 be the operator I_{x_0} with $x = 00\dots 0$. Then D is defined by

$$D = -H_n I_0 H_n. \quad (4.31)$$

A direct computation of the matrix elements of D [120, 150] shows that all off-diagonal elements are $\frac{2}{N}$ and all diagonal elements are $-1 + \frac{2}{N}$ (recalling that $N = 2^n$ here). Hence

$$D|x\rangle = -|x\rangle + \frac{2}{N} \sum_y |y\rangle. \quad (4.32)$$

D has a simple geometrical interpretation as being ‘‘inversion about the mean’’. For any state $|\psi\rangle = \sum a_x |x\rangle$ let $D|\psi\rangle = \sum a'_x |x\rangle$ and let $\bar{a} = \frac{1}{N} \sum a_x$ denote the average amplitude for the state $|\psi\rangle$. Using (4.32) we get

$$a'_x = -a_x + \frac{2}{N} \sum_y a_y = \bar{a} - (a_x - \bar{a}). \quad (4.33)$$

Writing $\Delta a_x = a_x - \bar{a}$ we have that $a_x = \bar{a} + \Delta a_x$ and $a'_x = \bar{a} - \Delta a_x$ so that the values of the amplitudes are just reflected in the mean \bar{a} .

To perform Grover’s algorithm we begin with an equal superposition $|\psi_0\rangle = \frac{1}{\sqrt{N}} \sum |x\rangle$ which may be prepared, for example, by applying H_n to $|0\dots0\rangle$. This state corresponds to examining the database at all positions in equal superposition. Our aim is to modify $|\psi_0\rangle$ to concentrate the amplitude at $x = x_0$. The algorithm consists of repeatedly applying the operator DI_{x_0} giving a sequence of states $|\psi_k\rangle$:

$$\begin{aligned} |\psi_0\rangle &= \frac{1}{\sqrt{N}} \sum |x\rangle \\ |\psi_{k+1}\rangle &= DI_{x_0} |\psi_k\rangle. \end{aligned} \quad (4.34)$$

Using our expressions for D and I_{x_0} it is easy to see that the amplitudes of all $|x\rangle$ ’s with $x \neq x_0$ remain equal to each other so that each $|\psi_k\rangle$ has the form

$$|\psi_k\rangle = \alpha_k \sum_{x \neq x_0} |x\rangle + \beta_k |x_0\rangle, \quad (4.35)$$

where α_k and β_k are also real. Using the matrix elements of D and I_{x_0} we can derive the recurrence relations:

$$\begin{aligned} \alpha_0 &= \beta_0 = \frac{1}{\sqrt{N}} \\ \alpha_{k+1} &= (1 - \frac{2}{N})\alpha_k - \frac{2}{N}\beta_k \\ \beta_{k+1} &= (1 - \frac{2}{N})\beta_k + (N - 1)\frac{2}{N}\alpha_k. \end{aligned} \quad (4.36)$$

Normalisation gives

$$\beta_k^2 + (N - 1)\alpha_k^2 = 1, \quad (4.37)$$

which suggests that we write $\alpha_k = \frac{1}{\sqrt{N-1}} \cos \theta_k$ and $\beta_k = \sin \theta_k$. It is then straightforward to verify [151] that the recurrence relations in (4.36) are satisfied by

$$\alpha_k = \frac{1}{\sqrt{N-1}} \cos(2k + 1)\theta, \quad \beta_k = \sin(2k + 1)\theta, \quad (4.38)$$

where θ is the angle given by $\sin \theta = \frac{1}{\sqrt{N}}$.

Thus β_k varies sinusoidally with the number of iterations k . We will have $\beta_k = 1$ if $(2k+1)\theta = \pi/2$ i.e. if $k = \frac{\pi - 2\theta}{4\theta}$. For large N , we have $\sin \theta = \frac{1}{\sqrt{N}} \approx \theta$ and then $k = \frac{\pi}{4}\sqrt{N} - \frac{1}{2}$ which is of order \sqrt{N} . Thus if we iterate the process for a number of steps given by the whole number nearest to this value of k , then x_0 may be obtained with a high probability (independent of N) by reading the final state in the standard basis (c.f. [151] for a further analysis of the probabilities involved.) This completes the algorithm.

Since Grover's original work, the basic ideas involved in the above algorithm have been extended to a variety of further applications such as estimating the mean and median of a database of N given numbers [152] and the analysis of the case of more than one marked item in a database [151, 153]. Using an ingenious combination of Grover's algorithm and Shor's algorithm, Brassard, Hoyer and Tapp have shown [153] that it is also possible to estimate the *number* of such marked items (rather than locating their positions). The underlying idea, broadly speaking, is to note that the amplitudes α_k and β_k above vary periodically with a period that is determined by the number of marked items. The periodicity is then estimated using the quantum Fourier transform, as described in preceding sections. It has also been shown [151, 153, 154] that, somewhat surprisingly at first sight, the unitary operation H_n in the definition of D may be replaced by almost any unitary operator U and the algorithm with the modified D still succeeds in finding x_0 in $O(\sqrt{N})$ steps.

Grover's algorithm provides a means of searching an exponentially large space of possibilities. Exponential searches in general are of fundamental importance in many branches of mathematics and computer science. Of particular interest is the situation in which the desired property (for which we are searching) can be verified to hold for any proposed item in *polynomial* time, i.e. intuitively the property itself is "computationally simple" to verify but we need to determine whether an example exists amongst an exponentially large number of candidates. As an illustrative example, suppose we are given a graph, described as a set of vertices and edges connecting selected vertices. A graph with n vertices may be coded as an $n \times n$ matrix of 0's and 1's with entry 1 in position ij if and only if there is an edge connecting vertex i to vertex j . We want to decide whether it is possible to find a closed path through the graph which visits each vertex once and only once. This is the so-called Hamiltonian circuit problem which has many important applications. Now given a graph, there is generally an exponential number of possible circuits (i.e. exponentially many as a function of the size of the description of the graph) but given any circuit it is easy to check in polynomial time whether it satisfies the required condition or not (i.e. just go around the circuit and see if it visits each vertex exactly once or not). In the theory of computation the class of all decision problems of this sort is called *NP* (c.f. [131, 132] for an extensive discussion). Intuitively for *NP* properties, it is "hard" to

find a satisfying instance but given a proposed instance, it is “easy” to check whether the property holds or not.

Many computational problems of great mathematical and practical interest lie in NP (c.f. [132] for a long and varied list of examples). Perhaps the most famous unsolved problem of classical complexity theory, the so-called $P \neq NP$ problem, is to establish whether every computational task in NP can in fact be solved in polynomial time or not. The motivating idea here is that if a property is “computationally simple” to verify then maybe the question of whether or not it held in a given structure, should also be able to be decided in polynomial time. Note that here we are not thinking of an exhaustive search amongst exponentially many candidates (which certainly must take exponential time) but of some clever analysis of the structure itself that generated the exponentially many possibilities. For example in the Hamiltonian circuit problem, is there a way of examining the description of the graph itself to see if it has a Hamiltonian circuit or not, instead of just unintelligently testing each circuit in turn?

Considering the intricacy and wide-ranging scope of some problems in NP [132] it would appear unlikely that they can be solved in polynomial time but this issue so far remains unproven, despite a great deal of attention! Note that some special mathematical properties of the particular structure of the problem would need to be invoked, e.g. in the Hamiltonian circuit problem the solution would be tantamount to developing some deep new theorem of graph theory.

Let us now return to the scenario of Grover’s search algorithm. Here the database was required to be *unstructured* (in contrast to the above remark) yet by quantum methods, we achieved a square root speed up over a direct exhaustive classical search. This speed up can be applied to a blind search in any NP problem. The crucial question now is this: can a search through an *unstructured* space of exponentially many candidates be *further* speeded up using quantum effects in some even more ingenious way? Indeed we have seen that exponentially large superpositions can be generated in linear time (4.3) and that these large superpositions can then be used to probe exponentially many values of a function using only a single query (c.f. (4.4)). In the early days of quantum computation, it was hoped that this effect might lead to a method of searching an exponentially large unstructured space of possibilities in polynomial time leading possibly to a quantum method of solving NP problems in polynomial time. For example given a graph we can look at all possible circuits in superposition but can we use this effect to determine, with high probability, whether there is a Hamiltonian circuit or not? This hope was dashed by Bennett, Bernstein, Brassard and Vazirani [155] who proved rigorously that no quantum process can speedup an unstructured search beyond the square root speed up exhibited in Grover’s algorithm. Roughly speaking the intuitive idea is that, although we can examine exponentially many candidates in superposition in one query, the registering of the desired property

will generally occur only with an exponentially small amplitude because of the exponential number of components in the superposition. Hence the process will have to be repeated an exponential number of times to register the property with any constant level of probability.

Thus in the context of quantum computation, just as in classical computation, if we are to solve NP problems in polynomial time, it will be essential to exploit the structure of the problem in some intelligent way. For example the exponential speedup in the algorithms of Simon and Shor makes use of special mathematical properties of the theory of periodicity via the techniques of Fourier analysis. Unfortunately the important question of the relation of the whole class NP to polynomial time computability, appears on the face of it to be no easier to resolve in the quantum context than in the context of classical computational complexity theory.

4.3 Quantum Gates and Quantum Computation with Trapped Ions

J.I. Cirac, P. Zoller, J.F. Poyatos

4.3.1 Introduction

It is clear from the preceding discussion in this chapter that quantum computation can offer amazing power. The question is: can we implement basic elements of quantum computation, such as quantum logic gates, and if so, how and in what kind of physical systems. Instead of a general discussion we will focus on one particular example. We will describe in some detail proposals related to the implementation of a quantum computer with trapped ions [156, 157]. In this scheme, each qubit is implemented as a superposition of the ground electronic state ($|0\rangle$) and the excited (metastable) state ($|1\rangle$) of an ion (see Fig. 4.9). It will be shown that a set of ions interacting with laser light and moving in a linear trap provides a realistic physical system to realise a quantum computer.

4.3.2 Quantum Gates with Trapped Ions

We will consider the situation where N ions are confined in a linear Paul trap, which is able to trap and confine the ions by means of a combination of static and ac electric fields (see Chap. 5). The ions basically move in only

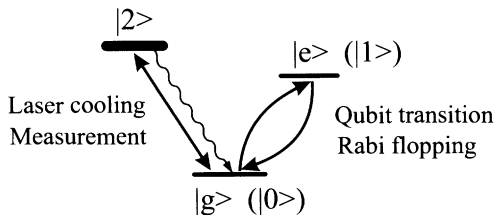


Fig. 4.9. Double resonance structure of the internal levels of a single ion. Those levels associated with the weak transition act as a qubit ($|0\rangle, |1\rangle$), while the third level, $|2\rangle$, connected to the $|0\rangle$ state by a dipole allowed transition is used for cooling and detection, by means of the quantum jump technique.

one dimension, the axial-direction, because in this direction the trapping potential is rather weak, and interact with different laser fields (Fig. 4.10).

The coupling of the motion of the ions is provided by the Coulomb repulsion which is much stronger than any other interaction for typical separation between the ions of a few optical wavelengths.

One of the initial advantages of the trapped ion system is that many of the required techniques to prepare and manipulate quantum states have already been developed for the purpose of high precision spectroscopy and frequency standards. Thus, Rabi floppings and measurements of the electronic states are both well developed tools, that will constitute basic parts of the computation. While Rabi flopping, i.e. coherent transitions between the internal states, are performed by applying a laser pulse for a fixed time (for example, a π pulse inverts completely the population from the excited to the ground state or vice versa), measurements of the internal quantum state are performed using the so-called quantum jump technique. Considering a double resonance situation, where one transition is strongly resonant, the other one being weaker, it is possible to measure the state of the selected levels chosen as qubits. This is done by using two laser beams tuned to each transition respectively. The state of the qubit will be measured by the presence or absence of spontaneously emitted light from the (dipole-allowed) strong transition, see Fig. 4.9. This scheme for detection has been proved to be of almost unit efficiency. On the other hand, we will also make use of laser cooling techniques to reduce the movement of the ions to small oscillations around their equilibrium position. In brief, laser cooling is based on the efficient use of radiation pressure, the momentum associated with every light beam. Such a momentum, negligible on a macroscopic scale, can nevertheless exert big enough forces on the atoms to considerably reduce their velocities (this force can be as big as $10^4 g$, where g is the acceleration due to gravity). An efficient way of using such forces is by means of the Doppler effect: in this way, ions moving opposite to the direction of propagation of the laser beam will experience a force able to considerably slow their motion.

Let us assume that the ions have been laser cooled in all three dimensions so that they merely undergo very small oscillations around the equilibrium position. In this case, the motion of the ions is described in terms of normal modes, being equivalent to a collection of uncoupled harmonic oscillators that can be quantized independently in the usual way. As a requirement, it is necessary to fulfill the so-called Lamb–Dicke limit for each mode, which physically means that the ion is confined in a region much smaller than the wavelength of the applied radiation.

The task of implementing a quantum computer will be equivalent to finding ways to implement single and two-qubit gates. Single qubit gates will be simple, since all we need is to induce Rabi flopping between the internal states of the qubit. As we already mentioned, this is a well known technique in the case of the trapped ions. Two-qubit gates will be more difficult to realise. The main difficulty is to find a way to connect quantum mechanically, i.e. maintaining the coherent superpositions, two qubits. To do this, we will consider the external degrees of freedom associated with the string of ions. In particular, we make use of the lowest quantized mode, the centre-of-mass (CM) motion describing the motion of all ions as if they were a joined single mass. The challenge is to swap information from the internal qubit onto the *quantum wire*, the CM motion. Once this is achieved, it will be possible to transfer the information from the *quantum wire* onto another selected qubit, realising in this way a coherent interaction between two qubits.

4.3.3 N Cold Ions Interacting with Laser Light

This section will be a little bit more technical, showing in more detail how to describe the system of ions and lasers and its ability to realise quantum computation. We consider the interaction of a given ion i with a standing laser wave (a travelling wave could be studied in the same way). The Hamiltonian describing this situation, in a frame rotating with the laser frequency, is given by $H = H_{\text{ex}} + H_{\text{int}} + H_{\text{las}}$, where ($\hbar = 1$)

$$\begin{aligned} H_{\text{ex}} &= \sum_{k=1}^N \nu_k a_k^\dagger a_k, \\ H_{\text{int}}^i &= -\frac{\delta_i}{2} \sigma_z^i, \\ H_{\text{las}}^i &= \frac{\Omega_i}{2} \sin(k_L r_i + \phi_i) (\sigma_i^+ + \sigma_i^-). \end{aligned} \tag{4.39}$$

Here, $\delta_i = \omega_L^i - \omega_0^i$ is the laser detuning (ω_L^i being the frequency of the laser and ω_0^i the frequency associated with the qubit transition), ν_k is the frequency of the different normal modes, Ω_i is the Rabi frequency¹ (the rate of coherent

¹ This name is due to I. I. Rabi who developed the initial idea of using an oscillator-driven magnetic field to induce transitions between internal levels of atoms and molecules.

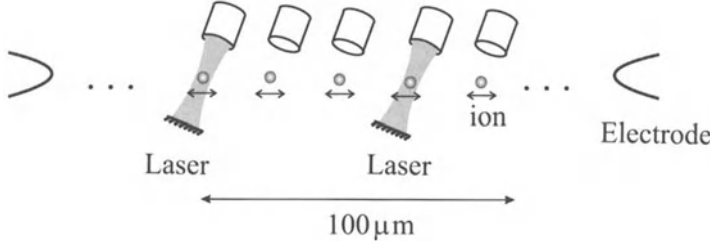


Fig. 4.10. N ions in a linear trap interacting with laser light. The motion of the ions is used as a data bus among qubits.

evolution induced by the applied laser field), k_L the laser wave vector (the laser beam is normally applied in a direction oblique to the trap axis, in this case k_L will be given by $k_\theta = k_L \cos(\theta)$, see Fig 4.10), ϕ_i is the phase describing the situation of the ion with respect to the standing wave and r_i is the position of the ion (expressed in general as a linear combination of the normal modes). In addition, we have used the Pauli operators associated with a two-level (spin 1/2) atom, and the creation (annihilation) operators associated with the quantized harmonic oscillator.

When a laser beam acts on one of the ions it will induce transitions between the (internal) ground and excited levels and can change the state of the collective normal modes. However, within the Lamb–Dicke limit, and considering weak enough laser intensities, only the CM motion will be modified. Under these limits the interaction with the laser will take the form

$$\begin{aligned} H_{\text{las}}^i &\approx H_a^i + H_b^i \\ &= \frac{\Omega_i^a}{2} (\sigma_i^+ + \sigma_i^-) + \frac{\Omega_i^b}{2} \frac{\eta_{\text{cm}}}{\sqrt{N}} (a_{\text{cm}} \sigma_i^+ + a_{\text{cm}}^\dagger \sigma_i^-), \end{aligned} \quad (4.40)$$

where η_{cm} is the Lamb–Dicke parameter associated with ν_z , the confinement frequency in the axial direction which coincides with the frequency of the CM mode. The above Hamiltonian is only valid when either $\Omega_1^a \neq 0$ ($\delta_a = 0$) or $\Omega_1^b \neq 0$ ($\delta_b \approx -\nu_z$). This means that we will find two available interactions modifying (b), or not modifying (a), the motion of the ions.

We show now how to realise quantum gates between one or two qubits making use of the above described interactions. Single-qubit quantum gates are easy to implement, since they imply only individual rotations of a single ion, without modifying its motional state. They can be realised using a laser at resonance with the internal transition frequency ($\delta_i = 0$) with the ion localised at the antinode of the standing wave laser beam. We have seen that the evolution in this case is given by the Hamiltonian H_a^i , inducing the following rotation

$$\begin{aligned} |g\rangle_i &\rightarrow \cos(k_L \pi/2) |g\rangle_i - ie^{i\phi} \sin(k_L \pi/2) |e\rangle_i, \\ |e\rangle_i &\rightarrow \cos(k_L \pi/2) |e\rangle_i - ie^{-i\phi} \sin(k_L \pi/2) |g\rangle_i. \end{aligned}$$

On the other hand, two qubit gates will be more difficult to implement. We consider first the laser frequency to be chosen in such a way that $\delta_i = -\nu_z$, i.e. it excites only the CM mode, and the ion localised at the node of the standing wave laser beam. The interaction with the laser is now given by the above H_b^t Hamiltonian. Applying a laser for a fixed time $t = k\pi/(\Omega_b^b \eta_z / \sqrt{N})$ (a $k\pi$ pulse) the states will evolve in the following way

$$\begin{aligned} |g\rangle_i|1\rangle &\rightarrow \cos(k_L\pi/2)|g\rangle_i|1\rangle - ie^{i\phi}\sin(k_L\pi/2)|e'\rangle_i|0\rangle, \\ |e'\rangle_i|0\rangle &\rightarrow \cos(k_L\pi/2)|e'\rangle_i|0\rangle - ie^{-i\phi}\sin(k_L\pi/2)|g\rangle_i|1\rangle, \\ |g\rangle|0\rangle &\rightarrow |g\rangle|0\rangle, \end{aligned} \quad (4.41)$$

where $|0\rangle$ ($|1\rangle$) denotes of the CM mode with zero (one) phonon, ϕ is the phase of the laser and $|e'\rangle$ can be either the state $|1\rangle$ of the qubit considered (denoted $|e\rangle$) or an auxiliary electronic state selectively excited. (This selective excitation can be realised by means of different polarisations or frequencies. Experimentally frequencies seem to be better controlled than polarisations). A two-qubit logic quantum gate can be implemented as follows: (i) using a π pulse focused on the first ion, we swap the internal state of the first ion to the motional state of the CM mode, (ii) introduce a conditional sign flip by means of a 2π pulse on the second ion using the auxiliary level $|e'\rangle_i$, and (iii) a π pulse will swap back the quantum state of the CM mode to the internal state of the first ion. The complete evolution will be given by

$$\begin{array}{ccccccc} (i) & & (ii) & & (iii) & & \\ |g\rangle_1|g\rangle_2|0\rangle & \longrightarrow & |g\rangle_1|g\rangle_2|0\rangle & \longrightarrow & |g\rangle_1|g\rangle_2|0\rangle & \longrightarrow & |g\rangle_1|g\rangle_2|0\rangle, \\ |g\rangle_1|e\rangle_2|0\rangle & \longrightarrow & |g\rangle_1|e\rangle_2|0\rangle & \longrightarrow & |g\rangle_1|e\rangle_2|0\rangle & \longrightarrow & |g\rangle_1|e\rangle_2|0\rangle, \\ |e\rangle_1|g\rangle_2|0\rangle & \longrightarrow & -i|g\rangle_1|g\rangle_2|1\rangle & \longrightarrow & i|g\rangle_1|g\rangle_2|1\rangle & \longrightarrow & |e\rangle_1|g\rangle_2|0\rangle, \\ |e\rangle_1|e\rangle_2|0\rangle & \longrightarrow & -i|g\rangle_1|e\rangle_2|1\rangle & \longrightarrow & -i|g\rangle_1|e\rangle_2|1\rangle & \longrightarrow & -|e\rangle_1|e\rangle_2|0\rangle. \end{array} \quad (4.42)$$

In this way, the net effect of the interaction will be a sign flip only when both ions are in the (internal) excited state. Note that before and after the gate the CM mode is in the vacuum state $|0\rangle$. Finally, making use of these operations we can realise logical gates employing *n-qubits* among every set of ions.

4.3.4 Quantum Gates at Non-zero Temperature

We have seen in the previous section how the system consisting of a set of ions in a linear trap appears to be a promising candidate for realistic implementations of quantum computations in the lab. The basic requirements for computing with laser cooled trapped ions seem to be precise control of the Hamiltonian operations, a high degree of decoherence and cooling of ions to the vibrational ground state to prepare a pure initial state for the collective phonon mode. We will not enter into the first two problems, since these are more related to the issues of error correction and decoherence that will be

discussed in Chap. 7, but we will show now how the restriction of cooling to the zero temperature limit can be overcome.

Let us consider the case of two ions in a linear trap. The novel idea is to use the movement of one of the ions' motional wave packet to the right or to the left depending on the absorption or emission of a laser induced photon, after which, the position of a second ion in the trap will be conditioned to the dynamics experienced by the first one. In this way one can enforce a position-dependent change of the internal state of the second ion. The result is a logic quantum gate essential for computation, i.e., the final internal state of the second ion depends on the initial internal state of the first one.

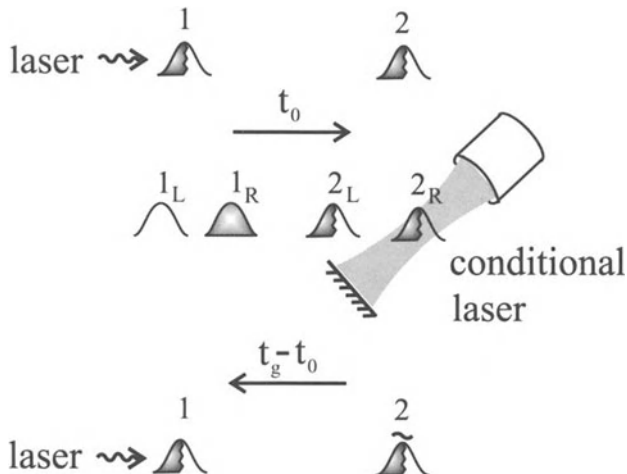


Fig. 4.11. Lasers and wave packet configuration for a two-qubit gate at non zero-temperature. After the realisation of the gate, the internal state of the target qubit (ion 2), will change or not (denoted with the tilde), depending on the internal state of the control qubit (ion 1), i.e. kick right or left due to stimulated photon absorption or emission. Here, the dark (light) filling of the wave packets stands for the internal excited (ground) states. See text for more details.

In some sense, we borrow ideas from atom interferometry, where atom wave packets are usually split into different parts, each one undergoing different dynamics, and joined at the end of the process to study the experienced evolution, as a kind of optical interference analysis.

We will show in particular how the two-qubit gate operation can be implemented. Firstly, by means of a laser beam, ion 1 is kicked left or right depending on its internal state due to photon absorption (emission). Thus, the other ion will experience a kick via the Coulomb repulsion conditional on the internal state of the ion 1. The corresponding wave packet would evolve into two possible spatial wavepackets which are entangled to the internal state of the control ion (denoted 1_R , 1_L , ... standing for ion 1 to the right, to the

left, etc). Provided the spatial splitting of these wave packets is sufficiently large (at a given time t_0), we can manipulate the internal state of the target ion, ion 2, depending on its spatial position, i.e. depending on the state of the control ion (ion 1), and thus implement a gate operation on the qubits. With time, these atomic wave packets will oscillate in the trap, and with a proper sequence of laser pulses this momentum transferred to the two ions can be undone to restore the original motional state (at time t_g), see Fig. 4.11. The motional state of the ion will then factorise from the internal atomic state before and after the gate, independent of whether it is in a mixed or a pure state, i.e. independent of the temperature.

In summary, in this section we have introduced a promising system to implement quantum computation. We have discussed proposals of conditional dynamics with ions considering two completely different situations, namely at zero and non-zero temperature. A proof of principle of the zero-temperature proposal was already reported by the group of D. Wineland at NIST [158] which indicates the building of small scale ion trap quantum computers will become feasible in the very near future. In the following chapter several aspects of the experimental realisation of quantum logic gates will be presented.

5. Experiments Leading Towards Quantum Computation

5.1 Introduction

The basic theoretical ideas of quantum computation have been explained in the previous chapter. But how feasible is it to actually construct a quantum computer? Realising that even a single quantum gate requires two strongly interacting quantum systems highly isolated from environmental disturbances, forces us to temper our optimism. This chapter presents several experimental techniques and results which indicate that a small number of highly controlled, strongly interacting, quantum systems are conceivable. However, whether or not it is possible to scale up to practical quantum computation remains to be seen.

Three experimental methods have succeeded in realising the proper experimental conditions for small-scale quantum-logic operations. They are based on cavity quantum electrodynamics (cavity QED), trapped ions, and nuclear magnetic resonances (NMR). The first two methods implement one of the simplest coupled quantum-mechanical systems: a two-level system coupled to a quantum oscillator. To stress this common feature, Sect. 5.2 presents the cavity QED experiments in parallel with the corresponding experiments on trapped ions.

The cavity QED experiments have been particularly successful in demonstrating fundamental features of quantum mechanics, like the quantum Rabi oscillation, presented in Sect. 5.2.3, Schrödinger's cat states and quantum decoherence, presented in Sect. 5.2.4. These experiments demonstrate in a beautiful way basic quantum logic operations; however, it seems very difficult to perform a large number of such operations with these techniques.

With respect to the scaling-up problem, trapped ion experiments seem more promising since it is possible to store and cool a string of ions in a linear trap. This string can be considered as a register of qubits where each qubit (stored on a single ion) can be addressed by tightly focused laser beams. In Sects. 5.2.5 to 5.2.12 it is demonstrated that quantum logic on the level of single ions can be performed and Sect. 5.3 provides a general overview of the experiments aimed towards quantum computation with strings of ions.

The third method under investigation for quantum computation, based on nuclear magnetic resonances (NMR), has already demonstrated a small

sequence of simple quantum-logic operations. NMR involves transitions between the Zeeman sub-levels of an atomic nucleus in a magnetic field. The frequencies of NMR signals from nuclei inside molecules depend on the precise chemical environment of the nucleus. This allows one to address different nuclear spins inside single molecules. The spins play the role of qubits, and via the strong spin-coupling interactions inside molecules they interact with one another. This provides the basic ingredients for quantum computation. Section 5.4 describes the principles of NMR quantum computation.

More speculative routes to performing quantum logic are based on solid state devices. Although a breakthrough in the fabrication of such devices would be extremely important, this field of research has not yet developed enough to be included here.

5.2 Cavity QED-Experiments: Atoms in Cavities and Trapped Ions

H.C. Nägerl, D. Leibfried, F. Schmidt-Kaler, J. Eschner, R. Blatt, M. Brune, J.M. Raimond, S. Haroche

5.2.1 A Two-Level System Coupled to a Quantum Oscillator

An atom in an optical cavity or ions in a trap can, to a good approximation, be considered as a two-level system coupled to a quantum harmonic oscillator. In the former case, a two-level atom is coupled to the cavity resonant mode. In the latter case, two internal states of one ion (hyperfine or metastable energy levels) are coupled to the vibrational degrees of freedom of the ions in the trap. Both systems can thus be characterized by the same interaction. The interaction (Jaynes–Cummings) Hamiltonian [159] can be written as:

$$H_{\text{int}} = -\hbar \frac{\Omega}{2} (a\sigma^+ + a^\dagger\sigma^-), \quad (5.1)$$

where a and a^\dagger are the annihilation and creation operators for the quantum oscillator, σ^+ and σ^- are the raising and lowering operators for the two-level system, and Ω is the coupling amplitude. This Hamiltonian describes emission or absorption of photons (in the case of cavity QED experiments) or phonons (in the case of trapped ion experiments) associated to an atomic or ionic transition. When the harmonic oscillator mode is exactly at resonance with the two-level system, the interaction term describes real energy exchange. When the systems are off resonance, the energy transfer processes are virtual and the interaction results in a phase shift of the atomic levels.

The key point is to realise the strong coupling regime, where the simple interaction of (5.1) dominates all relaxation processes, such as atomic spontaneous emission, photon/phonon damping, and decoherence caused by thermal noise. A convincing experimental realisation of the simplest matter-field system demonstrates elementary quantum logic operations. At the same time, it provides severe tests of our understanding of the least intuitive aspects of quantum theory, such as non-local entanglement and mesoscopic state superpositions.

Cavity QED developed both in the optical and the microwave domains, the basic principles of the experiments being extremely similar. For a review of these two classes of experiments, see [160]. In the optical domain, optical atomic transitions are coupled to very high finesse cavities. The strong coupling regime has been realised and investigated. This section will focus on the microwave domain. Long-lived, easily detected, circular Rydberg atoms are strongly coupled to the millimeter-wave radiation contained in a high- Q superconducting cavity. Atoms traveling at thermal velocities across the cavity get entangled with the field mode. The lifetimes of both the cavity field and the atomic two-level system are much longer than the interaction time. Therefore, the field and atom remain entangled even after the atom has left the cavity. The joint quantum state of the field and atom may thus be further investigated or manipulated at will.

The second class of experiments described in this section involves ions that are confined in an electromagnetic harmonic trap. The quantum oscillator is a specific mode of vibration of the ions. It is coupled, by laser pulses, to the internal state of the ionic two-level system. With well chosen pulses of laser light, the interaction of the ion motion with the internal state is, to an excellent approximation, described by the Jaynes–Cummings-type of Hamiltonians. Long coherence times of both the ionic two-level system and the vibration mode are achieved with techniques developed for ionic frequency standards.

In spite of a completely different experimental environment, the atom-cavity and trapped-ion experiments implement the same simple model. Therefore, any experiment designed for cavity QED can be translated in the context of ion traps, and vice versa. Moreover, the achievements of these two techniques are quite comparable. The next sections review cavity QED experiments in the microwave domain and trapped-ion experiments involving a Jaynes–Cummings interaction, followed by a comparison of the possible perspectives for quantum computation for both techniques.

5.2.2 Cavity QED with Atoms and Cavities

The general scheme of cavity QED experiments with atoms in microwave resonators is presented in this section. Experimental and theoretical details can be found elsewhere [160, 161].

Circular Rydberg atoms offer unprecedented tools for the realisation of cavity QED experiments. These atoms with their high-lying energy levels [162, 163], having principal quantum numbers n of the order of 50 and maximum orbital and magnetic quantum numbers, behave as huge antennae strongly coupled to millimetre-wave radiation. The dipole-matrix element on the transition between the circular states $n = 51$ ($|e\rangle$) and $n = 50$ ($|g\rangle$) at 51.099 GHz is as high as 1250 atomic units. When placed in a weak directing electric field, which avoids mixing with other levels in the hydrogenic multiplicity, these levels have a long lifetime, of the order of 30 ms, and behave as a true two-level system. Furthermore, they can be detected in a selective and sensitive way by the field-ionization method.

In the millimetre-wave domain, superconducting materials allow very high quality cavities. Centimetre-sized Fabry–Perot type cavities with niobium mirrors are used in the experiments. At low temperatures such as 0.6 K, the quality factor is in the range of 10^8 to 10^9 , corresponding to a photon storage time T_r of a few hundred microseconds up to a few milliseconds. This is much longer than the atom–cavity interaction time which is a few tens of microseconds for atoms at thermal velocities. At these low temperatures, the thermal field is quite negligible and the probability of finding the cavity in its ground state is above 98%.

The experimental set-up used in Ecole Normale, Paris [164]–[168], is sketched in Fig. 5.1. Its core is cooled to 0.6 K by a ${}^3\text{He}$ - ${}^4\text{He}$ cryostat. The atoms, initially effusing from an oven O , are velocity selected with the help of a laser beam at an angle with respect to the atomic beam propagation by velocity-selective optical pumping in zone V . The velocity-selected atoms are then prepared in box B in one of the states $|e\rangle$ or $|g\rangle$ by a succession of laser pulses and adiabatic radiofrequency transitions [163]. The preparation is pulsed and produces bursts of circular atoms at well defined times, with well controlled velocities between 200 and 400 m/s with a ± 2 m/s precision. The position of the atoms is known at any time with a ± 1 mm precision. Selective transformations can thus be applied on different atoms crossing the apparatus. The average number of atoms in each burst is kept below one, so that the probability of preparing two atoms at the same time remains small.

The superconducting cavity C is made of two spherical niobium mirrors, 2.7 cm apart. It sustains a transversal electromagnetic Gaussian mode with a 6 mm waist. When required, the cavity can be filled either by the atoms themselves through the process of resonant atom–field coupling or by a microwave source S injecting a coherent field. The cavity can be tuned in and out of resonance with the atomic transition by adjusting the mirrors’ distance or by modifying the atomic transition frequency through an electric field applied across the mirrors.

Before entering C , the atoms cross a low- Q auxiliary cavity R_1 in which a classical microwave pulse can mix levels $|e\rangle$ and $|g\rangle$. Each atom crosses C in a few 10 μs during which there is a strong interaction between the atom and the

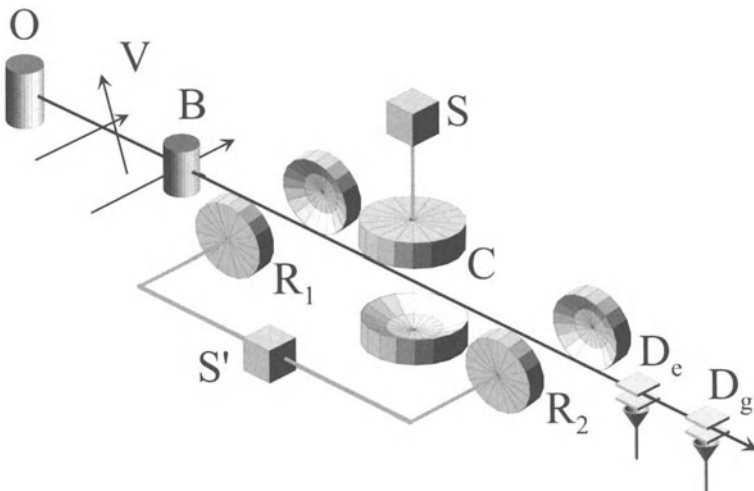


Fig. 5.1. Scheme of the atom–cavity experimental set-up.

cavity field. The atom–field coupling amplitude (Ω in the Jaynes–Cummings interaction) is $\Omega/2\pi = 50$ kHz for an atom at the centre of the cavity. This corresponds to the exchange rate of a single photon between an atom and the cavity mode. When the atom moves across the cavity, the coupling $\Omega(\mathbf{r})$ is a Gaussian function of its position. After C , a pulse of classical, resonant microwave may mix $|e\rangle$ and $|g\rangle$ again in the auxiliary cavity R_2 . Finally, the atoms reach two state-selective field-ionization detectors D_e and D_g , which count atoms in states $|e\rangle$ and $|g\rangle$ with a 40% efficiency.

An experimental sequence consists in sending one or two atoms, separated by a well defined interval, across the system and detecting them in D_e or D_g . The same sequence is repeated many times, with a repetition period of 1.5 ms which is longer than the cavity damping time, so that the field in C is in the same initial state at the beginning of each sequence. Statistics from repeated sequences are then extracted. Samples for joint two-atom probabilities correspond typically to 15000 events, recorded in about two hours. Two types of experiments have been performed. In the first one, presented in Sect. 5.2.3, the atoms and the cavity mode are at exact resonance which leads, via energy exchange, to entanglement of the atomic and field energies. In the second, presented in Sect. 5.2.4, the atoms and cavity are not at resonance and therefore the interaction produces atomic or cavity energy shifts, resulting in a phase entanglement.

5.2.3 Resonant Coupling: Rabi Oscillations and Entangled Atoms

Consider the case in which the cavity is tuned in resonance with the $|e\rangle \rightarrow |g\rangle$ atomic transition. Single photons can be emitted or absorbed by the single

atom in C [161]–[169] with a continuous stream of atoms, such cumulative emissions lead to the micromaser operation [170]. Such a single-photon single-atom interaction system has been used to demonstrate the quantum Rabi oscillation [171], direct evidence for field quantisation, a quantum memory [167], entanglement between two atoms [168], and single photon absorption-free detection [169].

The simplest experiment is performed by sending an atom in level $|e\rangle$ into the cavity and measuring the probability that it flips from $|e\rangle$ to $|g\rangle$ (zones R_1 and R_2 are not used) [165]. The measurement is repeated for various atom–cavity interaction times t , obtained either by changing the atomic velocity, or by Stark tuning the atomic transition into resonance with the cavity for a fraction of the crossing time.

Figure 5.2(A) shows the Rabi oscillation signal versus effective interaction time t in the case that the cavity field is initially in the vacuum state. The points are experimental and the line is a theoretical fit. The effective interaction time t , calculated from the experimental parameters, takes into account the Gaussian variation of the coupling inside the cavity. Four complete Rabi oscillations are observed, at a frequency close to $\Omega/2\pi = 50$ kHz. They correspond to the basic Jaynes–Cummings process: the reversible evolution of the atom between $|e\rangle$ and $|g\rangle$, correlated to the emission and absorption of one photon. The damping of the oscillations is caused by experimental imperfections. This vacuum Rabi oscillation signal is the time domain counterpart of the vacuum Rabi splitting observed in the spectrum of the atom–empty cavity system [172, 173].

Figures 5.2(B–D) show the oscillation signal when the cavity initially contains a coherent field with an average photon number equal, respectively for each figure, to $n = 0.40(\pm 0.02)$, $0.85(\pm 0.04)$ and $1.77(\pm 0.15)$. The oscillation involves several frequency components, corresponding to the various photon numbers present in the field. The beating between them gives rise to a collapse and a revival of the oscillations [171]. The Fourier transforms of the Rabi signals, shown in Fig. 5.2(a–d), exhibit peaks at the frequencies $\Omega\sqrt{n+1}$ corresponding to the Rabi frequency in the field of n photons ($n = 0$ to 3). The Rabi frequency, proportional to the amplitude for a classical field, is thus a discrete quantity. This provides a *direct evidence of field quantization in a box*. Figures 5.2(α – δ) show the Fourier components amplitudes, which give directly the photon number distribution. The small peak at $\Omega\sqrt{2}$ in Fig. 5.2(a) is due to the residual thermal field, which has an average photon number at 0.8 K of 0.06.

Besides providing a visceral evidence of field energy quantization, this experiment demonstrates that the atom–cavity resonant interaction dominates the relaxation processes. The resulting atom–field entanglement can be used to create or manipulate quantum entanglement, thus providing the basis for elementary quantum computation operations.

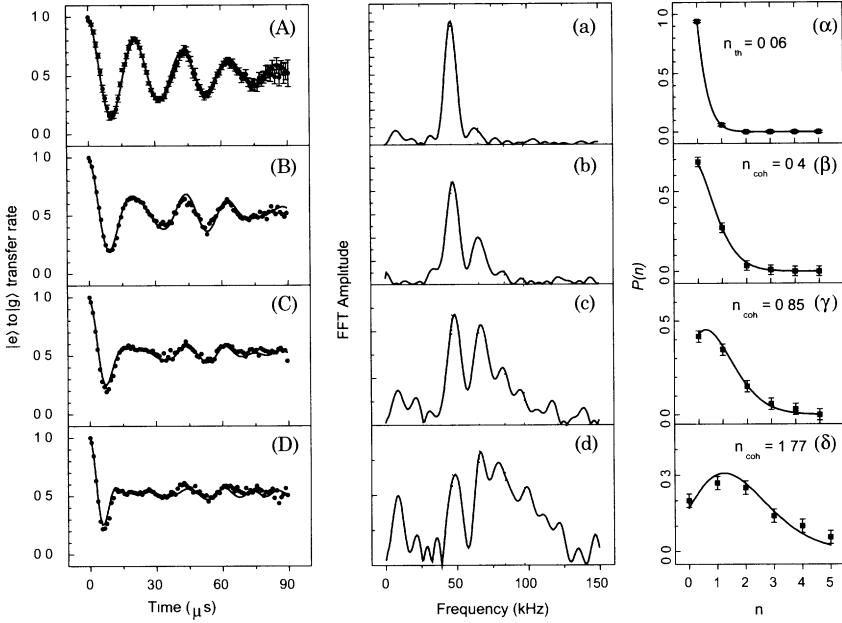


Fig. 5.2. Quantum Rabi oscillations. (A), (B), (C) and (D): Rabi nutation signals (A): no injected field and 0.06 (± 0.01) thermal photon on average; (B), (C) and (D): coherent fields with 0.40 (± 0.02), 0.85 (± 0.04) and 1.77 (± 0.15) photons on average. The points are experimental; the solid lines are theoretical fits. (a), (b), (c), (d): corresponding Fourier transforms. Frequencies ranging as the square roots of successive integers are indicated by vertical lines. (α), (β), (γ), (δ): photon number distribution inferred from experimental signals (points). Solid lines: theoretical thermal (α) or coherent((β) , (γ), (δ)) distributions.

Atom–field entanglement has first been used to realise a very simple device: a quantum memory holding a single qubit in the cavity. This memory is written by a first atom and read by a second. In the simplest situation, the first atom enters the empty cavity in state $|e\rangle$. The effective interaction time t is such that $\Omega t = \pi$. Therefore, the atom exits C in $|g\rangle$, leaving a one-photon state in C . The second atom, entering the cavity in state $|g\rangle$ after a delay T , absorbs this photon, provided it has not spontaneously decayed, and ends up in state $|e\rangle$. The decay of the probability of finding the second atom in $|g\rangle$ versus T measures the lifetime of a single photon in the cavity. Not surprisingly, it is equal to the classical field energy damping time T_r [167].

One can also send into the empty cavity an atom prepared in a superposition of $|e\rangle$ and $|g\rangle$ states with equal weights by a microwave $\pi/2$ pulse in R_1 (frequency ν). The $|e\rangle$ component of the atomic state emits, with unit probability, a photon in C , while the $|g\rangle$ component remains unaltered. The atomic state superposition is thus mapped onto the field as a superposition of 0 and 1 photon states, and the atom exits C in state $|g\rangle$. The field in C

has an average photon number equal to $1/2$ and a well defined phase, directly related to that of the microwave fields in R_1 . The phase information has been carried by the atom from R_1 to C .

The field is read out by a second atom, prepared in state $|g\rangle$ after a delay T , which again undergoes a π pulse in C . The quantum coherence is then mapped onto this atom, as a superposition of $|e\rangle$ and $|g\rangle$ states, leaving the cavity empty. A $\pi/2$ pulse is applied to the second atom in R_2 , with the same frequency ν and phase as the one applied on the first atom in R_1 . The cavity R_2 followed by D_e and D_g thus acts as a detector of the superposition state of the second atom, including phase information. The probability of detecting this atom in $|e\rangle$ or $|g\rangle$ oscillates versus ν , as in the usual Ramsey fringes situation. At variance with the usual situation, the two pulses are acting on two different atoms and the coherence is transferred between them via the cavity field in C . Figures 5.3(a–c) show the fringe signals indicating the coherence transfer for three different time intervals between atoms. When this time increases, the fringe period and the fringe amplitude decrease. The contrast reduction reveals the field decay in C . The decay time is twice as long as T_r , since this experiment involves a superposition of the $|1\rangle$ and $|0\rangle$ Fock (photon-number) states, the second being undamped.

In this experiment, a qubit is transferred between two atoms via a one-photon field. In the intermediate state, the cavity field is a highly non-classical superposition of one- and zero-photon states. Such an atom-to-field mapping process is essential in a proposed implementation of a cavity QED quantum gate [174].

The same scheme, under slightly different conditions, may be used to prepare and manipulate non-local atom–field or atom–atom entanglement [175]. A first atom sent into the empty cavity in state $|e\rangle$ undergoes a $\pi/2$ pulse ($\Omega t = \pi/2$). The atom and the cavity are then in the entangled state $|e, 0\rangle + |g, 1\rangle$. Atom–atom entanglement can be produced by sending a second atom prepared in state $|g\rangle$ across C with an interaction time such that $\Omega t = \pi$. The photon left by the first atom is absorbed by the second with unit probability, leaving the cavity empty and the atoms in the entangled state:

$$|\Psi_{\text{EPR}}\rangle = \frac{1}{\sqrt{2}} (|e_1, g_2\rangle - |g_1, e_2\rangle), \quad (5.2)$$

where the indices label the first and the second atom respectively.

This is an Einstein–Podolsky–Rosen pair of entangled particles [21]. The atoms can be represented by a spin one-half particle, the $|e\rangle$ and $|g\rangle$ states corresponding to the $+1/2$ and $-1/2$ states quantized along a direction Oz . $|\Psi_{\text{EPR}}\rangle$ is then the rotationally invariant “spin-zero” state, which means that the two spins should be anti-correlated in the sense that they will always be detected with opposite projections along any quantization axis. To illustrate this, choose an axis in the xOy plane in a direction making an angle ϕ with Ox . The spin eigenvectors along this axis are of the form $|e\rangle \pm e^{i\phi}|g\rangle$ and the state $|\Psi_{\text{EPR}}\rangle$ can be written (within an overall phase factor) as:

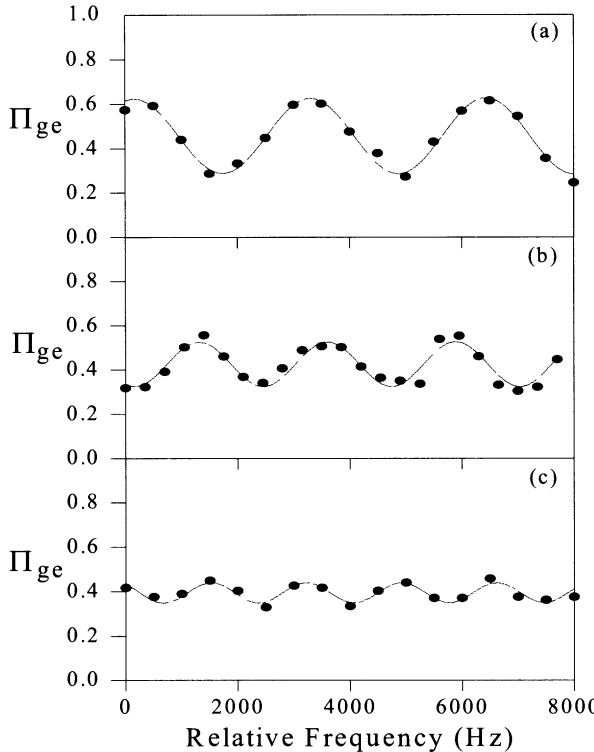


Fig. 5.3. Transfer of coherence between two atoms: conditional probability $\Pi_{ge}(\nu)$ of detecting the second atom in $|e\rangle$ provided the first one is detected in $|g\rangle$, versus the frequency ν of the microwave pulses applied to the first atom in R_1 and to the second in R_2 . The delays between the two microwave pulses in R_1 and R_2 are 301, 436 and 581 μs respectively from (a) to (c).

$$|\Psi_{\text{EPR}}\rangle = (|e_1\rangle + e^{i\phi}|g_1\rangle)(|e_2\rangle - e^{i\phi}|g_2\rangle) - (|e_1\rangle - e^{i\phi}|g_1\rangle)(|e_2\rangle + e^{i\phi}|g_2\rangle) \quad (5.3)$$

depicting the anti-correlation.

To analyse the entanglement in the energy basis (Oz axis), we detect the state of the atoms after they leave C . Ideally, the joint probabilities of detecting the atoms in the various combinations of $|e\rangle$ and $|g\rangle$ should be $P_{eg} = P_{ge} = 1/2$, $P_{ee} = P_{gg} = 0$. We find instead $P_{eg} = 0.44$, $P_{ge} = 0.27$, $P_{ee} = 0.06$, $P_{gg} = 0.23$. The difference is due to the decay of the photon stored in C between the passage of the two atoms, and to various other imperfections. A quantitative analysis shows that EPR pairs of atoms have been produced with a purity of 63% [168].

The anti-correlation property expressed by Eq. (5.3) is analysed by applying to both atoms a $\pi/2$ pulse in R_2 . The spin rotation in R_2 , followed by a detection along the Oz direction, is equivalent to a detection along a

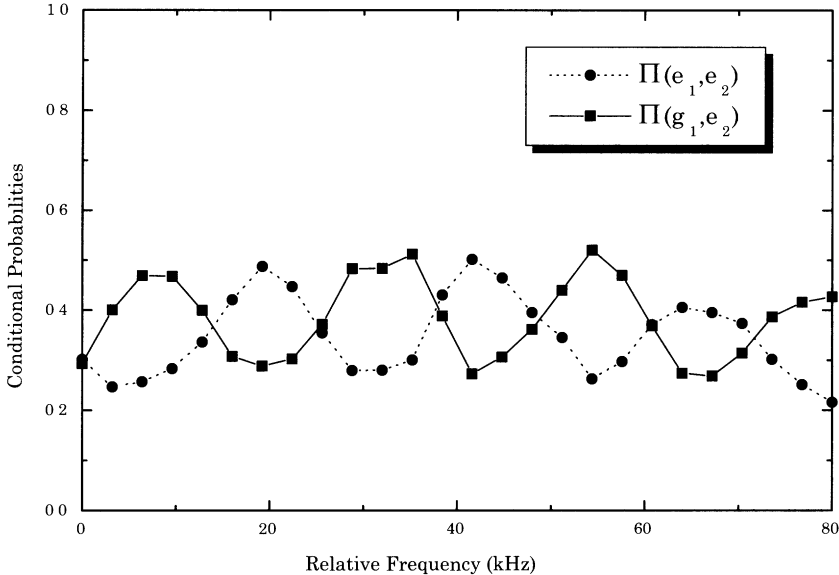


Fig. 5.4. EPR atomic entanglement: conditional probabilities $\Pi(e_1, e_2)$ (circles) and $\Pi(g_1, e_2)$ (squares) of measuring the second atom in state $|e\rangle$ when the first one has been found in $|e\rangle$ or $|g\rangle$ respectively, plotted versus the frequency ν of the pulses in R_2 . The lines connecting the experimental points have been added for visual convenience.

quantization axis in the horizontal plane. To be more specific, a detection in $|e\rangle$ or $|g\rangle$ after R_2 , corresponds to an atomic superposition $|e\rangle \pm e^{i\phi}|g\rangle$ before R_2 , where ϕ is the phase of the pulse applied in R_2 (+ sign for $|e\rangle$). According to the anti-correlation, the second atom should thus be projected by this measurement on the superposition pointing in the direction opposite the measured direction of the first atom. If both atoms were crossing R_2 simultaneously, a perfect anti-correlation between $|e\rangle$ and $|g\rangle$ detectors should be observed. In fact, the coherence of the second atom, delayed by time T , and the field in R_2 precess during the time interval T . The final probability of detecting the second atom in $|e\rangle$ or $|g\rangle$ depends upon the phase accumulated between the atomic coherence and the microwave in R_2 . This phase slip is proportional to the atom/Ramsey field frequency difference and to the flight time T . This is again a Ramsey fringes situation. However, the two microwave pulses are applied to different atoms and the phase is transferred between them through a non-local quantum correlation.

Figure 5.4 shows the conditional probabilities Π_{e_1, e_2} (Π_{g_1, e_2}) of detecting the second atom in $|e\rangle$, when the first is in $|e\rangle$ ($|g\rangle$) versus the frequency ν in the Ramsey zones. The modulations reveal the coherence of the state of the second atom. They are out of phase since the phase of the second atom changes by π when the first atom is detected in $|g\rangle$ instead of $|e\rangle$.

The experimental data demonstrate the preparation of controlled entanglement of two qubits (here, two atoms separated by approx. 1.5 cm). By combining resonant and dispersive interactions, this scheme can be extended to prepare triplets of atoms of the form $|e, e, e\rangle - |g, g, g\rangle$ [175]–[177].

The resonant atom–field interaction has also been used to perform the absorption-free detection of a single photon stored in the cavity [169]. The heart of the method is the conditional phase shift experienced by an atom crossing the cavity in level g and undergoing a 2π Rabi rotation in a single photon field. When the atom crosses an empty cavity (initial state $|g, 0\rangle$), it is unaffected by the interaction. When the cavity contains one photon, the atom–cavity system undergoes the transformation $|g, 1\rangle \rightarrow -|g, 1\rangle$. The π phase shift of the global wavefunction is similar to the one of a spin $1/2$ undergoing a 2π rotation in real space. This conditional phase shift can be tested by Ramsey interferometry on a transition connecting g to a reference level i uncoupled to the cavity field. The observation of the phase shift amounts to detecting the photon in the cavity. At variance with most photo-detectors, the photon is left in the cavity after the interaction with the “meter” atom. This experiment is thus equivalent to a quantum non-demolition measurement of a single photon field, restricted to the subspace spanned by the zero and one photon states. Moreover, the conditional dynamics at the heart of the method can be viewed as a quantum logic gate.

5.2.4 Dispersive Coupling: Schrödinger’s Cat and Decoherence

Consider now the case in which the atomic transition frequency ω_0 and the field mode frequency ω differ by δ , where δ is large compared to Ω and to the cavity linewidth. Under this condition, energy conservation prevents the emission or absorption of photons by the atoms and the interaction with the cavity is purely dispersive. The atom–field energy entanglement, as described in the previous section, is replaced by an entanglement of the atomic state with the phase of the radiation field, which can be considered to be classical. A microscopic degree of freedom controls thus a “macroscopic” quantity. This entanglement is a prototype of a quantum measurement and allows us to explore the weirdness of quantum mechanics at an unusual scale.

Let a circular Rydberg atom interact with a small coherent field in C , with cavity-field amplitude α and an average photon number $|\alpha|^2$, typically between 0 and 10. Since the vacuum Rabi frequency is a Gaussian function of the atomic position inside the cavity, the interaction is turned on and off adiabatically. This makes photon exchange between the atom and the cavity field very unlikely, even at small atom–cavity detunings ($\delta/2\pi = 100$ to 700 kHz). Therefore, the interaction results only in line shifts. The cavity mode is shifted by $\pm\Omega^2/4\delta$ for the atom at the centre of the cavity. This shift, resulting from the effect of the index of refraction of a single atom, takes the opposite value for an atom in states $|e\rangle$ or $|g\rangle$ [161]. It can reach up to

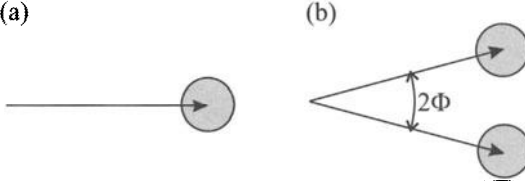


Fig. 5.5. (a): Pictorial representation in phase space of a coherent field state. (b) Components of the field in (5.4) correlated to the atomic states $|e\rangle$ and $|g\rangle$.

± 6 kHz for $\delta/2\pi = 100$ kHz, corresponding to an index per atom 15 orders of magnitudes larger than the ones of “ordinary atoms”.

The frequency shift, produced by the passage of a single atom through the cavity, results in a phase shift of the coherent cavity field by $\pm\Phi = \pm\Omega^2 t/4\delta$, where t is the effective interaction time. The phase shift is typically of the order of one radian. This atom–field interaction can be used to generate a non-classical superposition of field states with different phases. The atom is prepared in a superposition of $|e\rangle$ and $|g\rangle$ by a $\pi/2$ pulse in R_1 . When it crosses C , it simultaneously imparts to the field two opposite phase shifts, $\pm\Phi$. The combined atom–field system thus becomes

$$|\Psi\rangle = \frac{1}{\sqrt{2}} (|e, \alpha e^{i\Phi}\rangle + |g, \alpha e^{-i\Phi}\rangle) . \quad (5.4)$$

This is an entangled state, the energy of the atom being correlated to the phase of the cavity field. The coherent field can be represented as an arrow in phase space whose length and direction are associated to the amplitude and phase, as illustrated in Fig. 5.5(a). The tip of the arrow lies in a circle of unit radius describing the quantum uncertainties of the field. Equation (5.4) allows to see this arrow as a “meter needle” assuming two different directions correlated to the atomic state, as shown in Fig. 5.5(b). The interaction realises a “measurement” in which the “field arrow” is used to determine the energy of the atom. One can also adopt Schrödinger’s metaphor [178]: the $+\Phi$ and $-\Phi$ field components are then analogous to the “live” and “dead” states of the famous cat entangled to an atom in a superposition of excited and ground states.

After leaving the cavity and before detection, the atom undergoes another $\pi/2$ pulse in R_2 , phase coherent with the one in R_1 . The probability P_g of detecting the atom in $|g\rangle$ is measured as function of the frequency ν applied in R_1 and R_2 . Figure 5.6(a) shows the experimental result for the case of no photons in the cavity field and for a detuning $\delta/2\pi = 712$ kHz. The atomic state can be transferred from $|e\rangle$ to $|g\rangle$ either in R_1 (crossing C in state $|g\rangle$) or in R_2 (crossing C in state $|e\rangle$). Since the atom does not leave any trace of its presence inside the cavity, these two paths cannot be distinguished and the corresponding amplitudes interfere, leading to oscillations (Ramsey fringes) in P_g .

Figures 5.6(b–d) show the experimental results for a coherent cavity field with an average of 9.5 photons and for decreasing atom–cavity detunings. The smaller the detuning, the larger the separation of the field components in C will be. The inserts in Fig. 5.6(b–d) illustrate the phase information of the field which is a record of the atomic state. Such Welcher-Weg (which-way) information, even unread, must destroy the interference effect according to the complementarity principle. A quantitative analysis shows that the fringe signal is ruled by the overlap integral between the two field components, its modulus yielding the fringe contrast and its phase the one of the Ramsey fringes. For large Φ , the overlap is small and the fringes disappear. For small Φ , fringes are observed, albeit with a reduced contrast. The signals show convincingly that the cavity acts as a meter for the atomic state. Moreover, the phase shift of the fringes for large detunings provide a precise determination of the photon number.

The quantum superposition of the mesoscopic field, resulting from the above preparation and detection scheme of the atom passing the cavity, is fragile and subject to decoherence, especially when $|\alpha|^2$ and/or Φ become large [179]–[186]. In order to monitor the evolution from a quantum superposition to a statistical mixture, the “cat state” of the field is probed with a second atom, crossing the cavity after a delay T [166, 186]. The probe produces the same phase shifts as the first atom. It splits each of the two field components, caused by the first atom, into two parts. This means that the final field state exhibits four components, two of which coincide at zero phase. Whenever the two atoms crossed C in the $|e\rangle, |g\rangle$ or in the $|g\rangle, |e\rangle$ combination, the phase returns to its initial value. After the atomic states mixing in R_2 , there is no information left on the path followed ($|e\rangle, |g\rangle$ or $|g\rangle, |e\rangle$), since the second atom has partially erased [187] the information left in the field by the first one. The contributions of these two paths thus lead, in the joint probabilities P_{ee} , P_{eg} , P_{ge} and P_{gg} , and in the correlation signal $\eta = P_{ee}/(P_{ee} + P_{eg}) - P_{ge}/(P_{ge} + P_{gg})$, to the presence of interference terms.

If the state superposition survives during T , η ideally takes the value 1/2, whereas it vanishes when the field state is a mere statistical mixture. The experimental values of η versus T are shown in Fig. 5.7 for two different “cat” states (depicted in the inserts). The points are experimental and the curves theoretical [188]. The maximum value is 0.18 only, due to the limited contrast of the Ramsey interferometer. Decoherence occurs within a time much shorter than the cavity damping time and is more efficient when the separation between the cat components is increased. It shows that we observe a non-trivial relaxation mechanism, whose time constants drastically depend upon the initial state.

Decoherence is due to the loss of photons out of the cavity. Each “escaping” photon can be described as a small “Schrödinger kitten” copying in the environment the phase information contained in C . The mere fact that this “leaking” information could be read out is enough to wash out the interfer-

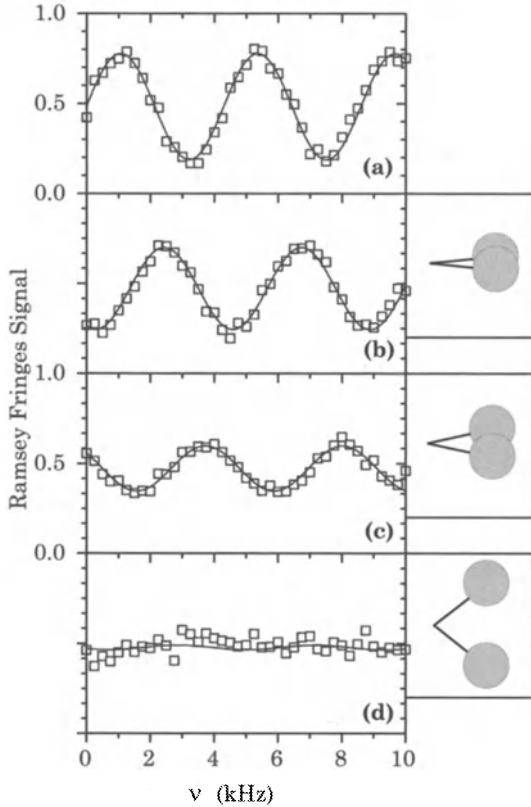


Fig. 5.6. Ramsey fringes in the probability versus ν of detecting the atom in level $|g\rangle$: (a) C empty, $\delta/2\pi = 712$ kHz; (b) to (d) C stores a coherent field with $|\alpha| = \sqrt{9.5} = 3.1$, $\delta/2\pi = 712$, 347 and 104 kHz respectively. Points are experimental and curves are sinusoidal fits. Inserts show the phase space representation of the field components left in C .

ence effects related to the quantum coherence of the “cat”. In this respect, decoherence is a complementarity phenomenon. The short decoherence time of the Schrödinger cat states presented above, about T_{cav}/n , is explained by this approach. The larger the photon number, the shorter is the time required to leak a single “photon-copy” into the environment. This experiment verifies the basic features of decoherence and vividly exhibits the fragility of quantum coherences in large systems. Extrapolation of quantum mechanical superposition states to macroscopic scale leads to an almost instantaneous decoherence, validating the Copenhagen interpretation of quantum measurement for any practical purpose. This experiment also provides interesting insight into the difficulties which have to be overcome in order to produce and control large-scale quantum entanglement, namely that quantum decoherence appears to be the major limitation to large scale quantum information processing.

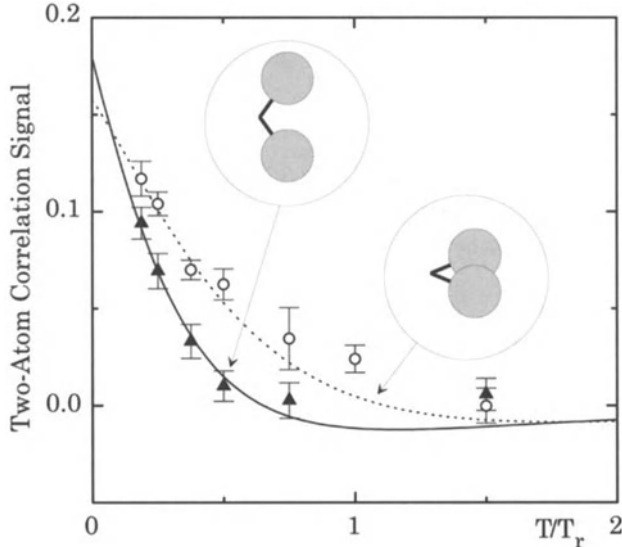


Fig. 5.7. Decoherence of a Schrödinger cat: two-atom correlation signal η versus T/T_r for $\delta/2\pi = 170$ kHz (circles) and $\delta/2\pi = 70$ kHz (triangles). Dashed and solid lines are theoretical. Insets: pictorial representations of corresponding field components separated by 2Φ .

A further discussion of the limits to quantum computation, without quantum error correction schemes, is given in Sect. 7.3.

5.2.5 Trapped-Ion Experiments

One or a few ions stored in radio-frequency Paul traps offer an ideal environment to study the dynamics of simple quantum systems, and, with the aid of laser pulses, the investigator can tailor the interaction of those simple systems almost at will. An especially interesting scenario is created by substituting the photon field of cavity QED, as described in the previous sections, by the harmonic oscillator describing the motion of the ion(s) in the external trapping potential. A suitable light field can couple two internal electronic levels of the ion(s), $|g\rangle$ and $|e\rangle$, to the external vibrational motion at frequency ω with an interaction Hamiltonian of the form [189]–[192]:

$$H_{\text{int}} = -\hbar G \left(\sigma^+ e^{i\eta(a^\dagger + a) - i\delta t} + \sigma^- e^{-i\eta(a^\dagger + a) + i\delta t} \right), \quad (5.5)$$

where $\eta = \delta k \sqrt{\hbar/(2m\omega)}$ is the Lamb–Dicke parameter with the modulus δk of the wavevector (or a wavevector difference if the systems are coupled by Raman transitions), $(a^\dagger + a)$ the position operator in terms of the harmonic oscillator ladder operators and G is a coupling strength, proportional to the amplitude of the coupling light field. This interaction Hamiltonian is

inherently richer than the Jaynes–Cummings Hamiltonian, (5.1), but reduces to the latter by choosing the detuning of the light field with respect to the energy difference of the two internal states to be $\delta = -\omega$ and in the limit $\eta\sqrt{\langle(a^\dagger + a)^2\rangle} \ll 1$. In general any detuning with $\delta = (n' - n)\omega$ (n, n' integer numbers) will resonantly drive transitions between the states $|g, n\rangle$ and $|e, n'\rangle$, and thus lead to another effective interaction Hamiltonian. In addition, the coupling strength G is not fixed by dipole matrix elements and the mode volume of the cavity, as is the case in the experiments presented in the previous sections, but can be varied by an appropriate choice of the light intensity.

The techniques to realise the situation described above in a laboratory have grown out of the efforts to build frequency standards with trapped and cooled ions [193]–[195]. Dynamical trapping of charged particles in radiofrequency (rf) traps was first proposed and experimentally verified by W. Paul in 1958 [196]. A rf electric field, generated by an appropriate electrode structure, creates a pseudo-potential confining a charged particle [197]. For the trapping of *single* atomic ions the electrodes have typical dimensions of a few millimetres down to about 100 μm . The rf fields are in the 10–300 MHz range, with a peak to peak voltage of hundreds of Volts. The motion of a particle confined in such a field involves a fast component synchronous to the applied driving frequency (micro motion) and the slow (secular) motion in the dynamically created pseudo-potential. For a quadrupole (rf) field geometry, the pseudo-potential is harmonic and the quantized secular motion of the trapped ion is very accurately described by a quantum harmonic oscillator. For a more detailed description of different types of Paul traps and their special properties we refer to Sect. 5.3.2.

For frequency standards, the trapped ions should offer at least one long lived, narrow transition that can be either in the microwave (for example, a ground state hyperfine transition) or the optical range (for example a transition to a metastable excited state). To reduce Doppler shifts and other adverse effects related to the motion, laser cooling of the ions is a very convenient tool. This cooling mechanism was proposed in 1975 by Wineland and Dehmelt [198] and experimentally observed in 1978 [199]. For experiments with fundamental quantum systems and quantum logic applications the requirements are almost identical. The narrow transition now forms the well isolated two-level system, while laser cooling is the key tool to initialise the harmonic oscillator of the motion in a well defined state.

5.2.6 Choice of Ions and Doppler Cooling

Although an ion trap is very deep (several eV potential well depth) and will hold almost every ion, only a few ions are suitable for cavity QED-like experiments. They should exhibit energy levels appropriate for the realisation of a two-level system with negligible decoherence by spontaneous decay, and should also allow for optical cooling and detection. The ions of choice have

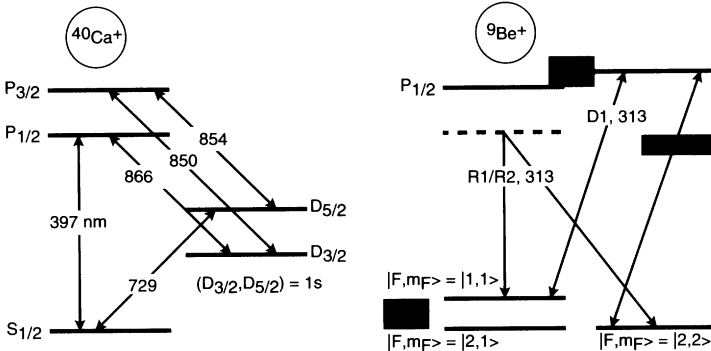


Fig. 5.8. $^{40}\text{Ca}^+$ and $^9\text{Be}^+$ level scheme. The wavelengths of the different transitions are indicated. For $^{40}\text{Ca}^+$, the lifetimes of the excited states are indicated too.

typically one electron in the outermost shell (hydrogenic ions) and a correspondingly simple electronic level structure. The two-level system can either be provided by two hyperfine ground states or by a long-lived metastable electronic state [200]. Most of the relevant experiments have been done with $^9\text{Be}^+$ by the NIST ion storage group in Boulder [201], but other groups are also gearing up to work on quantum logic and coherent control, as e.g. IBM Almaden ($^{138}\text{Ba}^+$), JPL in Los Angeles [202] ($^{199}\text{Hg}^+$), the MPQ in Garching [203] ($^{25}\text{Mg}^+$), Los Alamos National Laboratory [204] ($^{40}\text{Ca}^+$) and the Universities of Mainz [205] ($^{40}\text{Ca}^+$), Hamburg [206] ($^{138}\text{Ba}^+$, $^{171}\text{Yb}^+$) and Innsbruck [207] ($^{40}\text{Ca}^+$, $^{138}\text{Ba}^+$). The following discussion will concentrate on $^9\text{Be}^+$, where hyperfine ground states form the two-level system, and on $^{40}\text{Ca}^+$, where an optically excited metastable level is used. The level schemes of $^{40}\text{Ca}^+$ and $^9\text{Be}^+$ are shown in Fig. 5.8.

Cooling is required to realise a well defined initial state of vibration for the trapped ions. The most obvious choice is the ground state [208], but trapping states have also been proposed [209]. Most of the kinetic energy can already be extracted by Doppler cooling. This technique is based on the fact that atoms moving towards a laser source can be excited if the laser frequency is slightly detuned to the red (Doppler shift) with respect to the optical transition. The motion of the atoms will slow down due to scattering of photons. The momentum transfer due to absorption constantly adds up while it averages to zero for spontaneous emission which is spread over a 4π solid angle. Thus, the motional energy or equivalently the temperature of the ions is reduced. The mean final energy which can be reached by this technique is given by the Doppler cooling limit $E_D = \hbar\Gamma/2$ where Γ denotes the natural width of the excited state of the cooling transition. The same procedure is applied for trapped ions if the vibrational frequency (the secular frequency ω_i along the respective axis) is smaller than the natural line width Γ . Here, the required motion towards the laser source is provided by the

periodic vibration of the ions in the trap and, as in the case of free atoms, the final temperature for this cooling process is $T_D = E_D/k_B$ [210] (typically on the order of a few milliKelvin).

For most ions the optical transition used for Doppler cooling is in the ultra violet. For ${}^9\text{Be}^+$, the ${}^2\text{S}_{1/2}$ to ${}^2\text{P}_{3/2}$ transition at 313 nm is used, while for ${}^{40}\text{Ca}^+$ the corresponding transition is at 397 nm. Coincidentally, the linewidth is about 20 MHz in both Be^+ and Ca^+ . The cooling light is generated by frequency doubling a dye or a Ti:Sapphire laser respectively. In Ca^+ the $\text{P}_{1/2}$ level may decay to a metastable $D_{3/2}$ level and one needs an additional laser diode at 866 nm to repump the ions. In both cases Doppler cooling leads to a thermal state of motion with a temperature of about 1 mK, but $\langle n_D \rangle$ the corresponding mean number of vibrational quanta in the harmonic oscillator depends on the trap stiffness. For the trap used in the Be^+ experiments at NIST $\omega/2\pi$ was 11.2 MHz leading to $\langle n_D \rangle \simeq 1.3$ [211], while for the much weaker symmetry axis of the linear trap used for Ca^+ in Innsbruck ($\omega/2\pi \simeq 100\text{--}180$ kHz) $\langle n_D \rangle \simeq 50$ [212]. The design of traps is determined by a tradeoff between the spacing between the ions, which one wishes to be large enough to address each ion by single laser beams [213], and the cooling schemes which one wishes to keep as simple as possible. The Innsbruck ion trap has an ion spacing of about 15 micrometres whereas the NIST ion trap has a spacing of 1–2 micrometres.

For a single ion the notion of temperature is used in an ergodic sense, i.e. the average over repeated measurements will eventually reveal the final energy (or temperature). For motional frequencies ω_i larger than Γ it is more appropriate to consider the spectral structure of the cooling transition. Due to the vibrational motion of a trapped ion, the absorption spectrum acquires sidebands at $(\omega_0 \pm n\omega)$ where ω_0 denotes the transition frequency. The strength of these sidebands is given by the vibrational energy. It is possible to use these sidebands to obtain optical cooling below the Doppler limit. This method will be explained in the next section.

5.2.7 Sideband Cooling

To a good approximation a trapped ion can be treated as a quantum mechanical harmonic oscillator. As indicated in Fig. 5.9 for motion along one axis, the internal states of a single two-level atom are dressed with a harmonic oscillator level structure similar to a molecular structure, where the vibrational states are given by the trap frequency along this axis. These levels can then be conveniently labeled by the internal degrees of freedom $|e\rangle, |g\rangle$ (describing electronic excitation) and the external degrees of freedom $|n\rangle$ (i.e., motional excitation of the harmonic oscillator). For ions in a string the spectral structure is much richer, but the procedures and techniques outlined in this section are applicable, after some modification, to ion strings as well (see Sect. 5.3.3).

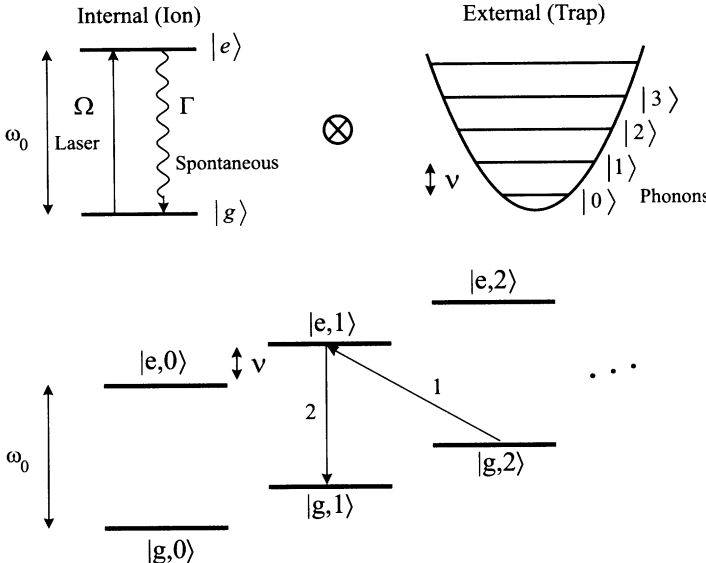


Fig. 5.9. Level scheme of a single two-level ion trapped in a harmonic potential. Sideband cooling is achieved by a photon absorption inducing the transition $|g, n\rangle \rightarrow |e, n-1\rangle$ indicated by arrow 1, and the subsequent decay (via spontaneous emission or an additional optical pump process) dominantly into $|g, n-1\rangle$ (see arrow 2).

Very efficient cooling is obtained by tuning the laser frequency such that absorption occurs on the lower sideband of the vibrational motion. This absorption is due to the transition $|g, n\rrangle \rightarrow |e, n-1\rangle$ (e.g. arrow 1 in Fig. 5.9). Subsequent spontaneous emission appears predominantly on the carrier frequency, i.e. $|e, n-1\rangle \rightarrow |g, n-1\rangle$ (arrow 2 in Fig. 5.9) and thus the average excitation of the mechanical oscillation is effectively damped by one vibrational quantum. One can also actively repump to $|g, n-1\rangle$ via a fast decaying third level. If the photon recoil energy E_{rec} in the decay is much smaller than an oscillator energy quantum, the motional state changes only with probability $E_{\text{rec}}/(\hbar\omega)$. On average the recoil is not absorbed by the ion's motion, but rather by the whole trap structure. When these steps are repeated a sufficient number of times, the ion is finally left in the ground state with high probability, since once $|g, 0\rangle$ is reached, it decouples from both laser fields (dark state).

In the experiments performed on Be^+ , Raman transitions, that is transitions induced by two laser beams R1 and R2 indicated by R1/R2 in Fig. 5.8, couple two (hyperfine ground) states with a frequency difference of $\omega_{\text{HF}}/(2\pi) \simeq 1.25$ GHz via a virtual third level. The Raman beams are produced by detuning a frequency doubled dye laser from the ${}^2\text{S}_{1/2}-{}^2\text{P}_{3/2}$ transition by approx. 12 GHz and splitting it into two components about 1.25 GHz apart with an acousto-optical modulator (AOM). In this way the frequency

difference and relative phase of the two components can be controlled with rf-accuracy, and not too high demands are put on the absolute stability of the laser. In the NIST experiment no special precautions are taken to spectrally narrow the dye laser which has a linewidth of approximately 1 MHz. For resolved sideband cooling, the frequency difference is tuned to $\omega_{\text{HF}} - \omega$ (red sideband). The cooling cycle then proceeds as described above, with the repumping induced by excitation on the $^2S_{1/2}$ to $^2P_{3/2}$ dipole transition also used for Doppler cooling [211].

For Ca^+ , the metastable $D_{5/2}$ level, indicated in Fig. 5.8, with a spontaneous lifetime of approx. 1 second, can be used together with the ground state for resolved sideband cooling techniques. Again, motional quanta are removed by inducing transitions with the exciting laser detuned by ω to the red of the narrow resonance. In contrast to Raman transitions, the laser has to exhibit a good absolute frequency stability to resolve motional sidebands, so care has to be taken in the stabilisation. The setup used at Innsbruck University consists of a Ti:Sapphire laser at 729 nm, stabilised to a thermally and acoustically insulated reference cavity suspended in vacuum. The finesse of the cavity is 250 000 and preliminary tests suggest a laser linewidth of better than 1 kHz. In principle the recoilless return to the ground state could serve as a means of repumping, but the 1 second lifetime of the metastable state would make cooling very slow. To speed up the cooling cycle the ions are repumped to the ground state via the quickly decaying $P_{3/2}$ level. In this manner a single Hg^+ ion was cooled to the ground state in one dimension by the NIST group in 1989 [214]. In Ca^+ , the repumping transition can be driven by a laser diode at 854 nm. Ground-state cooling of a single ion, and recently the ground-state cooling of various modes of vibration for two ions, has been observed in a spherical Paul trap at the University of Innsbruck [215]. The first cooling to the ground state of collective modes of motion of two trapped $^9\text{Be}^+$ ions has been reported in Ref. [216].

Obviously, ground state cooling is easier if Doppler cooling results in a low mean oscillator quantum number. In this case, only few resolved sideband cooling cycles are necessary to reach the vibrational ground state. For the stiff NIST trap, 5 Raman cooling cycles are enough to end up in the ground state 98% of the time [211]. In the case of Ca^+ in the spherical Innsbruck trap, 99.9% motional ground-state occupation (at a 4.5 MHz trap frequency) was measured after a cooling period of 6.4 ms [215]. Here the cooling rate was a few kHz. In the case of the linear Innsbruck trap, which has a lower trap frequency and consequently higher vibrational quantum numbers after Doppler cooling, the difficulty of ground-state cooling is enforced. However, the advantage of the linear trap, as mentioned above, is a wider ion-to-ion spacing, which simplifies individual addressing for quantum gate operations. Furthermore, low heating, as low as one phonon per 190 ms, has been observed which is related to the relatively large trap dimensions of 1.4 mm [215].

5.2.8 Electron Shelving and Detection of Vibrational Motion

The quantized motion of a small number of ions couples only very weakly to the environment and it is hard to detect it directly. In contrast, the internal electronic state can be detected in a very convenient way by the so-called “electron shelving” method proposed by Dehmelt [217]. This situation is quite similar to the “classical” cavity QED experiments, where the photon field is confined inside the superconducting cavity and hard to access, but can be inferred indirectly by measurements on the Rydberg atoms after their interaction with the oscillator mode.

The basic idea of the “electron shelving” method is very simple. A three-level system is needed consisting of a ground state $|g\rangle$, a metastable excited state $|e\rangle$, and a short lived excited state $|p\rangle$. The ground state is now coupled to the excited state $|e\rangle$ for some time, leaving the system in some superposition $\alpha|g\rangle + \beta|e\rangle$. If the $|g\rangle \rightarrow |p\rangle$ transition is now driven, the short-lived state $|p\rangle$ will be excited and decay if, and only if, the system collapses into $|g\rangle$. The fact that a photon is emitted with the decay of $|p\rangle$, that could, in principle, be observed, constitutes a measurement on the superposition. The measurement yields the result $|g\rangle$ with probability $|\alpha|^2$, corresponding to the excitation and decay of $|p\rangle$, and the result $|e\rangle$ with probability $|\beta|^2$, corresponding to the absence of excitation and decay of $|p\rangle$. Even if the efficiency for detecting the photon from one decay of $|p\rangle$ is very low (typically 10^{-3}), one can keep re-exciting the system and scatter millions of photons, eventually detecting a few of them provided the state is reduced to $|g\rangle$. If the state is “shelved” in the metastable state $|e\rangle$ no scattering will happen. In every single experiment the answer will be either $|g\rangle$ (scattered photons detected) or $|e\rangle$ (no scattered photons detected), thus measuring these states with almost 100 % detection efficiency and destroying all coherences between $|g\rangle$ and $|e\rangle$.

Averaged over many experiments, the number of tries where scattered photons are observed will be proportional to $|\alpha|^2$. As an example of the efficiency of this method, Fig. 5.10 shows the light scattered from a single Ca^+ ion into a photomultiplier during continuous excitation on the $S_{1/2} \rightarrow P_{1/2}$ transition at 397 nm. When the Ca^+ ion is in the $S_{1/2}$ state it scatters about 2000 photons in 100 ms into the photomultiplier. At certain times, for example around $t = 20$ s, the ion is excited into the $D_{5/2}$ state with a weak beam at 729 nm and the rate drops to about 150 events in 100 ms, given by the number of dark counts of the imperfect photomultiplier and some 397 nm light directly scattered from the exciting beam into the detector. Obviously, the two states can be well discriminated with good precision within 1 ms, and the average dark time is about 1 second, the radiative lifetime of the $D_{5/2}$ state.

With minor modifications the quantum shelving method can also be applied to distinguish between hyperfine ground states, as is necessary in experiments with ${}^9\text{Be}^+$. Since $|g\rangle$ is chosen to be the state with maximum m_F

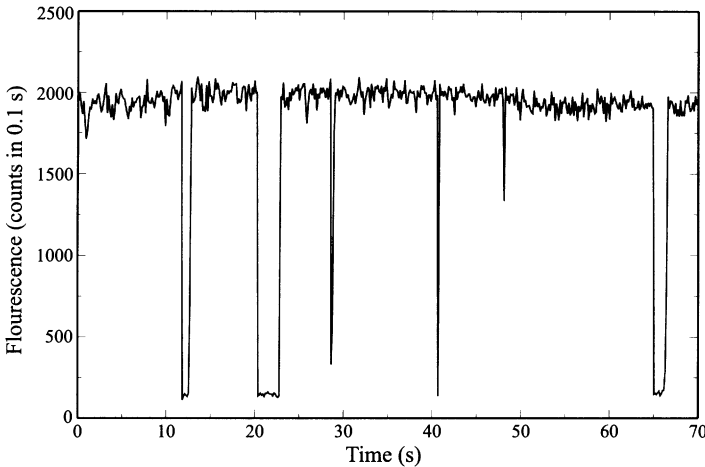


Fig. 5.10. Quantum jumps of a single $^{40}\text{Ca}^+$ ion. If the ion makes the transition to the metastable $D_{5/2}$ state, the fluorescence drops. After a mean time equal to the lifetime of the excited state ($\tau \simeq 1$ s), a spontaneous transition returns the ion to the ground state and the fluorescence returns to the higher level.

($F = 2, m_F = 2$), one can excite a cycling transition to the $^2\text{P}_{3/2}$ ($F = 3, m_F = 3$) state using σ^+ circular polarised laser light (D2 in Fig. 5.8) leaving the ion no other decay channel but the one back to $|g\rangle$. A combination of experimental imperfections in producing the polarised light σ^+ and off resonant excitations can lead to optical pumping into non-scattering states, reducing the detection efficiency [218].

5.2.9 Coherent States of Motion

The production of coherent states of light using cavity QED has been discussed in Sect. 5.2.3. Here we describe the production of coherent states of motion for a ion(s) in a trap. Starting from the ground state, coherent states of motion can be produced by coupling the ion(s) to a classical force resonant with the oscillation frequency. The most convenient way is to expose the ions to an electric driving field at ω . Depending on the magnitude, phase and duration of the drive the emerging coherent states are described by a complex parameter α with $|\alpha|^2 = \bar{n}$, the mean quantum number of the oscillator.

With more than one ion, normal modes can be excited by dialing in their resonant frequencies. Care has to be taken that the exciting field has the correct geometry. The centre-of-mass mode will be driven by a homogenous field, the stretch mode needs some field curvature, and higher order modes will need higher moments of the field. A couple of movies taken of large coherent states ($\bar{n} \simeq 100000$) in a string of up to seven ions can be seen on the home page of the Innsbruck group [207] and are also displayed in Fig. 5.11. The field inhomogeneity in this experiment was large enough to excite the

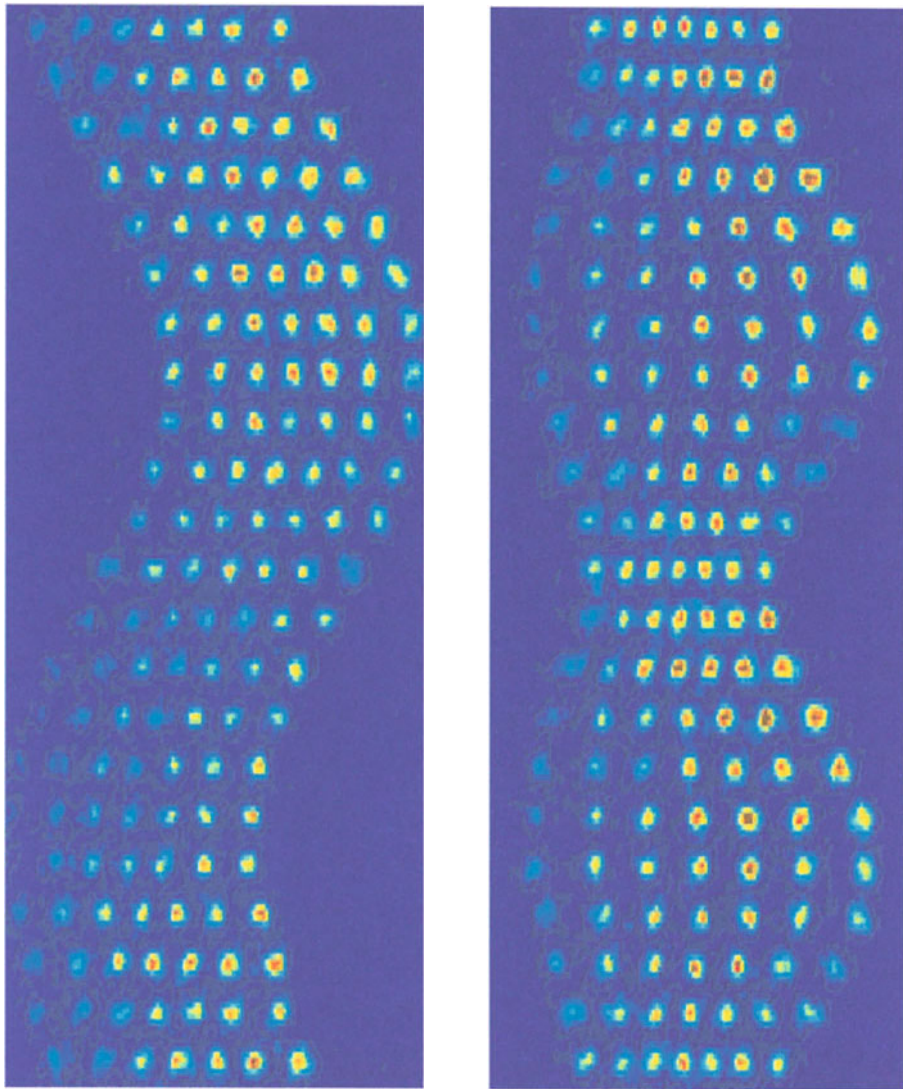


Fig. 5.11. Experimental demonstration of (a) the breathing mode and (b) the centre-of-mass motion of a string of 7 ions. The figures are compilations of snapshots taken of the string of ions at fixed time intervals (short compared to the time scale of the vibrational motion).

lowest two normal modes. Figure 5.11(a) shows the stretch or breathing mode and Fig. 5.11(b) shows the centre-of-mass motion. The pictures were taken stroboscopically with a slow scan CCD camera.

Instead of using the electric charge of the ions and electric external fields to induce the coherent excitation of vibrational modes one can use the in-

ternal state of the ions interacting with laser light fields. Two laser (Raman) beams with a frequency difference equal to ω will not induce internal state transitions, but will coherently excite higher and higher vibrational modes. As a result the ion(s) will (collectively) oscillate with the harmonic oscillator frequency ω , driven by the beating of the two light fields. Since each of the two laser (Raman) beams is near resonance with the $^2S_{1/2}$ to $^2P_{1/2}$ transition, an oscillating dipole force acts on the ion. By polarising the Raman beams σ^+ , one can even make this force dependent on the internal state: For $|g\rangle$ there is no coupling state in the $^2P_{1/2}$ hyperfine manifold, so only the $|e\rangle$ state will feel the dipole force. This point will be crucial for creating Schrödinger's cat type states as described in Sect. 5.2.11. Both techniques to produce coherent states have been used by the NIST group on a single trapped Be^+ ion.

For coherent states with a small mean vibrational quantum number the amplitude of the vibrational motion is too small to be resolved with a camera, and it is very difficult to detect the motion of the ion directly. Instead, one can couple the vibrational motion to the internal two-state system.

To measure the vibrational motion, that is, to determine the populations of phonon-number states $|n\rangle$, we first induce "blue sideband" transitions by laser light, frequency-detuned to the blue by $\delta = +\omega$. These transitions between $|g, n\rangle$ and $|e, n+1\rangle$ are indicated in Fig. 5.12. By using continuous laser light, Rabi oscillations will be induced between the levels indicated by the arrows in Fig. 5.12.

With the blue-detuned laser on, the probability $P_g(t)$ that an ion originally in internal state $|g\rangle$ is still there after time t is given by

$$P_g(t) = \frac{1}{2} \left[1 + \sum_{n=0}^{\infty} P_n \cos(2\Omega_{n,n+1}t) e^{-\gamma_n t} \right], \quad (5.6)$$

where P_n is the probability of finding the atom in the n th motional number state and $\Omega_{n,n+1}$ is the exchange frequency between $|g, n\rangle$ and $|e, n+1\rangle$. In the limit discussed in connection with (5.5), $\Omega_{n,n+1} = \Omega_0 \eta \sqrt{n+1}$. The key

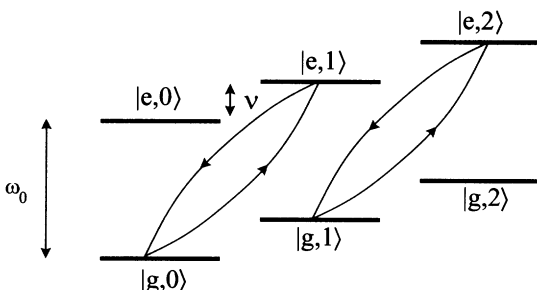


Fig. 5.12. Level scheme of a single two-level ion trapped in a harmonic potential. The arrows indicate Rabi oscillations between the levels $|g, n\rangle$ and $|e, n+1\rangle$. The Rabi frequency depends on n .

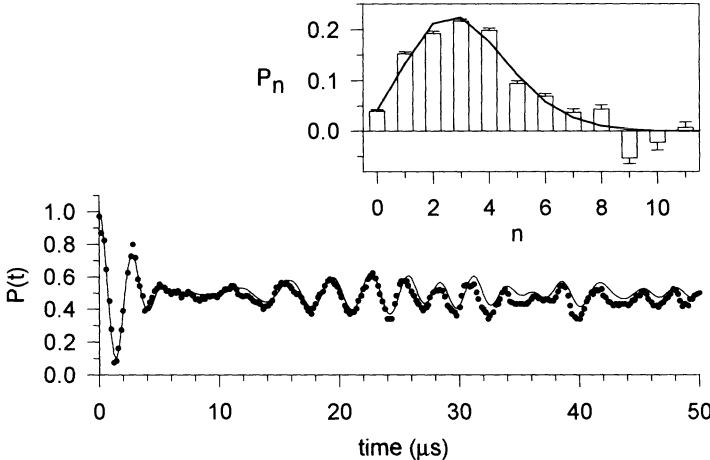


Fig. 5.13. P_g for a coherent state. The solid line is a fit of the data (dots) to a sum of number states having a coherent state distribution. The fitted value for the mean quantum number is $\bar{n} = 3.1 \pm 0.1$. The inset shows the amplitudes of the number state components (bars) with a fit to a Poisson distribution, corresponding to $\bar{n} = 2.9 \pm 0.1$ (line). (Reproduced from Ref. [220])

point is that the frequencies are different for all pairs $(n, n+1)$, thus a Fourier transform of $P_g(t)$ will yield all probabilities P_n . Data points are taken by shining in the blue sideband radiation for time t and then measuring the internal state of the ion with the “shelving” technique as discussed in the previous section. In the limit of many experiments for each time t (1000 experiments in practice) one can deduce $P_g(t)$. The time traces can then be Fourier transformed to get the probability distribution of motional levels P_n . The experimentally determined signal $P_g(t)$ and its Fourier transform for a $\bar{n} = 3.1$ coherent state of a single Be^+ ion are shown in Fig. 5.13. The trace is very similar to the cavity-QED results shown in Fig. 5.2. After a quick collapse around $6 \mu s$, the signal revives at $t \approx 12 \mu s$. Another collapse and revival is visible from $32 \mu s$ to $45 \mu s$ before the signal is finally washed out by decoherence.

5.2.10 Wigner Function of the One-Phonon State

The P_n , as determined in the previous section, correspond directly to the diagonal elements ρ_{nn} of the density matrix ρ and at first glance this seems to be all one can determine. But one can circumvent this problem by coherently shifting the initial motional state. Experimentally this is done exactly as creating coherent states. Instead of shifting the ground state, $|\alpha\rangle = U(\alpha)|0\rangle$, the initial state of motion is now shifted, $|\Psi_{\text{mot}}, \alpha\rangle = U(\alpha)|\Psi_{\text{mot}}\rangle$. Then the occupation of the different number states $|\langle n|U(\alpha)|\Psi_{\text{mot}}\rangle|^2$ is measured as described in Sect. 5.2.9. By doing that with a sufficient number of different

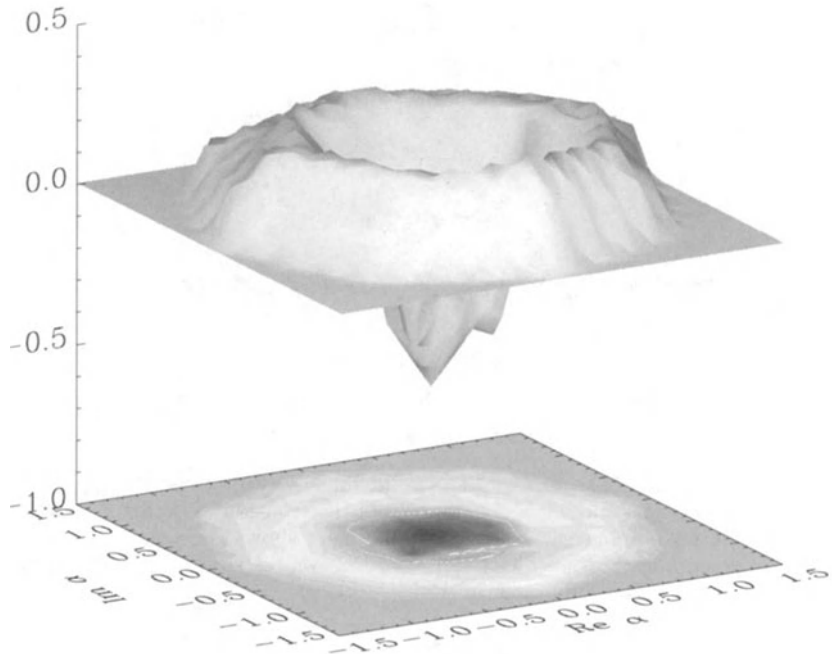


Fig. 5.14. Surface and contour plots of the reconstructed Wigner function $W(\alpha)$ of an approximate $n = 1$ number state. The negative values of $W(\alpha)$ around the origin highlight the non-classical nature of this state. (Reproduced from Ref. [219])

shift parameters α , one can reconstruct the off-diagonal elements of the density matrix in the number state basis or the Wigner function of the initial motional state [219].

Starting from the ground state of motion and with the tools at hand that are offered by the Hamiltonian given in (5.5), motional states can almost be created at will. In practice thermal states, number (Fock) states, squeezed states, Schrödinger cat type and other superpositions of number states of a single ion [219]–[221] have all been created and analysed by the NIST group.

Number states are created from the ground state by alternating π -pulses on the blue and red sideband. This sequence makes the ion climb the following ladder: $|g, 0\rangle \rightarrow |e, 1\rangle \rightarrow |g, 2\rangle \rightarrow \dots$ and so forth. Number states up to $n = 16$ have been created this way. Their signal $P_g(t)$ is a simple sinusoid whose frequency increases roughly proportional to $\sqrt{n+1}$ with deviations caused by the fact that η is nonzero ($\eta = 0.202$, see Fig. 1 in [220]). More interesting is the Wigner function which exhibits negative regions for number states when n is odd. The experimentally determined Wigner function of the $|n\rangle = |1\rangle$ number state is depicted in Fig. 5.14. The experimentally determined Wigner function is negative around the origin, in good agreement with theory.

5.2.11 Squeezed States and Schrödinger Cats with Ions

Squeezed vacuum states can be produced analogously to an optical parametric oscillator by driving the ion at 2ω either with an electric field or with two Raman beams detuned accordingly. Squeezed vacuum states with a ratio of quadrature variances of 40 (16 dB noise suppression in the squeezed quadrature) [220] have been created experimentally. Unfortunately in contrast to squeezed light, there is no sensitive measurement application so far that could make use of this astonishing degree of squeezing.

Schrödinger's cat type states of the exact same form as (5.4) but involving the motion of the ion instead of a photon field have been created in Be^+ [221]. After laser cooling to the $|g, n = 0\rangle$ state, represented by Fig. 5.15 (a), the Schrödinger cat state is created by applying several sequential pulses of the Raman beams.

A $\pi/2$ -pulse on the carrier frequency splits the wave function into an equal superposition of states $|g, 0\rangle$ and $|e, 0\rangle$ as indicated in Fig. 5.15 (b). Then polarised Raman beams detuned relative to one another by ω excite *only* the motion correlated with the $|e\rangle$ component to a coherent state $|\alpha\rangle$ as described in Sect. 5.2.9 and indicated in Fig. 5.15 (c). Figure 5.15 (d) illustrates how a π -pulse on the carrier then swaps the internal states of the superposition. Figure 5.15 (e) indicates how a second pulse of polarised Raman beams excites the motion correlated with the new $|e\rangle$ component to a second coherent state $|\alpha e^{i\phi}\rangle$. After this step the state has the desired form

$$|\Psi\rangle = \frac{1}{\sqrt{2}} (|e\rangle |\alpha e^{i\phi}\rangle + |g\rangle |\alpha e^{-i\phi}\rangle) . \quad (5.7)$$

The relative phase ϕ is determined by the phases of the rf difference frequencies of the Raman beams, which is easily controlled by phase-locking the rf sources. In examining the decoherence properties of this state, one has

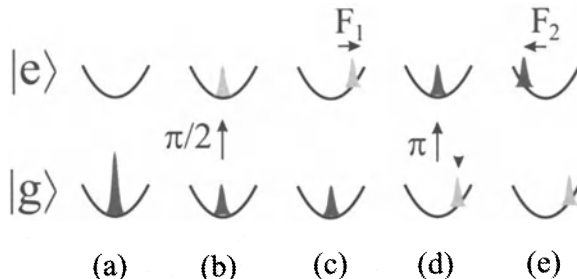


Fig. 5.15. Creation of Schrödinger cat states with ions. (a) Initial state $|g, n = 0\rangle$. (b) A $\pi/2$ -pulse creates the state $|g, 0\rangle$ and $|e, 0\rangle$. (c) Excitation of a coherent state of vibrational motion via optical interaction between polarised Raman beams and $|e\rangle$. (d) A π -pulse interchanges the internal state populations. (e) Finally another coherent state is excited for the new $|e\rangle$ component, creating the Schrödinger cat state.

to live with the drawback that it is not as well characterized and modeled as the decay of a cavity mode. On the other hand, the variety of possible interactions may enable the experimentalist to engineer a reservoir at will [222]. This artificial reservoir will largely determine the decoherence as long as the coupling is adjusted in a way that the induced dissipation timescales are much shorter than those of the dissipation observed without reservoir.

5.2.12 Quantum Logic with a Single Trapped ${}^9\text{Be}^+$ Ion

Trapped and cooled ions interacting with laser fields are strong candidates for the experimental implementation of quantum gates as described in Sect. 4.3. This was first pointed out by Cirac and Zoller [156]. The quantum information is stored in the qubits made up by the internal levels of the ions, while the normal modes of external motion, shared by all ions in the trap, can serve as the “data bus” to entangle the internal states (see Sect. 5.3.7). Up to now, several groups have cooled ions in a linear trap to the point where they form crystalline strings (see e.g. Fig. 5.11). Cooling to the ground state of motion for two ions has been achieved and work is in progress to demonstrate ground-state cooling for strings containing higher numbers of ions.

In an experiment performed in 1995, the NIST group created a quantum controlled-NOT gate between the internal two-state system of one ion ($|g\rangle$ and $|e\rangle$, target bit) and its motion in the trap ($|n=0\rangle$ and $|n=1\rangle$, control bit), thus demonstrating that it is possible to read from the “data bus” the harmonic motion [223]. A sequence of three laser pulses was applied to perform the gate:

1. A $\pi/2$ pulse on the carrier generated a linear superposition of $|g\rangle$ and $|e\rangle$.
2. A 2π pulse on the blue sideband of an auxiliary transition connecting $|e\rangle$ and $|aux\rangle$ introduced a conditional phase shift on the $|e\rangle$ part of the superposition. This sideband only couples $|e\rangle$ and $|aux\rangle$ if the motion is in $|n=1\rangle$, then the phase of the $|e\rangle$ -part is reversed.
3. Finally a $-\pi/2$ pulse on the carrier led to constructive or destructive interference for one of the states, depending on whether or not the conditional phase shift was acquired by the $|e\rangle$ -part.

To get a more intuitive picture one can think of the whole sequence as a Ramsey experiment on resonance. Starting in $|g\rangle$ the first $\pi/2$ -pulse creates the superposition $|g\rangle + |e\rangle$. Then, depending on whether or not $n = 0$, the superposition remains untouched or a phase shift is introduced for the excited part (i.e., $|g\rangle - |e\rangle$, only if $n = 1$). The last step is a $-\pi/2$ pulse. Hence without the phase shift the internal state returns to $|g\rangle$, but if the phase shift occurred ($n = 1$) it will be flipped to $|e\rangle$. The control qubit remains unchanged during the process. The NIST group measured the truth table for the controlled-NOT operation implemented in this way and also demonstrated the coherence of the gate (see Figs. 2 and 3 in Ref. [223]).

5.2.13 Comparison and Perspectives

In the preceding sections experiments on quantum information and quantum computing based on cavity QED and trapped ions have been described. Even if cavity QED and ion-trap experiments basically implement Jaynes–Cummings type Hamiltonians and thus the same dynamics, each technique has its own assets and drawbacks. The essential differences between the two techniques are presented in this section.

The initial state preparation involves standard technology for microwave cavity QED since the ground state of the cavity may be reached by cryogenic cooling to ^3He temperature. The generation of a velocity-selected beam of long-lived circular Rydberg atoms involves an excitation by some standard infrared diode lasers and a radiofrequency field. Laser cooling of ions mostly involves ultraviolet light sources. Cavity QED experiments realise rigorously the Jaynes–Cummings interaction, while the coupling for ions in a trap is only an approximation of the Jaynes–Cummings Hamiltonian in the limit of small Lamb–Dicke parameter. On the other hand, the coupling of trapped ions with the oscillator mode provides more freedom and can be tailored at will to realise more sophisticated functions than the basic Jaynes–Cummings interaction. The atomic/ionic decoherence is practically negligible for both Rydberg states of atoms and hyperfine/metastable states of ions. Concerning the harmonic oscillator mode, the losses of the superconducting cavity are fairly well understood and can be modeled. The only adjustable parameter of decoherence, the cavity quality factor, is determined independently by classical microwave techniques. For ions in traps, the sources of vibrational decoherence are not yet fully understood. The calculation of “fundamental” sources of decoherence such as damping induced by the image charge of the ion in the electrode structure or background gas collisions, result in order of magnitude lower heating rates than observed experimentally [215, 218]. This “anomalous” heating will be further studied and may eventually be overcome since there are no known fundamental reasons for it.

To perform interesting operations for quantum information, it is necessary to manipulate at least a few quantum bits. Using present techniques, cavity QED experiments relying on a beam of circular Rydberg atoms crossing a cavity turn out to be quite difficult with more than two or three consecutive atoms. As discussed above, the average number of atoms per pulse has to be kept well below one to avoid two-atom events. Three or four atom coincidences are very rare and the acquisition time increases exponentially with the number of atoms. This limitation does not affect ion trap experiments. Trapping a few ions in a linear trap is relatively easy. Individual addressing of single ions with well-focused laser pulses is feasible. Provided the collection of ions is cooled to the vibrational ground state, quantum logic operations involving a few qubits can be realised.

Another major asset of the ion trap experiments is the possibility of detecting the ion’s state with almost 100% quantum efficiency, using the quan-

tum shelving methods. Experiments testing the Bell inequalities on entangled trapped ions, for instance, could very easily close the detection efficiency loophole which is still open in the other experiments involving photons or even atoms (in cavity QED it seems that there is no prospect of increasing the detection efficiency far above 90%).

It thus seems that “classical” cavity QED experiments are more suited for investigations of decoherence and entanglement with a limited number of atoms involved (up to about four) in a very well controlled system. The preparation of an entangled triplet of atoms of the GHZ type is currently being performed. Further studies of decoherence will also be undertaken. In particular, it is possible to directly determine the Wigner function of the cavity field [224]. This would allow an in-depth understanding of the decoherence of a Schrödinger cat state. Finally, experiments with two separate superconducting cavities could yield non-local mesoscopic states, combining two most intriguing features of the quantum world.

In ion traps the reconstruction of the Wigner function has already been demonstrated, but the absence of theoretical models and the unclear nature of the decoherence process in ion traps complicates its understanding. Ion traps are also promising as a tool to investigate quantum logic on a moderate scale, involving perhaps up to a dozen qubits and a few hundred operations. However the implementation of the Shor factorisation algorithm (see Sect. 4.2) with “interesting” numbers to break classical cryptographic codes requires at least 400 qubits which seems out of reach with current knowledge and technology [225].

New ways have to be found to overcome fundamental limits such as spontaneous emission, but the implementation of error correction and code stabilisation techniques (Chap. 7) might offer a way of tackling these issues. En route, there are many interesting quantum information processing operations already accessible with a few qubits, for example entanglement purification. These “information-enriched” states could also be used to improve the performance of frequency standards using ions in traps (Sect. 7.6).

Beyond all possible applications, experiments on simple fundamental systems interacting in a well controlled environment will give us a glimpse of the most intimate features of quantum mechanics.

5.3 Linear Ion Traps for Quantum Computation

*H.C. Nägerl, F. Schmidt-Kaler, J. Eschner, R. Blatt,
W. Lange, H. Walther*

5.3.1 Introduction

Having achieved almost perfect control of the quantum state of a single ion, as shown in Sect. 5.2, attention has turned to systems of several ions with well controlled interactions between them [226]. Manipulations of their overall quantum state include the preparation of entangled states that have no classical counterpart. Moreover, the possibility of entangling massive particles offers prospects for new experiments including measurements with Bell states and GHZ states [176] which would allow new tests of quantum mechanics. Entanglement of particles offers the possibility to study the process of quantum measurement in detail and to investigate the phenomenon of decoherence [183, 221].

Due to its unique properties, a string of ions in a linear trap has been proposed for the realisation of quantum logic gates [156], the basic building blocks of a quantum computer. This device operates with quantum registers made up of quantum bits (qubits) which can be manipulated analogously to classical bits by using gate operations. Ion trap quantum gates rely on the entanglement of internal degrees of freedom of the ions (electronic excitation) and the collective motion (vibrational excitation) of the trapped string to logically combine the qubits. The quantum mechanical analogue of a classical XOR-gate is the so-called controlled-NOT operation which can be realised using a well defined series of laser pulses to address two different ions in the string. It has been shown that a controlled-NOT gate is a universal quantum gate, so that in principle arbitrary computations can be carried out using just this two-ion quantum gate and one-bit rotations [227]. The realisation of these gate operations based on a string of ions is of fundamental interest since all basic algorithms could be tested using just a string of trapped ions.

In this section, the specific properties of linear ion traps are summarised and their use for quantum computation is discussed. In Sect. 5.3.2 we review the operation of ion traps and various realisations of linear traps are described. In Sect. 5.3.3 we present the techniques required to achieve cooling to the ground state of motion, a necessary prerequisite for realising quantum gates with strings of ions. Ordered structures of ions are briefly discussed in Sect. 5.3.4. In Sects. 5.3.5 to 5.3.9 the specific techniques needed for the operation of quantum gates for, e.g., state preparation and manipulation, common mode excitations and the readout of the internal electronic state with unit detection efficiency are reviewed and discussed.

5.3.2 Ion Confinement in a Linear Paul Trap

Charged particles, such as atomic ions, can be confined by electromagnetic fields, either by using a combination of a static electric and magnetic field (Penning trap) or a time dependent inhomogeneous electric field (Paul trap) [197]. For the application of trapped ions as quantum bits and registers, the Paul trap, and especially its linear variant, seem favorable [228].

In order to confine a particle a restoring force \mathbf{F} is required, for example, $\mathbf{F} \propto -\mathbf{r}$ where \mathbf{r} is the distance from the origin of the trap. Such forces may be obtained with a quadrupole potential $\Phi = \Phi_0(\alpha x^2 + \beta y^2 + \gamma z^2)/r_0^2$, where Φ_0 denotes a voltage applied to a quadrupole electrode configuration, r_0 is the characteristic trap size and the constants α, β, γ determine the shape of the potential. For example, the three-dimensional confinement in a Paul trap is described by $\alpha = \beta = -2\gamma$, while for $\alpha = -\beta, \gamma = 0$ the quadrupole mass filter is obtained. The three-dimensional Paul trap provides a confining force with respect to a single point in space and therefore is mostly used for single ion experiments or for the confinement of large centro-symmetric ion clouds. In order to realise a quantum register with trapped ions, linear arrays of ions, i.e. ion strings, are required. Therefore, in most cases one employs the linear variant of the Paul trap, which is based on the quadrupole mass filter potential. The latter potential provides confining forces in the two directions perpendicular to the z -axis, but the motion along the z -axis is not affected. For axial confinement, additional electrodes must be employed. Radial confinement of the ions requires a dc-voltage U_{dc} and an ac-voltage $V_{ac} \cos(\Omega t)$ applied to the electrodes. Near the trap axis this creates a potential of the form

$$\Phi = \frac{U_{dc} + V_{ac} \cos(\Omega t)}{2r_0^2} (x^2 - y^2), \quad (5.8)$$

where r_0 denotes the distance from the trap axis to the surface of one of the electrodes. If only a dc-voltage is applied, (5.8) represents a saddle potential which leads to stable confinement in one direction only, as shown in Fig. 5.16. However, with the time dependent (ac) voltage, trapping is obtained. As can be seen from Fig. 5.16, reversing the sign of the ac-voltage leads to confinement in the previously unstable direction. With an appropriately chosen frequency Ω , particles can be trapped indefinitely. As is inferred from (5.8), the potential is ideally created using hyperbolically shaped electrodes (see Fig. 5.17a). For simplicity they are usually approximated by cylindrical rods as in Fig. 5.17b, or more elaborate shapes (Fig. 5.17c), depending on the requirements for laser access and diagnostics. Axial confinement is provided by an additional static potential U_{cap} applied along the z -axis using additional ring electrodes (Fig. 5.17b) or segmented parts of the rod electrodes (Fig. 5.17c). This creates a static harmonic well in the z direction which is characterized by the longitudinal trap frequency

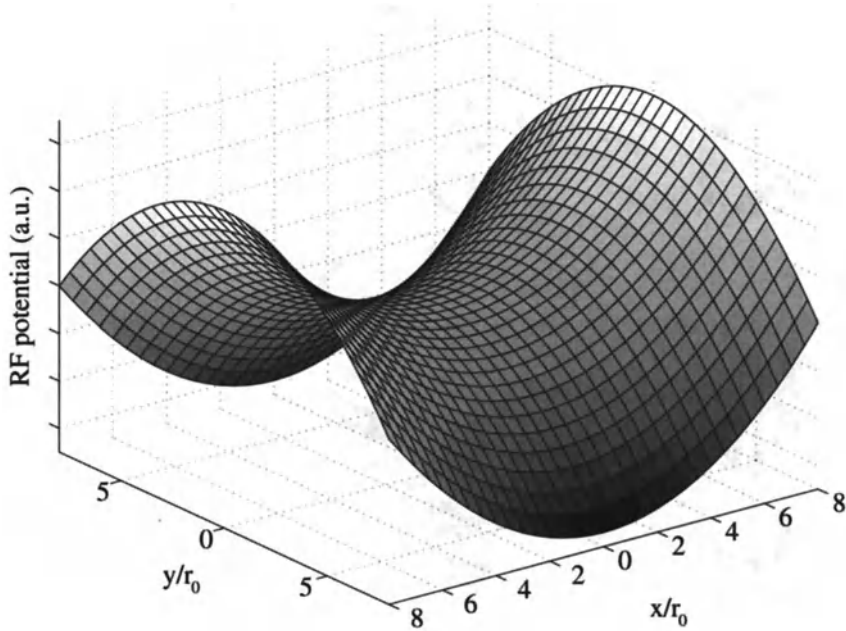


Fig. 5.16. Saddle potential of the rf-Paul trap. Confinement of a charged particle near $x = y = 0$ is achieved by rapid alternation of the sign of the potential

$$\omega_z = \sqrt{2\kappa q U_{\text{cap}} / mz_0^2}. \quad (5.9)$$

Here, m and q denote the ion mass and charge, z_0 is half the length between the axially confining electrodes, and κ is an empirically determined geometric factor of order unity which accounts for the particular electrode configuration. In principle, exact values of κ can be obtained either numerically or, in some cases, analytically. From a practical point of view, however, using a measured value of κ suffices to describe the experimental data. In the x and y directions, the equations of motion resulting from (5.8) are given by the Mathieu equations [228]

$$\frac{d^2 u_x}{d\tau^2} + (a_x + 2q_x \cos(2\tau)) u_x = 0 \quad (5.10)$$

$$\frac{d^2 u_y}{d\tau^2} + (a_y + 2q_y \cos(2\tau)) u_y = 0, \quad (5.11)$$

where

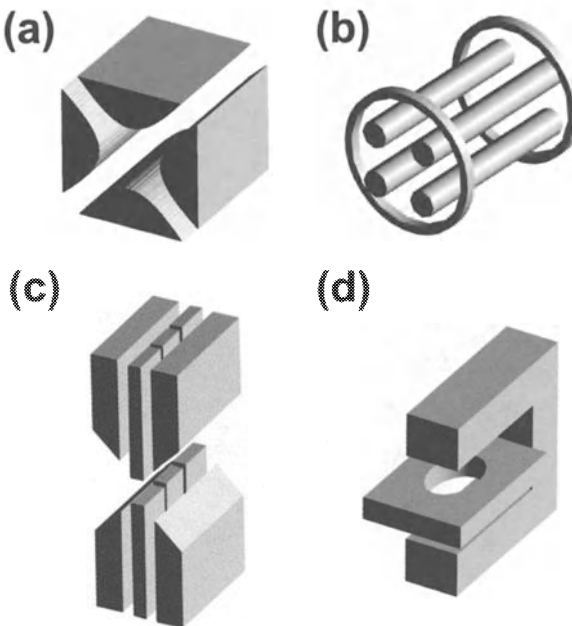


Fig. 5.17. Various realisations of the linear ion trap. (a) Linear quadrupole trap; (b) four rod trap; (c) linear end cap trap; (d) Paul trap with elongated ring electrode.

$$a_x = \frac{4q}{m\Omega^2} \left(\frac{U_{dc}}{r_0^2} - \frac{\kappa U_{cap}}{z_0^2} \right) \quad (5.12)$$

$$a_y = -\frac{4q}{m\Omega^2} \left(\frac{U_{dc}}{r_0^2} + \frac{\kappa U_{cap}}{z_0^2} \right) \quad (5.13)$$

$$q_x = -q_y = \frac{2qV_{ac}}{m\Omega^2 r_0^2} \quad (5.14)$$

$$\tau = \frac{\Omega t}{2}. \quad (5.15)$$

The general solution of (5.10,5.11) can be found as an infinite series of harmonics of the trap frequency Ω [197]. In practice, the condition that $a_i < q_i^2 \ll 1, i = x, y$ is usually fulfilled, allowing for an analytical approximate solution to the equations of motion. It consists of a harmonic secular motion (macromotion) at frequencies ω_i with a superimposed micromotion at the trap's driving frequency Ω ,

$$u_i(t) = A_i \cos(\omega_i t + \varphi_i) \left[1 + \frac{q_i}{2} \cos(\Omega t) \right], i = x, y. \quad (5.16)$$

The amplitude A_i and the phases φ_i depend on the initial conditions, and the secular frequencies are given by

$$\omega_i = \beta_i \frac{\Omega}{2}, \quad \beta_i \approx \left[a_i + \frac{q_i^2}{2} \right]. \quad (5.17)$$

In this limit and for $U_{\text{dc}} = 0$ (which is usually chosen), the micromotion is negligibly small and a confined ion oscillates as if trapped in a harmonic pseudopotential Ψ in the radial direction, given by

$$q\Psi = q \frac{|\nabla \Phi|^2}{4m\Omega^2} = \frac{1}{2} m\omega_r^2(x^2 + y^2) \quad (5.18)$$

with the radial secular frequency $\omega_r \approx qV_{\text{ac}}/(\sqrt{2}m\Omega r_0^2)$.

A major advantage of a linear Paul trap (compared with a three-dimensional Paul trap used for the storage of single ions) is that the micromotion completely vanishes for ions confined to the z -axis. The motion is then a pure harmonic oscillation in the static potential providing axial confinement.

Although the use of linear traps for quantum registers with ions seems favorable, an elongated version of the three-dimensional Paul trap can be used as well to provide strings of two and three ions [216]. Such a device consists of an elliptically shaped ring electrode and two end cap electrodes (Fig. 5.17d) and the ion string is oriented along the long axis of the ring electrode. With this geometry, much higher trap frequencies are possible than with a linear trap, which is an advantage for optical cooling (see Sects. 5.2.7 and 5.3.3). On the other hand, there is always residual micromotion which may cause rf-heating of the string.

5.3.3 Laser Cooling and Quantum Motion

In order to store quantum information in a well-defined way, the quantum state of each single ion in a string of ions has to be carefully prepared. This is achieved with laser cooling techniques in a way similar to that described in Sect. 5.2.7 for a single trapped ion. The final stage of cooling will also be a sideband cooling technique which eventually prepares the ion string in the motional ground state. However, the appearance of distinct modes of vibration of the string, with different frequencies, modifies the cooling process. In particular, the picture of sideband cooling as described in Sect. 5.2.7 does not generally hold for two or more ions. The important difference is that the incommensurate frequencies of the vibrational modes lead to a quasi-continuous energy spectrum rather than a spectrum of discrete equidistant levels, as for one single mode of vibration. The energy levels of the system are now labeled by the internal state $|g\rangle$ or $|e\rangle$ and the motional state $|\mathbf{n}\rangle$ where $\mathbf{n} = (n_1, n_2, \dots)$ is the vector of quantum numbers of the modes of vibration with frequencies $\omega = (\omega_1, \omega_2, \dots)$. Correspondingly, the resonance spectrum for transitions $|g, \mathbf{n}\rangle$ to $|e, \mathbf{m}\rangle$ exhibits sidebands which are much more densely spaced than for a single ion, and by tuning the laser to one specific frequency, all sideband transitions around that frequency, in an interval of the linewidth γ of the transition, are excited simultaneously.

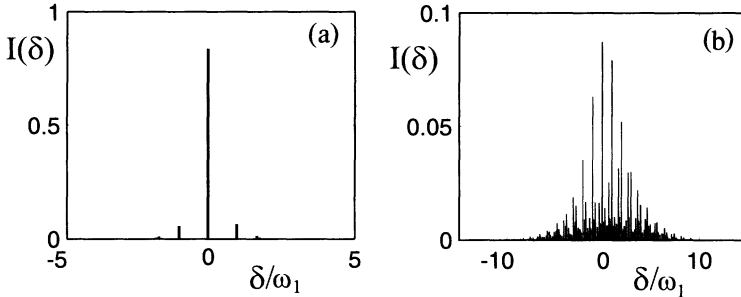


Fig. 5.18. Resonance spectrum of two trapped ions inside (a) and outside (b) the Lamb–Dicke regime. The optical transition without change of the motional state, at detuning zero, is shown together with its vibrational sidebands at their respective detunings. Inside the Lamb–Dicke regime (a) only the fundamental sidebands at $\delta = \omega_{1,2}$ are significant, which involve the exchange of just one vibrational quantum. Outside the Lamb–Dicke regime (b), many sidebands appear which involve changes in the excitation of both modes by one or more quanta. Taken from [229].

More precisely, two cases have to be distinguished [229]. If the sideband cooling happens in the Lamb–Dicke regime, i.e. if only vibrational states n_j and $n_{j\pm 1}$ are appreciably coupled by the recoil of the light interaction, only first-order sidebands contribute, while the exchange of more than one vibrational quantum is suppressed. The sideband spectrum is simple, see Fig. 5.18a, and tuning to one of the sidebands leads to cooling of the respective mode, as for a single ion. Yet the situation is not exactly the same because the other modes, which do not interact with the laser, are heated due to spontaneous emission, so that different settings of the detuning, or a sufficiently large linewidth γ , are required to reach the ground state for all modes.

The other case, i.e. sideband cooling outside the Lamb–Dicke regime, applies to most of the currently pursued implementations of quantum logic with linear ion traps. An example of a sideband spectrum for this case with a string of two ions is shown in Fig. 5.18b. Obviously, if the laser is tuned to a certain frequency below resonance, a set of transitions is excited which involve changes in the excitation of both modes by one or more quanta. In this case, in contrast to the Lamb–Dicke regime, both modes are cooled simultaneously. Furthermore, there appears a new dependence of the cooling rate on the linewidth γ of the transition: The cooling rate increases nonlinearly with the linewidth because first the rate for absorption-emission cycles is proportional to γ , and second the number of levels to which an initial state is coupled, and hence the number of channels through which the ion string is cooled, also increases with γ . Consideration of the cooling rate, i.e. the total cooling time, is important if, after Doppler cooling, many vibrational quanta are still excited. This is typically the case in linear ion-trap experiments.

It has been shown by numerical calculations [229] that both inside and outside the Lamb–Dicke regime, sideband cooling can be used to bring two ions to their motional ground state. Outside of the Lamb–Dicke regime, the strong dependence of the cooling rate on the linewidth γ of the transition can be exploited to optimise the cooling time, by adjusting γ in the course of the cooling process.

The ion species employed for the cooling does not necessarily have to be the same as that used for the desired quantum calculation. At the Max-Planck Institute for Quantum Optics in Garching, an experiment is set up in which a linear string containing magnesium and indium ions is employed. Indium can be sideband cooled to the ground state very efficiently [230], while magnesium would be used to carry the quantum information. The separation of cooling and computation allows the continuous cooling of all normal modes without disturbing the contents of the quantum register.

As a last experimental consideration for laser cooling to the vibrational ground state in Paul traps, we mention that any residual stray electric fields have to be carefully compensated. Such fields may be caused by patch fields on the electrodes and will result in ions being pushed away from the trap axis. Consequently, ions undergo residual micromotion which can prevent proper optical cooling. Stray fields are compensated by the application of dc-potentials to additional electrodes in order to push the ions back to the trap axis. This is routinely done in all three spatial dimensions with single trapped ions in ordinary Paul traps. A similar technique can be applied in linear ion traps. In the case of a string of ions, careful alignment of all electrodes is an important precondition for the cancellation of micromotion.

5.3.4 Ion Strings and Normal Modes

In a linear ion trap, ions can be confined and optically cooled such that they form ordered structures [212, 231]. If the radial confinement is strong enough, ions arrange themselves in a linear pattern along the trap axis at distances determined by the equilibrium of the Coulomb repulsion and the potential providing axial confinement. Figure 5.19 shows an example of a string of Ca^+ ions in a linear trap.

The equilibrium positions of the ions may be numerically determined. If the trap potential is sufficiently harmonic, the positions can be described by a single parameter, the axial frequency ω_z (5.9) [212, 232]. Small displacements of the ions from their equilibrium positions cannot be described in terms of the motion of individual ions since the Coulomb interaction couples the charged particles. Instead, the motion of the ion string must be described in terms of normal modes of the entire chain vibrating at distinct frequencies [156, 232]. As an example, consider two ions confined in a linear ion trap. The first normal mode corresponds to an oscillation of the entire chain of ions moving back and forth as if they were rigidly joined. This oscillation is referred to as the *centre-of-mass mode* (COM) of the string [232]. The second

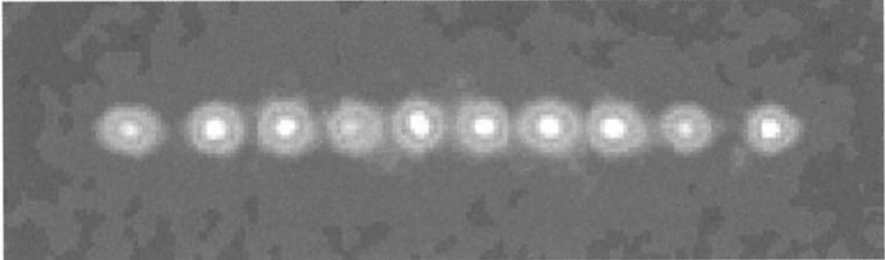


Fig. 5.19. Example of a string of ions in a linear Paul trap. The average distance between two ions is about $10 \mu\text{m}$. The exposure time for the CCD camera was 1 s. The measured resolution of the imaging system consisting of lens and CCD camera is better than $4 \mu\text{m}$. See also Ref. [231] for comparison.

normal mode corresponds to an oscillation where the ions move in opposite directions. More generally, this so-called *breathing mode* describes a string of N ions moving with an amplitude proportional to their mean distance from the trap center. Figure 5.11a and b in Sect. 5.2.9 shows the stroboscopic observation made at the university of Innsbruck of the breathing mode and the centre-of-mass motion for a string of 7 ions.

Explicit calculation of the normal modes (eigenmodes) and the respective eigenfrequencies of an ion string yield the following simple results [200, 232]: (i) for a one-dimensional string consisting of N ions there are exactly N normal modes and normal frequencies; (ii) the center of mass mode has a frequency which is exactly equal to the frequency of a single ion; (iii) higher order frequencies are nearly independent of the ion number N , and are given by $(1, 1.732, 2.4, 3.05(2), 3.67(2), 4.28(2), 4.88(2), \dots) \omega_z$, where the numbers in brackets indicate the maximum frequency deviation as N is increased from 1 to 10 ions, (iv) the relative amplitudes of the normal modes have to be evaluated numerically (at least for strings with more than 3 ions, see equation (28) in Ref. [232]).

After loading the trap with a string of ions, normal modes can be excited by applying additional ac-voltages to either one of the ring electrodes or to the compensation electrodes [212]. The normal mode excitation can be observed as an increase of the spot width on the CCD camera long before there is a dip in the fluorescence collected by the photomultiplier. The frequency measured for the breathing mode agrees (to within 1%) with the expected frequency of $\sqrt{3}$ times the centre-of-mass frequency. Figure 5.20 shows the excitation of the centre-of-mass mode (158.5 kHz) for two excitation amplitudes and the excitation of the breathing mode (276.0 kHz) for 5 ions. In order to excite the breathing mode it was necessary to apply voltages which are typically about 300 times higher than the ones needed for excitation of the centre-of-mass mode (3 V compared to 0.01 V). Excitations of higher order modes were not observed with the ac-voltages available in the setup of [212]. This is due to the fact that the exciting field is nearly uniform along the ion string, meaning

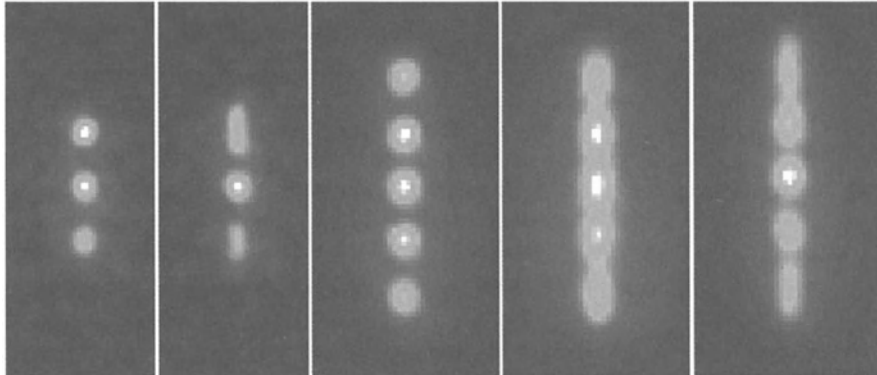


Fig. 5.20. Vibrational excitation of a string of five ions by an externally applied ac-voltage. From left to right: no excitation, weak and strong excitation of the COM-mode (158.5 kHz), excitation of the breathing mode (276.0 kHz).

that the higher modes which need field gradients across the ions are much less efficiently excited.

The COM vibration is excited with a uniform field and therefore is very susceptible to field fluctuations whose spatial variation is usually small on a length scale given by the ion distance. In contrast, the excitation of higher order modes requires large field gradients. Therefore, unwanted excitation occurs much less frequently for higher order modes. Note that during a quantum computation, vibrational quanta in the ion chain are generated by Raman sideband transitions induced by laser interaction with a single ion.

5.3.5 Ions as Quantum Register

Quantum information may be stored in an ion by preparing it in either one of two distinct electronic states $|g\rangle$, $|e\rangle$ or in any superposition of them. An obvious requirement for the choice of these states is that both should have a radiative lifetime sufficiently long for the computation to finish before coherence is destroyed by spontaneous decay. One possibility is to use the ground state of the ion and a metastable excited state, or even two metastable states. Lifetimes can be on the order of seconds (an example being the 2D levels in $^{40}\text{Ca}^+$, Fig. 5.21b), which should be sufficient for simple quantum calculations. Even longer lifetimes are possible if one uses two hyperfine components of the ground state, which are stable with respect to electric dipole decay [216, 228]. Examples include $^9\text{Be}^+$, $^{25}\text{Mg}^+$ and $^{43}\text{Ca}^+$, with beryllium being shown in Fig. 5.21c. Also, in the case of ions which do not possess hyperfine structure, information may be stored in the ground state by exploiting its Zeeman substructure. Note that since ions usually have two Zeeman ground states, this approach precludes qubit operations which use auxiliary ionic levels like the phase gate described below. Together the internal states of N

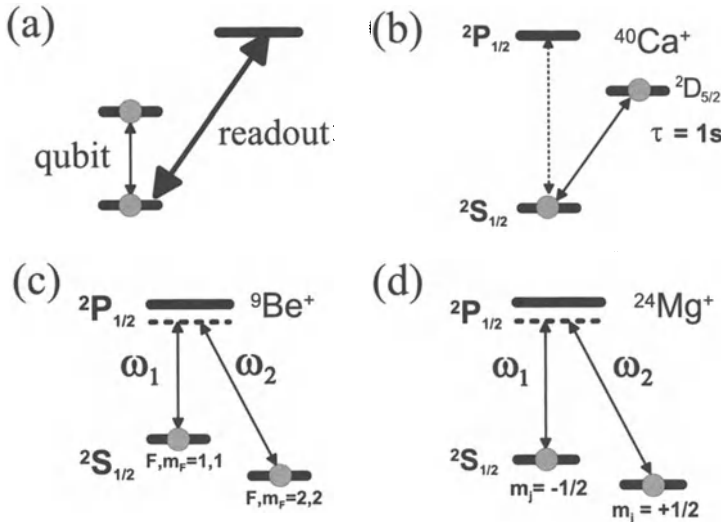


Fig. 5.21. Level scheme of trapped ions used for quantum computation. (a) Three level scheme with slow qubit transition and fast transition for efficient readout; (b) qubit stored in ground state and a metastable state; (c) qubit stored in hyperfine ground states; (d) qubit stored in Zeeman sublevels.

ions in the trap span the $2N$ dimensional Hilbert space in which the quantum computation evolves.

5.3.6 Single-Qubit Preparation and Manipulation

Prior to performing a quantum calculation, input data must be loaded into the quantum register. This process corresponds to the excitation of each of the N ions to a certain electronic quantum state. This is most conveniently achieved by laser manipulation of the internal states of the ions. A prerequisite is that each of the ions can be addressed individually by a laser beam. The separation of neighbouring ions in the trap is on the order of $10 \mu\text{m}$, so that the laser must be focused to this size in order to avoid cross-excitation of the ions. A suitable scheme for addressing the ions is to deflect a single laser beam by means of the acousto-optic or electro-optic effect, sequentially pointing it to each ion in the chain. This has been experimentally demonstrated by the Innsbruck group [213].

Preparation of the input state of a given qubit proceeds in two steps. First the qubit is erased by transferring the ion to one of the two basis states ($|g\rangle$ or $|e\rangle$), for example by optical pumping. From this well-determined initial state an arbitrary superposition state ($\alpha|g\rangle + \beta|e\rangle$) of the qubit may be excited by using a resonant laser pulse of variable length to drive a Rabi oscillation between the two qubit-states. If a π -pulse is used, the qubit is flipped to the orthogonal state, and for shorter pulses a superposition state of the qubit

is prepared. The technique of Rabi flopping is also used if unconditional single-qubit rotations are required during a quantum calculation to coherently modify the contents of a quantum register.

The details of how the Rabi flopping is accomplished depend on the level structure used. If the qubit states are separated by optical frequencies, a single-photon transition is employed. In the case of hyperfine states, or Zeeman substates of the same electronic level, two Raman beams are used connecting the qubit states through an intermediate virtual level close to an excited state of the ion.

5.3.7 Vibrational Mode as a Quantum Data Bus

The operations described so far manipulate single qubits independently of each other. For useful computations (logic operations) however, it is necessary to provide a strong coupling between the qubits, so that the dynamics of any ion in the chain may be conditional on the state of other ions. By far the strongest interaction between ions in a trap is their Coulomb repulsion, which in equilibrium is balanced by the external trapping potential. As was indicated in Sect. 5.3.4, the ions perform oscillations around this equilibrium position, which are highly correlated. Of particular interest for coupling ions in different positions of a linear trap is the centre-of-mass (COM) mode of oscillation, in which all the ions oscillate in phase in the direction of the trap axis. Cirac and Zoller [156] have shown how the COM-mode may be used to transfer quantum information between ions which can possibly be at widely separated positions of the chain.

Initially, the COM-vibration must be cooled to its quantum mechanical ground state, which may be accomplished with the technique of resolved sideband cooling described in Sect. 5.3.3. Quantum information may then be transferred from any ion in the string to the COM-mode by the following procedure: One ion is selectively illuminated by a focused laser beam and through a π -pulse on the first red-detuned vibrational sideband of the ionic resonance, the internal state of this ion is mapped to an external (vibrational) state of the ion chain (see Fig. 5.22a). As a result, the ground state and the first excited state of the COM-vibration are found in a superposition corresponding to the superposition of the lower and upper qubit state that was originally present in the ion. Due to the correlated COM-motion, all ions in the chain undergo the same oscillatory motion and hence have access to the same quantum information. The task of performing a quantum gate, i.e., of changing the state of an ion conditional on the state of another ion is therefore reduced to the task of changing the ionic state conditional on the vibrational state of the COM-mode (see Fig. 5.22b), as explained in the following section. The oscillation of the ions acts like a quantum bus, linking the qubit registers along the chain. After the operation on the second ion has been performed, step (a) must be reversed in order to restore the vibrational

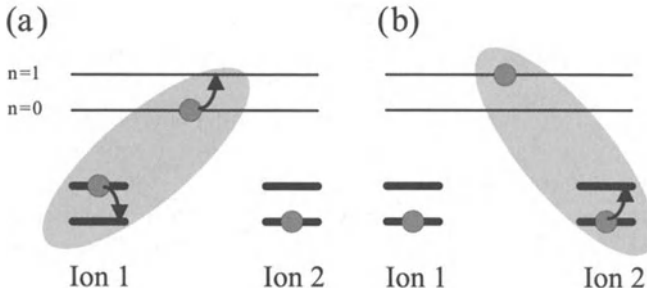


Fig. 5.22. Vibrational mode of an ion as a quantum data bus. (a) With the first laser pulse the state of ion 1 is mapped to the COM mode; (b) the state of ion 2 is changed conditional on the state of the COM mode.

mode to its ground state and at the same time return the first ion to its initial state.

5.3.8 Two-Bit Gates in an Ion-Trap Quantum Computer

The essential step of the Cirac–Zoller proposal for an ion-trap quantum computer is the realisation of a two-bit quantum gate, with the vibrational state of the COM-mode and the internal state of one ion as input qubits. In the following, we will describe gates in which the vibrational mode acts as the control bit, conditioning the state change in the target ion.

The most straightforward gate is one in which only one combination of basis states will lead to a modification of the output. This is the case for the so-called phase gate, in which the wavefunction of the system acquires a phase shift of π (change of sign) if both input qubits are in the upper state and is left unchanged in all other cases. To realise the change of sign of the wavefunction it is sufficient to apply a 2π -pulse to the ion. In order to obtain the required conditional dynamics, the pulse should be on a transition which couples only to the upper internal state of the ion. This requires the presence of an auxiliary electronic level, which could be another Zeeman substate or a different electronic level. Conditioning on the vibrational state is achieved by tuning to the first blue COM-sideband, which only leads to a transition if at least one vibrational quantum is present. Note that by construction, no more than one vibrational quantum may be excited in this scheme.

Other gates are possible by combining the phase gate with single qubit rotations. An example is the controlled NOT (CNOT) gate (see Sect. 5.2.12), in which the target bit is flipped depending on the state of the control bit. This may be realised by applying a (resonant) $\pi/2$ -pulse before and after the phase gate, corresponding to a temporary change of the computational basis to $|g\rangle \pm |e\rangle$. A CNOT gate for a single qubit using its vibrational mode as the control bit has been experimentally demonstrated [211].

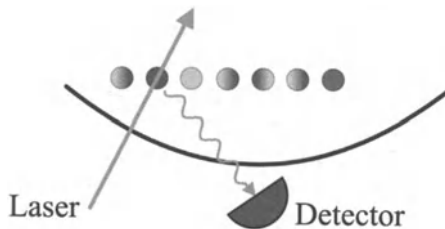


Fig. 5.23. State measurements on ion qubits. Each ion is individually addressed with a laser beam tuned to the readout transition (cf. Fig. 5.21a) and the fluorescence monitored.

In some cases it may be useful to obtain the CNOT directly, for example when no suitable auxiliary levels are available in the ion's level scheme. To do this one can exploit the fact that the coupling between internal and external degrees of freedom depends nonlinearly on the number of excited vibrational quanta [233]. For a suitable choice of parameters, a resonant pulse will act as a 2π -pulse if the system is in its lowest vibrational state, but as a π -pulse if one vibrational quantum is present, so that only in the latter case will the ion's state be flipped.

5.3.9 Readout of the Qubits

At the end of the quantum computation it is necessary to read out the result of the calculation, i.e., determine the state of the qubit register. Clearly this involves a projection of the state of the ions onto the basis states used for the detection.

The ion trap quantum computer has the advantage that the readout can be achieved with nearly 100% detection efficiency by applying a method first demonstrated for the detection of quantum jumps in single ions [234] (see Sect. 5.2.8). Each ion is subsequently illuminated by a laser tuned to a fast transition which is coupled to only one of the qubit states and the emitted fluorescent light is detected (Fig. 5.23). The presence of scattered light indicates occupation of the coupled state, its absence occupation of the orthogonal basis state. Superposition states may be probed by rotating the qubit prior to detection.

5.3.10 Conclusion

In the above sections we have outlined the principle of operation of an ion trap and its application to the task of performing quantum computations. Currently, a string of ions in a linear trap seems to be a most promising candidate for demonstrating the basic concept of a quantum computer. The principal benefits of the system are the long decoherence times of the internal states of the ions and the ability to prepare, coherently control and read

out the states of the qubits by means of laser pulses. Among the quantum computation schemes implemented experimentally so far, ion traps have, at least theoretically, the largest potential for being scaled up to provide qubit registers long enough to run useful quantum algorithms.

In a realistic ion trap quantum computer, practical issues limit the size of calculations that may be implemented. Electromagnetic field fluctuations and collisions with background gas in the vacuum chamber may lead to decoherence rates larger than the radiative decay rates of the internal states of the ion. Even more restrictive is decoherence of the vibrational states of the ion string. For a single $^{198}\text{Hg}^+$ ion, a transition out of the zero-point vibrational level occurred in 0.15 s [214], while in the case of $^9\text{Be}^+$ a lifetime of 1 ms [211] was measured. For experimental data on $^{40}\text{Ca}^+$ see Ref. [215]. These processes put an upper limit on the number of operations that may be performed with a quantum computer before coherence is lost. However, in view of the recent experimental results [212, 216], some of the more technical limitations may be overcome using a breathing mode as the quantum data bus.

Additional problems affect the performance of a quantum computer during logic operations. Processes compromising the fidelity of the system evolution are inaccurate timing of the laser pulses, errors in the detunings, intensities and phases of the laser beams, and deviations between the laser focus and the ion positions. However, such errors may be taken care of eventually by an implementation of error correcting codes and protocols.

Although the number of ions that may be stored in the trap should only be limited by the size of the trap and the laser power available for cooling, only a string of two ions has been successfully cooled to the ground state of motion so far [216]. This number is likely to increase in the near future to a few tens of ions, but the thousands of qubits and billions of laser pulses needed, for example, to implement Shor's algorithm for factorising nontrivial numbers seems to be beyond experimental reach at present. However, ion traps offer the best prospects for testing small networks of quantum gates as well as schemes for quantum error correction. In this way the ion trap provides an ideal environment for synthesizing, manipulating and probing highly entangled quantum states of a string of ions.

5.4 Nuclear Magnetic Resonance Experiments

J.A. Jones

5.4.1 Introduction

Nuclear magnetic resonance (NMR) is the study of transitions between the Zeeman levels of an atomic nucleus in a magnetic field. Described so simply, it is hard to see why anyone would be interested in it, but NMR is in fact one of the most important spectroscopic techniques available in the molecular sciences [235, 236]. This is because the frequencies of NMR signals depend subtly on the precise chemical environment of the nucleus, and so careful study of a molecule's NMR spectrum allows its structure to be determined.

NMR has long been considered as a possible technology for implementing quantum computers. Superficially the idea is attractive, as nuclear spins provide a good source of qubits, and it is fairly simple to construct quantum logic gates. There is, however, one major problem: it is difficult to place an NMR quantum computer in a well defined initial state, which appears essential for any interesting computation. This problem was solved recently by two separate approaches [237]–[239], and since then progress has been rapid.

Because of the importance of NMR in the molecular sciences, there has been extensive technical development of NMR spectrometers. Huge sums of money have been spent on optimising every component, and commercial spectrometers are widely available with performances close to the theoretical limits. Modern spectrometers are extremely complex devices, but they are easily controlled, and with a little assistance even the most nervous theoretician should be able to perform simple NMR experiments.

5.4.2 The NMR Hamiltonian

The NMR Hamiltonian can in the worst case be rather complex [236, 240, 241], but in many cases much of this complexity can be ignored. Firstly I will only consider spin- $\frac{1}{2}$ nuclei (such as ^1H , ^{13}C , ^{15}N , ^{19}F , and ^{31}P), as these nuclei do not experience many of the interactions which occur in high-spin nuclei. These nuclei are also the most important for current implementations of NMR quantum computers, as the two spin states of a spin- $\frac{1}{2}$ nucleus provide a natural two-level system for implementing a qubit. Secondly I shall assume that the NMR sample is a fluid (normally either a pure liquid or a solution). Rapid molecular motion in fluids greatly simplifies the NMR Hamiltonian, as anisotropic interactions can be replaced by their isotropic average, which is often zero. NMR signals from spin- $\frac{1}{2}$ nuclei in fluids are

typically rather narrow, and so such studies are often referred to as “high resolution” NMR [242].

Two interactions are particularly important in high resolution NMR. The first of these is of course the Zeeman interaction. In the presence of a magnetic field B_z , directed along the z -axis, the degeneracy of the two spin states ($I_z = \pm \frac{1}{2}\hbar$) is lifted by the Zeeman interaction

$$\mathcal{H} = -\gamma I_z B_z, \quad (5.19)$$

where γ (the gyromagnetic ratio) is a constant characteristic of the nucleus. The Zeeman splitting corresponds to a frequency of around 500 MHz for ^1H nuclei in typical NMR magnets, and so NMR experiments are performed using radio frequency (RF) radiation.

It is not practical to use conventional spatial localisation techniques to pick out individual molecules, as the spacing between molecules (a few Å) is small compared with the wavelength of the RF radiation, and in any case the individual molecules are undergoing rapid motion. Instead, the combined signal from all the molecules is detected. This has important consequences for NMR experiments, as they are implemented not on individual spin systems but on statistical ensembles of such systems. It is, however, possible to distinguish between different nuclei in the same molecule. Electrons surrounding the nuclei act to shield them from the magnetic field, thus modifying the apparent gyromagnetic ratio. The extent of this shielding depends on the chemical environment of the nucleus, and thus nuclei in different environments have slightly different transition frequencies.

The second important interaction in high resolution NMR is scalar coupling (J-coupling). This is not simple dipole–dipole coupling, which is averaged out by rapid molecular tumbling, but a more subtle effect related to the Fermi contact interaction. When the coupling between two nuclei, I and S , is small compared with the difference between their NMR frequencies (weak coupling) the coupling Hamiltonian takes the simple form

$$\mathcal{H} = J_{IS} I_z S_z, \quad (5.20)$$

where J_{IS} , the spin–spin coupling constant, depends on details of the molecular structure. This coupling is directly observable in NMR spectra as a splitting (of size J_{IS}) in the NMR signals corresponding to each nucleus.

A simple example: Figure 5.24 shows the chemical structure of deuterated cytosine. Cytosine is one of the four “bases” which are used to encode information in DNA, and has recently been used to implement an NMR quantum computer [243]. For this purpose three of the hydrogen nuclei in the molecule were replaced by deuterium, which can be easily achieved by dissolving it in D_2O . The ^1H spectrum of this molecule on a 500 MHz NMR spectrometer is shown in Fig. 5.25. Each of the two ^1H nuclei gives rise to a pair of signals, called a doublet. The two doublets occur at a frequency of about 500 MHz,

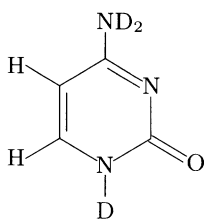


Fig. 5.24. The structure of partially deuterated cytosine obtained by dissolving cytosine in D₂O; the three protons bound to nitrogen nuclei exchange with solvent deuterons, leaving two ¹H nuclei as an isolated two spin system (all other nuclei can be ignored).



Fig. 5.25. The ¹H NMR spectrum of partially deuterated cytosine. Each pair of lines is the NMR signal from one of the two ¹H nuclei.

with a separation between them of 763 Hz; the small splitting within each doublet (7.2 Hz) is due to spin–spin coupling between the nuclei.

5.4.3 Building an NMR Quantum Computer

While several different models of quantum computing have been considered, the most common approach is based on quantum logic circuits. Such a quantum computer has four main elements which must be implemented. The first of these, qubits, is easy, as the two spin states of a spin- $\frac{1}{2}$ nucleus provide an ideal two-level system. The remaining elements are slightly more complex.

Quantum gates: Quantum logic circuits are constructed by interconnecting qubits with quantum gates. While many different gates are possible it is well known that any gate can be constructed using a suitable combination of one qubit and two qubit gates [244]. One qubit gates correspond to rotations of a single spin within its own Hilbert space, and these can be readily achieved using RF fields. Two qubit gates, such as the controlled-NOT gate, are more complex as they involve conditional dynamics, and thus require an interaction between the two qubits. In NMR the scalar coupling (J-coupling) is well suited to this purpose: while scalar coupling does not have exactly the form required to construct traditional controlled gates it can be easily combined

with one qubit gates to make them [245]. For example the controlled-NOT gate can be achieved by placing a controlled phase shift gate (which performs the transformation $|11\rangle \rightarrow -|11\rangle$, while leaving the other basis states unchanged) between a pair of one qubit Hadamard gates applied to the target qubit. The controlled phase shift can itself be achieved by combining evolution under the scalar coupling, which results in a two qubit phase rotation, with single qubit phase shift gates [245].

The CLEAR operator: Quantum logic gates transform qubits from one state to another. Clearly this is only useful if the qubits start off in some well defined input state. In practice it is sufficient to have some method for reaching any single state, as other initial states can then be reached by applying one bit gates. The obvious choice of initial state is to have all qubits in the $|0\rangle$ state, corresponding to a CLEAR operation.

In principle CLEAR should be easy to implement as it takes the quantum computer to its energetic ground state, which can be achieved by some cooling process. Unfortunately this approach is not practical in NMR as the energy gap between Zeeman levels is small compared with the Boltzmann energy at any reasonable temperature. At room temperature the energy gap is so small compared to kT that the population of all the states will be almost equal, with only small deviations (around one part in 10^4) from the average. No NMR signal will be observed from the average population, as the signals from different molecules will cancel out, but a small signal can be seen which arises from the deviations away from the average.

For a molecule containing a single isolated nucleus, that is a computer with a single qubit, it is easy to reach an effective $|0\rangle$ state: at thermodynamic equilibrium the deviation from equal populations is just a slight excess in the (low energy) $|0\rangle$ state compared with the (slightly higher energy) $|1\rangle$ state. Unfortunately this simple approach does not work for larger systems, as the pattern of population deviations is more complicated, and does not have the desired form. This apparent inability to implement CLEAR made NMR an impractical quantum computing technology for many years.

Towards the end of 1996 two separate approaches were discovered for solving this problem. The first approach, due to Cory and coworkers [237, 238], uses complex NMR pulse sequences to modify the populations of different spin states, eventually creating the desired pattern, and thus a state equivalent to the desired initial state. An alternative approach, due to Chuang and Gershenfeld, works by separating the spin system into many different subsystems [239, 246]. Within these subsystems the equilibrium pattern of populations has the desired form, and so the desired starting state is accessible. While this approach is theoretically elegant, it is complicated to apply in practice, and has not been widely used. More recent approaches, such as temporal averaging [247], are conceptually related to that of Cory et al., and will not be described further. A detailed comparison of the various methods has been made by Havel and coworkers [248].

Output: Finally it is necessary to have some method for reading out the final answer. Typically this is obtained by reading the values of one or more qubits which finish the calculation in eigenstates. In an NMR quantum computer this corresponds to determining whether the population of the $|0\rangle$ state is higher than that of the $|1\rangle$ state, or vice versa. It is not practical to determine these populations directly, but an equivalent measurement is easily made by applying a 90° excitation RF pulse. This creates a coherent superposition of $|0\rangle$ and $|1\rangle$ which then oscillates in the magnetic field. The relative populations can then be determined by observing the size and phase of this oscillatory signal. The absolute phase of the signal is meaningless, but it is possible to incorporate a reference signal, so that only relative phases need be measured.

Some quantum algorithms produce a result occupying two or more qubits, and in this case two different approaches are possible. The first approach is to excite only one of the corresponding spins; in this case the states of the other spins can be monitored by examining the multiplet structure of the observed spin. Alternatively it is possible to excite all the spins and observe them simultaneously; in this case the state of each spin can be determined directly from the phase of its NMR signal.

NMR quantum computers have a potential advantage over other designs in that it is not necessary for the answer to be stored as an eigenstate. It is instead possible to observe some superpositions directly. This possibility arises because of the ensemble average implicit in any NMR measurement. While measurements on a single spin system cause superpositions to collapse, the equivalent effect is not seen in ensemble averages. Thus it is possible, for example, to monitor two complementary observables continuously and simultaneously. This mode of operation could be useful in future experiments.

5.4.4 Deutsch's Problem

The concepts described above can be illustrated using an NMR quantum computer designed to implement an algorithm to solve Deutsch's problem [138, 249]. This problem is described in detail in Sect. 4.2.4, and only a brief summary will be given here. Consider a binary function

$$f(x) : B \mapsto B, \quad (5.21)$$

and suppose we have a corresponding operator U_f , such that

$$|x\rangle |y\rangle \xrightarrow{U_f} |x\rangle |y \oplus f(x)\rangle. \quad (5.22)$$

Clearly it is possible to build quantum circuits to determine $f(0)$ and $f(1)$, as shown in Fig. 5.26a. Deutsch's problem is the determination of $f(0) \oplus f(1)$ with only a single application of U_f (corresponding to a single evaluation of f). This is impossible on a classical computer, but can be achieved on a quantum computer using the circuit shown in Fig. 5.26b.

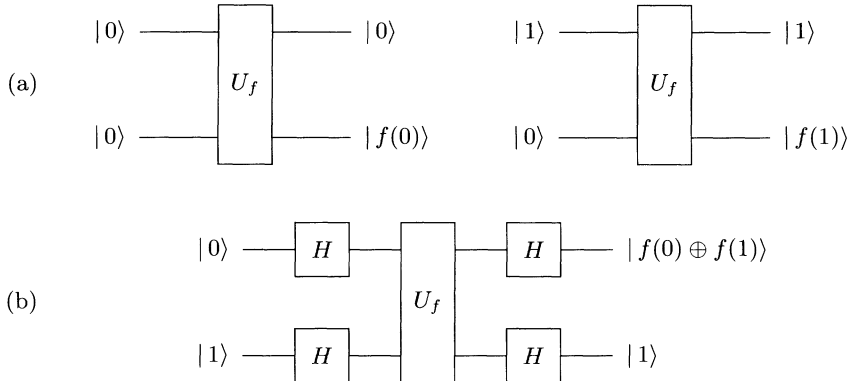


Fig. 5.26. (a) Quantum circuits to determine $f(0)$ and $f(1)$ for a binary function. (b) A quantum circuit to determine $f(0) \oplus f(1)$ with a single application of U_f (Deutsch's problem). H represents the single qubit Hadamard gate.

This circuit has been implemented on our two qubit NMR quantum computer based on partially deuterated cytosine [243] (similar results have also been obtained by Chuang et al. using a two qubit NMR quantum computer based on chloroform [250]). In our NMR quantum computer each doublet corresponds to the signal from one qubit. The value of the qubit can be determined from the phase of the corresponding signal: a positive signal corresponds to a qubit in the $|0\rangle$ state, while a negative signal corresponds to a qubit in the $|1\rangle$ state.

As mentioned above, the absolute phase of an NMR signal is not meaningful, as it depends on a variety of experimental factors. Relative phases are, however, meaningful, and so it is possible to obtain “absolute” phases by adjusting the spectrum so that the phase of a reference signal is correct. The relative phases of signals in two different experiments can also be meaningful if the two experiments are acquired in an identical fashion, and so it is possible to use a reference signal from one experiment to correct signals from another experiment. This is the approach adopted in the results discussed below.

Experimental results from a classical algorithm to determine $f(0)$ are shown in Fig. 5.27. In this algorithm the left hand pair of lines (corresponding to the first qubit) indicates the input value, while the right hand pair of lines (corresponding to the second qubit) indicate the output value. Results are shown for the four possible binary functions, listed in Table 5.1. As expected

Table 5.1. The four possible binary functions mapping one bit to another.

x	$f_{00}(x)$	$f_{01}(x)$	$f_{10}(x)$	$f_{11}(x)$
0	0	0	1	1
1	0	1	0	1

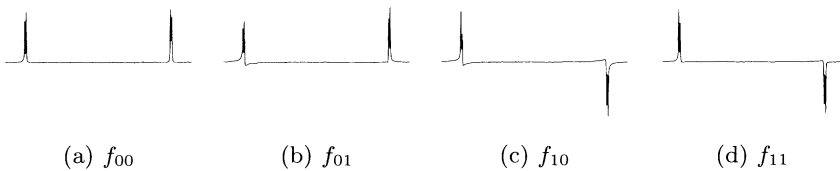


Fig. 5.27. Experimental results from an NMR quantum computer determining $f(0)$; the result is shown for each of the four possible binary functions, f .



Fig. 5.28. Experimental results from an NMR quantum computer determining $f(1)$; the result is shown for each of the four possible binary functions, f .

the left hand signals are always positive, indicating the input value (0), while the right hand signals are positive when $f(0) = 0$ (for f_{00} and f_{01}) and negative when $f(0) = 1$ (for f_{10} and f_{11}). The absolute phase of these spectra is unknown, but this was solved by adjusting the phase of spectrum (a) such that the left hand signal was positive, and then applying the same phase correction to all the other spectra.

These plots do not clearly show the fine structure within each doublet, but this is not particularly important as within this implementation of a quantum computer all the lines in the multiplet should have the same sign, as is indeed observed. Ideally this sign would be simply positive or negative, but in practice the lineshapes observed are slightly more complex. Similarly all the lines should have the same height, while the experimental results show substantial variations. These lineshape and height distortions arise from errors in the computer. For the most part these errors are systematic, in that they arise because the computer does not implement quantum gates perfectly correctly. It should be possible to reduce these errors by careful optimisation of the NMR pulse sequences used to implement gates.

The same algorithm can be used to determine $f(1)$: all that is needed is to change the input value. The results of this approach are shown in Fig. 5.28. In this case the left hand signals are always negative, indicating the new input value (1), while the right hand signals can be either negative or positive. As expected this signal is positive when $f(1) = 0$ (for f_{00} and f_{10}) and negative when $f(1) = 1$ (for f_{01} and f_{11}). Note that the same phase correction was used

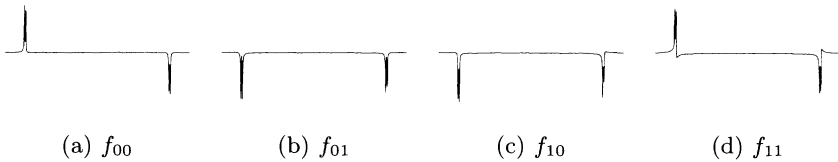


Fig. 5.29. Experimental results from an NMR quantum computer determining $f(0) \oplus f(1)$ (Deutsch's problem); the result is shown for each of the four possible binary functions, f .

for these spectra as for those in Fig. 5.27, showing that relative phases can be defined for two different experiments performed under identical conditions.

Finally, this quantum computer can also be used to implement an algorithm to solve Deutsch's problem (determining $f(0) \oplus f(1)$). The results are shown in Fig. 5.29. In this case there is no input bit, as the quantum computer uses a superposition of the two possible inputs, and the answer is encoded as the phase of the left hand signals. The second qubit is simply a working bit, and both starts and ends the computation in state $|1\rangle$. As expected the right hand signals are always negative, while the left hand signals are positive for f_{00} and f_{11} (for which $f(0) \oplus f(1) = 0$), and negative for f_{01} and f_{10} (for which $f(0) \oplus f(1) = 1$).

5.4.5 Quantum Searching and Other Algorithms

Since the discovery that it is possible to generate effectively pure starting states in NMR quantum computers progress has been extremely rapid. Two qubit computers have been used to implement Grover's quantum search algorithm with a two qubit search space [251]–[253]. This allows a single item to be located in a search over four items with a single query; the algorithm begins with the quantum computer in the state $|00\rangle$ and ends in the state corresponding to the matching item ($|00\rangle$, $|01\rangle$, $|10\rangle$, or $|11\rangle$). This algorithm has been implemented on our cytosine quantum computer [252], and the results are shown in Fig. 5.30. The results shown are slightly better than those published earlier [252]; they were acquired using modified pulse sequences as described in [254].

While NMR quantum computers are capable of performing a simple Grover search, for which there is only one item to be found, difficulties arise in the general case when more than one item matches the search criteria. In this case a conventional quantum computer will return one of the matching items at random, while an NMR implementation will return some sort of ensemble average over all the matches, and it is difficult or impossible to deduce anything useful from this ensemble result. It is, however, possible to overcome this problem by using a closely related approach, approximate quantum counting [254].

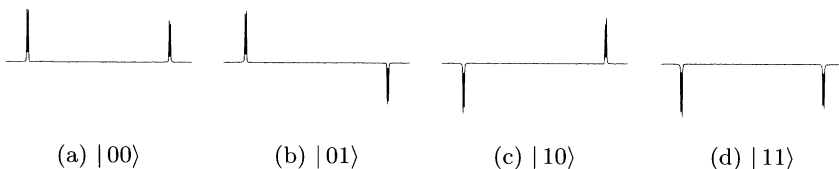


Fig. 5.30. Experimental results from an NMR quantum computer implementing Grover's quantum search over a two qubit search space; the result is shown for each of the four possible matching items.

Three qubit systems have been studied, but have largely been used to demonstrate interesting quantum phenomena, such as GHZ states [255, 256], simple error correction protocols [257, 258], and teleportation [259]. They have also been used, however, to implement the three qubit Deutsch–Jozsa algorithm [260]. A partial demonstration of the Deutsch–Jozsa algorithm on a five-qubit system has also been given [261].

5.4.6 Prospects for the Future

There are several major problems which might act to limit the size of real NMR quantum computers based on the current approach. The most widely discussed problems are the exponential loss of signal intensity with increasing numbers of qubits, followed by the effects of decoherence. In fact these effects are unlikely to be very important as other problems are likely to become visible first. Nevertheless it is useful to discuss these issues and how they might be tackled.

Exponential signal loss: The exponential loss in signal with increasing numbers of qubits arises as a result of the need to distill an effective pure state from the thermal equilibrium density matrix. Adding an additional qubit means adding an additional spin, doubling the number of spin states in the system and thus doubling the number of ways in which a flip of the state of any one spin can occur. Distilling out an effective pure state is equivalent to selecting only one of these possible transitions, with a consequent loss in signal intensity [262]. Note that this problem is not confined to NMR, but will also arise in *any* ensemble quantum computation working in the high temperature regime ($\Delta E \ll kT$).

Clearly this exponential fall off in signal is a potential limit, but in practice its importance has been overstated. NMR spectra can be acquired with a fairly high signal-to-noise ratio (the spectrum in Fig. 5.25 has a ratio of about 800), and thus the signal loss will only be a serious problem for NMR computers containing ten qubits or more. It is possible to increase the signal-to-noise ratio by a variety of simple means, such as signal averaging or increasing the sample size, or by more subtle approaches such as optical pumping [263].

A different approach, suggested by Schulman and Vazirani [264] is to use computational methods to purify a collection of low fidelity qubits. It is not practical to apply this approach directly to a thermal ensemble, but if used in combination with other methods for increasing the initial polarisation, such as optical pumping, it may prove useful.

Decoherence: Decoherence (that is, the conversion of coherent superpositions into incoherent mixtures by random processes) is another potential problem, which is common to all implementations of quantum computers. Any quantum superposition has a characteristic decoherence time, and it is necessary to ensure that any calculations are completed in a time which is not too long compared with the decoherence time (although error correction techniques allow this time scale to be extended). In NMR quantum computers this time is generally related to the spin–spin relaxation time, T_2 , although this is a simplification as T_2 is the decoherence time of a single spin coherence, and the decoherence times for multi-spin coherences can be quite different. Nevertheless T_2 does give a very approximate idea of the appropriate time scale, which for the NMR computers currently being investigated (based on small molecules in solution) is of the order of a few seconds.

The relevant parameter for a quantum computer is not the decoherence time itself, but the ratio of the decoherence time to the time taken to execute a quantum gate. For simple two-bit gates, such as the controlled-NOT, this time is comparable to the inverse of the scalar spin–spin coupling (around 5–150 ms), suggesting that it should be possible to implement tens or hundreds of gates. It is true that systems with much larger values of T_2 are known, but such systems cannot be used to build NMR quantum computers of the current design as they do not have the spin–spin interactions necessary to build quantum gates.

Other problems: Far more important than either of the problems discussed above are two other problems: the problem of selectively addressing spins, and the problem of the growth in the complexity of gates with increasing numbers of spins.

The problem of selectively addressing different spins is simple to understand. In conventional quantum computers individual qubits are distinguished by the spatial locations of the corresponding physical systems, but this approach cannot be used in NMR. Instead qubits are distinguished by the different NMR transition frequencies of their corresponding spins. Unfortunately this frequency range is rather narrow (typically only a few thousand Hz), and it is difficult to perform completely selective excitations on spins whose frequencies are close together [265]. This is one major source of the distortions clearly visible in the experimental spectra (Figs. 5.27–5.30). Clearly this problem will be more serious in systems with more spins, as it will be harder to ensure that all the spins are separated by substantial frequency gaps.

Because of this most authors have preferred to study heteronuclear spin systems, such as NMR computers based on the ^1H - ^{13}C spin pair in chloroform. This is much simpler than the corresponding homonuclear problem, as the transition frequencies of the two spins now differ by hundreds of MHz, and spin-selective excitation is essentially trivial. This approach has allowed rapid progress with two spin and three spin systems, but it cannot be extended indefinitely as there are only a small number of different nuclei which are suitable, and in any event most NMR spectrometers are not capable of dealing with more than two or three different nuclei at the same time. Thus any NMR quantum computer involving more than a few qubits will have to face the problems of selectively addressing spins.

A second, more subtle, problem is the increasing complexity of quantum logic gates in multispin systems. Ideally it would be possible to take a two qubit gate, developed for a two qubit computer, and use it in a three or four qubit computer without major modification. With NMR quantum computers this may prove tricky. The interactions which form the basis of gates, in particular spin–spin coupling, are part of the background NMR Hamiltonian, under which the spin system evolves in the absence of specific excitation. Quantum logic gates are formed by modulating the intensity of different elements of this background Hamiltonian, to give an effective Hamiltonian which has the desired form. This process, however, becomes more difficult in the presence of additional qubits, as it is necessary not only to modulate the interactions between the spins involved in the gate, but also to modulate any interactions with the additional spins so as to effectively remove them [266]. In the worst case a system of N spins has a total of $\frac{1}{2}N(N + 1)$ one and two-spin interactions in the background Hamiltonian, of which only three are relevant to forming any particular two qubit gate. Although this problem is not quite as serious as it might initially appear [267]–[269] cancelling out all these irrelevant interactions may prove to be the hardest aspect of building NMR quantum computers with more than a handful of qubits.

Alternative approaches: Mindful of the potential problems outlined above, some researchers have begun to think about radically different approaches to building quantum computers with NMR systems. So far none of these ideas have been demonstrated, and they bear little resemblance to “conventional” NMR quantum computers.

One feature common to many of these speculative schemes is the use of solid samples instead of fluids. This has many significant consequences for NMR studies, both helpful and unhelpful. Individual molecules will remain approximately stationary in a solid sample, and so spatial localisation techniques could in principle be used to selectively excite particular spins. The long wavelength of RF radiation precludes direct approaches, but techniques developed for NMR imaging [270] do allow spatial discrimination between spins. It will be difficult to achieve atomic resolution with this approach, however, partly because of the difficulty of constructing sufficiently powerful

field gradients, but also because the low sensitivity of NMR makes it impractical to directly detect single spins [270]. Calculations suggest a limiting resolution of about $1\mu\text{m}$, so it will be necessary to use clusters of spins rather than individual nuclei.

A second consequence of moving to the solid state is a substantial change in the NMR Hamiltonian, as anisotropic interactions are no longer averaged to their isotropic values. In particular the direct dipole-dipole coupling between spins is the largest spin-spin interaction. This coupling is much larger than scalar coupling, allowing the implementation of more rapid logic gates, but has the disadvantage that every spin is coupled to all other nearby spins. This makes it difficult to use the coupling in the selective manner needed for logic gates, and can also lead to rapid decoherence.

A recent proposal due to Kane [271] confronts these problems in a most ingenious way, combining solid state NMR with conventional silicon microchip technology. It envisages the use of isolated ^{31}P atoms in a silicon matrix, with electrostatic gates, both to control the excitation of individual spins and to modulate couplings between them. Single spin detection would be achieved by using the nuclear spin to control a single electron transfer process. While this proposal is well beyond the scope of current technology, it is likely that many of the requirements will have been attained within the next ten years.

5.4.7 Entanglement and Mixed States

It has recently been suggested that NMR might not be a quantum mechanical technique at all! When assessing this claim, it should be remembered that “quantum mechanical” is used here with a technical meaning of “provably non-classical”. As NMR experiments are conducted in the high temperature regime (kT is large compared with the splitting between energy levels), the density matrix describing a nuclear spin system is always close to the maximally mixed state, and such states can always be decomposed [272] as a mixture of product states (that is, states containing no entanglement between different nuclei). As NMR states are describable without invoking entanglement, they can therefore be described using classical models (although these classical models may be somewhat contrived). However, while classical models can be used to describe an individual NMR state, it is not clear that such models can be used to describe the evolution of the state during an NMR experiment [273]. The significance of these conclusions remains controversial and unclear.

5.4.8 The Next Few Years

NMR provides the most powerful technology for implementing quantum computers currently available, and is likely to remain so for several more years. Several small NMR quantum computers have been built, and quantum algorithms have been implemented upon them.

In the next few years it seems likely that NMR computers with three to five qubits will become routine, and that larger systems will be under investigation. It seems unlikely, however, that NMR systems with many more than ten qubits will be built without a major change in approach. In the longer term, approaches such as Kane's solid state NMR computer may prove extremely promising.

6. Quantum Networks and Multi-Particle Entanglement

6.1 Introduction

The basic concepts of quantum entanglement have been presented in previous chapters. In this chapter various advanced topics of quantum entanglement will be discussed. Section 6.2 describes a scheme for establishing entanglement between atoms at spatially separated nodes through the exchange of photons. In this way a quantum network can be built combining the virtues of trapped atom/ion systems, i.e. long storage times and local quantum state processing, with the advantages of quantum optics, i.e. flexible and reliable quantum communication over long distances.

Section 6.3 addresses entangled states of more than two particles. Such states are not only important in the field of quantum information but were initially introduced by Greenberger, Horne and Zeilinger (GHZ) to address the Einstein–Podolsky–Rosen (EPR) conflict of local realism with quantum mechanics in a most conclusive way. It is shown how three-photon GHZ entanglement can be generated and why entanglement between more than two particles illustrates quantum properties that are completely incomprehensible from any classical local-realistic viewpoint.

In Sect. 6.4 it is shown that entanglement between more than two particles is a very delicate concept. In fact, entanglement between more than two particles cannot be defined in a unique way. Measures are introduced to quantify the entanglement, and related topics such as entanglement distillation and the relative entropy of entanglement will be explained.

6.2 Quantum Networks I: Entangling Particles at Separate Locations

H.-J. Briegel, S. J. van Enk, J. I. Cirac, and P. Zoller

6.2.1 Interfacing Atoms and Photons

Quantum networks consist of spatially separated nodes where qubits are stored and locally manipulated, and quantum communication channels connecting the nodes. Exchange of information within the network is accomplished by sending qubits through the channels. A physical implementation of such a network could consist e.g. of clusters of trapped atoms or ions representing the nodes, with optical fibres or similar photon “conduits” providing the quantum channels, as shown in Fig. 6.1.

Atoms and ions are particularly well suited for storing qubits in long-lived internal states, and recently proposed schemes for performing quantum gates between trapped atoms or ions provide an attractive method for local processing within an atom/ion node [156, 274, 275]. On the other hand, photons clearly represent the best qubit-carrier for fast and reliable communication over long distances [276, 277]. In this section, we describe a scheme [278] to implement an interface between the atoms and the photons, i.e. between the nodes and the communication channels of the network. This scheme allows quantum transmission with (in principle) unit efficiency between distant atoms 1 and 2. The possibility of combining local quantum processing with quantum transmission between the nodes of the network opens the possibility for a variety of novel applications ranging from entangled-state cryptography [279] and teleportation [280] to more complex activities such as multi-particle communication and distributed quantum computing [281, 282].

The basic idea of the scheme is to utilise strong coupling between a high-Q optical cavity and the atoms [276] forming a given node of the quantum network. By applying laser beams, one first transfers the internal state of

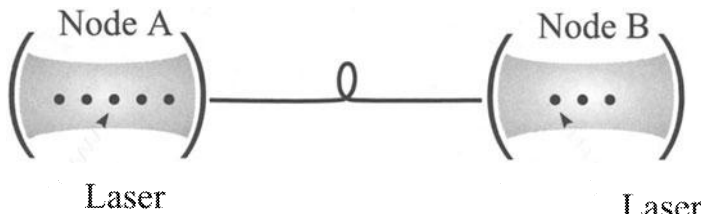


Fig. 6.1. Element of a quantum network. Atoms in high-Q cavities are used to locally store and process quantum information; photons are used to transfer quantum information between spatially separated “nodes” of the network.

an atom at the first node to the optical state of the cavity mode. The generated photons leak out of the cavity, propagate as a wavepacket along the transmission line, and enter an optical cavity at the second node. Finally, the optical state of the second cavity is transferred to the internal state of an atom. Multiple-qubit transmissions can be achieved by sequentially addressing pairs of atoms (one at each node), as entanglements between arbitrarily located atoms are preserved by the state-mapping process. The distinguishing feature of the protocol is that, by controlling the atom-cavity interaction, one can avoid the reflection of the wavepackets from the second cavity, effectively switching off the dominant loss channel that would be responsible for decoherence in the communication process.

6.2.2 Model of Quantum State Transmission

A simple configuration of quantum transmission between two nodes consists of two atoms 1 and 2 which are strongly coupled to their respective cavity modes, see Fig. 6.2.

The Hamiltonian describing the interaction of each atom with the corresponding cavity mode is ($\hbar = 1$):

$$\begin{aligned} \hat{H}_i &= \omega_c \hat{a}_i^\dagger \hat{a}_i + \omega_0 |r\rangle_i \langle r| + g(|r\rangle_i \langle g| \hat{a}_i + \text{h.c.}) \\ &\quad + \frac{1}{2} \Omega_i(t) [e^{-i[\omega_L t + \phi_i(t)]} |r\rangle_i \langle e| + \text{h.c.}] \quad (i = 1, 2). \end{aligned} \quad (6.1)$$

Here, \hat{a}_i and \hat{a}_i^\dagger are the annihilation and creation operators for cavity mode i with frequency ω_c . The states $|g\rangle$, $|r\rangle$, and $|e\rangle$ form a three-level system of excitation frequency ω_0 (Fig. 6.2), and the qubit is stored in a superposition of the two degenerate ground states. The states $|e\rangle$ and $|g\rangle$ are coupled by a Raman transition [274, 275, 283], where a laser of frequency ω_L excites the atom from $|e\rangle$ to $|r\rangle$ with a time-dependent Rabi frequency $\Omega_i(t)$ and phase $\phi_i(t)$, followed by a transition $|r\rangle \rightarrow |e\rangle$ which is accompanied by emission of a photon into the corresponding cavity mode, with coupling constant g . In order to suppress spontaneous emission from the excited state during the Raman process, we assume that the laser is strongly detuned from the atomic

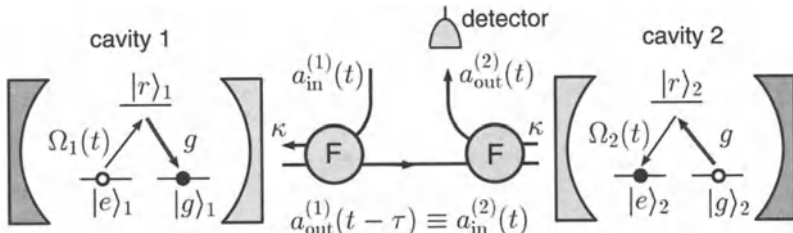


Fig. 6.2. Schematic representation of unidirectional quantum transmission between two atoms in optical cavities connected by a quantized transmission line.

transition $|\Delta| \gg \Omega_{1,2}(t), g, |\dot{\phi}_{1,2}|$ (with $\Delta = \omega_L - \omega_0$). In such a case, one can eliminate adiabatically the excited states $|r\rangle_i$. The new Hamiltonian for the dynamics of the two ground states becomes, in a rotating frame for the cavity modes at the laser frequency,

$$\begin{aligned}\hat{H}_i = & -\delta\hat{a}_i^\dagger\hat{a}_i + \frac{g^2}{\Delta}\hat{a}_i^\dagger\hat{a}_i|g\rangle_i\langle g| + \delta\omega_i(t)|e\rangle_i\langle e| \\ & -ig_i(t)\left[e^{i\phi_i(t)}|e\rangle_i\langle g|a_i - \text{h.c.}\right]. \quad (i = 1, 2)\end{aligned}\quad (6.2)$$

The first term involves the Raman detuning $\delta = \omega_L - \omega_c$. The next two terms are AC-Stark shifts of the ground states $|g\rangle$ and $|e\rangle$ due to the cavity mode and laser field, respectively, with $\delta\omega_i(t) = \Omega_i(t)^2/(4\Delta)$. The last term is the familiar Jaynes–Cummings interaction, with an effective coupling constant $g_i(t) = g\Omega_i(t)/(2\Delta)$. Here we ignore for the moment the small effects produced by spontaneous emission during the Raman process. The notation $|e\rangle$ as “excited” and $|g\rangle$ as “ground” state is motivated by this analogy with the Jaynes–Cummings Model.

The aim is to select the time-dependent Rabi frequencies and laser phases¹ to accomplish the *ideal quantum transmission*

$$\begin{aligned}& (c_g|g\rangle_1 + c_e|e\rangle_1)|g\rangle_2 \otimes |0\rangle_1|0\rangle_2|\text{vac}\rangle \\ & \rightarrow |g\rangle_1(c_g|g\rangle_2 + c_e|e\rangle_2) \otimes |0\rangle_1|0\rangle_2|\text{vac}\rangle,\end{aligned}\quad (6.3)$$

where $c_{g,e}$ are complex numbers; in general, they have to be replaced by unnormalised states of other “spectator” atoms in the network. In (6.3), $|0\rangle_i$ and $|\text{vac}\rangle$ represent the vacuum state of the cavity modes and the free electromagnetic modes connecting the cavities. Transmission will occur by photon exchange via these modes.

In the present context, it is convenient to formulate the problem in the language of quantum trajectories [284, 285]. Let us consider a fictitious experiment where the output field of the second cavity is continuously monitored by a photodetector (see Fig. 6.2). The evolution of the quantum system under continuous observation, conditional upon observing a particular trajectory of counts, can be described by a pure state wavefunction $|\Psi_c(t)\rangle$ in the system Hilbert space (where the radiation modes outside the cavity have been eliminated). During the time intervals when no count is detected, this wavefunction evolves according to a Schrödinger equation with non-hermitian effective Hamiltonian

$$\hat{H}_{\text{eff}}(t) = \hat{H}_1(t) + \hat{H}_2(t) - i\kappa\left(\hat{a}_1^\dagger\hat{a}_1 + \hat{a}_2^\dagger\hat{a}_2 + 2\hat{a}_2^\dagger\hat{a}_1\right). \quad (6.4)$$

Here, κ is the cavity loss rate, which is assumed to be the same for the first and the second cavity. The detection of a count at time t_r is associated with a quantum jump according to $|\Psi_c(t_r + dt)\rangle \propto \hat{c}|\Psi_c(t_r)\rangle$, where $\hat{c} = \hat{a}_1 + \hat{a}_2$

¹ One could also modulate the cavity transmission, but this is technically more difficult.

[285, 286]. The probability density for a jump (detector click) to occur during the time interval from t to $t + dt$ is $\langle \Psi_c(t) | \hat{c}^\dagger \hat{c} | \Psi_c(t) \rangle dt$ [285, 286].

6.2.3 Laser Pulses for Ideal Transmission

We wish to design the laser pulses in both cavities in such a way that ideal quantum transmission condition (6.3) is satisfied. A necessary condition for the time evolution is that a quantum jump (detector click, see Fig. 6.2) never occurs, i.e. $\hat{c}|\Psi_c(t)\rangle = 0 \forall t$, and thus the effective Hamiltonian will become a hermitian operator. In other words, the system will remain in a *dark state* of the cascaded quantum system. Physically, this means that the wavepacket is not reflected from the second cavity. We expand the state of the system as

$$\begin{aligned} |\Psi_c(t)\rangle &= |c_g|gg\rangle|00\rangle \\ &+ |c_e| \left[\alpha_1(t)e^{-i\phi_1(t)}|eg\rangle|00\rangle + \alpha_2(t)e^{-i\phi_2(t)}|ge\rangle|00\rangle \right. \\ &\quad \left. + \beta_1(t)|gg\rangle|10\rangle + \beta_2(t)|gg\rangle|01\rangle \right]. \end{aligned} \quad (6.5)$$

Ideal quantum transmission (6.3) will occur for

$$\alpha_1(-\infty) = \alpha_2(+\infty) = 1, \quad \phi_1(-\infty) = \phi_2(+\infty) = 0. \quad (6.6)$$

The first term on the RHS of (6.5) does not change under the time evolution generated by H_{eff} . Defining symmetric and antisymmetric coefficients $\beta_{1,2} = (\beta_s \mp \beta_a)/\sqrt{2}$, we find the following *evolution equations*

$$\dot{\alpha}_1(t) = g_1(t)\beta_a(t)/\sqrt{2}, \quad (6.7)$$

$$\dot{\alpha}_2(t) = -g_2(t)\beta_a(t)/\sqrt{2}, \quad (6.8)$$

$$\dot{\beta}_a(t) = -g_1(t)\alpha_1(t)/\sqrt{2} + g_2(t)\alpha_2(t)/\sqrt{2}, \quad (6.9)$$

where we have chosen the laser frequencies $\omega_L + \dot{\phi}_{1,2}(t)$ so that $\delta = g^2/\Delta$ and

$$\dot{\phi}_{1,2}(t) = \delta\omega_i(t) \quad (6.10)$$

in order to compensate the AC-stark shifts; thus (6.7–6.9) are decoupled from the phases. The *dark state condition* implies $\beta_s(t) = 0$, and therefore

$$\dot{\beta}_s(t) = g_1(t)\alpha_1(t)/\sqrt{2} + g_2(t)\alpha_2(t)/\sqrt{2} + \kappa\beta_a(t) \equiv 0, \quad (6.11)$$

as well as the normalisation condition

$$|\alpha_1(t)|^2 + |\alpha_2(t)|^2 + |\beta_a(t)|^2 = 1. \quad (6.12)$$

We note that the coefficients $\alpha_{1,2}(t)$ and $\beta_s(t)$ are real.

The mathematical problem is now to find pulse shapes $\Omega_{1,2}(t) \propto g_{1,2}(t)$ such that the conditions (6.6–6.9, 6.11) are fulfilled. In general this is a difficult problem, as imposing conditions (6.6, 6.11) on the solutions of the

differential equations (6.7–6.9) gives functional relations for the pulse shape whose solution are not obvious. We shall construct a class of solutions guided by the following physical idea. Let us consider that a photon leaks out of an optical cavity and propagates away as a wavepacket. Imagine that we were able to “time reverse” this wavepacket and send it back into the cavity; then this would restore the original (unknown) superposition state of the atom, provided we would also reverse the timing of the laser pulses. If, on the other hand, we are able to drive the atom in a transmitting cavity in such a way that the outgoing pulse were already symmetric in time, the wavepacket entering a receiving cavity would “mimic” this time reversed process, thus “restoring” the state of the first atom in the second one. Thus, we look for solutions satisfying the *symmetric pulse condition*

$$g_2(t) = g_1(-t) \quad (\forall t). \quad (6.13)$$

This implies $\alpha_1(t) = \alpha_2(-t)$, and $\beta_a(t) = \beta_a(-t)$. The latter relation leads to a symmetric shape of the photon wavepacket propagating between the cavities.

Suppose that we specify a pulse shape $\Omega_1(t) \propto g_1(t)$ for the second half of the pulse in the first cavity ($t \geq 0$)². We wish to determine the first half $\Omega_1(-t) \propto g_1(-t)$ (for $t > 0$), such that the conditions for ideal transmission (6.3) are satisfied. From (6.6, 6.11) we have

$$g_1(-t) = -\frac{\sqrt{2}\kappa\beta_a(t) + g_1(t)\alpha_1(t)}{\alpha_2(t)}, \quad (t > 0). \quad (6.14)$$

Thus, the pulse shape is completely determined provided we know the system evolution for $t \geq 0$. However, a difficulty arises when we try to find this evolution, since it depends on the yet unknown $g_2(t) = g_1(-t)$ for $t > 0$ [see (6.7–6.9)]. In order to circumvent this problem, we use (6.11) to eliminate this dependence in (6.7, 6.9). This gives

$$\dot{\alpha}_1(t) = g_1(t)\beta_a(t)/\sqrt{2}, \quad (6.15)$$

$$\dot{\beta}_a(t) = -\kappa\beta_a(t) - \sqrt{2}g_1(t)\alpha_1(t) \quad (6.16)$$

for $t \geq 0$. These equations have to be integrated with the initial conditions

$$\alpha_1(0) = \left[\frac{2\kappa^2}{g_1(0)^2 + \kappa^2} \right]^{\frac{1}{2}} \quad (6.17)$$

$$\beta_a(0) = [1 - 2\alpha_1(0)^2]^{\frac{1}{2}} \quad (6.18)$$

which follow immediately from $\alpha_1(0) = \alpha_2(0)$, and (6.11, 6.12) at $t = 0$. Given the solution of (6.15, 6.16), we can determine $\alpha_2(t)$ from the normalisation

² $\Omega_1(t)$ has to be such that $\alpha_1(\infty) = 0$. This is fulfilled if $\Omega_1(\infty) > 0$, which also guarantees that the denominator in (6.14) does not vanish for $t > 0$.

(6.12). In this way, the problem is solved since all the quantities appearing on the RHS of (6.14) are known for $t \geq 0$. It is straightforward to find analytical expressions for the pulse shapes, for example by specifying $\Omega_1(t) = \text{const}$ for $t > 0$.

6.2.4 Imperfect Operations and Error Correction

We have assumed that all operations involved in the transmission process, e.g. the state mapping from the atom to the cavity field via laser pulses, are perfect and did not pay special attention to absorption losses and decoherence in the communication channel. In reality, of course, such processes will always occur with a certain probability. The optical cavity–fibre system, together with the Raman pulses, is an example of a *noisy quantum channel*. Generally speaking, quantum noise tends to diminish the fidelity of the transmission and to destroy the quantum correlations that are ideally established between the nodes. This effect becomes particularly dominant if the nodes are separated by a long distance, where long is defined in comparison with the coherence length and/or absorption length of the channel. Fortunately, since the advent of quantum error correction [287] and entanglement purification [288], there are some tools to fight the effects of quantum noise and decoherence. In Sect. 8.6, we will describe how an efficient error correction can be implemented in above quantum network, correcting transmission errors to all orders. This will allow communication with high fidelity over a short distance. For long distance communication, where the error probability grows exponentially with the length of the channel, we develop a concept of a quantum repeater that plays a role analogous to amplifiers in classical communication.

6.3 Multi-Particle Entanglement

D. Bouwmeester, J.-W. Pan, M. Daniell, H. Weinfurter, A. Zeilinger

6.3.1 Greenberger–Horne–Zeilinger states

Entanglement between many particles is essential for most quantum communication schemes, e.g. error-correction schemes and secret key distribution networks, and for quantum computation. However, the original motivation for the discussion and the generation of entangled states for more than two particles, so called Greenberger–Horne–Zeilinger (GHZ) states, stems from a different direction [289, 290]. Namely from the debate about whether or not quantum mechanics is a complete theory. Although it is not the intention to

give a detailed exposure of this fundamental philosophical discussion here, a brief presentation will be given in order for the reader to obtain a better understanding of the quantum information stored in many-particle entangled system and why their quantum properties are in strong conflict with Einstein's notion of locality. The presentation is structured around an experimental realisation of three-photon entanglement, which, in its own right, is important for the field of quantum information [291].

6.3.2 The Conflict with Local Realism

Greenberger, Horne and Zeilinger showed that quantum-mechanical predictions for certain measurement results on three entangled particles are in conflict with local realism in cases where quantum theory makes definite, i.e. non-statistical, predictions [289]–[294]. This is in contrast to the case of Einstein–Podolsky–Rosen experiments with two entangled particles testing Bell's inequality, where the conflict with local realism only arises for statistical predictions [21, 23, 295, 296, 297].

How are the quantum predictions of a three-photon GHZ-state in stronger conflict with local realism than the conflict for two-photon states?³ To answer this, consider the state

$$\frac{1}{\sqrt{2}}(|H\rangle_1|H\rangle_2|H\rangle_3 + |V\rangle_1|V\rangle_2|V\rangle_3), \quad (6.19)$$

where H and V denote horizontal and vertical polarisations. This state indicates that the three photons are in a quantum superposition of the state $|H\rangle_1|H\rangle_2|H\rangle_3$ (all three photons are horizontally polarised) and the state $|V\rangle_1|V\rangle_2|V\rangle_3$ (all three photons are vertically polarised). This specific state is symmetric with respect to the interchange of all photons which simplifies the arguments below, however the line of reasoning holds for any other maximally entangled three-photon state.

Consider now some specific predictions following from state (6.19) for polarisation measurements on each photon in either a basis rotated through 45° with respect to the original H/V basis, denoted by H'/V' , or in a circular polarisation basis denoted by L/R (left-handed, right-handed). These new polarisation bases can be expressed in terms of the original ones as

$$|H'\rangle = \frac{1}{\sqrt{2}}(|H\rangle + |V\rangle), \quad |V'\rangle = \frac{1}{\sqrt{2}}(|H\rangle - |V\rangle), \quad (6.20)$$

$$|R\rangle = \frac{1}{\sqrt{2}}(|H\rangle + i|V\rangle), \quad |L\rangle = \frac{1}{\sqrt{2}}(|H\rangle - i|V\rangle). \quad (6.21)$$

Let us denote $|H\rangle$ by the vector $(1,0)$ and $|V\rangle$ by the vector $(0,1)$; they are thus the two eigenstates of Pauli operator σ_z , with the corresponding

³ For two-photon states Hardy [298] has found situations where local realism predicts that a specific result occurs *sometimes* and quantum mechanics predicts that the same result *never* occurs [299].

eigenvalues +1 and -1. One can also easily verify that $|H'\rangle$ and $|V'\rangle$ or $|R\rangle$ and $|L\rangle$ are two eigenstates for Pauli operator σ_x or σ_y with the values +1 and -1, respectively. We will refer to a measurement in the H'/V' basis as an x measurement and in the L/R basis as a y measurement.

Representing state (6.19) in the new bases one obtains predictions for measurements of these new polarisations. For example, in the case of measurement of circular polarisation on, say, both photon 1 and 2, and measurement of linear polarisation H' and V' on photon 3, denoted as a yyx measurement, the state becomes

$$\frac{1}{2} \left(|R\rangle_1 |L\rangle_2 |H'\rangle_3 + |L\rangle_1 |R\rangle_2 |H'\rangle_3 + |R\rangle_1 |R\rangle_2 |V'\rangle_3 + |L\rangle_1 |L\rangle_2 |V'\rangle_3 \right). \quad (6.22)$$

This expression has a number of significant implications. Firstly, a specific result that is obtained in any individual or two-photon joint measurement is maximally random. For example, photon 1 will exhibit polarisation R or L with the same probability of 50%.

Secondly, because only those terms yielding a -1 product for a yyx measurement appear in the expression, one realises that, given the results of measurements on two photons, it is possible to predict with certainty what the result of a corresponding measurement performed on the third photon will be. For example, suppose photon 1 and 2 are both found to exhibit right-handed (R) circular polarisation (i.e., both having the value +1). By the third term in the expression above, photon 3 will definitely be V' polarised (i.e., having the value -1).

By cyclic permutation, analogous expressions are obtained for any case of the measurement of circular polarisation on two photons and V' - H' polarisation on the remaining one. Again, only those terms which give a -1 product are the possible outcomes in a xyx or an xyy measurement. Thus, the measurement result both for circular polarisation and for linear H' , V' polarisation can be predicted with certainty for any one of these photons given the result of appropriate measurements on the other two.

Now let us analyse the implications of these predictions from the point of view of local realism. First note that the predictions are independent of the spatial separation of the photons and independent of the relative time order of the measurements. Let us thus consider the experiment to be performed such that the three measurements are performed simultaneously in a given reference frame, say, for conceptual simplicity, in the reference frame of the source. Employing the notion of Einstein locality implies that no information can travel faster than the speed of light. Hence the specific measurement result obtained for any photon must not depend on which specific measurement is performed simultaneously on the other two nor on the outcome of these measurements. The only way then to explain from a local realist point of view the perfect correlations discussed above is to assume that each photon

carries elements of reality for all the measurements considered and that these elements of reality determine the specific measurement result [289, 290, 294].

Let us now consider a measurement of linear H' , V' polarisation on all three photons, i.e. an xxx measurement. What outcomes are possible here if elements of reality exist? State (6.19) and its permutations imply that whenever the result H' [V'] is obtained for any one photon, the other two photons must carry opposite [identical] circular polarisations. Suppose that for three specific photons, one finds, say, the result V' for photons 2 and 3. Because photon 3 is a V' , both photon 1 and 2 must carry identical circular polarisations; and because photon 2 is a V' , both photons 1 and 3 must carry identical circular polarisations. Clearly, if these circular polarisations are elements of reality, then all three photons must carry identical circular polarisations. Thus, if photons 2 and 3 have identical circular polarisations, then photon 1 must necessarily carry linear polarisation V' . Thus the existence of elements of reality leads to the conclusion that the result $|V'_1\rangle|V'_2\rangle|V'_3\rangle$ is one possible outcome if one elects to measure H' , V' polarisations of all three particles, i.e. if an xxx measurement is performed. By parallel constructions, one can verify that the only four possible outcomes are

$$|V'_1\rangle|V'_2\rangle|V'_3\rangle, |H'_1\rangle|H'_2\rangle|V'_3\rangle, |H'_1\rangle|V'_2\rangle|H'_3\rangle, \text{ and } |V'_1\rangle|H'_2\rangle|H'_3\rangle. \quad (6.23)$$

How do these predictions of local realism compare with those of quantum physics? Expressing the state given in (6.19) in terms of H' , V' polarisation yields

$$\begin{aligned} & \frac{1}{2} (|H'\rangle_1 |H'\rangle_2 |H'\rangle_3 + |H'\rangle_1 |V'\rangle_2 |V'\rangle_3 \\ & + |V'\rangle_1 |H'\rangle_2 |V'\rangle_3 + |V'\rangle_1 |V'\rangle_2 |H'\rangle_3). \end{aligned} \quad (6.24)$$

Comparing the terms given in (6.23) with the terms in (6.24) one observes that whenever local realism predicts that a specific result definitely occurs for a measurement on one of the photons given the results for the other two, quantum physics definitely predicts the opposite result. Thus, while in the case of Bell's inequalities for two photons the difference between local realism and quantum physics happens for statistical predictions of the theory, here any statistics is only due to inevitable measurement errors occurring in any and every experiment of classical or quantum physics.

6.3.3 A Source for Three-Photon GHZ Entanglement

Proposals for the creation of entanglement between more than two particles have been made for experiments with photons [300], atoms [301] and ions (see Sect. 4.3), and three nuclear spins within a single molecule have been prepared such that they locally exhibit three-particle correlations [302]. In this section the first experimental observation of polarisation entanglement of three spatially separated photons is described [291]. The method used for

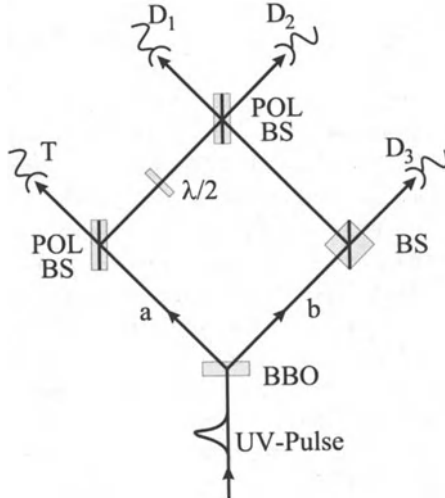


Fig. 6.3. Schematic drawing of the experimental setup for the demonstration of Greenberger–Horne–Zeilinger entanglement for spatially separated photons. Conditional on the registration of one photon at the trigger detector T, the three photons registered at D_1 , D_2 , and D_3 exhibit the desired GHZ correlations.

the experiment is a further development of the techniques that have been used in experiments on quantum teleportation [76] (Sect. 3.7) and entanglement swapping [86] (Sect. 3.10).

As proposed in Ref. [300], the main idea is to transform two pairs of polarisation entangled photons into three entangled photons and a fourth independent photon.⁴ Figure 6.3 is a schematic drawing of the experimental setup. Pairs of polarisation entangled photons are generated by a 200 fs pulse of UV-light which passes through a BBO crystal (see Sect. 3.4.4). The pair creation is such that the following polarisation entangled state is obtained [26]:

$$\frac{1}{\sqrt{2}}(|H\rangle_a|V\rangle_b + e^{i\chi}|V\rangle_a|H\rangle_b). \quad (6.25)$$

This state represents a superposition of the possibility that the photon in arm a is horizontally polarised and the one in arm b is vertically polarised $|H\rangle_a|V\rangle_b$, with the opposite possibility $|V\rangle_a|H\rangle_b$.

In the rare event that two such pairs are created by the passage of a single UV pulse through the crystal the setup is designed such that detection of one photon at each of the four detectors (four-fold coincidence) corresponds to the observation of the state

⁴ The method developed to obtain three-particle entanglement from a source of pairs of entangled particles can be extended to obtain entanglement between many more particles [303].

$$\frac{1}{\sqrt{2}} (|H\rangle_1 |H\rangle_2 |V\rangle_3 + |V\rangle_1 |V\rangle_2 |H\rangle_3) , \quad (6.26)$$

by the detectors D₁, D₂ and D₃. This can be understood in the following way. When a four-fold coincidence recording is obtained, one photon in path *a* must have been transmitted by the polarising beamsplitter (Pol BS) in path *a* and therefore must have had horizontal polarisation upon detection by the trigger detector T. Its companion photon in path *b* must then be vertically polarised, and it has 50% chance of being transmitted by the beamsplitter (see Fig. 6.3) towards detector D₃ and 50% chance of being reflected by the beamsplitter towards the final polarising beamsplitter where it will be reflected to D₂. In the former case, the counts at detectors D₁ and D₂ are due to the second pair. One photon of this second pair travels via path *a* and must necessarily be *V* polarised in order to be reflected by the polarising beamsplitter in path *a*; thus its companion, taking path *b*, must be *H* polarised and after reflection at the beamsplitter in path *b* (with a 50% probability) it will be transmitted by the final polarising beamsplitter and arrive at detector D₁. The photon detected by D₂ therefore must be *H* polarised since it came via path *a* and had to transit the last polarising beamsplitter. Note that this latter photon was initially *V* polarised but after passing the $\lambda/2$ plate (at 22.5°) it became polarised at 45° which gave it a 50% chance of arriving as an *H* polarised photon at detector D₂. Thus one concludes that if the photon detected by D₃ is the companion of the T photon, then the coincidence detection by D₁, D₂, and D₃ corresponds to the detection of the state

$$|H\rangle_1 |H\rangle_2 |V\rangle_3 . \quad (6.27)$$

By a similar argument one can show that if the photon detected by D₂ is the companion of the T photon, the coincidence detection by D₁, D₂, and D₃ corresponds to the detection of the state

$$|V\rangle_1 |V\rangle_2 |H\rangle_3 . \quad (6.28)$$

In general, the two possible states (6.27) and (6.28) corresponding to a four-fold coincidence recording will not form a coherent superposition, i.e. a GHZ state, because they could, in principle, be distinguishable. Besides possible lack of mode overlap at the detectors, the exact detection time of each photon can reveal which state is present. For example, state (6.27) is identified by noting that T and D₃, or D₁ and D₂, fire nearly simultaneously. To erase this information it is necessary that the coherence time of the photons is substantially longer than the duration of the UV pulse (approx. 200 fs) [304]. This can be achieved by detecting the photons behind narrow band-width filters (3.6 nm bandwidth) which yield a coherence time of approx. 500 fs. Thus, the potential to distinguish between states (6.27) and (6.28) largely vanishes, and, by a basic rule of quantum mechanics, the state detected by a coincidence recording of D₁, D₂, and D₃, conditional on the

trigger T, is the quantum superposition given in (6.26). Rigorously speaking, this erasure technique is perfect, hence produces a pure GHZ state, only in the limit of infinitesimal pulse duration and infinitesimal filter bandwidth, but detailed calculations [305] reveal that the experimental parameters given above are sufficient to create a clearly observable entanglement, up to about 80% purity, consistent with the experimental data given below. The plus sign in (6.26) follows from the following more formal derivation. Consider two down-conversions producing the product state

$$\frac{1}{2} (|H\rangle_a |V\rangle_b - |V\rangle_a |H\rangle_b) (|H\rangle'_a |V\rangle'_b - |V\rangle'_a |H\rangle'_b) . \quad (6.29)$$

Here it is initially assumed that the components $|H\rangle_{a,b}$ and $|V\rangle_{a,b}$ created in one down-conversion might be distinguishable from the components $|H\rangle'_{a,b}$ and $|V\rangle'_{a,b}$ created in the other one. The evolution of the individual components of state (6.29) through the apparatus towards the detectors T, D₁, D₂, and D₃ is given by

$$|H\rangle_a \rightarrow |H\rangle_T , \quad |V\rangle_b \rightarrow \frac{1}{\sqrt{2}}(|V\rangle_2 + |V\rangle_3) , \quad (6.30)$$

$$|V\rangle_a \rightarrow \frac{1}{\sqrt{2}}(|V\rangle_1 + |H\rangle_2) , \quad |H\rangle_b \rightarrow \frac{1}{\sqrt{2}}(|H\rangle_1 + |H\rangle_3) . \quad (6.31)$$

Identical expressions hold for the primed components. Inserting these expressions into state (6.29) and restricting ourselves to those terms where only one photon is found in each output we obtain

$$-\frac{1}{4\sqrt{2}} \{ |H\rangle_T (|V\rangle'_1 |V\rangle_2 |H\rangle'_3 + |H\rangle'_1 |H\rangle'_2 |V\rangle_3) + |H\rangle'_T (|V\rangle_1 |V\rangle'_2 |H\rangle_3 + |H\rangle_1 |H\rangle_2 |V\rangle'_3) \} . \quad (6.32)$$

If the experiment is now performed such that the photon states from the two down-conversions are indistinguishable, one finally obtains the desired state (up to an overall minus sign)

$$\frac{1}{\sqrt{2}} |H\rangle_T (|H\rangle_1 |H\rangle_2 |V\rangle_3 + |V\rangle_1 |V\rangle_2 |H\rangle_3) . \quad (6.33)$$

Note that the total photon state produced by the setup, i.e., the state before detection, also contains terms in which, for example, two photons enter the same detector. In addition, the total state contains contributions from single down-conversions. The four-fold coincidence detection acts as a projection measurement onto the desired GHZ state (6.33) and filters out the unwanted terms. The efficiency for one UV pump pulse to yield such a four-fold coincidence detection is very low (of the order of 10^{-10}). Fortunately, 7.6×10^7 UV-pulses are generated per second, which yields about one double pair creation and detection per 150 seconds. Triple and multiple pair creations can be completely neglected.

6.3.4 Experimental Proof of GHZ Entanglement

To experimentally demonstrate that GHZ entanglement can be obtained by the method described above, one first has to verify that, conditional on a photon detection by the trigger T, both the $H_1H_2V_3$ and the $V_1V_2H_3$ component are present and no others. This was done by comparing the count rates of the eight possible combinations of polarisation measurements, $H_1H_2H_3$, $H_1H_2V_3$, ..., $V_1V_2V_3$. The observed intensity ratio between the desired and undesired states was 12:1. Existence of the two terms as just demonstrated is a necessary but not yet sufficient condition for demonstrating GHZ entanglement. In fact, there could in principle be just a statistical mixture of those two states. Therefore, one has to prove that the two terms coherently superpose. This was done by a measurement of linear polarisation of photon 1 along $+45^\circ$, bisecting the H and V direction. Such a measurement projects photon 1 into the superposition

$$|+45^\circ\rangle_1 = \frac{1}{\sqrt{2}}(|H\rangle_1 + |V\rangle_1), \quad (6.34)$$

which implies that the state (6.33) is projected into

$$\frac{1}{\sqrt{2}}|H\rangle_T|+45^\circ\rangle_1(|H\rangle_2|V\rangle_3 + |V\rangle_2|H\rangle_3). \quad (6.35)$$

Thus photon 2 and 3 end up entangled as predicted under the notion of “entangled entanglement” [306]. Rewriting the state of photon 2 and 3 in the 45° basis results in the state

$$\frac{1}{\sqrt{2}}(|+45^\circ\rangle_2|+45^\circ\rangle_3 - |-45^\circ\rangle_2|-45^\circ\rangle_3). \quad (6.36)$$

This means that if photon 2 is found to be polarised along -45° , photon 3 is also polarised along the same direction. The absence of the terms $|+45^\circ\rangle_2|-45^\circ\rangle_3$ and $|-45^\circ\rangle_2|+45^\circ\rangle_3$ is due to destructive interference and thus indicates the desired coherent superposition of the terms in the GHZ state (6.33). The experiment therefore consisted of measuring four-fold coincidences between the detector T, detector 1 behind a $+45^\circ$ polariser, detector 2 behind a -45° polariser, and measuring photon 3 behind either a $+45^\circ$ polariser or a -45° polariser. In the experiment, the difference in arrival time of the photons at the final polariser, or more specifically, at the detectors D₁ and D₂, was varied.

The data points in Fig. 6.4a are the experimental results obtained for the polarisation analysis of the photon at D₃, conditioned on the trigger and the detection of two photons polarised at 45° and -45° by the two detectors D₁ and D₂, respectively.

The two curves show the four-fold coincidences for a polariser oriented at -45° (squares) and $+45^\circ$ (circles) in front of detector D₃ as function of the

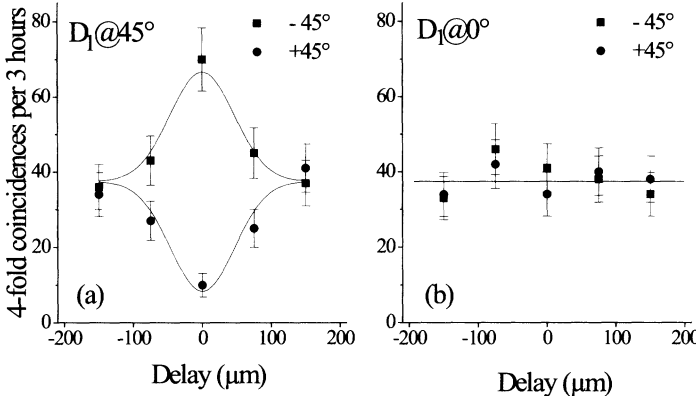


Fig. 6.4. Experimental confirmation of GHZ entanglement. Graph (a) shows the results obtained for polarisation analysis of the photon at D_3 , conditional on the trigger and the detection of one photon at D_1 polarised at 45° and one photon at detector D_2 polarised -45° . The two curves show the four-fold coincidences for a polariser oriented at -45° and 45° respectively in front of detector D_3 as function of the spatial delay in path a . The difference between the two curves at zero delay confirms the GHZ entanglement. By comparison (graph (b)) no such intensity difference is found, as predicted, if the polariser in front of detector D_1 is set at 0° .

spatial delay in path a . From the two curves it follows that for zero delay the polarisation of the photon at D_3 is oriented along -45° , in accordance with the quantum-mechanical predictions for the GHZ state. For non-zero delay, the photons travelling via path a towards the second polarising beamsplitter and those traveling via path b become distinguishable. Therefore increasing the delay gradually destroys the quantum superposition in the three-particle state.

Note that one can equally well conclude from the data that at zero delay, the photons at D_1 and D_3 have been projected onto a two-particle entangled state by the projection of the photon at D_2 onto -45° . The two conclusions are only compatible for a genuine GHZ state.

For an additional confirmation of state (6.33) measurements have been performed conditional on the detection of the photon at D_1 under 0° polarisation (i.e. V polarisation). For the GHZ state $(1/\sqrt{2})(H_1H_2V_3 + V_1V_2H_3)$ this implies that the remaining two photons should be in the state V_2H_3 which cannot give rise to any correlation between these two photons in the 45° detection basis. The experimental results of these measurement are presented in Fig. 6.4b. The data clearly indicate the absence of two-photon correlations and thereby confirm the observation of GHZ entanglement between three spatially separated photons.

Recall that the GHZ entanglement is only observed under the condition that both the trigger photon and the three entangled photons are detected.

This implies that the four-fold coincidence detection plays the double role both of projecting into the desired GHZ state (6.26) and of performing a specific measurement on the state.

This might raise doubts about whether such a source can be used to test local realism. Actually the same doubts had also been raised for the former Bell-type experiments involving indistinguishability of photons [307, 308]. Although these experiments have successfully produced certain long-distance quantum-mechanical correlations, in the past it was generally believed [309], [310] that they could never, not even their idealised versions, be considered as genuine tests of local realism. However, Popescu, Hardy and Zukowski [311] showed that this general belief is wrong and that the above experiments indeed constitute (modulo the usual detection loopholes) true tests of local realism. Following the same line of reasoning, Zukowski [312] has shown that the above GHZ entanglement source enables one to perform a three-particle test of local realism. In essence, the GHZ argument for testing local realism is based on detection events and knowledge of the underlying quantum state is not even necessary. It is indeed enough to consider only the four-fold coincidences discussed above and ignore totally the contributions by the other terms.

6.3.5 Experimental Test of Local Realism Versus Quantum Mechanics

How can one experimentally address the conflict between local realism and quantum mechanics using the GHZ entanglement source described in the previous section? As explained in Sect. 6.3.2, one first has to perform a set of experiments for yyx , yxy and xyy . Each of the three experiments has in principle 2^3 possible outcomes.

Figure 6.5 indicates the experimentally obtained probabilities for each of the 3×2^3 possible outcomes. Here, in order to compare with the GHZ reasoning for state (6.19) given in Sect. 6.3.2, we have simply redefined the polarisation states of photon 3 in (6.26), that is, the notation $|H\rangle_3$ and $|V\rangle_3$ have been interchanged.

From the values of the maxima and minima in Fig. 6.5 one concludes that with $71\% \pm 4\%$ accuracy, i.e. with a visibility of $(\langle \max \rangle - \langle \min \rangle) / (\langle \max \rangle + \langle \min \rangle) = 0.71 \pm 0.04$, the terms that are expected to be present and those that are expected to be absent can be identified. Although the limited visibility is mainly explained by the finite length of the pump-pulse and the finite bandwidth of the frequency filters (see Sect. 6.3.3), it is appropriate, if not compulsory, for a fundamental test of local realism versus quantum mechanics to consider the data shown in Fig. 6.5 as being obtained from measurements on an ensemble of three particles emerging from a black box. In this way no presuppositions about the source of GHZ entanglement are included in the following demonstration of the conflict with local realism. From the data in Fig. 6.5, and taking a local realistic point of view, i.e., assuming that

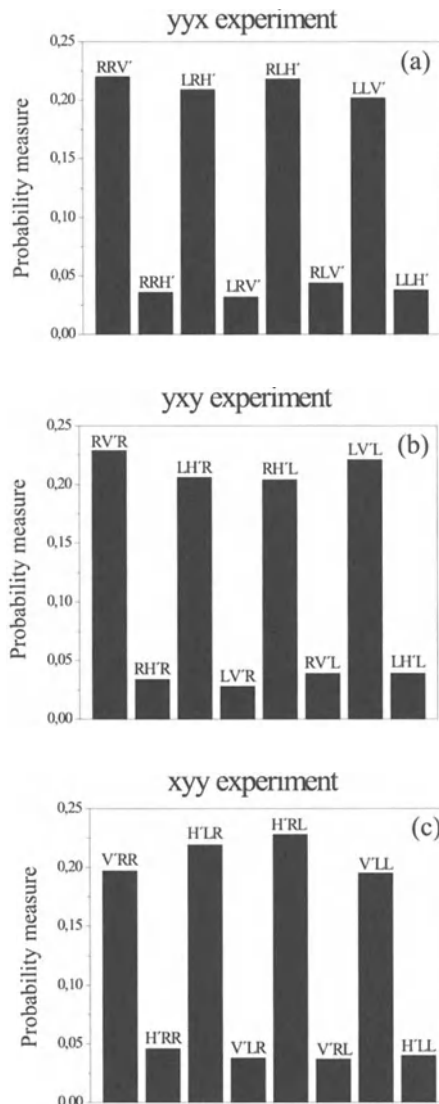


Fig. 6.5. Experimentally determined probabilities of all the possible outcomes of (a) a *yyx* measurement, (b) a *xxy* measurement and (c) an *xyy* measurement.

the outcome of a certain measurement on one particle is independent of the result of any measurement that has been performed on another particle that is specially separated from the former, one can predict (following the arguments given in Sect. 6.3.2) the possible outcomes for an *xxx* measurement. These predictions are shown in Fig. 6.6a.

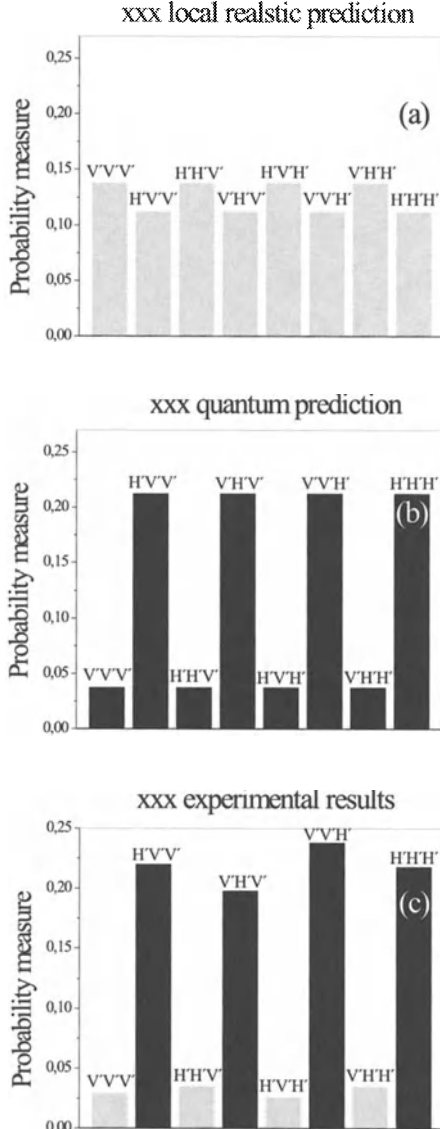


Fig. 6.6. (a): Local realistic predictions for the probabilities of the eight three-particle correlations for an *xxx* measurement (based on data given in Fig. 6.5). (b): The corresponding quantum-mechanical predictions. (c): The experimental results, which are in strong conflict with the local realistic predictions and in agreement with the quantum-mechanical predictions within experimental accuracy.

The predictions following from quantum mechanics are shown in Fig. 6.6b. These later predictions follow from the argument that the data in Fig. 6.5 indicate the presence of entangled three-particle systems with a purity of

about 71%. Finally, Fig. 6.6c shows the experimental results for an xxx measurement.

The results are in strong conflict with the local realism predictions and in full agreement with the quantum mechanical predictions. Actually, within the experimental uncertainty, the experimental data clearly show that only those triple coincidences predicted by quantum mechanics, see (6.24), occur and that those predicted by local realism, see (6.23), are absent. In this sense, the described experiment constitutes the first three-particle test of local realism without inequalities [313].

Since no real experiment can fully fulfill the perfect correlation condition required by the original reasoning of GHZ, a local realist may argue that the GHZ predictions can never be perfectly tested in the laboratory and thus he/she might not be convinced by the above analysis. To face this difficulty, a number of Bell-type inequalities for N -particle GHZ states have been derived [314]–[316]. All these works show that quantum mechanical predictions for GHZ states violate these inequalities by an amount that grows exponentially with N . For instance, the optimal Bell-type inequality for a three-particle GHZ state given by Mermin reads as follows

$$|\langle xyy \rangle + \langle yxy \rangle + \langle yyx \rangle - \langle xxx \rangle| \leq 2, \quad (6.37)$$

where, for example, $\langle xyy \rangle$ denotes the expectation value of the product of the eigenvalues for x , y , and y , measurements on particles 1, 2, and 3, respectively. The necessary visibility to violate this Bell-type inequality for a three-particle GHZ state is 50% [314]. The visibility observed in the above GHZ experiment is about 70% and clearly surpasses the 50% limit. Substituting the experimental results into the left-hand side of inequality (6.37) gives

$$|\langle xxy \rangle + \langle yxy \rangle + \langle yyx \rangle - \langle xxx \rangle| = 2.83 \pm 0.09. \quad (6.38)$$

Therefore, the experimental results violate the inequality (6.37) by over 9 standard deviations, which concludes the demonstration of the conflict with local realism. It should be pointed out that the above test does not provide the final verdict for local realistic theories. Some “loopholes” are still open since the experiments have not been performed with a high-efficiency and space-like separated detection method.

6.4 Entanglement Quantification

V. Vedral, M.B. Plenio, P.L. Knight

6.4.1 Schmidt Decomposition and von Neumann Entropy

A composite quantum system is one that consists of a number of quantum subsystems. When those subsystems are entangled it is impossible to ascribe a definite state vector to any one of them. A simple example of a composite quantum system is a pair of two polarisation entangled photons (see Sect. 3.4.4). The composite system is mathematically described by

$$|\Psi^-\rangle_{12} = \frac{1}{\sqrt{2}}(|H\rangle_1|V\rangle_2 - |V\rangle_1|H\rangle_2). \quad (6.39)$$

The property that is described is that the direction of polarisation of the two photons is orthogonal along any axis. One can immediately see from (6.39) that neither of the photons possesses a definite state (polarisation) vector. The best that one can say is that if a measurement is made on one photon, and it is found, say, to be vertically polarised ($|V\rangle$), then the other photon is certain to be horizontally polarised ($|H\rangle$). This type of description however can not be applied to a general composite system, unless the former is written in a special form. This motivates us to introduce the so called Schmidt decomposition [317], which not only is mathematically convenient, but also gives a deeper insight into correlations between the two subsystems.

The Schmidt decomposition shows that any state of two subsystems A and B (one of dimension N and the other of dimension $M \leq N$) can be written as

$$|\Psi_{AB}\rangle = \sum_{i=1}^N c_i |u_i\rangle |v_i\rangle, \quad (6.40)$$

where $\{|u_i\rangle\}$ is a basis for subsystem A and $\{|v_i\rangle\}$ is a basis for subsystem B . There are two important observations to be made, which are absolutely fundamental to understanding correlations between the two subsystems in a joint pure state:

- The reduced density matrices of both subsystems, written in the Schmidt basis, are diagonal and have the same positive spectrum. We find the reduced density matrix of the subsystem A by tracing the joint state $\rho_{AB} = |\Psi_{AB}\rangle\langle\Psi_{AB}|$ over all states of the subsystem B , so that

$$\rho_A = \text{Tr}_B \rho_{AB} := \sum_q \langle v_q | \rho | v_q \rangle = \sum_p |c_p|^2 |u_p\rangle \langle u_p|. \quad (6.41)$$

Analogously we find $\rho_B = \sum_p |c_p|^2 |v_p\rangle \langle v_p|$.

- If a subsystem is N dimensional it can be entangled with no more than N orthogonal states of another one.

We would like to point out that the Schmidt decomposition is, in general, impossible for more than two entangled subsystems. Mathematical details of this fact are exposed in [318]. To clarify this, however, we consider three entangled subsystems as an example. Here, our intention would be to write a general state such that by observing the state of the one of the subsystems would instantaneously and with certainty tell us the state of the other two. But this is impossible in general since one can perform a measurement on one of the three subsystems such that the remaining two subsystems are entangled systems (see Sect. 6.3.4). Clearly, involvement of even more subsystems complicates this analysis even further. The same reasoning applies to mixed states of two or more subsystems (i.e. states whose density operator is not idempotent $\rho^2 \neq \rho$), for which we cannot have the Schmidt decomposition in general. This reason alone is responsible for the fact that the entanglement of two subsystems in a pure state is simple to understand and quantify, while for mixed states, or states consisting of more than two subsystems, the question is much more involved.

To quantify entanglement in a pure state of two subsystems we introduce the following “measure of uncertainty” in a state of a quantum system.

Definition. The von Neumann entropy of a quantum system described by a density matrix ρ is defined as [319]

$$S_N(\rho) := -\text{Tr}(\rho \ln \rho) . \quad (6.42)$$

(We will drop the subscript N whenever there is no possibility of confusion). So entanglement between A and B can be understood as follows. The uncertainty in the system B before we measured A is $S(\rho_B)$, where ρ_B is the reduced density matrix of system B . After the measurement there is no uncertainty, i.e. if we obtain $\{|u_i\rangle\}$ for A , then we know that the state of B is $\{|v_i\rangle\}$. So the information gained is $S(\rho_B) = S(\rho_A)$. Thus A and B are most entangled when their reduced density matrices are maximally mixed. Specialising to two qubits, a maximally entangled state is e.g. $\frac{1}{\sqrt{2}}(|00\rangle + |11\rangle)$.

There is also another physical interpretation of this measure of entanglement for pure states. Namely it can be shown [117] that the amount of entanglement that can be distilled locally from a pure state of the form $a|00\rangle + b|11\rangle$ is limited by the reduced entropy of that pure state. On the other hand, if we want to create, by local operations, an ensemble of systems each in the state $a|00\rangle + b|11\rangle$ then the average amount of entanglement per pair that we need to share initially is again given by the reduced entropy of that pure state.

For mixed states the Schmidt decomposition no longer exists, so that the reduced entropy is no longer a good measure of entanglement. A way to proceed in quantifying entanglement turns out to be via entanglement

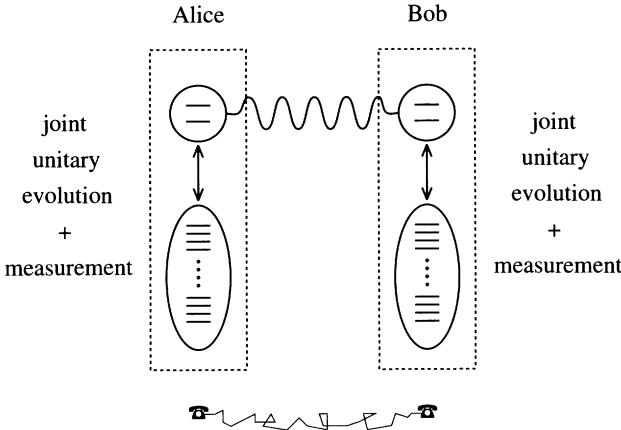


Fig. 6.7. Quantum state purification methods allow local general measurements as indicated by the dashed boxes. An additional multilevel system interacts with our qubit and subsequently the multilevel system is measured. This is the most general form of measurement. Also allowed is classical communication, here symbolised by the telephones.

purification procedures. We first formalise general purification procedures and then, based on that, show three different ways of quantifying entanglement.

6.4.2 Purification Procedures

There are three different ingredients involved in procedures aiming at distilling locally a subensemble of highly entangled states from an original ensemble of less entangled states.

1. *Local general measurements* (LGM): these are performed by the two parties A and B separately and are described by two sets of operators satisfying the completeness relations $\sum_i A_i^\dagger A_i = \mathbf{I}$ and $\sum_j B_j^\dagger B_j = \mathbf{I}$. The joint action of the two is described by $\sum_{i,j} A_i \otimes B_j = \sum_i A_i \otimes \sum_j B_j$, which is again a complete general measurement, and obviously local. Any local general measurement on a system can be implemented by letting it interact with an additional system and then measuring this additional system. The situation is depicted in Fig. 6.7.
2. *Classical communication* (CC): this means that the actions of A and B can be correlated. This can be described by a *complete measurement* on the whole space $A + B$ and is not necessarily decomposable into a sum of direct products of individual operators (as in LGM). If ρ_{AB} describes the initial state shared between A and B then the transformation involving ‘LGM+CC’ would look like

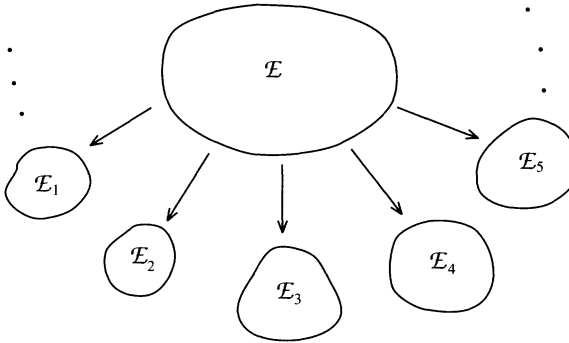


Fig. 6.8. Subselection according to the result of local measurements is the key ingredient of a quantum state purification procedure. The initial ensemble \mathcal{E} is decomposed into subensembles \mathcal{E}_i . Some of these subensembles may have a higher entanglement per pair than the original ensemble.

$$\rho_{AB} \longrightarrow \sum_i A_i \otimes B_i \rho_{AB} A_i^\dagger \otimes B_i^\dagger, \quad (6.43)$$

i.e. the actions of A and B are ‘correlated’.

3. *Post-selection* (PS) is performed on the *final ensemble* according to the above two procedures (Illustrated in Fig. 6.8). Mathematically this amounts to the general measurement not being complete, i.e. we leave out some operations. The density matrix describing the newly obtained ensemble (the subensemble of the original one) has to be renormalised accordingly. Suppose that we kept only the pairs where we had an outcome corresponding to the operators A_i and B_j , then the state of the chosen subensemble would be

$$\hat{\rho}_{AB} \longrightarrow \frac{A_i \otimes B_j \rho_{AB} A_i^\dagger \otimes B_j^\dagger}{\text{Tr}(A_i \otimes B_j \rho_{AB} A_i^\dagger \otimes B_j^\dagger)}, \quad (6.44)$$

where the denominator provides the necessary normalisation.

Any manipulation involving either of the above three elements or their combination is called a *purification procedure*. It should be noted that the three operations described above are local. This implies that the entanglement of the total ensemble cannot increase under these operations. However, classical correlations between the two subsystems *can* be increased, even for the whole ensemble, if we allow classical communication.

We assume the following definition: a state ρ_{AB} is disentangled (also called separable) if and only if

$$\rho_{AB} = \sum_i p_i \rho_A^i \otimes \rho_B^i, \quad (6.45)$$

where $\sum_i p_i = 1$ and $p_i \geq 0$ for all i . Otherwise it is said to be entangled. Note that all the states in the above expansion can be pure. This is because each ρ^i can be expanded in terms of its eigenvectors. So, in the above sum we can in addition require that $\rho_A^i{}^2 = \rho_A^i$ and $\rho_B^i{}^2 = \rho_B^i$ for all i . This fact will be used later in this section.

6.4.3 Conditions for Entanglement Measures

It can be proven that, out of certain states, it is possible to distill maximally entangled states by means of LGM+CC+PS a subensemble of maximally entangled states [50]. The disentangled states, of course, yield no entanglement through purification, but the converse is not true in general; namely, if a state is entangled then this does not necessarily imply that it can be purified [320]. The question remains open as to how much entanglement a certain state contains. This question is not entirely well defined unless we state what physical circumstances characterise the amount of entanglement. This immediately implies that a measure of entanglement is non-unique, as will be seen shortly. Before we define three different measures of entanglement we state four conditions that every measure of entanglement has to satisfy [321, 322].

- E1. $E(\sigma) = 0$ iff σ is separable.
- E2. Local unitary operations leave $E(\sigma)$ invariant, i.e. $E(\sigma) = E(U_A \otimes U_B \sigma U_A^\dagger \otimes U_B^\dagger)$.
- E3. The expected entanglement cannot increase under LGM+CC+PS given by $\sum V_i^\dagger V_i = I$, i.e.

$$\sum_i \text{tr}(\sigma_i) E(\sigma_i / \text{tr}(\sigma_i)) \leq E(\sigma) , \quad (6.46)$$

where $\sigma_i = V_i \sigma V_i^\dagger$.

- E4. For pure states the measure of entanglement has to reduce to the entropy of the reduced density operator.

Condition E1 ensures that disentangled and only disentangled states have a zero value of entanglement. Condition E2 ensures that a local change of basis has no effect on the amount of entanglement. Condition E3 is intended to abolish the possibility of increasing entanglement by performing local measurements aided by classical communication. It takes into account the fact that we have a certain knowledge of the final state. Namely, when we start with n states σ we know exactly which $m_i = n \times \text{Tr}(\sigma_i)$ pairs will end up in the state σ_i after performing a purification procedure. Therefore we can separately access the entanglement in each of the possible subensembles described by σ_i . Clearly the total entanglement at the end should not exceed the original entanglement, which is stated in E3. This, of course, does not exclude the possibility that we can select a subensemble whose entanglement per pair is higher than the original entanglement per pair. The fourth condition has been introduced as a consistency criterion because the measure

of entanglement for pure states is unique. We now introduce three different measures of entanglement which obey E1–E4. Note that we might wish to relax condition E4. This would allow us more possible measures of entanglement which might have applications in special situations. We will give an example later in this section.

First we discuss the entanglement of formation (sometimes also called the entanglement of creation) [323]. Bennett et al. define the entanglement of creation of a state $\hat{\rho}$ by

$$E_c(\rho) := \min \sum_i p_i S(\rho_A^i) \quad (6.47)$$

where $S(\rho_A) = -\text{Tr} \rho_A \ln \rho_A$ is the von Neumann entropy and the minimum is taken over all the possible realisations of the state, $\hat{\rho}_{AB} = \sum_j p_j |\psi_j\rangle\langle\psi_j|$ with $\hat{\rho}_A^i = \text{Tr}_B(|\psi_i\rangle\langle\psi_i|)$. The entanglement of creation cannot be increased by the combined action of LGM+CC and therefore satisfies all the four conditions E1–E4 [323]. The physical basis of this measure presents the number of singlets that must be invested in order to create a given entangled state. It should also be added that a closed form of this measure has been found recently [324].

Related to this measure is the entanglement of distillation [323]. It defines an amount of entanglement of a state σ as a proportion of singlets that can be distilled using a purification procedure. As such it is dependent on the efficiency of a particular purification procedure and can be made more general only by introducing some sort of universal purification procedure. Unlike the entanglement of formation there is no closed form analytical expression for the entanglement of distillation. However, some upper bounds can be provided and we come back to this later.

We now introduce a third measure of entanglement which may actually give rise to a whole family of good entanglement measures. It can be seen that this measure is intimately related to the entanglement of distillation by providing an upper bound for it [322].

If \mathcal{D} is the set of all disentangled states (see Fig. 6.9), the measure of entanglement for a state σ is then defined as

$$E(\sigma) := \min_{\rho \in \mathcal{D}} D(\sigma || \rho), \quad (6.48)$$

where D is any measure of *distance* (not necessarily a metric) between the two density matrices ρ and σ such that $E(\sigma)$ satisfies the above conditions E1–E4.

Now an important question is what condition a candidate for $D(\sigma || \rho)$ has to satisfy in order for E1–E4 to hold for the entanglement measure? Necessary and sufficient conditions are not known, although a set of sufficient conditions exists [321]. Without going into any mathematical detail (see [322] if necessary) we present one measure that satisfies E1–E4 and one measure that only satisfies E1–E3.

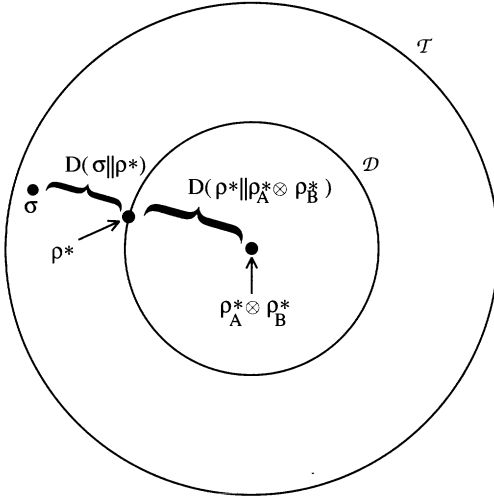


Fig. 6.9. The set of all density matrices, \mathcal{T} is represented by the outer circle. Its subset, a set of disentangled states \mathcal{D} is represented by the inner circle. A state σ belongs to the entangled states, and ρ^* is the disentangled state that minimises the distance $D(\sigma||\rho)$, thus representing the amount of quantum correlations in σ . State $\rho_A^* \otimes \rho_B^*$ is obtained by tracing ρ^* over A and B . $D(\rho^*||\rho_A^* \otimes \rho_B^*)$ represent the classical part of the correlations in the state σ .

6.4.4 Two Measures of Distance Between Density Matrices

We first state that E1-E4 hold for the quantum relative entropy, i.e. when $D(\sigma||\rho) = S(\sigma||\rho) := \text{Tr} \{\sigma(\ln \sigma - \ln \rho)\}$ [322]. Note that the quantum relative entropy is not a true metric, as it is not symmetric and does not satisfy the triangle inequality. In the next subsection the reasons for this will become clear. A question arises as to why the entanglement is not defined as $E(\sigma) = \min_{\rho \in \mathcal{D}} S(\rho||\sigma)$. Since the quantum relative entropy is asymmetric this gives a different result to the original definition. However, the major problem with this convention is that for maximally entangled states this measure is infinite. Although this does have a sound statistical interpretation (see the next section) it is hard to relate it to any physically reasonable scheme (e.g. a purification procedure). This is the prime reason for excluding this convention from any further considerations. The measure of entanglement generated by the quantum relative entropy will hereafter be referred to as the relative entropy of entanglement. An important result is that (for a proof see [322])

Theorem. For pure states the relative entropy of entanglement is equal to the von Neumann reduced entropy.

This is physically a very satisfying property of an entanglement measure, because it is already known that for pure states the von Neumann reduced entropy is a good measure of entanglement.

We also state an important result, that the entanglement of creation E_c is never smaller than the relative entropy measure of entanglement E . We will show later that this property has the important implication that the amount of entanglement that we have to invest to create a given quantum state is usually larger than the entanglement that one can recover using quantum state distillation methods.

Theorem. $E_c(\sigma) \leq E(\sigma) = \min_{\rho \in \mathcal{D}} S(\sigma || \rho)$.

We add that both the entanglement of creation and the relative entropy of entanglement can be calculated easily for the Bell diagonal states [321]. It turns out that for these states the entanglement of formation is substantially larger than the relative entropy of entanglement.

A “closed form” for the relative entropy of entanglement is not yet known, and a computer search is necessary to find the minimum ρ^* , for each given σ . However, we can numerically find the amount of entanglement for two spin-1/2 particles very efficiently using methods described in the next section.

An example of a measure of entanglement that satisfies conditions E1–E3 but not E4 is given by the (modified) Bures metric, i.e. when $D(\sigma || \rho) = D_B(\sigma || \rho) := 2 - 2F(\sigma, \rho)$, where $F(\sigma, \rho) := [\text{Tr}\{\sqrt{\rho}\sigma\sqrt{\rho}\}^{1/2}]^2$ is the so-called fidelity (or Uhlmann’s transition probability). We can, as in the case of the quantum relative entropy, calculate the measure of entanglement in this case for some simple states. For example, for maximally entangled states we obtain $E = 1$. Following the lines of the above proof it can be shown that for a general pure state $\alpha|00\rangle + \beta|11\rangle$ ⁵ the entanglement is $4\alpha^2\beta^2$. In general, a computer search is necessary, as in the previous case. We now turn to describing this general computer calculation of a relative entropy of entanglement.

6.4.5 Numerics for Two Spin 1/2 Particles

As there is no closed analytical formula for the relative entropy of entanglement, we have to resort to a numerical search to find the entanglement of a general quantum state σ . Such a search can be performed efficiently using some results from convex analysis [325]. In the following we introduce one basic definition and one important result from convex analysis [325]. From this point onwards we concentrate on the quantum relative entropy as a measure of entanglement although most of the considerations are of a more general nature. The following theorem is crucial for our minimisation problem as it shows that we do not have to have an infinite number of parameters in the decomposition of a disentangled state in (6.45) to search over.

Caratheodory’s theorem. Let $A \subset \mathbf{R}^N$. Then any $x \in \text{co}(A)$ has an expression of the form $x = \sum_{n=1}^{N+1} p_n a_n$ where $\sum_{n=1}^{N+1} p_n = 1$, and, for $n = 1, \dots, N+1$, $p_n \geq 0$ and $a_n \in A$.

⁵ That this is, indeed, the most general form can be seen for the Schmidt decomposition [317].

A direct consequence of Caratheodory's theorem is that any state in \mathcal{D} can be decomposed into a sum of at most $(\dim(H_1) \times \dim(H_2))^2$ products of pure states. So, for two spin-1/2 particles there are at most 16 terms in the expansion of any disentangled state in (6.45). In addition, each pure state can be described using two real numbers, so that there are altogether at most $15 + 16 \times 4 = 79$ real parameters needed to completely characterize a disentangled state in this case.

We note that this efficient computer search provides an alternative criterion for deciding when a given state σ of two spin-1/2 systems is disentangled, i.e. of the form given in (6.45). The already existing criterion is the one given by Peres and the Horodecki family. It states that a state is disentangled iff its partial trace is a negative operator (see the second and third references in [326]). This criterion is only valid for two spin 1/2, or one spin 1/2 and one spin 1 systems. In the absence of a more general analytical criterion, our computational method provides a way of deciding this question.

At the end of this section we mention *additivity* as an important property desired from a measure of entanglement, i.e. we would like to have

$$E(\sigma_{12} \otimes \sigma_{34}) = E(\sigma_{12}) + E(\sigma_{34}) , \quad (6.49)$$

where systems 1 + 2 and systems 3 + 4 are entangled separately from each other. The exact definition of the left hand side is

$$E(\sigma_{12} \otimes \sigma_{34}) = \min_{p_i, \rho_{13}, \rho_{24}} S(\sigma_{12} \otimes \sigma_{34} || \sum_i p_i \rho_{13}^i \otimes \rho_{24}^i) . \quad (6.50)$$

Why should we choose this form? One would originally assume that $\sigma_{12} \otimes \sigma_{34}$ should be minimised by the states of the form $(\sum_i p_i \rho_1^i \otimes \rho_2^i) \otimes (\sum_j p_j \rho_3^j \otimes \rho_4^j)$. However, Alice and Bob can also perform arbitrary unitary operation on their subsystems (i.e. locally). This obviously leads to the creation of entanglement between 1 and 2 and between 3 and 4 and hence the form in (6.50). Additivity is, of course, already true for the pure states as can be seen from the proof above, when our measure reduces to the von Neumann entropy. For a more general case we have not been able to provide any analytical proof, so that the above property remains a conjecture. However, for two spin-1/2 systems, our program has not found any counter-example. We will therefore assume this property to hold. A direct consequence of this and E3 is that the relative entropy of entanglement is an upper bound on the efficiency of any purification procedure. Namely if we start with n pairs in the state σ and obtain m singlets as a result of a purification procedure then

$$n \times E(\sigma) \geq m \ln 2 , \quad (6.51)$$

i.e. the efficiency m/n is always bounded by $E(\sigma)$. Since $E(\sigma)$ can be smaller than the entanglement of creation, this implies that the entanglement of creation and distillation are not necessarily equal.

6.4.6 Statistical Basis of Entanglement Measure

Let us see how we can interpret our entanglement measure in the light of experiments, i.e. statistically [327]. We first show how the notion of relative entropy arises in classical information theory as a measure of distinguishability of two probability distributions. We then generalise this idea to the quantum case, i.e. to distinguishing between two quantum states (for a discussion of distinguishability of pure quantum states see e.g. [328]). We will see that this naturally leads to the notion of the quantum relative entropy. It is then straightforward to extend this concept to explain the relative entropy of entanglement. Suppose we would like to check if a given coin is “fair”, i.e. if it generates a “head–tail” distribution of $f = (1/2, 1/2)$. If the coin is biased then it will produce some other distribution, say $uf = (1/3, 2/3)$. So, our question of the coin fairness boils down to how well we can differentiate between two given probability distributions given a finite number, n , of experiments to perform on one of the two distributions. In the case of a coin we would toss it n times and record the number of 0’s and 1’s. What is the probability that a fair coin will be mistaken for an unfair one with the distribution of $(1/3, 2/3)$ given n trials on the fair coin? For large n the answer is [327, 329] (Sanov’s theorem)

$$p(\text{fair} \rightarrow \text{unfair}) = e^{-nS_{cl}(uf||f)} , \quad (6.52)$$

where $S_{cl}(uf||f) = 1/3 \ln 1/3 + 2/3 \ln 2/3 - 1/3 \ln 1/2 - 2/3 \ln 1/2$ is the classical relative entropy for the two distributions. So,

$$p(\text{fair} \rightarrow \text{unfair}) = 3^n 2^{-\frac{5}{3}n} , \quad (6.53)$$

which tends exponentially to zero with $n \rightarrow \infty$. In fact we see that already after ~ 20 trials the probability of mistaking the two distributions is vanishingly small, $\leq 10^{-10}$.

In quantum theory we therefore state a law analogous to Sanov’s theorem (see also [327]),

Theorem. (Quantum Sanov’s Theorem). The probability of *not* distinguishing two quantum states (i.e. density matrices) σ and ρ after n measurements is

$$p(\rho \rightarrow \sigma) = e^{-nS(\sigma||\rho)} . \quad (6.54)$$

It can be claimed with certainty that the above presents the lower limit to the probability of confusing ρ with σ after performing n measurements on ρ [327]. In fact, this bound is reached asymptotically as proved in [330], and the measurements achieving this are projectors independent of the state σ [331]. Now the interpretation of the relative entropy of entanglement becomes immediately transparent [327]. The probability of mistaking an entangled state σ for a closest, disentangled state, ρ , is $e^{-n \times \min_{\rho \in \mathcal{D}} S(\sigma, \rho)} = e^{-nE(\sigma)}$. If

entanglement of σ is greater, then it takes fewer measurements to distinguish it from a disentangled state (or, fixing n , there is a smaller probability of confusing it with some disentangled state). Let us give an example. Consider a state $(|00\rangle + |11\rangle)/\sqrt{2}$, known to be a maximally entangled state. The closest to it is the disentangled state $(|00\rangle\langle 00| + |11\rangle\langle 11|)/2$ [321]. To distinguish these states it is enough to perform projections onto $(|00\rangle + |11\rangle)/\sqrt{2}$. If the state that we are measuring is the above mixture, then the sequence of results (1 for a successful projection, and 0 for an unsuccessful projection) will contain on average an equal number of 0's and 1's. For this to be mistaken for the above pure state the sequence has to contain all n 1's. The probability for that is 2^{-n} , which also comes from using (6.54). If, on the other hand, we performed projections onto the pure state itself, we would then never confuse it with a mixture, and from (6.54) the probability is seen to be $e^{-\infty} = 0$.

We see that the above treatment does not refer to the number (or indeed dimensionality) of the entangled systems. This is a desired property as it makes our measure of entanglement universal. The extensions to three or more systems are straightforward [322, 327]. (See also Sect. 8.5 on multiparticle entanglement purification).

7. Decoherence and Quantum Error Correction

7.1 Introduction

The main obstacle for the experimental implementations of quantum state processing is quantum decoherence. In Sect. 7.2 it is shown that decoherence of the state of a quantum system can be viewed as the consequence of entanglement between the quantum system and its environment. Section 7.3 illustrates the seemingly devastating effect of decoherence due to spontaneous decay for an ion-trap quantum computer.

One of the most important achievements in the field of quantum information is the discovery of methods to overcome the problem of decoherence. These methods are called quantum error correction schemes and are introduced in Sect. 7.4. The methods make use of the fact that the state of a single qubit can be encoded on entangled states of several qubits. Symmetry properties of these entangled states, together with the fact that quantum noise can be digitized by projection measurements, enables the detection and correction of quantum errors. Since entangled states are themselves more vulnerable to decoherence than single-qubit states, there is a trade-off between correcting and inducing quantum errors for such schemes. The general theory of quantum error correction and the issue of fault tolerance will be addressed in Sect. 7.5. A good illustration of a realistic error correction procedure is the problem of creating a frequency standard using Ramsey spectroscopy and this is presented in Sect. 7.6.

Another route to overcome decoherences is to distill from a large set of entangled particles, that has been degraded in purity by decoherence, a subset of particles with enhanced entanglement purity. Entanglement purification is the topic of Chap. 8.

7.2 Decoherence

A.K. Ekert, G.M. Palma, K.A. Suominen

7.2.1 Decoherence: Entanglement Between Qubits and Environment

As described in Chap. 4 of this book a quantum computer can be viewed as a sort of “programmable interferometer” where different computational paths are designed in such a way as to interfere constructively on the desired result. In order for such interference to take place the evolution of the computer must be coherent, i.e. unitary. Any deviation from unitarity due to decoherence would spoil the interference visibility.

Decoherence appears whenever our qubits are coupled with their environment. To illustrate the origin of decoherence mechanisms let us assume that the qubit–environment coupling induces a joint unitary time evolution of the following form

$$|0\rangle|E\rangle \xrightarrow{U(t)} |0\rangle|E_0(t)\rangle \quad |1\rangle|E\rangle \xrightarrow{U(t)} |1\rangle|E_1(t)\rangle, \quad (7.1)$$

where $|E\rangle$ is some fixed initial state of the environment, and $U(t)$ is the joint unitary time evolution operator. In (7.1) the environment acts as a measuring apparatus which acquires information on the states of our qubit [332]. When the initial state of the qubit is a linear superposition of states $|0\rangle$ and $|1\rangle$, $U(t)$ will introduce entanglement between qubit and environment:

$$(a_0|0\rangle + a_1|1\rangle) \otimes |E\rangle \xrightarrow{U(t)} a_0|0\rangle|E_0(t)\rangle + a_1|1\rangle|E_1(t)\rangle. \quad (7.2)$$

Decoherence is due exactly to such entanglement, since nonunitarity emerges once we trace over the environment degrees of freedom. The reduced density matrix of the qubit corresponding to state (7.2) is given by

$$\rho_q(t) = \text{Tr}_E \varrho_{q+E} = \begin{bmatrix} |a_0|^2 & a_0 a_1^* \langle E_1 | E_0 \rangle \\ a_1 a_0^* \langle E_0 | E_1 \rangle & |a_1|^2 \end{bmatrix}. \quad (7.3)$$

In most cases states $|E_0(t)\rangle, |E_1(t)\rangle$ become more orthogonal in time (i.e. more and more information on the qubit state leaks into the environment) and we can conveniently write

$$\langle E_0(t) | E_1(t) \rangle = e^{-\Gamma(t)}, \quad (7.4)$$

where $\Gamma(t)$ is a function of time whose specific form will depend on the details of the coupling between qubit and environment [333]. Its value depends

on the type of qubits and their interaction with the environment and can vary from 10^4 s for nuclear spins in a paramagnetic atom to 10^{-12} s for electron–hole excitations in the bulk of a semiconductor [334]. As a consequence the particular kind of entanglement described by (7.2) kills the off-diagonal matrix elements of the density matrix – the so-called “coherences” – while leaving the diagonal ones, known as “populations” unaffected. This effect is known as dephasing. We will describe later the effects of other kind of qubit–environment entanglement. From the complexity viewpoint it is important to know how the characteristic decoherence time scales with the size of our quantum computer. To this end let us introduce a model of qubit–environment coupling which generates a time evolution of the kind described in (7.1). We will model our environment as a bath of harmonic oscillators [333, 335] and we will assume that the interaction Hamiltonian between a single qubit and its environment is of the form

$$H = \frac{1}{2}\sigma_z\omega_0 + \sum_{\mathbf{k}} b_{\mathbf{k}}^\dagger b_{\mathbf{k}}\omega_k + \sum_{\mathbf{k}} \sigma_z(g_{\mathbf{k}} b_{\mathbf{k}}^\dagger + g_{\mathbf{k}}^* b_{\mathbf{k}}), \quad (7.5)$$

where $\omega_k, b_{\mathbf{k}}^\dagger, b_{\mathbf{k}}$ are, respectively, the frequency and the creation and annihilation bosonic operators of the \mathbf{k} mode of our bath of harmonic oscillators, and σ_z is a Pauli pseudospin operator. The first and the second term on the r.h.s. of (7.5) describe, respectively, the free evolution of the qubit and of the environment, and the third term describes the interaction between the two. The state of the combined system (qubit + environment) is described by a density operator $\varrho(t)$ which at time $t = 0$ is assumed to be

$$\varrho(0) = |\psi\rangle\langle\psi| \otimes \prod_{\mathbf{k}, \mathbf{k}'} |0_{\mathbf{k}}\rangle\langle 0_{\mathbf{k}'}| = \rho(0) \otimes |vac\rangle\langle vac|, \quad (7.6)$$

where $|\psi\rangle$ is the initial state of our qubit and $|vac\rangle = \prod_{\mathbf{k}} |0_{\mathbf{k}}\rangle$ is the vacuum state of all the bath modes. Since $[\sigma_z, H] = 0$, the populations of the qubit density matrix, $\rho(t) = \text{Tr}_R \varrho(t)$ are not affected by the environment, which in our model simply erodes quantum coherence as anticipated. This model is *exactly* soluble and allows a clear analysis of the mechanism of entanglement between qubit and environment which, as we have discussed, is believed to be at the core of most decoherence processes.

It can be easily shown that the time evolution operator $U(t)$ in the interaction picture is a conditional displacement operator for the field [333], the sign of the displacement being dependent on the logical value of the qubit. $U(t)$ will therefore induce a dynamics of the kind described in (7.2) with

$$|E_0\rangle = \prod_{\mathbf{k}} |- \phi_{\mathbf{k}}\rangle \quad |E_1\rangle = \prod_{\mathbf{k}} |\phi_{\mathbf{k}}\rangle, \quad (7.7)$$

where the states $|\phi_{\mathbf{k}}\rangle$ are coherent states of amplitude $\phi_{\mathbf{k}} = g_{\mathbf{k}}(1 - e^{\omega_k t})/\omega_k$. A detailed calculation of $\Gamma(t)$ and an extension of the analysis to the finite temperature case can be found in [333, 335].

7.2.2 Collective Interaction and Scaling

We now have all the ingredients to analyse the decoherence of a register on n qubits [333]. The Hamiltonian in this case will read

$$H = \frac{1}{2} \sum_i \sigma_{z,i} \omega_0 + \sum_{\mathbf{k}} b_{\mathbf{k}}^\dagger b_{\mathbf{k}} \omega_k + \sum_{i,\mathbf{k}} \sigma_z (g_{i,\mathbf{k}} b_{\mathbf{k}}^\dagger + g_{i,\mathbf{k}}^* b_{\mathbf{k}}), \quad (7.8)$$

where the coupling constants $g_{i,\mathbf{k}}$ will now depend on the position of the i^{th} qubit. The entanglement induced by this Hamiltonian will be of the form

$$\left(\sum_{i_1 \dots i_n} c_{i_1 \dots i_n} |i_1 \dots i_n\rangle \right) \otimes |vac\rangle \xrightarrow{U(t)} \sum_{i_1 \dots i_n} c_{i_1 \dots i_n} |i_1 \dots i_n\rangle |E_{i_1, i_2, \dots, i_n}\rangle, \quad (7.9)$$

where i_n labels the logical value of the n^{th} qubit. The bath of harmonic oscillators will be characterized by a coherence length λ_c over which its fluctuations are correlated. The form of states $|E_{i_1 \dots i_n}\rangle$ can be instructively obtained in two limiting cases of physical relevance, depending on the ratio between the physical size of our register and λ_c .

Short λ_c : In this case each qubit will feel its own independent environment and will decohere individually. We will have

$$|E_{i_1, i_2, \dots, i_n}\rangle = |E_{i_1}\rangle |E_{i_2}\rangle \cdots |E_{i_n}\rangle, \quad (7.10)$$

where the $|E_{i_n}\rangle$ are the same as in (7.7) and the density operator matrix elements will decay as

$$\rho_{i_1 \dots i_n, j_1 \dots j_n}(t) = \rho_{i_1 \dots i_n, j_1 \dots j_n}(0) \langle E_{i_1} | E_{j_1} \rangle \langle E_{i_2} | E_{j_2} \rangle \cdots \langle E_{i_n} | E_{j_n} \rangle. \quad (7.11)$$

The fastest decay will occur for

$$\rho_{11 \dots 1, 00 \dots 0}(t) = \rho_{11 \dots 1, 00 \dots 0}(0) \langle E_1 | E_0 \rangle^n = \rho_{11 \dots 1, 00 \dots 0}(0) e^{-n\Gamma(t)}. \quad (7.12)$$

Long λ_c : When λ_c is sufficiently long we can assume that all the qubits collectively interact with the same environment, i.e. we can assume $g_{i,\mathbf{k}} = g_{\mathbf{k}}$ for all qubits. $U(t)$ will then be a conditional displacement operator of amplitude depending on the logical value of *all* qubits in our register. More explicitly

$$|E_{i_1 \dots i_n}\rangle = \prod_{\mathbf{k}} | -\{(-1)^{i_1} + (-1)^{i_2} \cdots (-1)^{i_n}\} \phi_{\mathbf{k}} \rangle. \quad (7.13)$$

The fastest decay will occur for

$$\rho_{11 \dots 1, 00 \dots 0}(t) = \rho_{11 \dots 1, 00 \dots 0}(0) \langle E_{11 \dots 1} | E_{00 \dots 0} \rangle = \rho_{11 \dots 1, 00 \dots 0}(0) e^{-n^2\Gamma(t)}. \quad (7.14)$$

The physical origin of the n^2 in the exponent can be easily understood by noting that $|E_{00\dots 0}\rangle, |E_{11\dots 1}\rangle$ are the tensor product of coherent states of amplitude $n\phi_{\mathbf{k}}$.

The above discussion shows how the decay of coherences of a register of n qubits scales as $\exp[-Poly(n)\gamma(t)]$, with $Poly(n) \sim n$ for independent interaction with the environment and $Poly(n) \sim n^2$ for collective interaction.

7.2.3 Subspace Decoupled From Environment

If collective interactions lead to faster decay rates it should be noted that it also leads to the appearance of subspaces decoupled from the environment. As (7.13) clearly shows, states with an equal number of 0 and 1 do not get entangled with the environment and therefore are not prone to decoherence. In other words the interaction does not displace the amplitude of the field modes. This suggests the possibility of using this decoupled subspace to implement a simple form of redundant coding. Let us suppose that we can manufacture in our laboratory a quantum register of $2L$ qubits composed of pairs of qubits close enough to each other so that each pair is effectively interacting with the same reservoir. Different pairs can interact with different reservoirs, although the results we are going to illustrate are not modified if all the qubits interact with the same reservoir. We could then encode the logical states as follows

$$|\tilde{0}\rangle = |0,1\rangle, \quad |\tilde{1}\rangle = |1,0\rangle. \quad (7.15)$$

The idea is that if we use a pair of qubits to encode a bit we might effectively decouple the register from the environment.

Several problems remain open with this kind of coding. First of all we should make sure that such states are also robust also with respect to other channels of decoherence (we will come to this question in the next section). Secondly the problem remains of how to prepare such states (states which are decoupled from the environment are often also decoupled from external probes) and how to read them (this will imply collective measurements). Finally, it is not yet clear how to perform quantum computation confined within such subsystems. Qubit–qubit controllable interactions might turn out to be useful tools for implementing gate operation [336, 337].

7.2.4 Other Find of Couplings

In the remainder of this section we would like to discuss which of the results obtained survives once we take into account more realistic mechanisms for qubit–environment interaction. The model we will briefly analyse is one commonly used to describe a broad range of physical phenomena, like the exchange of photons between the electromagnetic field and a two-level atom

in quantum optics [338]. In this model the Hamiltonian of a system of n identical qubits coupled with the reservoir of harmonic oscillators will be

$$H = \frac{1}{2} \sum_i \sigma_{z,i} \omega_0 + \sum_{\mathbf{k}} b_{\mathbf{k}}^\dagger b_{\mathbf{k}} \omega_k + \sum_{i,\mathbf{k}} (g_{i,\mathbf{k}} \sigma_{-,i} b_{\mathbf{k}}^\dagger + g_{i,\mathbf{k}}^* \sigma_{+,i} b_{\mathbf{k}}), \quad (7.16)$$

where $\sigma_{-,i}$ and $\sigma_{+,i}$ are the lowering and raising operators for qubit i .

The dynamics generated by (7.16) cannot be solved exactly. However, under the so called Born–Markov approximation, the time evolution of the qubit reduced density operator can be described by a master equation [338, 339]. If the spacing between the qubits is smaller than the wavelength of the resonant modes it is reasonable to assume $g_{i,\mathbf{k}} \sim g_0$, and the desired master equation will be:

$$\frac{d\rho}{dt} = i\omega_0 \rho - \frac{\gamma}{2} (S_+ S_- \rho + \rho S_+ S_- - 2 S_- \rho S_+), \quad (7.17)$$

where we have introduced the collective operators $S_z = \sum_i \sigma_{z,i}$, $S_{\pm} = \sum_{\pm i} \sigma_{\pm}$ and the decay constant $\gamma \propto |g_0|^2 \delta(\omega_k - \omega_0)$.

The dynamics described by (7.17) is clearly nonunitary. The nonunitarity is again due to entanglement between qubit and environment, although this is less evident than in the exactly soluble model analysed in the previous section.

In the case of dissipation of a single qubit the reduced density at time t will be

$$\rho(t) = \begin{pmatrix} (1 - \rho_{11})e^{-\gamma t} & \rho_{10} e^{-\frac{\gamma}{2}t} \\ \rho_{01} e^{-\frac{\gamma}{2}t} & \rho_{11} e^{-\gamma t} \end{pmatrix}, \quad (7.18)$$

which shows clearly that this model of coupling induces decoherence *and* decay of the populations.

In order to illustrate the characteristics of collective interaction in this new scenario it is instructive to discuss the decay of the entangled Bell states $|\Psi_{\pm}\rangle = \frac{1}{\sqrt{2}}\{|01\rangle \pm |10\rangle\}$. The probability amplitude for the decay into state $|00\rangle$ is proportional to the matrix element of operator S_+

$$\langle \Psi_{\pm} | S_+ | 00 \rangle = \frac{1}{\sqrt{2}} \{ \langle 01 | \sigma_{+2} | 00 \rangle \pm \langle 10 | \sigma_{+1} | 00 \rangle \}. \quad (7.19)$$

This shows clearly how the probability *amplitudes* for the decay of the $|\Psi_{+}\rangle$ state interfere constructively leading to a decay rate twice the decay rate of a single qubit while they interfere destructively for the $|\Psi_{-}\rangle$ state. For a large number n on qubits the collective decay will lead to decay constants scaling from $n\gamma$ to $n^2\gamma$, while the singlet collective state will be decoupled from the environment. This is the well known phenomenon of superradiance vs. subradiance [339, 340]. Again this suggests the possibility of using the

subradiant subspaces of a register of n qubits [341]. Of course also in this case all the difficulties we have mentioned in the previous section remain.

To conclude, we would like to point out that, although different models will lead to different physical decay mechanisms and will need different techniques for their treatment, many of the qualitative features of decoherence processes do not depend on the specific model of coupling. In particular all decoherence processes will lead to a nonunitary time evolution of the quantum register. Furthermore collective interaction will enhance the decay of some register subspaces and will inhibit the decay of others. Therefore our considerations on the scaling of the decoherence time with the size of our quantum computer and on collective encoding remain valid regardless of the details of the coupling with the environment.

7.3 Limits to Quantum Computation Due to Decoherence

M.B. Plenio, P.L. Knight

The previous section presented models to describe decoherence and dissipation of an array of qubits, implemented e.g. on a string of ions (see Chap. 5). After these general considerations we will now estimate how serious the impact of noise will be on a quantum computer. In particular we would like to see how many quantum operations we can possibly perform for example with an ion trap quantum computer of which the principles have been described in Sect. 4.3 and Chap. 5 [156]. We will not discuss here many of the other potential implementations of a quantum computer such as nuclear magnetic resonance schemes [342, 343] (see also Sect. 5.4).

There are many possible mechanisms that produce noise in a quantum computer. In this subsection we will discuss only the effect of spontaneous emission from the ions [344]–[347] because the analysis is quite instructive. Other mechanisms such as noise in the centre-of-mass mode [348], laser instabilities and cross-talking between different ions due to their small spatial separation [349] will not be discussed here. For these effects we refer the reader to the cited literature.

Now we want to estimate the effect of spontaneous emission on a quantum computer. To do this we use as a benchmark the algorithm for the factorisation of large numbers [350]. The discussion can easily be generalised to other algorithms. As was shown in Sect. 4.2, finding factors of a large number on a classical computer is a hard problem and cannot be done efficiently. On a quantum computer, however, an efficient algorithm has been found. Under ideal conditions this algorithm would allow a quantum computer to find factors of a large number exponentially faster than on a classical computer.

We will now discuss what the largest number is that one can factorise on a quantum computer if we assume that the only source of error is spontaneous emission from ions. To simplify the analysis, we do not consider the possibility of quantum error correction here but refer the reader to literature [346] and to the next section of this chapter.

Consider the following experimental setup: A string of ions is placed in a linear ion trap and cooled to the motional ground state. Each qubit is represented by a metastable optical transition in the ion. The internal structure of the ions we are considering is shown in Fig. 7.1). The qubit is represented by the atomic levels 0 and 1. Transitions are driven by a laser with Rabi frequency Ω_{01} and spontaneous emissions from level i can occur at a rate $2\Gamma_i$. The existence of the additional level 2 is important and will be discussed later. Of course more sophisticated methods for the representation of the qubit are possible, e.g. in Zeeman sub-levels, but the analysis becomes more complicated while the conclusions are similar. Therefore we refer the reader to the literature [346].

Our aim is the factorisation of an L -bit number, which means a number which is not larger than 2^L . From Shors' algorithm [350], we know that this task can be performed using ϵL^3 elementary operations such as one-bit gates, CNOT gates and Toffoli gates. Networks that perform this task have been designed [351] and it turns out that the algorithm requires of order $5L$ qubits to factorise an L bit number.

How long does it take to perform all the necessary gates? It takes 1.5 times as long to implement a Toffoli gate than it takes to make a CNOT gate [156]. Therefore it is enough to calculate the time required to perform a CNOT gate. Single bit gates will not be considered because they can be implemented much faster. The reason is that, unlike for a CNOT gate, the implementation of a single bit gate does not require an excitation of the centre-of-mass mode (see Sect. 5.2.9).

The implementation of a CNOT gate requires

$$\tau_{el} = 4\pi \frac{\sqrt{5L}}{\eta \Omega_{01}} . \quad (7.20)$$

Here $5L$ is the number of ions in the trap, Ω_{01} is the Rabi frequency of the laser that drives the qubit transition and η is the Lamb–Dicke parameter (see Chap. 5 for experimental details). Therefore the total time required to perform the factorisation of an L bit number is the number of required CNOT gates multiplied by τ_{el} . We find

$$T = \frac{4\pi\sqrt{5L}}{\eta\Omega} \epsilon L^3 . \quad (7.21)$$

Obviously there are free parameters in this expression. In particular we could imagine that we could increase the Rabi frequency as much as we like to permit a very rapid calculation. This would allow us to avoid spontaneous

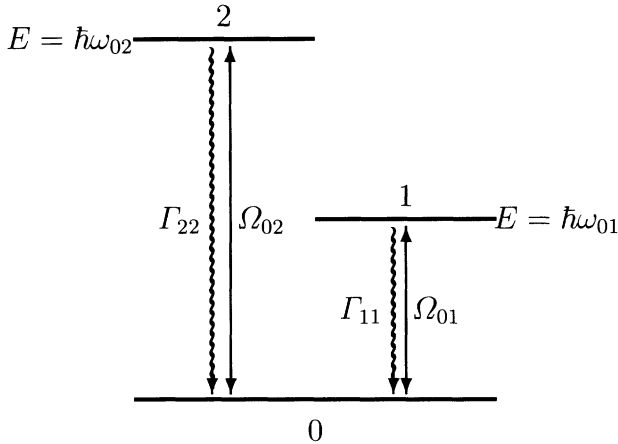


Fig. 7.1. Schematic level scheme of the ions used in quantum computation. The $0 \leftrightarrow 1$ transition represents the qubit. It is driven by a laser of Rabi frequency Ω_{01} . Level 1 has a spontaneous decay rate $2\Gamma_{11}$ which is assumed to be small. The laser which is resonant with the $0 \leftrightarrow 1$ transition inevitably couples level 0 also to other non-resonant levels such as level 2. The Rabi frequency on that transition is then Ω_{02} and the decay rate $2\Gamma_{22}$ is usually much larger than $2\Gamma_{11}$. The effective Rabi frequency on the $0 \leftrightarrow 2$ transition is very small as the laser is detuned by $\Delta_{02} \gg \Omega_{02}$.

emission from the upper level of the qubit. However, this is not so easy. The reason for this is the fact that the Rabi frequency of a transition and the decay constant of that transition are related to each other by

$$\frac{\Omega^2}{\Gamma} = \frac{6\pi c^3 \epsilon_0}{\hbar \omega_{01}^3} E^2 , \quad (7.22)$$

where E is the electric field strength of the laser, c is the speed of light, ϵ_0 is the permittivity of free space, and ω_{01} the transition frequency. Still one could imagine increasing the electric field strength of the laser E arbitrarily. Obviously there are some upper limits to that process. If E is so strong that it exceeds the electric field between the electron and the nucleus then the ion will ionize immediately. This limit, however, is quite high and other effects are more relevant. In fact at high field strengths of the laser we cannot continue to assume that the ion has only two relevant energy levels. Other energy levels will contribute to the dynamics, as they might obtain some small population due to off-resonant transitions to them. This situation is presented in Fig. 7.1. In addition to the qubit levels 0 and 1 there are other, far detuned levels around. We summarise the effect of all existing auxiliary levels by assuming one additional energy level 2 that couples to the lower qubit state 0. Because the laser is far detuned from the $0 \leftrightarrow 2$ transition the population in the upper level will be small. Nevertheless, spontaneous emission from that level may take place, especially because this auxiliary level

could well have a very short lifetime. The stronger the electric field of the applied laser, the larger the population in this auxiliary level. Therefore we have a trade-off between spontaneous emission from the upper qubit level and spontaneous emission from the auxiliary level. The faster the computation, the lower the spontaneous emissions from the upper qubit state 1 but the greater the spontaneous emissions from the auxiliary level.

In the following we calculate the probability p_{tot} of an emission from either level 1 or level 2. The aim is to minimise this probability. This minimisation then leads to an intensity-independent limit to the size of the number that can be factorised by a quantum computer in the presence of spontaneous emission.

During all the quantum computation, on average half of the qubits are in the upper state. Therefore the probability of a spontaneous emission occurring from the upper level during the whole computation is given by

$$p_1 = \frac{1}{2} 2 \Gamma_{11} 5 L T . \quad (7.23)$$

On the other hand, the auxiliary level is populated only during the interaction of the ion with the laser. Therefore the probability of suffering a spontaneous emission from an auxiliary level is given by

$$p_2 = \frac{\Omega_{02}^2}{8 \Delta_{02}} 2 \Gamma_{22} T . \quad (7.24)$$

If we now use (7.22), which gives

$$\frac{\Omega_{01}^2}{\Gamma_{11}} = \frac{\omega_{02}^3}{\omega_{01}^3} \frac{\Omega_{02}^2}{\Gamma_{22}} , \quad (7.25)$$

and define

$$x = \sqrt{\frac{\Omega_{01}^2}{\Gamma_{11}}} , \quad (7.26)$$

we obtain, using (7.21),

$$p_{tot} = p_1 + p_2 \quad (7.27)$$

$$= \frac{4\pi\sqrt{5L}}{\eta} \epsilon L^4 \sqrt{\Gamma_{11}} \left[\frac{1}{x} + \frac{1}{L} \frac{\omega_{01}^3}{\omega_{02}^3} \frac{\Gamma_{22}^2}{4\Delta_{02}^2 \Gamma_{11}} x \right] . \quad (7.28)$$

We can minimise this expression with respect to x and obtain for the minimum

$$p_{min} = \frac{4\pi\sqrt{5}\epsilon L^4}{\eta} \sqrt{\frac{\omega_{01}^3}{\omega_{02}^3}} \sqrt{\frac{\Gamma_{22}^2}{\Delta_{02}^2}} . \quad (7.29)$$

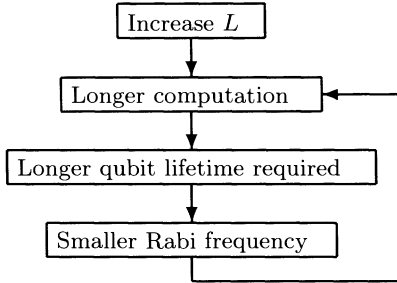


Fig. 7.2. The strong L dependence in (7.30) is due to a positive feedback. If we try to increase L our computation becomes longer. That requires a longer lifetime of the qubit which reduces the achievable Rabi frequency on the qubit transition. This lengthens the computation even more.

To ensure that with a high probability there is no spontaneous emission during the quantum computation, we require $p_{min} \ll 1$. We can therefore transform (7.29) into an upper bound on L which is given by

$$L_{max}^8 \approx \frac{\eta^2 \Delta_{02}^2}{80 \Gamma_{22}^2 \pi^2 \epsilon^2} \left(\frac{\omega_{02}}{\omega_{01}} \right)^3. \quad (7.30)$$

The reader might wonder where the power of L^8 in (7.30) originates from. The reason is a positive control loop as shown in Fig. 7.2.

To see whether this is a serious limitation we need to plug some numbers into the equation. We will use values for realistic ions, i.e. ions that are being used in ion trap experiments.

In Table 7.1 (which is taken from [346]) we can see the results for some real atoms. The resulting limits for the factorisable numbers are really small. This

Table 7.1. For several possible systems the upper limit on the bitsize L of the number N that can be factorised on a quantum computer is calculated. A qubit is stored in a metastable optical transition. The atomic levels which are abbreviated in Fig. 7.1 by 0, 1 and 2 are given. The atomic data are inserted into (7.30) and the result is given in the last row of the table.

Ion	Ca^+	Hg^+	Ba^+
level 0	$4s^2 S_{1/2}$	$5d^{10} 6s^2 {}^2S_{1/2}$	$6s^2 S_{1/2}$
level 1	$3d^2 D_{5/2}$	$5d^9 6s^2 {}^2D_{5/2}$	$5d^2 D_{5/2}$
level 2	$4s^2 P_{3/2}$	$5d^{10} 6p^2 {}^2P_{1/2}$	$6s^2 P_{3/2}$
$\omega_{01} [s^{-1}]$	$2.61 \cdot 10^{15}$	$6.7 \cdot 10^{15}$	$1.07 \cdot 10^{15}$
$\omega_{02} [s^{-1}]$	$4.76 \cdot 10^{15}$	$11.4 \cdot 10^{15}$	$4.14 \cdot 10^{15}$
$\Gamma_{22} [s^{-1}]$	$67.5 \cdot 10^6$	$5.26 \cdot 10^8$	$58.8 \cdot 10^6$
$L(\eta = 0.01)$	2.2	1.6	4.5

shows that even noise from spontaneous emission places serious limitations on quantum computation. This is the reason why scientists in this field have been highly motivated to develop methods that are able to correct the errors generated by noise such as spontaneous emission. These methods will be presented in the next section and in fact they can improve the limitations that we have derived in this chapter.

7.4 Error Correction and Fault-Tolerant Computation

C. Macchiavello, G.M. Palma

7.4.1 Symmetrisation Procedures

The first proposed remedy for quantum noise in quantum computation was based on a symmetrisation procedure [352]. We briefly summarise here the basic idea. Suppose you have a quantum system, you prepare it in some initial state $|\Psi_i\rangle$ and you want to implement a prescribed unitary evolution $|\Psi(t)\rangle$ or you simply want to preserve $|\Psi_i\rangle$ for some period of time t . Now, suppose that instead of a single system you can prepare R copies of $|\Psi_i\rangle$ and subsequently you can project the state of the combined system onto the symmetric subspace i.e. the subspace containing all states which are invariant under any permutation of the sub-systems. The claim is that frequent projections on the symmetric subspace will reduce errors induced by the environment. The intuition behind this concept is based on the observation that a prescribed error-free storage or evolution of the R independent copies starts in the symmetric sub-space and should remain in that sub-space. Therefore, since the error-free component of any state always lies in the symmetric subspace, upon successful projection it will be unchanged and part of the error will have been removed. Note, however, that the projected state is generally not error-free since the symmetric subspace contains states which are not of the simple product form $|\psi\rangle|\psi\rangle\dots|\psi\rangle$. Nevertheless it has been shown that the error probability will be suppressed by a factor of $1/R$ [353].

We illustrate here this effect in the simplest case of two qubits. The projection into the symmetric subspace is performed in this case by introducing the symmetrisation operator

$$S = \frac{1}{2}(P_{12} + P_{21}), \quad (7.31)$$

where P_{12} represents the identity and P_{21} the permutation operator which exchanges the states of the two qubits. The symmetric projection of a pure state $|\Psi\rangle$ of two qubits is just $S|\Psi\rangle$, which is then renormalised to unity.

It follows that the induced map on mixed states of two qubits (including renormalisation) is

$$\rho_1 \otimes \rho_2 \longrightarrow \frac{S(\rho_1 \otimes \rho_2)S^\dagger}{\text{Tr}S(\rho_1 \otimes \rho_2)S^\dagger}. \quad (7.32)$$

The state of either qubit separately is then obtained by the partial trace over the other qubit.

Let us assume that the two copies are initially prepared in a pure state $\rho_0 = |\Psi\rangle\langle\Psi|$ and that they interact with independent environments. After some short period of time δt the state of the two copies $\rho^{(2)}$ will have undergone an evolution

$$\rho^{(2)}(0) = \rho_0 \otimes \rho_0 \quad \longrightarrow \quad \rho^{(2)}(\delta t) = \rho_1 \otimes \rho_2, \quad (7.33)$$

where $\rho_i = \rho_0 + \varrho_i$ for some Hermitian traceless ϱ_i . We will retain only terms of first order in the perturbations ϱ_i so that the overall state at time δt is

$$\rho^{(2)} = \rho_0 \otimes \rho_0 + \varrho_1 \otimes \rho_0 + \rho_0 \otimes \varrho_2 + O(\varrho_1 \varrho_2). \quad (7.34)$$

We can calculate the average purity of the two copies before symmetrisation by calculating the average trace of the squared states:

$$\frac{1}{2} \sum_{i=1}^2 \text{Tr}((\rho_0 + \varrho_i)^2) = 1 + 2\text{Tr}(\rho_0 \tilde{\varrho}), \quad (7.35)$$

where $\tilde{\varrho} = \frac{1}{2}(\varrho_1 + \varrho_2)$. Note that $\text{Tr}(\rho_0 \tilde{\varrho})$ is negative, so that the expression above does not exceed 1. After symmetrisation each qubit is in state

$$\rho_s = [1 - \text{Tr}(\rho_0 \tilde{\varrho})]\rho_0 + \frac{1}{2}\tilde{\varrho} + \frac{1}{2}(\rho_0 \tilde{\varrho} + \tilde{\varrho} \rho_0) \quad (7.36)$$

and has purity

$$\text{Tr}(\rho_s^2) = 1 + \text{Tr}(\rho_0 \tilde{\varrho}). \quad (7.37)$$

Since $\text{Tr}\rho_s^2$ is closer to 1 than (7.35), the resulting symmetrised system ρ_s is left in a purer state.

Let us now see how the fidelity changes by applying the symmetrisation procedure. The average fidelity before symmetrisation is

$$F_{bs} = \frac{1}{2} \sum_i \langle \Psi | \rho_0 + \varrho_i | \Psi \rangle = 1 + \langle \Psi | \tilde{\varrho} | \Psi \rangle, \quad (7.38)$$

while after successful symmetrisation it takes the form

$$F_{as} = \langle \Psi | \rho_s | \Psi \rangle = 1 + \frac{1}{2} \langle \Psi | \tilde{\varrho} | \Psi \rangle. \quad (7.39)$$

The state after symmetrisation is therefore closer to the initial state ρ_0 .

For the generic case of R copies the purity of each qubit after symmetrisation is given by [353]

$$\text{Tr}(\rho_s^2) = 1 + 2 \frac{1}{R} \text{Tr}(\rho_0 \tilde{\varrho}) , \quad (7.40)$$

where now $\tilde{\varrho} = \frac{1}{R} \sum_{i=1}^R \varrho_i$, and the fidelity takes the form

$$\langle \Psi | \rho_s | \Psi \rangle = 1 + \frac{1}{R} \text{Tr}(\rho_0 \tilde{\varrho}) . \quad (7.41)$$

Formulae (7.40) and (7.41) must be compared with the corresponding ones before symmetrisation, i.e. (7.35) and (7.38). As we can see, ρ_s approaches the unperturbed state ρ_0 as R tends to infinity. Thus by choosing R sufficiently large and the rate of symmetric projection sufficiently high, the residual error at the end of a computation can, in principle, be controlled to lie within any desired small tolerance.

7.4.2 Classical Error Correction

A different class of error correcting techniques originates from an extension to the quantum realm of existing classical error correcting codes [354]. Indeed the problem of how to transmit and manipulate information reliably when errors can be induced by noise is present also in classical information theory. Before we begin our analysis of quantum error correcting codes it is therefore appropriate to briefly review how error correction is implemented in a classical scenario. In what follows a code will be a set of c binary sequences $\mathbf{w}_1 \cdots \mathbf{w}_c$, called codewords, of length n . During transmission or storage, some bits, due to the action of external noise, can undergo random flips. Bit flips are the only possible kind of classical error. If the channel is a binary symmetric memoryless channel (see Fig. 7.3) the set of possible received sequences $\mathbf{v}_1 \cdots \mathbf{v}_{2^n}$ is the set of all the 2^n binary sequences of length n . The task of the receiver is, given a received sequence \mathbf{v}_0 , to identify the most likely codeword \mathbf{w}_i sent by the transmitter, i.e. to identify the \mathbf{w}_i closest to \mathbf{v}_0 . In this context the distance between two binary sequences $d(\mathbf{w}, \mathbf{v})$, the so called Hamming distance, is measured by the number of digits in which the two strings differ. For a binary symmetric memoryless channel the \mathbf{w}_i with smallest Hamming distance $d(\mathbf{w}_i, \mathbf{v}_0)$ is also the most likely.

Clearly the larger the distance between codewords the better they are distinguishable in the presence of errors and therefore the more the code is robust against noise. If $d(\mathbf{w}_i, \mathbf{w}_j) \geq 2\eta + 1$ for $i \neq j$ then up to η errors can be corrected.

The Hamming bound provides an upper bound to the number of codewords c in a code able to correct up to η errors. Each codeword \mathbf{w}_i is the centre of a sphere of radius η containing all binary sequences \mathbf{v} with $d(\mathbf{w}_i, \mathbf{v}) \leq \eta$,

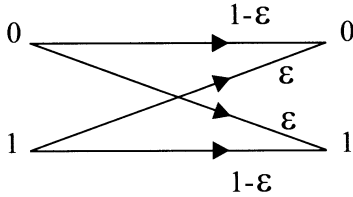


Fig. 7.3. In a binary symmetric channel each bit is transmitted with an error probability ϵ .

i.e. differing from \mathbf{w}_i in up to η locations. Figure 7.4 is an illustration of this situation for $\eta = 4$. If the code can correct the errors, these spheres must be disjoint. Obviously the number of sequences in each sphere times the number of spheres must be smaller than the total number of sequences of length n . Since each sphere contains a codeword \mathbf{w} plus all the sequences differing from it in $1, 2, \dots, \eta$ positions we must have

$$c \left\{ 1 + n + \binom{n}{2} + \binom{n}{3} + \dots + \binom{n}{\eta} \right\} = c \sum_{i=0}^{\eta} \binom{n}{i} \leq 2^n. \quad (7.42)$$

A family of codes which has proved very efficient is known for historical reasons as parity check codes [354]. In these codes the codewords \mathbf{w} are chosen in such a way as to satisfy a set of linear equations. The receiver tests whether the received sequence \mathbf{v} satisfies this set of linear relations. If \mathbf{v} fails the test the receiver corrects the smallest error which might have produced \mathbf{v} . Let's see in more detail how the code works. The set of linear equations the codewords must satisfy is characterized by a parity check matrix \mathbf{M} . Codewords \mathbf{w} are chosen to satisfy the relation

$$\mathbf{M} \cdot \mathbf{w} = 0. \quad (7.43)$$

For example codewords

$$\mathbf{w}_1 = 0000 \quad \mathbf{w}_2 = 0101 \quad \mathbf{w}_3 = 1110 \quad \mathbf{w}_4 = 1011 \quad (7.44)$$

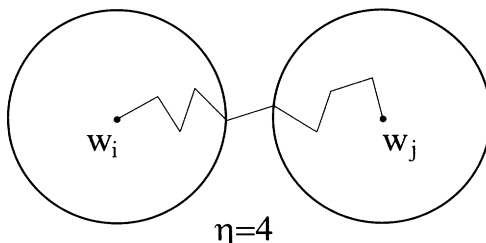


Fig. 7.4. In codes with $d(\mathbf{w}_i, \mathbf{w}_j) \geq 2\eta + 1$ disjoint spheres of radius η centred on each codeword contain all the sequences with up to η errors.

satisfy (7.43), with

$$\mathbf{M} = \begin{pmatrix} 1 & 0 & 1 & 0 \\ 0 & 1 & 1 & 1 \end{pmatrix} \quad (7.45)$$

where all the arithmetic is modulo 2. If the rank of \mathbf{M} is m than $k = n - m$ bits of our codeword can be specified arbitrarily while the remaining m digits are check digits determined by relation (7.43). The number of linearly independent codewords is therefore $c = 2^{n-m} = 2^k$ and the Hamming bound (7.42) can be rewritten as

$$2^k \sum_{i=0}^{\eta} \binom{n}{i} \leq 2^n \rightarrow 2^{n-k} = 2^m \geq \sum_{i=0}^{\eta} \binom{n}{i}, \quad (7.46)$$

which is a lower bound for the number of check digits. Suppose that the sequence \mathbf{w} is transmitted and that the sequence \mathbf{v} is received. The sequence $\mathbf{z} = \mathbf{w} - \mathbf{v}$, known as the error pattern, is a binary sequence with ones in the positions where an error has occurred and zeros elsewhere. If $\mathbf{z} \neq 0$ than \mathbf{v} fails the parity check: $\mathbf{M} \cdot \mathbf{v} = \mathbf{M} \cdot (\mathbf{w} + \mathbf{z}) = \mathbf{M} \cdot \mathbf{z} = \mathbf{s}$. The vector \mathbf{s} , known as error syndrome, is the sum of the columns of the parity check matrix in the location where \mathbf{z} has ones. For example if $\mathbf{w} = 1110$ is transmitted and $\mathbf{v} = 1000$ is received then $\mathbf{z} = 0110$ and, with \mathbf{M} as given by (7.45), $\mathbf{s} = 10$.

The task of the receiver, once an error syndrome \mathbf{s} is detected, is to identify the error patterns \mathbf{z} which might have produced \mathbf{s} and to correct the smallest one, i.e. the one with the smallest number of 1's. It should be noted that if our code can correct a single error the syndrome is simply the column where the error has occurred. If the columns of \mathbf{M} are different the receiver can easily identify the location of the error and correct it.

7.4.3 General Aspects of Quantum Error Correcting Codes

As soon as we try to extend the error correcting techniques illustrated above to the quantum scenario we immediately face two problems:

1. Due to external noise each qubit may not only flip its logical value but also decohere. In general it will get entangled with the environment, as was shown in Sect. 7.2.
2. We are not allowed to read the state of the qubit before the end of the computation. Failure to observe this rule leads to decoherence. We must therefore acquire knowledge on the location and nature of the error without acquiring knowledge on the state of the qubits.

We will show that the way out problem 2 is to use as “codevectors” $|\mathbf{w}\rangle$ entangled states of n qubits. The information we want to protect is therefore spread by the entanglement over all the n qubits. Reading (or decohering) only a few qubits will not lead to an irreversible loss of quantum information.

Codevectors are chosen in such a way that an error will move the $|\mathbf{w}\rangle$ into mutually orthogonal subspaces. Measurement of the syndrome will therefore reveal only which subspace $|\mathbf{w}\rangle$ has moved to. In what follows we will assume that each qubit can undergo an error with probability ϵ and that errors on different qubits are independent. With these assumptions the probability of errors on two qubits is of order $O(\epsilon^2)$. For sufficiently small values of ϵ we can reasonably assume that only one error has occurred. The probability of successful computation is $(1 - \epsilon)$. If we can implement a quantum error correction routine able to correct single errors the probability of success can be increased to $(1 - O(\epsilon^2))$. In general a code able to correct up to t errors increases the probability of successful computation to $(1 - O(\epsilon^{t+1}))$.

7.4.4 The Three Qubit Code

To gain some familiarity with quantum error correcting codes and to illustrate the ideas sketched above we will start by analyzing the three qubit code which can correct phase errors on a single qubit [355]. Suppose that each qubit of the qubit of a codeword can independently undergo an entanglement with the environment of the form (7.1). We will show that we can undo the effects of phase entanglement if we can correct phase errors, defined as

$$|0\rangle \longrightarrow |0\rangle \quad |1\rangle \longrightarrow -|1\rangle \quad (7.47)$$

due to the error operator σ_z . To this goal let us choose as codewords the following entangled states of three qubits:

$$\begin{aligned} |\mathbf{w}_0\rangle &= |000\rangle + |011\rangle + |101\rangle + |110\rangle, \\ |\mathbf{w}_1\rangle &= |111\rangle + |100\rangle + |010\rangle + |001\rangle. \end{aligned} \quad (7.48)$$

If only one qubit gets entangled with the environment, an arbitrary linear superposition of $|\mathbf{w}_0\rangle, |\mathbf{w}_1\rangle$ will become

$$\begin{aligned} (a_0|\mathbf{w}_0\rangle + a_1|\mathbf{w}_1\rangle)|E\rangle &\longrightarrow (a_0|\mathbf{w}_0\rangle_0 + a_1|\mathbf{w}_1\rangle_0)|E_0\rangle \\ &\quad + (a_0|\mathbf{w}_0\rangle_1 + a_1|\mathbf{w}_1\rangle_1)|E_1\rangle \\ &\quad + (a_0|\mathbf{w}_0\rangle_2 + a_1|\mathbf{w}_1\rangle_2)|E_2\rangle \\ &\quad + (a_0|\mathbf{w}_0\rangle_3 + a_1|\mathbf{w}_1\rangle_3)|E_3\rangle, \end{aligned} \quad (7.49)$$

where the error state $|\mathbf{w}_j\rangle_k$ is codeword j , ($j = 0, 1$) with a phase error on his k^{th} qubit ($k = 0$ labels no error). For example $|\mathbf{w}_0\rangle_2 = |000\rangle - |011\rangle + |101\rangle - |110\rangle$. The $|E_k\rangle$ are the corresponding environment states. Note that the error states are orthogonal:

$$_k\langle \mathbf{w}_j|\mathbf{w}_l\rangle_i = \delta_{jl}\delta_{ki}. \quad (7.50)$$

Codes in which error states are orthogonal are called non-degenerate. The error correction procedure is therefore the following:

- Project the code space onto the error subspaces spanned by $|\mathbf{w}_0\rangle_i |\mathbf{w}_1\rangle_i$
- Depending on the outcome of the measurement correct the appropriate qubit with a phase error applying σ_z . More explicitly, if the result of the above projection measurement is i , apply σ_z to the i th qubit (when $i = 0$ the state is not modified).

Note that at the end of the procedure the codevector and the environment are disentangled and that the amplitudes a_0, a_1 are not modified.

7.4.5 The Quantum Hamming Bound

We can now turn our attention to codes able to correct the most general kind of qubit–environment entanglement, which is of the form

$$|0\rangle|E\rangle \longrightarrow |0\rangle|E_{00}\rangle + |1\rangle|E_{01}\rangle \quad |1\rangle|E\rangle \longrightarrow |0\rangle|E_{10}\rangle + |1\rangle|E_{11}\rangle. \quad (7.51)$$

For a linear superposition of qubit states this can be conveniently written as

$$\begin{aligned} (a_0|0\rangle + a_1|1\rangle)|E\rangle &\longrightarrow (a_0|0\rangle + a_1|1\rangle)|E_0\rangle \\ &+ [\sigma_x(a_0|1\rangle + a_1|0\rangle)]|E_x\rangle \\ &+ [\sigma_z(a_0|0\rangle - a_1|1\rangle)]|E_z\rangle \\ &+ [\sigma_y(a_0|1\rangle - a_1|0\rangle)]|E_y\rangle, \end{aligned} \quad (7.52)$$

where σ_x is the error operator for bit flips, σ_z the error operator for phase flips defined in the previous paragraph and $\sigma_y = -i\sigma_z\sigma_x$ is the operator for both errors. As we can see from (7.52), a general qubit–environment interaction can be expressed as a superposition of unity and Pauli operators σ_x , σ_y and σ_z acting on the qubit. This means that the qubit state evolves into a superposition of an error-free component and three erroneous components, with errors of the σ_x , σ_y and σ_z type.

We can now easily translate into the quantum language the arguments which led us to the Hamming bound for “non-degenerate codes” [355] (less restrictive conditions hold for general quantum codes, see for example [323]). If a code with 2^q codevectors can correct up to η errors the codevectors $|\mathbf{w}\rangle$ and all the states which can be obtained from the $|\mathbf{w}\rangle$ with the action of up to η error operators must form a set of orthogonal states. The interaction with the entanglement will evolve each codevector as

$$\begin{aligned} |\mathbf{w}\rangle|E\rangle &\longrightarrow |\mathbf{w}\rangle|E_0\rangle + \sum_{i,k_i} |\mathbf{w}_i^{k_i}\rangle|E_i^{k_i}\rangle \\ &+ \sum_{ij,k_j k_j} |\mathbf{w}_{ij}^{k_i k_j}\rangle|E_{ij}^{k_i k_j}\rangle + \sum_{i j l, k_i k_j k_l} |\mathbf{w}_{ijl}^{k_i k_j k_l}\rangle|E_{ijl}^{k_i k_j k_l}\rangle \dots, \end{aligned} \quad (7.53)$$

where indices i, j, \dots label the qubits of the codevectors and the $k_i, k_j, \dots = x, y, z$ label the error on the corresponding qubit. If the code corrects up to

η errors, all the states with up to η errors which originate for each of the 2^q codevectors must be orthogonal. The number of orthogonal states must be smaller than the dimension of the Hilbert space of n qubits, and we have

$$2^q \sum_{i=0}^{\eta} 3^i \binom{n}{i} \leq 2^n \rightarrow 2^{n-q} \geq \sum_{i=0}^{\eta} 3^i \binom{n}{i} \quad (7.54)$$

which puts a lower bound on the number of check qubits $n - q$ of a quantum error correcting code able to correct up to η errors. The factor 3^i in (7.54) comes from the fact that in the quantum case three independent errors can occur for each qubit, at variance with the classical case, where the only kind of possible errors are bit flips.

7.4.6 The Seven Qubit Code

We are now ready to illustrate a quantum code which can correct any general error on a single qubit. Although five qubit codes exist [323, 356] with this property, as predicted by the quantum Hamming bound, for pedagogical reasons we will describe the seven qubit code introduced by Steane [357, 358]. First of all let us introduce the following parity check matrix:

$$\mathbf{M} = \begin{pmatrix} 0 & 0 & 0 & 1 & 1 & 1 & 1 \\ 0 & 1 & 1 & 0 & 0 & 1 & 1 \\ 1 & 0 & 1 & 0 & 1 & 0 & 1 \end{pmatrix}. \quad (7.55)$$

As all the columns of \mathbf{M} are different, if only one bit flip occurs the measurement of the syndrome will reveal the position of the qubit in error. We will use as starting ingredients to build the codevectors the (classical) sequences \mathbf{u} which satisfy the parity check $\mathbf{Mu} = 0$ and the corresponding states of seven qubits $|\mathbf{u}\rangle$ such that the logical value of the qubits corresponds to sequence \mathbf{u} . The codevectors $|\mathbf{w}_0\rangle, |\mathbf{w}_1\rangle$ are then defined as entangled superposition of states $|\mathbf{u}\rangle$ with an even and an odd number of 1's, respectively:

$$|\mathbf{w}_0\rangle = \sum_{even} |\mathbf{u}\rangle_e \quad |\mathbf{w}_1\rangle = \sum_{odd} |\mathbf{u}\rangle_0. \quad (7.56)$$

The final ingredient is a procedure to measure the syndrome. To this goal let us add three ancillary qubits, one for each bit of the syndrome, i.e. one for each row of \mathbf{M} (see Fig. 7.5). When matrix element $\mathbf{M}_{i,j} = 1$ than a CNOT gate is introduced, whose target is the ancillary qubit i and whose control is qubit j of the codevector.

If the initial codevector is $|\mathbf{v}\rangle$ and the initial vector of the ancillary qubits is $|0\rangle$ then the final vector of the ancillary qubits, the ancilla, will be $|\mathbf{s}\rangle = |\mathbf{Mv}\rangle$ corresponding to the value of the syndrome:

$$|\mathbf{v}\rangle \otimes |0\rangle_{anc.} \longrightarrow |\mathbf{v}\rangle \otimes |\mathbf{Mv}\rangle_{anc} \quad (7.57)$$

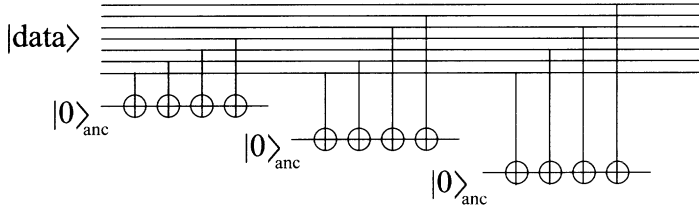


Fig. 7.5. Measurement of the bit-flip syndrome in the seven qubit code.

If only one error has occurred, a measurement of the ancilla will project the codevector either in the correct state or in a state with one bit flip. Furthermore the logical value of the ancilla will reveal the location of the qubit in error, which can then be corrected by applying operator σ_x .

The technique described above can easily be extended to correct also phase flips once we note that phase flips in base $|0\rangle, |1\rangle$ become bit flips in the Hadamard rotated basis. The problem therefore reduces to the correction of bit flips in the rotated basis. If we apply bitwise the Hadamard rotation each qubit will transform as

$$|0\rangle \longrightarrow |\tilde{0}\rangle \frac{1}{\sqrt{2}} \equiv (|0\rangle + |1\rangle), \quad |1\rangle \longrightarrow |\tilde{1}\rangle \frac{1}{\sqrt{2}} \equiv (|0\rangle - |1\rangle), \quad (7.58)$$

and the codevectors as

$$|\mathbf{w}_0\rangle \longrightarrow |\tilde{\mathbf{w}}_0\rangle \equiv \frac{1}{\sqrt{2}}(|\mathbf{w}_0\rangle + |\mathbf{w}_1\rangle), \quad |\mathbf{w}_1\rangle \longrightarrow |\tilde{\mathbf{w}}_1\rangle \equiv \frac{1}{\sqrt{2}}(|\mathbf{w}_0\rangle - |\mathbf{w}_1\rangle). \quad (7.59)$$

Note that $|\tilde{\mathbf{w}}_0\rangle, |\tilde{\mathbf{w}}_1\rangle$ satisfy the parity check. The procedure to correct phase errors is therefore the following: Apply a bitwise Hadamard rotation to the codevectors, correct the bit flips in the rotated basis, and rotate back to return to the original basis $|0\rangle, |1\rangle$ (see Fig. 7.6). The phase error will automatically be corrected. This shows that the seven qubit code can therefore correct any arbitrary phase and/or amplitude error in a single qubit.

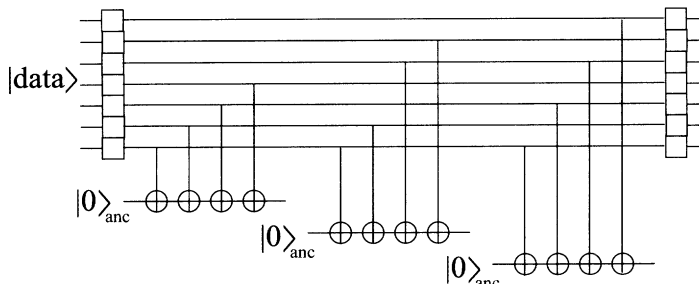


Fig. 7.6. Measurement of the phase-flip syndrome in the seven qubit code.

7.4.7 Fault-Tolerant Computation

So far, computational steps have been assumed to be error-free. In practice gate operations are themselves prone to errors. Furthermore, coding, decoding and error correction are also computational operations. The problem then arises of how to implement reliable computation using faulty circuits. We will illustrate in the remainder of this section the basic ideas behind fault-tolerant quantum computation [359]. As an example of how faulty gate operation can infect the quantum data beyond the recovery ability of our quantum error correcting codes, consider the measurement of the syndrome with the help of an ancillary qubit. The ancillary qubit is the target of several CNOT gates. Since, in a quantum CNOT, phase errors in the target act back on the control qubit, any phase error in the ancillary qubit can propagate to more than one data qubit. Note, however, that our code can correct only one error. Therefore, if the ancillary qubit contaminates two data qubits corruption is beyond recovery.

A way to confine the spreading of infection is to use separate ancillary qubits as targets of separate data qubits. The syndrome bit will then be inferred from a collective measurement of the ancillary qubits. Care must be taken however to make sure that such a procedure will give us information only on the errors and not on the state of the data qubits. The solution to this problem has been found by Shor. In his scheme the ancillary qubits are prepared in a linear superposition of states with an even number of 1's:

$$|Shor\rangle = \sum_{even} |\mathbf{x}\rangle \quad (7.60)$$

For instance the ancillary qubits – four for each syndrome bit – are prepared in state

$$\begin{aligned} |Shor\rangle = \frac{1}{\sqrt{8}} (& |0000\rangle + |0011\rangle + |0101\rangle + |1001\rangle + |0110\rangle \\ & + |1010\rangle + |1100\rangle + |1111\rangle). \end{aligned} \quad (7.61)$$

Each ancillary qubit will be the target of a different data qubit. At the end the value of the syndrome bit is inferred by measuring the parity of the bits in the ancillary state. This procedure ensures that measurement of the ancilla provides us with information only on the errors. Furthermore it guarantees that errors in the ancillary qubits will not spread in the data.

Our ambition, however, is not only to store data but also to perform computations on them. The easiest thing to do would be to decode the data, perform the desired computation and then to encode again. While decoded, however, data are vulnerable to external noise. Therefore, in order to protect our qubits we would like to perform computation directly on codevectors. Furthermore we would like to perform this computation in a fault-tolerant way in order to avoid propagation of errors. This is automatically achieved

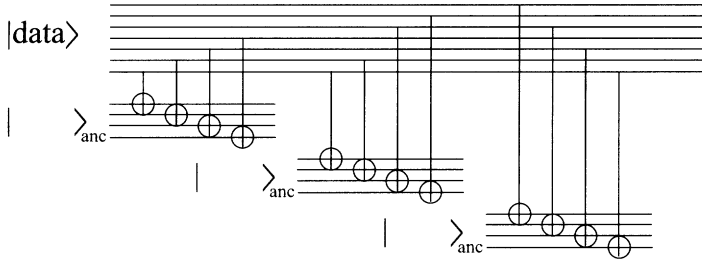


Fig. 7.7. Fault-tolerant measurement of the syndrome in the seven qubit code.

whenever we can construct gate operations on codevectors as bitwise operations on the single encoded qubits. We have shown in (7.58) that this is possible for the Hadamard rotation. It is also possible to implement the CNOT gate on codevectors pairwise on the code qubits of the control and target codevectors. These two gates alone, however, do not constitute a universal set. They can however be supplemented with a fault-tolerant version of the Toffoli gate in order to form such a universal set.

7.5 General Theory of Quantum Error Correction and Fault Tolerance

A. Steane

Introductory material and examples of quantum error correction (QEC) methods were given in the previous section. Here we will give a summary of the simplest aspects of the more general theory.

QEC is based on three central ideas: digitisation of noise, the manipulation of error operators and syndromes, and quantum error correcting code (QECC) construction. The degree of success of QEC relies on the physics of noise; we will turn to this after discussing the three central ideas.

7.5.1 Digitisation of Noise

“Digitisation of noise” is based on the observation that *any* interaction between a set of qubits and another system (such as the environment) can be expressed by a generalisation of (7.52):

$$|\phi\rangle |\psi\rangle_e \rightarrow \sum_i (E_i |\phi\rangle) |\psi_i\rangle_e \quad (7.62)$$

where each “error operator” E_i is a tensor product of Pauli operators acting on the qubits, $|\phi\rangle$ is the initial state of the qubits, and $|\psi\rangle_e$ are states of

the environment, not necessarily orthogonal or normalised. We thus express general noise and/or decoherence in terms of Pauli operators $\sigma_x, \sigma_y, \sigma_z$ acting on the qubits. These will be written $X \equiv \sigma_x, Z \equiv \sigma_z, Y \equiv -i\sigma_y = XZ$.

To write tensor products of Pauli matrices acting on n qubits, we introduce the notation $X_u Z_v$ where u and v are n -bit binary vectors. The non-zero coordinates of u and v indicate where X and Z operators appear in the product. For example,

$$X \otimes I \otimes Z \otimes Y \otimes X \equiv X_{10011} Z_{00110}. \quad (7.63)$$

Error correction is a process which takes a state such as $E_i |\phi\rangle$ to $|\phi\rangle$. Correction of X errors takes $X_u Z_v |\phi\rangle$ to $Z_v |\phi\rangle$; correction of Z errors takes $X_u Z_v |\phi\rangle$ to $X_v |\phi\rangle$. Putting all this together, we discover the highly significant fact that to correct *the most general possible* noise (7.62), it is sufficient to correct just X and Z errors.

7.5.2 Error Operators, Stabiliser, and Syndrome Extraction

We will now examine the mathematics of error operators and syndromes, using the insightful approach put forward by Gottesman [360] and Calderbank et. al. [361, 362], building on the first discoveries of Steane [357, 358] and Calderbank and Shor [363, 364].

Consider the set $\{I, X, Y, Z\}$ consisting of the identity plus the three Pauli operators. The Pauli operators all square to I : $X^2 = Y^2 = Z^2 = I$, and have eigenvalues ± 1 . Two members of the set only ever commute ($XI = IX$) or anticommute: $XZ = -ZX$. Tensor products of Pauli operators, i.e. error operators, also square to one and either commute or anticommute. N.B. the term ‘error operator’ is here just a shorthand for ‘product of Pauli operators’; such an operator will sometimes play the role of an error, sometimes of a parity check, c.f. classical coding theory, Sect. 7.4.2.

If there are n qubits in the quantum system, then error operators will be of *length* n . The *weight* of an error operator is the number of terms not equal to I . For example $X_{10011} Z_{00110}$ has length 5, weight 4.

Let $\mathcal{H} = \{M\}$ be a set of commuting error operators. Since the operators all commute, they can have simultaneous eigenstates. Let $\mathcal{C} = \{|u\rangle\}$ be the orthonormal set of simultaneous eigenstates all having eigenvalue +1:

$$M |u\rangle = |u\rangle \quad \forall |u\rangle \in \mathcal{C}, \forall M \in \mathcal{H}. \quad (7.64)$$

The set \mathcal{C} is a quantum error correcting code, and \mathcal{H} is its *stabiliser*. The orthonormal states $|u\rangle$ are termed *code vectors* or *quantum codewords*. In what follows, we will restrict attention to the case in which \mathcal{H} is a group. Its size is 2^{n-k} , and it is spanned by $n-k$ linearly independent members of \mathcal{H} . In this case \mathcal{C} has 2^k members, so it encodes k qubits, since its members span a 2^k dimensional subspace of the 2^n -dimensional Hilbert space of the whole

system. A general state in this subspace, called an *encoded state* or *logical state*, can be expressed as a superposition of the code vectors:

$$|\phi\rangle_L = \sum_{|u\rangle \in C} a_u |u\rangle. \quad (7.65)$$

Naturally, a given QECC does not allow correction of all possible errors. Each code allows correction of a particular set $\mathcal{S} = \{E\}$ of *correctable errors*. The task of code construction consists of finding codes whose correctable set includes the errors most likely to occur in a given physical situation. We will turn to this important topic in the next section. First, let us show how the correctable set is related to the stabiliser, and demonstrate how the error correction is actually achieved.

First, error operators in the stabiliser are all correctable, $E \in \mathcal{S} \forall E \in \mathcal{H}$, since these operators actually have no effect on a general logical state (7.65). If these error operators are themselves the only terms in the noise of the system under consideration, then the QECC is a noise-free subspace, also called decoherence-free subspace of the system.

There is a large set of further errors which do change encoded states but are nevertheless correctable by a process of extracting an error syndrome, and then acting on the system depending on what syndrome is obtained. We will show that \mathcal{S} can be any set of errors $\{E_i\}$ such that every product $E_1 E_2$ of two members is either in \mathcal{H} , or anticommutes with a member of \mathcal{H} . To see this, take the second case first:

$$E_1 E_2 M = -M E_1 E_2 \text{ for some } M \in \mathcal{H}. \quad (7.66)$$

We say that the combined error operator $E_1 E_2$ is *detectable*. This can only happen if

$$\begin{aligned} \text{either } & \{ME_1 = -E_1 M, ME_2 = E_2 M\} \\ \text{or } & \{ME_1 = E_1 M, ME_2 = -E_2 M\}. \end{aligned} \quad (7.67)$$

To extract the syndrome we measure all the observables in the stabiliser. To do this, it is sufficient to measure any set of $n - k$ linearly independent M in \mathcal{H} . Note that such a measurement has no effect on a state in the encoded subspace, since such a state is already an eigenstate of all these observables. The measurement projects a noisy state onto an eigenstate of each M , with eigenvalue ± 1 . The string of $n - k$ eigenvalues is the syndrome. Equations (7.67) guarantee that E_1 and E_2 have different syndromes, and so can be distinguished from each other. For, when the observable M is measured on the corrupted state $E|\phi\rangle_L$, (7.67) means a different eigenvalue will be obtained when $E = E_1$ than when $E = E_2$. Therefore, the error can be deduced from the syndrome, and reversed by re-applying the deduced error to the system (taking advantage of the fact that error operators square to 1).

Let us see how this whole process looks when applied to a general noisy encoded state. The noisy state is

$$\sum_i (E_i |\phi\rangle_L) |\psi_i\rangle_e . \quad (7.68)$$

The syndrome extraction can be done most simply by attaching an $n-k$ qubit ancilla a to the system, and storing in it the eigenvalues by a sequence of CNOT gates and Hadamard rotations. The exact network can be constructed either by thinking in terms of parity check information stored in the ancilla (c.f. Fig. 7.5), or by the following standard eigenvalue measurement method. To extract the $\lambda = \pm 1$ eigenvalue of operator M , prepare an ancilla in $(|0\rangle + |1\rangle)/\sqrt{2}$. Operate controlled- M with ancilla as control, system as target, then Hadamard rotate the ancilla. The final state of the ancilla is $[(1+\lambda)|0\rangle + (1-\lambda)|1\rangle]/2$. Carrying out this process for the $n-k$ operators M which span \mathcal{H} , the effect is to couple system and environment with the ancilla as follows:

$$|0\rangle_a \sum_i (E_i |\phi\rangle_L) |\psi_i\rangle_e \rightarrow \sum_i |s_i\rangle_a (E_i |\phi\rangle_L) |\psi_i\rangle_e . \quad (7.69)$$

The s_i are $(n-k)$ -bit binary strings, all different if the E_i all have different syndromes. A projective measurement of the ancilla will collapse the sum to a single term taken at random: $|s_i\rangle_a (E_i |\phi\rangle_L) |\psi_i\rangle_e$, and will yield s_i as the measurement result. Since there is only one E_i with this syndrome, we can deduce the operator E_i which should now be applied to correct the error!

This remarkable process can be understood as first forcing the general noisy state to ‘choose’ among a discrete set of errors, via a projective measurement, and then reversing the particular discrete error ‘chosen’ using the fact that the measurement result tells us which one it was. Alternatively, the correction can be accomplished by a unitary evolution consisting of controlled gates with ancilla as control, system as target, effectively transferring the noise (including entanglement with the environment) from system to ancilla.

We left out of the above the other possibility mentioned just before (7.66), namely that

$$E_1 E_2 \in \mathcal{H} . \quad (7.70)$$

In this case E_1 and E_2 will have the same syndrome, so are indistinguishable in the syndrome extraction process. However, this does not matter! We simply interpret the common syndrome of these two errors as an indication that the corrective operation E_1 should be applied. If it was E_1 that occurred, this is obviously fine, while if in fact E_2 occurred, the final state is $E_1 E_2 |\phi\rangle_L$ which is also correct! This situation has no analogue in classical coding theory. The quantum codes which take advantage of it are termed *degenerate* and are not constrained by the quantum Hamming bound, (7.54).

The discussion based on the stabiliser is useful because it focuses attention on operators rather than states. Quantum codewords are nevertheless

very interesting states, having a lot of symmetry and interesting forms of entanglement. The codewords in the QECC can readily be shown to allow correction of the set \mathcal{S} if and only if [323, 365]

$$\langle u | E_1 E_2 | v \rangle = 0 \quad (7.71)$$

$$\langle u | E_1 E_2 | u \rangle = \langle v | E_1 E_2 | v \rangle \quad (7.72)$$

for all $E_1, E_2 \in \mathcal{S}$ and $|u\rangle, |v\rangle \in \mathcal{C}, |u\rangle \neq |v\rangle$. In the case that $E_1 E_2$ always anticommutes with a member of the stabiliser, we have $\langle u | E_1 E_2 | u \rangle = \langle u | E_1 E_2 M | u \rangle = -\langle u | M E_1 E_2 | u \rangle = -\langle u | E_1 E_2 | u \rangle$, therefore $\langle u | E_1 E_2 | u \rangle = 0$. This is a nondegenerate code; all the code vectors and their erroneous versions are mutually orthogonal, and the quantum Hamming bound must be satisfied.

7.5.3 Code Construction

The power of QEC results from the physical insights and mathematical techniques already discussed, combined with the fact that useful QECCs can actually be found. Code construction is itself a subtle and interesting area, which we will merely introduce here.

First, recall that we require the members of the stabiliser all to commute. It is easy to show that $X_u Z_v = (-1)^{u \cdot v} Z_v X_u$, where $u \cdot v$ is the binary parity check operation, or inner product between binary vectors, evaluated in $GF(2)$. From this, $M = X_u Z_v$ and $M' = X_{u'} Z_{v'}$ commute if and only if

$$u \cdot v' + v \cdot u' = 0. \quad (7.73)$$

The stabiliser is completely specified by writing down the $n - k$ linearly independent error operators which span it. It is convenient to write these error operators by giving the binary strings u and v which indicate the X and Z parts, in the form of two $(n - k) \times n$ binary matrices H_x, H_z . The whole stabiliser is then uniquely specified by the $(n - k) \times 2n$ binary matrix

$$H = (H_x | H_z) \quad (7.74)$$

and the requirement that the operators all commute (i.e. that \mathcal{H} is an abelian group) is expressed by

$$H_x H_z^T + H_z H_x^T = 0, \quad (7.75)$$

where T indicates the matrix transpose.

The matrix H is the analogue of the parity check matrix for a classical error correcting code. The analogue of the generator matrix is the matrix $G = (G_x | G_z)$ satisfying

$$H_x G_z^T + H_z G_x^T = 0. \quad (7.76)$$

In other words, H and G are duals with respect to the inner product defined by (7.73). G has $n+k$ rows. H may be obtained directly from G by swapping the X and Z parts and extracting the usual binary dual of the resulting $(n+k) \times 2n$ binary matrix.

Note that (7.76) and (7.75) imply that G contains H . Let \mathcal{G} be the set of error operators generated by G , then also \mathcal{G} contains \mathcal{H} .

Since by definition (7.76), all the members of \mathcal{G} commute with all the members of \mathcal{H} , and since (by counting) there can be no further error operators which commute with all of \mathcal{H} , we deduce that all error operators not in \mathcal{G} anticommute with at least one member of H . This leads us to a powerful observation: if all members of \mathcal{G} (other than the identity) have weight at least d , then all error operators (other than the identity) of weight less than d anticommute with a member of \mathcal{H} , and so are detectable. Such a code can therefore correct all error operators of weight less than $d/2$.

What if the only members of \mathcal{G} having weight less than d are also members of \mathcal{H} ? Then the code can still correct all error operators of weight less than $d/2$, using property (7.70) (a degenerate code). The weight d is called the minimum distance of the code.

The problem of code construction is thus reduced to a problem of finding binary matrices H which satisfy (7.75), and whose duals G , defined by (7.76), have large weights. We will now write down such a code by combining well-chosen classical binary error correcting codes:

$$H = \left(\begin{array}{c|c} H_2 & 0 \\ \hline 0 & H_1 \end{array} \right), \quad G = \left(\begin{array}{c|c} G_1 & 0 \\ \hline 0 & G_2 \end{array} \right). \quad (7.77)$$

Here H_i , $i = 1, 2$, is the check matrix of the classical code C_i generated by G_i . Therefore $H_i G_i^T = 0$ and (7.76) is satisfied. To satisfy commutativity, (7.75), we force $H_1 H_2^T = 0$, in other words, $C_2^\perp \subset C_1$. By construction, if the classical codes have size k_1, k_2 , then the quantum code has size $k = k_1 + k_2 - n$. The quantum codewords are

$$|u\rangle_L = \sum_{x \in C_2^\perp} |x + u \cdot D\rangle, \quad (7.78)$$

where u is a k -bit binary word, x is an n -bit binary word, and D is a $(k \times n)$ matrix of coset leaders. These are the CSS (Calderbank–Shor–Steane) codes. Their significance is first that they can be efficient, and second that they are useful in fault-tolerant computing (see below).

By “efficient” we mean that there exist codes of given d/n whose rate k/n remains above a finite lower bound, as $k, n, d \rightarrow \infty$. The CSS codes have $d = \min(d_1, d_2)$. If we choose the pair of classical codes in the construction to be the same, $C_1 = C_2 = C$, then we are considering a classical code which contains its dual. A finite lower bound for the rate of such codes can be shown to exist [364]. This is highly significant: it means that QEC can be a very powerful method to suppress noise (see next section).

There exist QECCs more efficient than CSS codes. Good codes can be found by extending CSS codes, and by other methods. For illustration, we finish this section with the stabiliser and generator of the $[[n, k, d]] = [[5, 1, 3]]$ perfect code. It encodes a single qubit ($k = 1$), and corrects all errors of weight 1 (since $d/2 = 1.5$).

$$H = \left(\begin{array}{c|c} 11000 & 00101 \\ 01100 & 10010 \\ 00110 & 01001 \\ 00011 & 10100 \end{array} \right), \quad G = \left(\begin{array}{c|c} H_x & H_z \\ 11111 & 00000 \\ 00000 & 11111 \end{array} \right). \quad (7.79)$$

7.5.4 The Physics of Noise

Noise and decoherence are themselves a large subject. Here we will simply introduce a few basic ideas, in order to clarify what QEC can and cannot do. By ‘noise’ we mean simply any unknown or unwanted change in the density matrix of our system.

The statement (7.62) about digitisation of noise is equivalent to the statement that any interaction between a system of qubits and its environment has the form

$$H_I = \sum_i E_i \otimes H_i^e, \quad (7.80)$$

where the operators H_i^e act on the environment. Under the action of this coupling, the density matrix of the system (after tracing over the environment) evolves from ρ_0 to $\sum_i a_i E_i \rho_0 E_i$. QEC returns all terms of this sum having correctable E_i to ρ_0 . Therefore, the fidelity of the corrected state, compared to the noise-free state ρ_0 , is determined by the sum of all coefficients a_i associated with uncorrectable errors.

For a mathematically thorough analysis of this problem, see [365, 366]. The essential ideas are as follows. Noise is typically a continuous process affecting all qubits all the time. However, when we discuss QEC, we can always adopt the model that the syndrome is extracted by a projective measurement. Any statement such as ‘the probability that error E_i occurs’ is just a short-hand for ‘the probability that the syndrome extraction projects the state onto one which differs from the noise-free state by error operator E_i ’. We would like to calculate such probabilities.

To do so, it is useful to divide up (7.80) into a sum of terms having error operators of different weight:

$$H_I = \sum_{\text{wt}(E)=1} E \otimes H_E^e + \sum_{\text{wt}(E)=2} E \otimes H_E^e + \sum_{\text{wt}(E)=3} E \otimes H_E^e + \dots \quad (7.81)$$

There are $3n$ terms in the first sum, $3^2 n! / (2!(n-2)!)$ terms in the second, and so on. The strength of the system–environment coupling is expressed by

coupling constants which appear in the H_E^c operators. In the case where only the weight 1 terms are present, we say the environment acts independently on the qubits: it does not directly produce correlated errors across two or more qubits. In this case, errors of all weights will still appear in the density matrix of the noisy system, but the size of the terms corresponding to errors of weight w will be $O(\epsilon^{2w})$, where ϵ is a parameter giving the system–environment coupling strength.

Since QEC restores all terms in the density matrix whose errors are of weight $\leq t = d/2$, the fidelity of the corrected state, in the uncorrelated noise model, can be estimated as one minus the probability $P(t+1)$ for the noise to generate an error of weight $t+1$. This probability is approximately

$$P(t+1) \simeq \left(3^{t+1} \binom{n}{t+1} \epsilon^{t+1} \right)^2 \quad (7.82)$$

when all the single-qubit error amplitudes can add coherently (i.e. the qubits share a common environment), or

$$P(t+1) \simeq 3^{t+1} \binom{n}{t+1} \epsilon^{2(t+1)} \quad (7.83)$$

when the errors add incoherently (i.e. either separate environments, or a common environment with couplings of randomly changing phase). The significance of (7.82) and (7.83) is that they imply QEC works extremely well when t is large and $\epsilon^2 < t/3n$. Since good codes exist, t can in fact tend to infinity while t/n and k/n remain fixed. Therefore, as long as the noise per qubit is below a threshold around $t/3n$, almost perfect recovery of the state is possible. The ratio t/n constrains the rate of the code through the quantum Hamming bound or its cousins.

Such uncorrelated noise is a reasonable approximation in many physical situations, but we need to be careful about the degree of approximation, since we are concerned with very small terms of order ϵ^d . If we relax the approximation of completely uncorrelated noise, (7.82) and (7.83) remain approximately unchanged, if and only if the coupling constants in (7.81) for errors of weight t are themselves of order $\epsilon^t/t!$.

A very different case in which QEC is also highly successful is when a set of correlated errors, also called burst errors, dominate the system–environment coupling, but we can find a QEC whose stabiliser includes all these correlated errors. This is sometimes called ‘error avoiding’ rather than ‘error correction’ since by using such a code, we don’t even need to correct the logical state: it is already decoupled from the environment. The general lesson is that the more we know about the environment, and the more structure there exists in the system–environment coupling, the better able we are to find good codes.

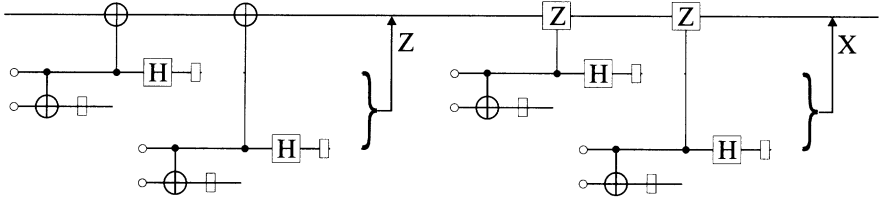


Fig. 7.8. Fault-tolerant syndrome extraction network

7.5.5 Fault-Tolerant Quantum Computation

The above discussion of QEC is relevant to high-fidelity communication down noisy quantum channels, but it is not yet clear how relevant it may be to quantum computing. This is because so far we have assumed the quantum operations involved in syndrome extraction are themselves noise-free. Therefore we are using processing power to combat noise, but it is not clear what degree of precision of the processing is necessary in order to gain something.

Fault-tolerant computation is concerned with processing information reliably even when every elementary operation, and every period of free evolution, is itself noisy. One way to approach this is to use QEC repeatedly, but with the syndrome extraction procedure carefully constructed in such a way that it corrects more noise than it introduces. Most of the essential new insights which permit us to do this were introduced by Shor [367] and helpfully discussed by Preskill [359]; see also [368]–[370]. Here we will adopt Shor’s general approach, but with significant improvements introduced by Steane [371, 372]. Note that this subject is much less mature than QEC; many avenues remain unexplored. Here we will concentrate on explaining one method to extract syndromes in the right way.

A complete fault-tolerant syndrome extraction network is shown in Fig. 7.8. For brevity, we consider the simplest case of a single-error correcting code; the ideas can be generalised to codes correcting many errors. The fundamental 2-state entities in the computer are called physical qubits. Each horizontal line in the network represents not a single physical qubit, but a block of n such qubits. Operators such as Hadamard and CNOT are applied across the relevant block or blocks, i.e. n operations, one for each qubit or pair of qubits.

The method relies on the careful use of repetition, on the fact that X and Z errors propagate differently, and on useful properties of CSS codes. Define an *error location* to be any 1 or 2-qubit gate on physical qubits (including preparation and measurement operations), or the free evolution of any single physical qubit during one timestep. The noise is assumed to be uncorrelated and stochastic, so that failures occur independently with probability $\sim \gamma$. The aim of the whole network is to achieve a single-error correction of the computer block, in such a way that no failure at a single location can result in an error of weight ≥ 2 in the computer block. The idea is that while the syndrome extraction must make single-qubit errors in the computer more

likely, these are the very ones which are correctable. The important thing is not to generate uncorrectable errors with $O(\gamma)$ probability.

We begin by introducing 2 ancilla blocks, and preparing each in the logical zero state $|0\rangle_L$. Each preparation is not fault tolerant, it will fail in such a way that the prepared state can have any error of any weight with probability $O(\gamma)$. Operate CNOT blockwise between the two ancillas, and measure all the bits of one of them in the computational basis. Here we are trying to verify that the correct state was prepared, using the fact that blockwise physical CNOT acts as a logical CNOT for a CSS code. Therefore, the measurement result should be a member of the classical code C_2^\perp (7.78). If it is not, then reprepare the pair of ancillas and repeat until it is. At this stage, the probability for the remaining unmeasured ancilla to have X errors of weight ≥ 2 is $O(\gamma^2)$, because it can only happen if failures occur in at least two locations. Note that the ancilla might still have Z errors of any weight.

Now couple the verified ancilla to the computer by blockwise physical CNOT. Once again, we use the fact that this acts as logical CNOT, so there should be no effect! In fact something does happen: X errors propagate from ancilla to computer, and Z errors propagate from computer to ancilla. This is a sneaky, and fault tolerant, way to gather the Z -error syndrome into the ancilla. We read it out by Hadamard transforming the ancilla (to convert Z errors to bit flips) and measuring all the bits of the ancilla in the computational basis. Here we have used the property, valid for a certain class of CSS codes, that blockwise physical H acts as logical H , so will keep the ancilla state in the encoded subspace, except for the Z errors which become X errors.

There is still no single error location which can produce a weight-2 error in the computer, but now we are in danger, since there are many locations where a single failure would lead to an incorrect syndrome. If we were to ‘correct’ the computer on the basis of the wrong syndrome, we would actually introduce more errors. Therefore, the whole of the process described up till now is repeated. We finally end up with two syndromes. If they agree, then the only way they can be wrong is if failures occurred at two different locations, an $O(\gamma^2)$ process, so we go ahead and believe them. If they disagree, a third syndrome must be extracted, and we act on the majority vote.

We have now completed the correction of Z errors in the computer (while generating further Z errors, which will be caught in the next round of correction). The second half of the network acts similarly, but now gathers up and corrects the X errors in the computer.

Note that the whole process depends on the fact that X and Z errors propagate differently. We can fault-tolerantly verify the ancilla against X errors, but only by accepting the risk of having high-weight Z errors in the ancilla. This is OK because those Z errors stay put; they don’t propagate up to the computer, they just make the syndrome wrong. We subsequently check for their presence by generating the syndrome again. Note also the

heavy reliance on useful properties of CSS codes, such as their behaviour under blockwise gates.

In a repeated series of error recoveries, each round of recovery corrects not just the errors developed in the computer during that round, but also the errors caused by the previous round (as long as they are correctable). It leaves uncorrected the errors it itself caused. The noise level accumulated after R rounds is therefore suppressed from $O(R\gamma)$ to $O(R\gamma^2 + \gamma)$, which is beneficial for large R and sufficiently small γ .

To complete the task of fault tolerant *computation*, not just memory storage, we need to be able to evolve the computer state through the desired quantum algorithm. We already saw how to perform logical Hadamard and CNOT operations on the state encoded by a CSS code: operate blockwise on the qubits. This is fault tolerant since each physical gate only connects to one physical qubit per block. To obtain a complete set of operations, we use the fact that the members of the continuous set of all gates can be approximated efficiently by using members of a discrete set. To complete the set, it is sufficient to have a fault-tolerant Toffoli gate, or one of a set of closely related gates, among which is the controlled- $\pi/2$ rotation. Shor [367] proposed a (somewhat obscure) network for Toffoli. It is possible to understand the construction as related to teleportation. Teleportation can be understood as a form of fault tolerant swap operation, and it is useful for moving information around fault-tolerantly in a quantum computer [372, 373]. These and other methods are under active investigation.

At the time of writing, fault-tolerant computation based on repeated QEC seems to be the most promising way to realise large quantum algorithms, though the requirements on the physical hardware, both in terms of computer size and noise level, remain formidable.

7.6 Frequency Standards

S.F. Huelga, C. Macchiavello, M.B. Plenio, A.K. Ekert

In this section the precision of frequency measurements based on trapped ions in the presence of decoherence is analysed. Different preparations of n two-level systems are considered as well as different measurements procedures. We show in particular that standard Ramsey spectroscopy on uncorrelated ions and optimal measurements on maximally entangled states provide the same resolution. We suggest the use of symmetrisation procedures to reduce the undesired effects of decoherence and show that these allow one to exceed even the optimal precision achievable with optimised initial preparation of the n -ions state and optimised measurement scheme.

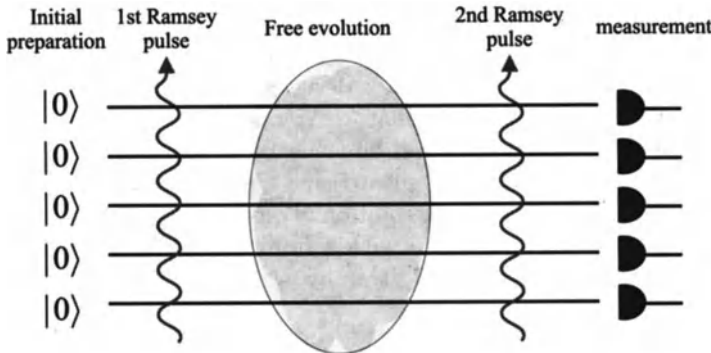


Fig. 7.9. Schematic representation of Ramsey-type spectroscopy with uncorrelated particles.

The aim of a frequency standard is to stabilise a reference oscillator to a given atomic frequency. The implementation of an optical frequency standard in an atomic trap according to standard Ramsey interferometry is illustrated in Fig. 7.9.

The ion trap is loaded with n ions initially prepared in the same internal state $|0\rangle$ (we denote by $|0\rangle$ and $|1\rangle$ the ground and the excited states of each ion). A Ramsey pulse of frequency ω is applied to all ions. The pulse shape and duration are carefully chosen so that it drives the atomic transition $|0\rangle \leftrightarrow |1\rangle$ of natural frequency ω_0 and prepares an equally weighted superposition of the two internal states $|0\rangle$ and $|1\rangle$ for each ion.

$$|0\rangle \rightarrow \frac{|0\rangle + |1\rangle}{\sqrt{2}} \quad |1\rangle \rightarrow \frac{-|0\rangle + |1\rangle}{\sqrt{2}} . \quad (7.84)$$

Next the system evolves freely for a time t . In a reference frame rotating at the oscillator frequency ω , the free evolution is governed by the Hamiltonian

$$H = -\hbar\Delta|1\rangle\langle 1| , \quad (7.85)$$

where $\Delta = \omega - \omega_0$ denotes the detuning between the classical driving field and the atomic transition. The evolution of the basis atomic states can then be represented as follows:

$$|0\rangle \rightarrow |0\rangle \quad |1\rangle \rightarrow e^{i\Delta t}|1\rangle , \quad (7.86)$$

and the frequency difference between the atomic transition and the reference oscillator leads to the accumulation of a relative phase. If we now apply a second Ramsey pulse, the probability that an ion is found in the state $|1\rangle$ is given by

$$P = \frac{1 + \cos(\Delta t)}{2} . \quad (7.87)$$

When this basic scheme is repeated yielding a total duration T of the experiment, the resulting interference curve of the measured population in the upper state allows us to deduce the oscillator detuning and subsequently to adjust the frequency of the reference oscillator. At this point, one question arises. What is the best precision that can be achieved in the measurement of the atomic frequency? More precisely, given T and a fixed given number of ions n , what is the ultimate limit to the resolution of our frequency standard?

The statistical fluctuations associated with a finite sample yield an uncertainty ΔP in the estimated value of P given by

$$\Delta P = \sqrt{P(1 - P)/N} , \quad (7.88)$$

where $N = nT/t$ denotes the actual number of experimental data (we assume that N is large). Hence the uncertainty in the estimated value of ω_0 is given by

$$|\delta\omega_0| = \frac{\sqrt{P(1 - P)/N}}{|dP/d\omega|} = \frac{1}{\sqrt{nTt}}. \quad (7.89)$$

This value is often referred to as the *shot noise limit* [374]. We should stress that this limit comes from the intrinsically statistical character of quantum mechanics, in contrast to other possible sources of technical noise. While the latter may eventually be reduced, the shot noise poses a fundamental limit to the achievable resolution in precision spectroscopy with n independent particles.

The theoretical possibility of overcoming this limit has been put forward recently [375, 376]. The basic idea is to prepare the ions initially in an entangled state. To see the advantage of this approach, let us consider the case of two ions prepared in the maximally entangled state

$$|\Psi\rangle = (|00\rangle + |11\rangle)/\sqrt{2}. \quad (7.90)$$

This state can be generated, for example, by the initial part of the network illustrated in Fig. 7.10. A Ramsey pulse on the first ion is followed by a controlled-NOT gate. After a free evolution period of time t the state of the composite system in the interaction picture rotating at the driving frequency ω reads

$$|\Psi\rangle = (|00\rangle + e^{2i\Delta t} |11\rangle)/\sqrt{2}. \quad (7.91)$$

The second part of the network allows to disentangle the ions after the free evolution period. The population in state $|1\rangle$ of the first ion will now oscillate at a frequency 2Δ :

$$P_2 = \frac{1 + \cos(2\Delta t)}{2}. \quad (7.92)$$

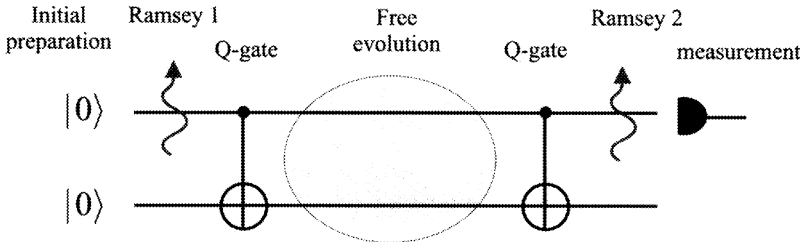


Fig. 7.10. Spectroscopy with two maximally entangled particles. The particles are entangled and disentangled by means of “controlled-NOT” gates.

This scheme can be easily generalised to the n -ion case by a sequence of controlled-NOT gates linking the first ion with each of the remaining ones. In this way, a maximally entangled state of n ions of the form

$$|\Psi\rangle = (|00\dots0\rangle + |11\dots1\rangle)/\sqrt{2} \quad (7.93)$$

is generated. The final measurement on the first ion, after the free evolution period and the second set of controlled-NOT gates, gives the signal

$$P_n = \frac{1 + \cos(n\Delta t)}{2}. \quad (7.94)$$

The advantage of this scheme is that the oscillation frequency of the signal is now amplified by a factor n with respect to the case of uncorrelated ions and the corresponding frequency uncertainty is

$$|\delta\omega_0| = \frac{1}{n\sqrt{Tt}}. \quad (7.95)$$

Note that this result represents an improvement of a factor $1/\sqrt{n}$ over the shot noise limit (7.89) by using the same number of ions n and the same total duration of the experiment T and it was argued that this is the best precision possible [377].

Let us now examine the same situation in a realistic experimental scenario, where decoherence effects are inevitably present. The main type of decoherence in an ion trap is dephasing due to processes that cause random changes in the relative phase of quantum states while preserving the population in the atomic levels. Important mechanisms that result in dephasing effects are collisions, stray fields and laser instabilities. We model the time evolution of the reduced density operator for a single ion ρ in the presence of decoherence by the following master equation [378]:

$$\frac{d\rho}{dt} = -i\Delta(\rho|1\rangle\langle 1| - |1\rangle\langle 1|\rho) + \gamma(\sigma_z\rho\sigma_z - \rho). \quad (7.96)$$

Equation (7.96) is written in a frame rotating at the frequency ω . By $\sigma_z = |0\rangle\langle 0| - |1\rangle\langle 1|$ we denote a Pauli spin operator. Here we have introduced the

decay rate $\gamma = 1/\tau_{dec}$, where τ_{dec} is the decoherence time. For the case of independent particles this will give rise to a broadening of signal (7.87):

$$P = (1 + \cos \Delta t e^{-\gamma t})/2. \quad (7.97)$$

As a consequence the corresponding uncertainty in the atomic frequency is no longer detuning-independent. We now have

$$|\delta\omega_0| = \sqrt{\frac{1 - \cos^2(\Delta t)e^{-2\gamma t}}{nTte^{-2\gamma t} \sin^2(\Delta t)}}. \quad (7.98)$$

In order to obtain the best precision it is necessary to optimise this expression as a function of the duration of each single measurement t . The minimal value is attained for

$$\Delta t = k\pi/2 \text{ (}k \text{ odd)} \quad t = \tau_{dec}/2 \quad (7.99)$$

provided that $T > \tau_{dec}/2$. Thus the minimum frequency uncertainty reads

$$|\delta\omega_0|_{opt} = \sqrt{\frac{2\gamma e}{nT}} = \sqrt{\frac{2e}{n\tau_{dec}T}}. \quad (7.100)$$

For maximally entangled preparation, the signal (7.94) in the presence of dephasing is modified as follows:

$$P_n = \frac{1 + \cos(n\Delta t)e^{-n\gamma t}}{2} \quad (7.101)$$

and the resulting uncertainty for the estimated value of the atomic frequency is now minimal when

$$\Delta t = k\pi/2n \text{ (}k \text{ odd)} \quad t = \tau_{dec}/2n. \quad (7.102)$$

Interestingly, we recover exactly the same minimal uncertainty as for standard Ramsey spectroscopy (7.100). This effect is illustrated in Fig.7.11. The modulus of the frequency uncertainty $|\delta\omega_0|$ is plotted as a function of the duration of each single experiment t for standard Ramsey spectroscopy with n uncorrelated particles and for a maximally entangled state with n particles.

In the presence of decoherence both preparations reach the same precision. This result can be intuitively understood by considering that maximally entangled states are much more fragile in the presence of decoherence: their decoherence time is reduced by a factor n and therefore the duration of each single measurement t has also to be reduced by the same amount. The previous conclusions hold whenever the total duration of the experiment exceeds the typical decoherence time. Hence, maximally entangled states are only advantageous for short term stabilisations. As far as long term experiments

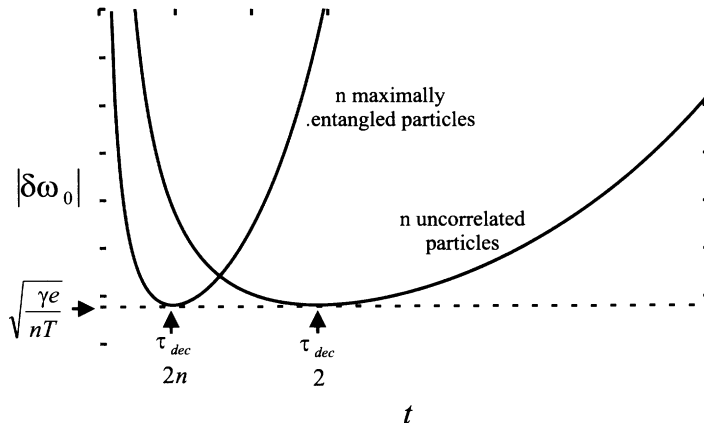


Fig. 7.11. Frequency uncertainty $|\delta\omega_0|$ as a function of the duration of a single shot t for maximally entangled and uncorrelated particles. Note that the minimum uncertainty is exactly the same for both configurations.

are concerned, it has been shown recently [379] that the best resolution is achieved using partially entangled preparations with a high degree of symmetry. The procedure involves both an optimisation of the initial preparation of the state of the n ions and the final measurement after the free evolution region. However, from a practical point of view, the expected improvement is modest. The optimal percentual improvement in the precision relative to the limit (7.100) is of the order of 10% for $n = 7$. Asymptotic limits for large n are still under investigation.

A very different approach to improving the resolution of a frequency standard by means of quantum entanglement is making use of error correction. As it has been shown in previous sections, these procedures can effectively reduce the amount of decoherence and dissipation in quantum systems. However, when established error correction protocols for phase-type errors are applied to this particular problem, difficulties arise. The use of error correction not only corrects phase errors due to environmental noise but also interferes with the desired change of relative phase in the atomic states that appears for a detuned oscillator, which is the quantity we want to estimate. This reduces the sensitivity of the frequency standard. Nevertheless, as will be shown, it is possible to *stabilise* the system against decoherence and overcoming the optimal resolution achievable in the spectroscopy of uncorrelated particles.

The key point is to realise that during the free evolution region, in the absence of decoherence, the state of n particles initially prepared in a state which is invariant under any permutation of the n ions always lies in the symmetric subspace of the Hilbert space of the composite system of the n ions (by symmetric subspace we mean the subspace which includes all the possible

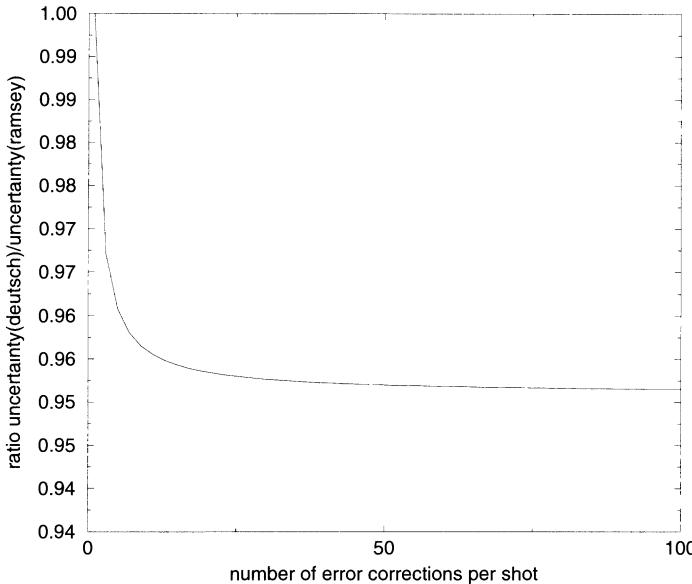


Fig. 7.12. Ratio of the uncertainty for standard Ramsey spectroscopy with and without symmetrisation for $n = 2$ as a function of the number of symmetrisation steps performed during the free evolution region.

states which are invariant under any permutation of the n ions). A projection of the global state into the symmetric subspace [380] would then yield a partial removal of events affected by environmental phase errors. Figure 7.12 shows the percentual precision improvement achievable with this technique for $n = 2$. In this case a standard Ramsey scheme with initially uncorrelated ions has been considered and repeated symmetrisation steps are applied during the free evolution region. After each symmetrisation step the ions are kept only if the symmetrisation is successful, otherwise they are discarded and reset to state $|0\rangle$ to start the scheme from the beginning. Although this reduces the number of experimental data available for statistics, Fig. 7.12 shows that it is a convenient strategy to improve the overall precision of the experiment.

The limits to the precision achievable with symmetrisation procedures for generic n and a generic initial preparation of the state of the ions are still under investigation.

It should be noted that the symmetrization method is an error detection method rather than an error correction method. The symmetrization method simply removes erroneous states instead of correcting them. Although the remaining ensemble contains less errors the statistics of the experiment becomes worse due to the smaller number of systems that remain in the symmetric subspace. Overall a small improvement results. The application of true quantum

error correction codes in frequency standards is currently being investigated. Progress in this direction could potentially lead to substantially improved frequency standards. But even a proof that quantum error correction and entanglement cannot improve the precision of frequency standards significantly would be very interesting.

In this section we have presented the application of entanglement and quantum error correction in frequency standards. The motivation for this is that it is an application of the ideas of quantum information theory that requires only small quantum resources. One direction of future research in quantum information theory is certainly the development of other applications that require only small resources. Such applications could then be realised experimentally in the near future.

8. Entanglement Purification

8.1 Introduction

In Chap. 7 the theory of quantum error correction was presented. The present chapter describes an alternative method of overcoming decoherence which is particularly useful for quantum state communication. The main idea is to distill from a large set of (pairs of) entangled particles, possibly degraded in entanglement purity by decoherence, a subset of particles with enhanced entanglement purity. Section 8.2 describes the general principles of entanglement purification. Specific examples are local filtering (Sect. 8.3), suitable for increasing the entanglement for pure states, and quantum privacy amplification (Sect. 8.4), designed to increase the security of quantum cryptography over noisy quantum channels. The generalisation of purification to multi-particle entanglement will be addressed in Sect. 8.5. Section 8.6 shows how to create maximally entangled EPR pairs between spatially distant atoms, each of them inside a high-Q optical cavity, by sending photons through a noisy channel, such as a standard optical fibre. As the absorption probability of photons during the transmission grows exponentially with the distance, so will the required number of repetitions for a successful transmission. Section 8.7 presents the quantum repeater method, which reduces the growth of the required number of operations as function of the transmission distance from exponential to polynomial.

8.2 Principles of Entanglement Purification

H.-J. Briegel

A central problem of quantum communication is the faithful transmission of quantum information from a party A (Alice) to some other party B (Bob) when the communication channel that connects A with B is noisy. The fidelity with which a quantum state is transmitted through a noisy quantum channel decreases, in general, exponentially with its length, so faithful transmission will be restricted to very short distances. This problem can be solved, in

principle, by the method of teleportation, which requires that A and B share a certain supply of pairs of particles in a maximally entangled state (EPR pairs). The question remains then, how can A and B create such entangled states if they can only communicate through noisy channels? Since entanglement cannot be created by local operations alone, A and B will have to send quantum bits through the channel at some point, to build up non-local quantum correlations. As these qubits interact with the channel, they are subject to decoherence and the resulting EPR pairs will not be maximally entangled, but instead be described by some mixed state with a certain entanglement fidelity. The idea of *entanglement purification* is to extract from a large ensemble of such low-fidelity EPR pairs a smaller sub-ensemble with sufficiently high fidelity, which may then be used for faithful teleportation [49, 74] (Chap. 3) or for quantum cryptography [46, 47] (Chap. 2).

From the quantum communication perspective, there is a natural connection between entanglement purification and quantum error correction. The theory of quantum error correction has primarily been developed to make quantum computation possible despite the effects of decoherence and imperfect apparatus, but it can, of course, also be used to correct transmission errors.¹ Entanglement purification, on the other hand, is a more specific but powerful tool for quantum communication purposes. By exploiting classical communication between the parties, it allows highly efficient two-way protocols that cannot be realised with quantum error correction techniques. Furthermore, the method is remarkably robust with respect to imperfect apparatus, which makes it very attractive for more advanced applications such as quantum repeaters [381]. A quantitative analysis of the connection between entanglement purification and quantum error correction is given in Ref. [323].

It should be emphasised that the issue of purifying (and quantifying) entanglement is of fundamental interest, regardless of the specific communicational applications that we have in mind *today*. We are likely to learn many more aspects of (multi-)particle entanglement in the future than we are presently aware of, and its applications might not be restricted to computational and communicational tasks. In any case, it will be good to have entangled states in our laboratory, and we need to know how to generate and to purify them efficiently.

So what is entanglement purification?

To illustrate the main ideas we first consider an ensemble of spin 1/2 particles that are partially polarised along a certain direction (z say). For simplicity, we may assume that we are dealing with an incoherent mixture of particles in state $|\uparrow\rangle \equiv |\text{spin up}\rangle$ and $|\downarrow\rangle \equiv |\text{spin down}\rangle$, respectively, represented by the density matrix

$$\rho = f|\uparrow\rangle\langle\uparrow| + (1-f)|\downarrow\rangle\langle\downarrow|, \quad (8.1)$$

¹ In fact, *classical* error correction was originally developed for just that purpose [32].

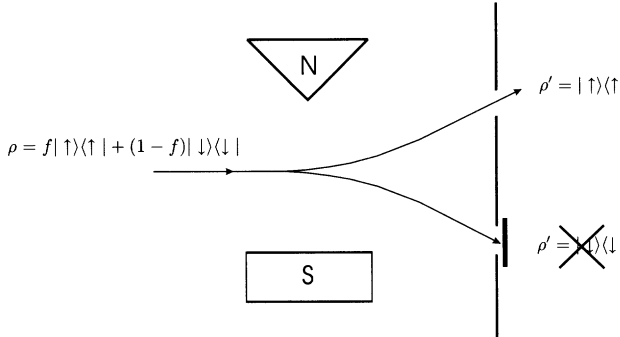


Fig. 8.1. Selection of spin-polarised atoms with Stern-Gerlach magnets: An inhomogeneous magnetic field in z direction, generated by two magnets (S and N), is used to spatially separate particles with different spin. For brevity, we call this arrangement a “Stern-Gerlach apparatus.”

although this restriction is not essential for the following argument. We can easily select the subensemble of particles in state $|\uparrow\rangle$ by measuring the particles’ spin along the z axis, e.g. by sending them through a Stern–Gerlach (SG) apparatus as shown in Fig. 8.1. By selecting only those particles that leave the apparatus along the upper path (which will be the case for a fraction f of all particles, on average), we will obviously create a subensemble of particles in the pure state $\rho' = |\uparrow\rangle\langle\uparrow|$. We could say that we have “purified” the whole ensemble by “distilling” the particles with the desired polarisation, although this terminology would sound rather forced, at this point.

For reasons that will become clear, imagine a slightly more complicated situation where, by some unknown mechanism, the particles are destroyed (e.g. absorbed) after they have passed through the SG apparatus! We only assume that the apparatus delivers us with a click if a particle goes through the upper hole in Fig. 8.1 and nothing otherwise, absorbing all of the particles. How could we use such a deficient apparatus to purify our ensemble? A possibility would be to not send the particles themselves through the SG apparatus but a *copy* of them, instead. Although it is impossible to copy a general quantum state (no-cloning theory, Sect. 2.2.2 [88]) it is possible to copy the selected *basis* states using an auxiliary particle C and the *measurement gate* (or CNOT gate). The measurement gate has been described in Sect. 1.6: If the initial state of the particle C is $|\uparrow\rangle_C$, its effect is to copy the

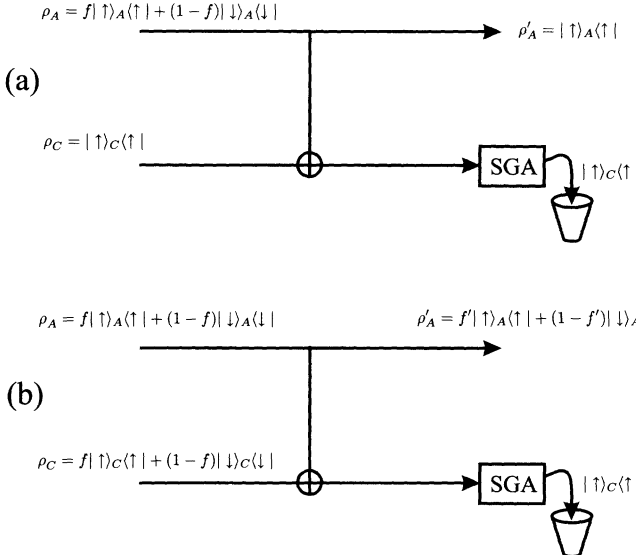


Fig. 8.2. Selection of spin-polarised atoms with a fictitious Stern–Gerlach (SG) apparatus that absorbs an atom upon measuring its state. The state of an atom of the impure ensemble (upper line) is copied (symbol \oplus) onto an auxiliary atom C (lower line), on which the destructive measurement is performed. The auxiliary atoms used in (a) are polarised in state $| \uparrow \rangle_C$; in (b) they are taken from the impure ensemble itself.

basis states $| \uparrow \rangle_A$ and $| \downarrow \rangle_A$ of particle A onto particle C.² ³

$$\begin{aligned} | \uparrow \rangle_A | \uparrow \rangle_C &\longrightarrow | \uparrow \rangle_A | \uparrow \rangle_C \\ | \downarrow \rangle_A | \uparrow \rangle_C &\longrightarrow | \downarrow \rangle_A | \downarrow \rangle_C . \end{aligned} \quad (8.2)$$

Applied to the ensemble (8.1), the measurement gate creates two (classically) correlated ensembles of the form⁴

$$\rho_{AC} = f| \uparrow \rangle_A \langle \uparrow | \otimes | \uparrow \rangle_C \langle \uparrow | + (1-f)| \downarrow \rangle_A \langle \downarrow | \otimes | \downarrow \rangle_C \langle \downarrow | . \quad (8.3)$$

² This means that any superposition $(\alpha| \uparrow \rangle_A + \beta| \downarrow \rangle_A)$ will be transformed by this gate according to

$$\begin{aligned} (\alpha| \uparrow \rangle_A + \beta| \downarrow \rangle_A) | \uparrow \rangle_C &\rightarrow \alpha| \uparrow \rangle_{AC} + \beta| \downarrow \rangle_{AC} \\ &\neq (\alpha| \uparrow \rangle_A + \beta| \downarrow \rangle_A)(\alpha| \uparrow \rangle_C + \beta| \downarrow \rangle_C) . \end{aligned}$$

The no-cloning principle [88] is therefore not violated.

³ More generally, the spin of the particle C is flipped under the condition that particle A is in state $| \downarrow \rangle_A$. That is, (8.2) together with the transformations $| \uparrow \rangle_A | \downarrow \rangle_C \longrightarrow | \uparrow \rangle_A | \downarrow \rangle_C$ and $| \downarrow \rangle_A | \downarrow \rangle_C \longrightarrow | \downarrow \rangle_A | \uparrow \rangle_C$ describe the full CNOT gate.

⁴ This is true if the auxiliary particles C are initially in the state $| \uparrow \rangle_C$.

If we now measure the spin value of an auxiliary particle, we still destroy *that* particle, but a click will indicate that the corresponding left-behind particle A is in the pure state $\rho'_A = |\uparrow\rangle_A\langle\uparrow|$ (see Fig. 8.2a). By measuring the copy of every particle, we simply check which of the particles are in the right state and can therefore select a purified subensemble.

Obviously, there is a catch: By assuming that we have auxiliary particles in the *pure* state $|\uparrow\rangle_C$ available, the whole purification idea seems to be pointless, since we could have used those auxiliary particles from the beginning, instead of our impure ensemble.

So what can we do if we do not have perfectly polarised spins for copying? The important point is that we may as well use particles taken from the impure ensemble itself, for this purpose. As long as $f > 1/2$, it is more likely that some randomly selected particle (for copying) is in the correct internal state $|\uparrow\rangle_C$ and can thus be used to check the unknown state of some other particle of the ensemble. To see this quantitatively, imagine that we divide the initial ensemble, which we want to purify, into two subensembles ρ_A and ρ_C of the same size (we write two different indices A and C to distinguish their roles in the measurement gate). Both subensembles will be described by the same density matrix (8.6), see also Fig. 8.2b. Now for every atom in the ensemble A, we pick an atom from the ensemble C and copy the state of A onto C with the aid of the measurement gate. After this procedure has been done for all particles, we obtain the following ensemble,

$$\begin{aligned} \rho_{AC} = & (f^2 |\uparrow\rangle_A\langle\uparrow| + (1-f)^2 |\downarrow\rangle_A\langle\downarrow|) \otimes |\uparrow\rangle_C\langle\uparrow| \\ & + f(1-f) (|\uparrow\rangle_A\langle\uparrow| + |\downarrow\rangle_A\langle\downarrow|) \otimes |\downarrow\rangle_C\langle\downarrow|. \end{aligned} \quad (8.4)$$

We now measure the state of the particles C and collect all those particles of the ensemble A, whose copy is found in state $|\uparrow\rangle_C$ (“click”), into a new ensemble. This new ensemble is then described by the density operator

$$\rho'_A = f' |\uparrow\rangle_A\langle\uparrow| + (1-f') |\downarrow\rangle_A\langle\downarrow| \quad (8.5)$$

with $f' = f^2/(f^2 + (1-f)^2)$. The simple function $f'(f)$ is identical to the one plotted in Fig. 8.4, where we will discuss the purification of mixed entangled states. For $f > 1/2$, we thus obtain a *purified ensemble* with a larger fraction $f' > f$ of particles in the state $|\uparrow\rangle_A$. If we iterate this procedure, as indicated by the staircase in Fig. 8.4, we are able to *distill* particles with a state arbitrarily close to the pure state $|\uparrow\rangle_A$, as long as the initial ensemble is sufficiently large.⁵

We are now ready to discuss the purification of mixed entangled states. Imagine that Alice and Bob want to purify an ensemble of *two*-particle entangled states ρ_{AB} , where their particles A and B are kept at different locations. Consider the following simple example

⁵ Strictly speaking, to distill pure states by this method, the initial ensemble has to be infinitely large.

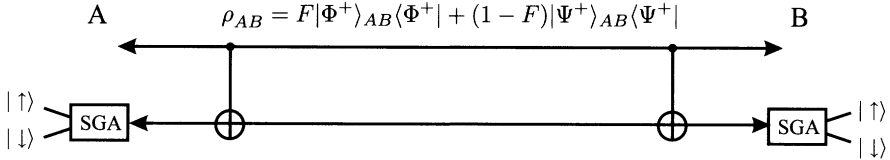


Fig. 8.3. Purification of a mixed-state ensemble of entangled states by local unitary operations, measurements, and classical communication.

$$\rho_{AB} = f|\Phi^+\rangle_{AB}\langle\Phi^+| + (1-f)|\Psi^+\rangle_{AB}\langle\Psi^+| \quad (8.6)$$

with the Bell states

$$|\Phi^+\rangle_{AB} = \{|\uparrow\uparrow\rangle_{AB} + |\downarrow\downarrow\rangle_{AB}\}/\sqrt{2}$$

and

$$|\Psi^+\rangle_{AB} = \{|\uparrow\downarrow\rangle_{AB} + |\downarrow\uparrow\rangle_{AB}\}/\sqrt{2}$$

and $1/2 < f < 1$. Unless $f = 1/2$, the state (8.6) is inseparable. We may regard (8.6) as a classical mixture of two ensembles of (pure) Bell states $|\Phi^+\rangle_{AB}$ and $|\Psi^+\rangle_{AB}$ of size f and $(1-f)$, respectively.⁶ Clearly, by sending both particles through a corresponding SG apparatus on each side, Alice and Bob can distinguish the two subensembles: For pairs in the state $|\Phi^+\rangle_{AB}$, both particles will leave the apparatus on similar paths (“up-up” or “down-down”) while for pairs in state $|\Psi^+\rangle_{AB}$ they will leave the apparatus along different paths (“up-down” or “down-up”), assuming that both Alice and Bob have aligned their SG apparatuses in the z -direction. On the other hand, this measurement will *destroy* any previously existing entanglement, and the particles will leave the apparatuses in a product state. The problem is therefore: How can Alice and Bob select the subensemble described by $|\Phi^+\rangle_{AB}$ if, by a local measurement, they destroy the entanglement?

To solve this problem, we may use our insights from the previous discussion of one-particle purification. Can Alice and Bob apply the trick with the measurement gate and send “copies” of A and B through the SG apparatuses, instead of the particles themselves? They can, in fact, if the initial state of the particles used for the copying is itself entangled. To see this, consider the situation where Alice and Bob share two pairs, one pair AB from the ensemble (8.6) and a second pair A'B' in the pure state $|\Phi^+\rangle_{A'B'}$. Now they copy the state of the pair AB onto the pair A'B' by applying the measurement gate of (8.2) on both sides, that is, between particles A and A', and B and B', respectively. The result of this operation can be summarised as follows:

⁶ The fraction $f = \langle\Phi^+|\rho_{AB}|\Phi^+\rangle_{AB}$ in (8.6) is also called the “entanglement fidelity” (or simply fidelity) of the mixed state ρ_{AB} with respect to the Bell state $|\Phi^+\rangle_{AB}$.

$$\begin{aligned} |\Phi^+\rangle_{AB}|\Phi^+\rangle_{A'B'} &\longrightarrow |\Phi^+\rangle_{AB}|\Phi^+\rangle_{A'B'} \\ |\Psi^+\rangle_{AB}|\Phi^+\rangle_{A'B'} &\longrightarrow |\Psi^+\rangle_{AB}|\Psi^+\rangle_{A'B'}. \end{aligned} \quad (8.7)$$

This bi-lateral (CNOT) operation obviously acts like a measurement gate for *pairs* where the states $|\Phi^+\rangle$ and $|\Psi^+\rangle$ play the analogs of $|\uparrow\rangle$ and $|\downarrow\rangle$ in (8.2). This means that, if Alice and Bob share some pairs in the state $|\Phi^+\rangle_{A'B'}$, they can use them to check the state of randomly chosen pairs of the ensemble (8.6) and thereby select the desired subensemble. The problem is, of course, that they do not have auxiliary pairs in the state $|\Phi^+\rangle_{AB}$! (otherwise there would be no need for purification). But – remember the previous discussion for single-particle states – Alice and Bob may equally well use pairs from the mixed ensemble itself, as long as the majority of them is in the right initial state $|\Phi^+\rangle$ (i.e. $f > 1/2$). So the protocol is very similar to that for the one-particle purification (see Fig. 8.3):

1. Alice and Bob pick randomly two pairs of the ensemble (8.6) and use one of the pairs to measure the state of the other pair; i.e.
2. they apply the CNOT gate between corresponding particles on each side;
3. they measure the state of the auxiliary pair, e.g. with two SG apparatuses as in Fig. 8.3 (and thus destroy its entanglement).

By keeping only those pairs for which the measurement results give the same spin value, (up-up or down-down) they can select a new ensemble that is described by the density operator

$$\rho'_{AB} = f'|\Phi^+\rangle_{AB}\langle\Phi^+| + (1-f')|\Psi^+\rangle_{AB}\langle\Psi^+|, \quad (8.8)$$

with a larger fraction $f' = f^2/(f^2+(1-f)^2) > f$ (for $f > 1/2$) of pairs in the state $|\Phi^+\rangle_{AB}$ (see Fig. 8.4). Note that, in order to compare the outcomes of their measurements and thus to decide which pairs to keep or to discard, Alice and Bob have to communicate and exchange classical information, which is an integral part of any purification protocol. By iterating this procedure as indicated by the staircase in Fig. 8.4, Alice and Bob can *distill* an ensemble of pairs with entanglement fidelity f arbitrarily close to unity.

It seems that with (8.6), we have discussed a rather special case of a mixed two-particle state, but the method also works for general states ρ_{AB} , as long as they contain a sufficiently large fraction $f = \langle\Phi_{\text{me}}|\rho_{AB}|\Phi_{\text{me}}\rangle > 1/2$ of particles in a maximally entangled state $|\Phi_{\text{me}}\rangle$.⁷ The first entanglement purification protocol for general mixed entangled states was given by Bennett et al. [49]. It allows one to distill from a large ensemble of entangled states with fidelity $f > 1/2$ a smaller ensemble of pairs with fidelity f arbitrarily close to unity. These pairs can then be used for faithful teleportation through

⁷ By this we mean any state that is, up to local unitary transformations on Alice's and Bob's particle, equivalent to one of the four (and thus to all) Bell states. Typically, at some point of a protocol that works with general mixed states ρ_{AB} , the dominant component $|\Phi_{\text{me}}\rangle$ of ρ_{AB} is transformed into the Bell state $|\Phi^+\rangle$ before the bilateral CNOT operation is applied.

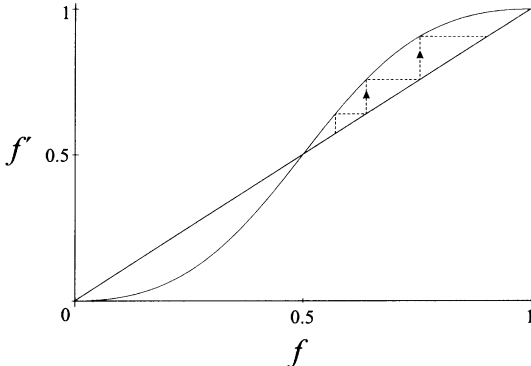


Fig. 8.4. Purification of mixed entangled states. For $f > 1/2$, the fidelity of the pairs (8.6) is increased to the value f' in (8.8). By iteration (staircase), one can distill high fidelity pairs from a large initial ensemble of low-fidelity pairs. Note that for this simple (so-called recurrence) method, more than 50% of all pairs are sacrificed in each step.

a noisy quantum channel. A second protocol, called “quantum privacy amplification,” (QPA) was given by Deutsch et al. [47]. Apart from differences in the details (such as the efficiency in producing singlets), both protocols use the measurement gate as a central ingredient to perform measurements on non-local entangled states without destroying their entanglement. The prime motivation of QPA lies in its application to entanglement-based quantum cryptography [46], by establishing a procedure that allows Alice and Bob, in principle, to *disentangle* a potential eavesdropper from a selected subset of pairs, which may subsequently be used for quantum key distribution. This method of quantum privacy amplification will be reviewed in Sect. 8.4

It should be emphasised that the method which we have described above to illustrate the idea of entanglement purification is not the only way of purifying entangled states. There are more sophisticated methods (using e.g. multi-particle measurements) that exploit ideas from classical information theory such as random hashing [49, 323] to increase the efficiency of the protocols. Another interesting and simple method, which is particularly suited for increasing the entanglement of *pure* states, is *local filtering* [117, 382], which will be described in more detail in Sect. 8.3. There have also been a series of further developments in the theory of entanglement purification since the first ideas were formulated a few years ago, but we cannot discuss these in this elementary introduction. Examples include the important notion of “bound entanglement” [383], the discussion of optimal purification protocols [322, 323, 384, 385], and the efficiency and the robustness of purification protocols under imperfect local operations [381, 386, 387]. A generalisation of entanglement purification for multi-particle entangled states is discussed in Sect. 8.5.

8.3 Local Filtering

B. Huttner, N. Gisin

For entanglement purification one considers an unlimited number of pairs of quantum systems, all in the same (possibly mixed) state ρ_{in} . The task is to extract from this a fraction of maximally entangled pure states, by using only local operations and classical communication. Let us first consider the case of a pure entangled state of two quantum systems $\rho_{\text{in}} = |\psi_{\text{in}}\rangle\langle\psi_{\text{in}}|$. We shall show that it can always be “purified” by local filtering to the 2-qubits singlet state $\frac{1}{\sqrt{2}}(|01\rangle - |10\rangle)$. This introduces the concept of local filtering, a particularly simple example of entanglement purification, and shows that for entanglement purification in general it suffices to consider purification towards singlet states [382].

Using the Schmidt decomposition, ψ_{in} can always be written as:

$$\psi_{\text{in}} = \sum_{j=1}^N c_j \alpha_j \otimes \beta_j \quad (8.9)$$

where $\{\alpha_j\}$ and $\{\beta_j\}$ are orthonormal bases of the Hilbert spaces of the 2 entangled quantum systems. Since the state ψ_{in} is assumed entangled, there are at least 2 non-vanishing c_j , hence we may assume $c_1 \neq 0$ and $c_2 \neq 0$. To purify ψ_{in} Alice, who holds the system in states α_j , and Bob, who holds the β_j , first measure the projectors $P_{\alpha_1} + P_{\alpha_2}$ and $P_{\beta_1} + P_{\beta_2}$, respectively. By classical communication, Alice and Bob keep only the pairs that give positive outputs to the measurements. These pairs are in the following state:

$$\psi_1 = c_1 \alpha_1 \otimes \beta_1 + c_2 \alpha_2 \otimes \beta_2. \quad (8.10)$$

Hence each subsystem involves only two orthogonal states, like qubits. Let us assume that $|c_1|^2 \geq |c_2|^2$, then Alice and Bob apply locally 2 filters F_A and F_B that attenuate α_1 and β_1 while letting α_2 and β_2 through unaffected. These filters are represented by the following positive operators:

$$F_A = \sqrt{\frac{|c_2|}{|c_1|}} P_{\alpha_1} + P_{\alpha_2} \quad \text{and} \quad F_B = \sqrt{\frac{|c_2|}{|c_1|}} P_{\beta_1} + P_{\beta_2}. \quad (8.11)$$

Using the classical communication channel, Alice and Bob select only those pairs of systems that passed both filters. (Actually, it suffices if only Alice or only Bob measures her (his) operator and act with a filter). Notice that such filters really exist. For example optical elements with polarisation-dependent loss are common. For an experimental example in quantum optics, see for instance [388]. The state of the filtered systems has equal weights on both product states:

$$\psi_2 = F_A \otimes F_B \psi_1 = \frac{|c_2|}{|c_1|} c_1 \alpha_1 \otimes \beta_1 + c_2 \alpha_2 \otimes \beta_2. \quad (8.12)$$

Finally, Alice and Bob only need to fix the relative phase between $\alpha_1 \otimes \beta_1$ and $\alpha_2 \otimes \beta_2$ to obtain the desired singlet state (up to an irrelevant global phase):

$$\psi_{\text{filtered}} = \alpha_1 \otimes \beta_1 - \alpha_2 \otimes \beta_2 \quad (8.13)$$

In full generality, the problem of entanglement purification is more complex (for more than 2 entangled systems, the general solution is not even known). However, the relatively simple filters presented above can also be used to purify some mixed states, as will be shown now. Inspired by the above results, let us consider the following mixture of 2-qubit states:

$$\rho_{\text{in}}(\lambda, c) = \lambda P_{\psi_c} + \frac{1-\lambda}{2} (P_{\psi_{11}} + P_{\psi_{00}}), \quad (8.14)$$

where λ and c are two real numbers between 0 and 1, and

$$\psi_c = c|10\rangle - \sqrt{1-c^2}|01\rangle, \quad \psi_{11} = |11\rangle, \quad \psi_{00} = |00\rangle. \quad (8.15)$$

Before showing how the state $\rho(\lambda, c)$ can be purified, we would like to prove that this state can never violate the Bell–CHSH inequality [12]. For this purpose, we use a powerful result by the Horodecki family [389], which applied to state $\rho(\lambda, c)$ concludes that for

$$\frac{1}{2-2c\sqrt{1-c^2}} < \lambda \leq \frac{1}{1+c^2(1-c^2)} \quad (8.16)$$

no violation of the Bell–CHSH inequality can happen. Hence $\rho(\lambda, c)$ is apparently local, though below we show that $\rho(\lambda, c)$ can be purified to singlet states and that consequently $\rho(\lambda, c)$ is in fact nonlocal.

The procedure to purify $\rho(\lambda, c)$ is actually quite similar to the example presented above: Alice and Bob apply the filters (8.11) with $c_1 = c$ and $c_2 = \sqrt{1-c^2}$. The filtered state reads:

$$\begin{aligned} \rho_{\text{filtered}}(\lambda, c) &= F_A \otimes F_B \rho_{\text{in}}(\lambda, c) F_A \otimes F_B = \\ &= \frac{1}{N} \left(2\lambda c \sqrt{1-c^2} P_{\text{singlet}} + \frac{1-\lambda}{2} (P_{\psi_{11}} + P_{\psi_{00}}) \right) \end{aligned} \quad (8.17)$$

with the normalisation factor $N = 2\lambda c \sqrt{1-c^2} + (1-\lambda)$.

Using again Horodeckis theorem [389], one sees that this state violates the Bell–CHSH inequality iff

$$\lambda > \frac{1}{1+2c\sqrt{1-c^2}(\sqrt{2}-1)}. \quad (8.18)$$

The upper and lower bounds on λ defined by the conditions (8.16) and (8.18) are compatible provided $c\sqrt{1 - c^2} \leq \sqrt{2} - 1$. Hence there are values of λ and c such that the state $\rho(\lambda, c)$ is “local”, in the sense that no Bell–CHSH inequality is violated, and such that the corresponding state filtered by the local environments, $\rho_{\text{filtered}}(\lambda, c)$, violates some Bell–CHSH inequality.

Above we have identified “local” \approx “no violation of Bell–CHSH inequality”. In this way the results appear somewhat more dramatic! But clearly this identification can and should be criticized. A state that is explicitly nonlocal after some local interactions does not deserve the qualification of local. An open question is whether the states $\rho(\alpha, \lambda)$ satisfying (8.16) and (8.18) admit a local hidden variable model reproducing all correlations. Since it does not violate any Bell–CHSH inequality, it is plausible that such a model exists. However, even if such a local hidden model exists, the state should be called nonlocal, because reproducing all correlations is not enough, as illustrated by the example presented above.

8.4 Quantum Privacy Amplification

C. Macchiavello

The purpose of entanglement purification schemes is to distill a subset of states with enhanced purity from a larger set of non-pure entangled states. The first scheme of this kind was proposed in [49] and it was shown that this allows faithful teleportation of quantum states via noisy channels. A subsequent more efficient purification scheme was presented in [47], named “quantum privacy amplification” (QPA) because it was designed for cryptographic purposes. Actually, it was proved that it leads to security of quantum cryptography over noisy channels (in the entanglement based scheme [46] also presented in Chap. 2). In this section we describe how the QPA scheme works.

Let us assume that pairs of qubits in maximally entangled states are generated and distributed to two users, Alice and Bob, via a noisy quantum channel. Because of the noise along the transmission channel the distributed pairs interacting with the environment get entangled with it, lose their purity and become mixed states. Acting on the received pairs, Alice and Bob want to enhance their purity. Let us assume that many pairs are distributed and the channel acts in the same way on all of them. We will describe the states of the pairs in the Bell basis representation

$$|\phi^\pm\rangle = \frac{1}{\sqrt{2}}(|00\rangle \pm |11\rangle) \quad (8.19)$$

$$|\psi^\pm\rangle = \frac{1}{\sqrt{2}}(|01\rangle \pm |10\rangle), \quad (8.20)$$

where $\{|0\rangle, |1\rangle\}$ represents a basis for each particle belonging to the pairs. We assume that each pair is initially generated in state $|\phi^+\rangle$ and denote by $\{a, b, c, d\}$ the diagonal components of the density operator ρ of the “noisy” pairs that Alice and Bob receive in the basis $\{|\phi^+\rangle, |\psi^-\rangle, |\psi^+\rangle, |\phi^-\rangle\}$. The first diagonal element $a = \langle\phi^+|\hat{\rho}|\phi^+\rangle$, which we call the ‘fidelity’, is the probability that the pair would pass a test for being in the state $|\phi^+\rangle$. The purpose of QPA is to drive the fidelity to 1 (which implies that the other three diagonal elements go to 0). We note that it is not necessary to specify the whole density matrix of the noisy pairs because in the QPA algorithm the off-diagonal elements do not contribute on average (i.e. averaging over the ensemble of distributed pairs at each step of the procedure) to the evolution of the diagonal ones and therefore they are not significant in the study of the efficiency of the scheme.

In the QPA procedure Alice and Bob divide the received noisy pairs into groups of two pairs each and perform the following operations on each group. Alice performs the unitary operation

$$U_A = \frac{1}{\sqrt{2}} \begin{pmatrix} 1 & -i \\ -i & 1 \end{pmatrix} \quad (8.21)$$

on each of her two qubits; Bob performs the inverse operation

$$U_B = \frac{1}{\sqrt{2}} \begin{pmatrix} 1 & i \\ i & 1 \end{pmatrix} \quad (8.22)$$

on his. Note that if the qubits are spin- $\frac{1}{2}$ particles and the computation basis is that of the eigenstates of the z components of their spins, then the two operations correspond respectively to rotations by $\pi/2$ and $-\pi/2$ about the x axis.

Then Alice and Bob each perform two instances of the quantum Controlled-NOT operation, described in Sect. 1.6,

$$\begin{array}{ccccc} \text{control} & \text{target} & \text{control} & \text{target} \\ |x\rangle & |y\rangle & \longrightarrow & |x\rangle & |x \oplus y\rangle \end{array} \quad (x, y) \in \{0, 1\}, \quad (8.23)$$

where one pair comprises the two control qubits and the other one the two target qubits, and \oplus denotes addition modulo two (a useful table describing the action of this bilateral Controlled-NOT operation in the Bell basis can be found in [49]). Alice and Bob then measure the target qubits in the computational basis (e.g. they measure the z components of the targets’ spins). If the outcomes coincide (e.g. both spins up or both spins down) they keep the control pair for the next round, and discard the target pair. If the outcomes do not coincide, both pairs are discarded. The basic operations of the QPA procedure are systematically reported in Fig. 8.5.

To see the effect of this procedure, let us assume that each pair is initially in the same state with diagonal elements $\{a, b, c, d\}$. In the case where the control qubits are retained, their density operator will have diagonal elements $\{A, B, C, D\}$ which depend, on average, *only* on the diagonal elements $\{a, b, c, d\}$:

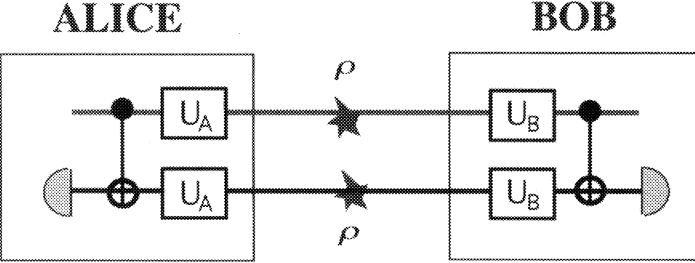


Fig. 8.5. Schematic representation of a QPA step. Alice performs operation U_A on her particles and a Controlled-NOT operation. Bob performs operation U_B and a Controlled-NOT operation. Alice and Bob then measure the target pair and keep the control pair for the next iteration if the results coincide.

$$A = \frac{a^2 + b^2}{p} \quad (8.24)$$

$$B = \frac{2cd}{p} \quad (8.25)$$

$$C = \frac{c^2 + d^2}{p} \quad (8.26)$$

$$D = \frac{2ab}{p}, \quad (8.27)$$

where $p = (a + b)^2 + (c + d)^2$ is the probability that Alice and Bob obtain coinciding outcomes in the measurements on the target pair. Equations (8.24–8.27) describe an elementary step of the QPA algorithm. The procedure is then iterated by applying again the above elementary step to the surviving pairs from the previous iteration. Note that if the average value of the fidelity is driven to 1 then each of the surviving pairs must individually approach the pure state $|\phi^+\rangle\langle\phi^+|$.

In passing we note that if the two input pairs are described by different density operators ρ and ρ' with diagonal elements $\{a, b, c, d\}$ and $\{a', b', c', d'\}$ respectively, then the retained control pairs will, on average, have diagonal elements given by:

$$A = \frac{aa' + bb'}{p} \quad (8.28)$$

$$B = \frac{c'd + cd'}{p} \quad (8.29)$$

$$C = \frac{cc' + dd'}{p} \quad (8.30)$$

$$D = \frac{ab' + a'b}{p}, \quad (8.31)$$

where $p = (a + b)(a' + b') + (c + d)(c' + d')$, which generalises (8.24–8.27).

Several interesting properties of the QPA map (8.24–8.27) can be easily verified. For example if at any stage the fidelity a exceeds $\frac{1}{2}$, then after one more iteration, it still exceeds $\frac{1}{2}$. Although a does not necessarily increase monotonically as a function of the number of iterations, our target point, $A = 1$, $B = C = D = 0$, is a fixed point of the map, and is the only fixed point in the region $a > \frac{1}{2}$. It can be easily seen analytically that it is a local attractor, namely that $A > a$ for a close to 1.

An analytical proof that it is also a global attractor in the region $a > \frac{1}{2}$ has been recently obtained [390]. The proof is based on showing that the function $f(a, b) = (2a - 1)(1 - 2b)$ is monotonic as a function of the number of iterations and asymptotically approaches unity. This implies that if we begin with pairs whose average fidelity exceeds $\frac{1}{2}$, but which are otherwise in an arbitrary state containing arbitrary correlations with the environment, then the states of pairs surviving after successive iterations always converge to the unit-fidelity pure state $|\phi^+\rangle$. It can also be shown [390] that the QPA procedure is always successful for any initial value $b > \frac{1}{2}$ (leading to the pure state $|\phi^+\rangle$) and for any initial value $c > \frac{1}{2}$ or $d > \frac{1}{2}$ (leading in this case to the pure state $|\psi^+\rangle$). In contrast, when none of the diagonal elements of the initial density operator exceeds 1/2 the procedure does not work.

Notice also that the QPA is capable of purifying a collection of pairs in any state ρ whose average fidelity with respect to at least one maximally entangled state (i.e. a Bell state or a state obtained from a Bell state via local unitary operations) is greater than $\frac{1}{2}$. This is due to the fact that any state of that type can be transformed into $|\phi^+\rangle$ via local unitary operations [73]. If we denote by \mathcal{B} the class of pure, maximally entangled states (the generalised Bell states) then the condition that the state ρ can be purified using the QPA is given by

$$\max_{\phi \in \mathcal{B}} \langle \phi | \rho | \phi \rangle > \frac{1}{2}. \quad (8.32)$$

The speed and the convergence behaviour of the procedure depends on the value of the diagonal elements of the initial density operator. As an example, in Fig. 8.6 we plot the fidelity as a function of the initial fidelity and the number of iterations, in cases where $a > \frac{1}{2}$ and $b = c = d$ initially.

The QPA procedure is rather wasteful in terms of discarded particles: at least one half of the particles (the ones used as targets) is lost at every iteration. Still the efficiency of this scheme compares favourably with the first proposed entanglement purification scheme described in [49] (about 1000 times more efficient for a close to 0.5, i.e. the number of surviving pairs is 1000 times bigger for a prescribed value of final fidelity).

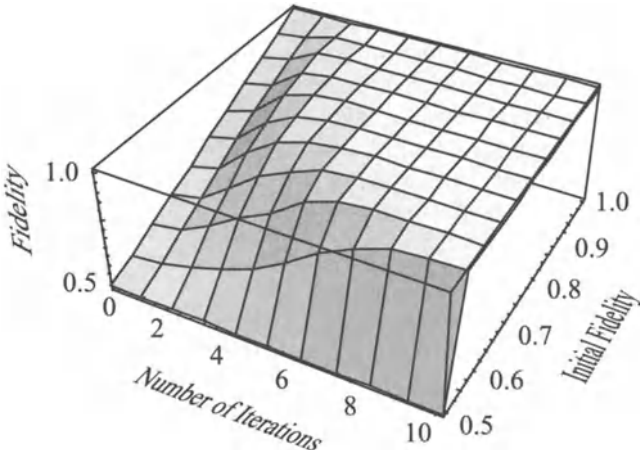


Fig. 8.6. Average fidelity as a function of the initial fidelity and the number of iterations for initial states with $b = c = d$.

8.5 Generalisation of Purification to Multi-Particle Entanglement

M. Murao, M.B. Plenio, S. Popescu, V. Vedral, P.L. Knight

In this section, direct purification protocols proposed in [391] are described for a wide range of mixed diagonal states of N particle entanglement. Although the procedures are not as general as those for two-particle purification of Bennett et al. [49] and Deutsch et al. [47], they are important for our understanding of multi-particle entanglement and have important practical applications. For many spin-1/2 particles, the maximally entangled states are

$$|\phi^\pm\rangle = \frac{1}{\sqrt{2}} (|00\cdots 0\rangle \pm |11\cdots 1\rangle), \quad (8.33)$$

together with those that are locally unitarily equivalent. The state for each particle is written in the $\{|0\rangle, |1\rangle\}$ basis; for three particles, these are called GHZ states [290].

Purification procedures [47, 49, 117, 382] “distill” from an ensemble of entangled *mixed* states a sub-ensemble of maximally entangled *pure* states by using local operations and classical communications. For two particles, the singlet state $|\psi^-\rangle = (|01\rangle - |10\rangle)/\sqrt{2}$, which is totally antisymmetric, is invariant under any bilateral rotation and plays an important role in these purification schemes.

However, for three or more particles, there is no maximally entangled state which is invariant under trilateral (multi-lateral) rotations (for a classification of entangled states based on invariance under local unitary transformations,

see [392]). Local rotations map maximally entangled states into a superposition of maximally entangled states (unless we have trivial rotations by $n\pi$ where n is an integer). This makes it more difficult to transform an *arbitrary* state into one of the Werner states, which makes the search for general purification protocols much less straightforward.

Although there is no maximally entangled state invariant under random bilateral rotations for $N \geq 3$ (where N is the number of entangled particles), we will call the state

$$\rho_W = x |\phi^+\rangle\langle\phi^+| + \frac{1-x}{2^N} \mathbf{1} \quad (8.34)$$

a “Werner-type state” because of the similarity with the two particle case. Note that we write $|\phi^+\rangle$ instead of $|\psi^-\rangle$ for convenience. The aim of purification is the distillation of a sub-ensemble in the state $|\phi^+\rangle$. The fidelity,

$$f = \langle\phi^+| \rho_W |\phi^+\rangle \quad (8.35)$$

of the Werner-type state is $f = x + (1-x)/2^N$. These Werner-type states are important practically, because mixed entangled states are likely to appear when one has an ensemble of initially maximally entangled states (for example, $|\phi^+\rangle$) of N particles, and then transmits the N particles to N different parties via noisy channels (Fig. 8.7).

Consider the effect of a noisy channel, whose action on each particle can be expressed by random rotations about random directions. Each noisy channel causes random rotations (around a random direction and by a random angle) with probability $1 - x$, but leaves the particle unaffected with probability x . The state after transmission through such a channel becomes the Werner-type state given by (8.34).

In the following, a protocol is presented (P1+P2 in Fig. 8.8), which can purify a Werner-type state, provided the fidelity of the initial mixed state is

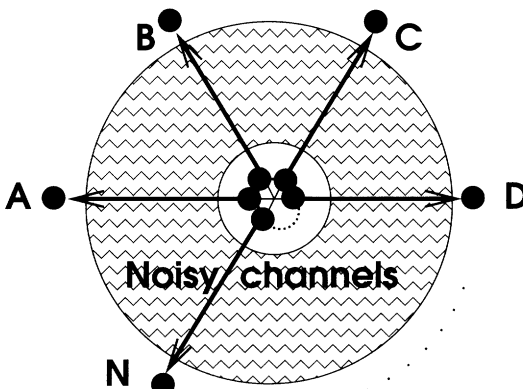


Fig. 8.7. Transmission of N particles in the maximally entangled state to different parties (A, B, C, D, ..., N) via noisy channels.

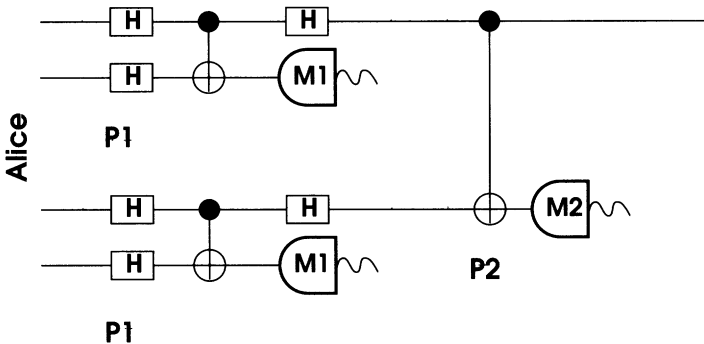


Fig. 8.8. Purification protocol P_1+P_2 . H is a Hadamard transformation, M_1 and M_2 are local measurement and classical communication. This diagram shows four particles belonging to Alice. Bob and others apply exactly the same procedure.

higher than a certain critical value. The advantage of this protocol is that Werner-type states for *any number of particles* can be *directly* purified.

In the protocol P_1+P_2 , each party (Alice, Bob et al.) perform iterations of the operations P_1 followed by P_2 on the particles belonging to them.

- The operation P_1 consists of a local Hadamard transformation which maps $|0\rangle \rightarrow (|0\rangle + |1\rangle)/\sqrt{2}$, $|1\rangle \rightarrow (|0\rangle - |1\rangle)/\sqrt{2}$, a local CNOT (Controlled NOT) operation and a measurement M_1 , and another local Hadamard transformation. In M_1 , we keep the control qubits if an even number of target qubits are measured to be in the state $|1\rangle$, otherwise the control qubits are discarded. For example when purifying for three particles, we only keep $|000\rangle$, $|011\rangle$, $|101\rangle$, $|110\rangle$.
- The operation P_2 consists of a local CNOT operation and a measurement M_2 in which we keep the control qubits if all target bits are measured to be in the same state, otherwise the control qubits are discarded. For example, when purifying three particles, we only keep $|000\rangle$ and $|111\rangle$. In this operation, the diagonal and off-diagonal elements of the density matrix are independent of each other, so that the off-diagonal elements do not affect the purification.

The purification scheme, however, is not restricted to Werner-states. There are several types of states which can be purified by the protocol P_1 or P_2 alone. For example, if the initial mixed state does not have any weight of the pairing state (we call the state $|\phi^-\rangle$ the “pairing state” of $|\phi^+\rangle$) and weights of other states are equal (or even when some weights are zero), iterations of the operation P_2 only are sufficient to purify the initial ensemble to the $|\phi^+\rangle$ state (see [391] for more in detail).

In the purification protocols discussed above, many-particle entangled states are *directly* purified. This is necessary for fundamental investigation of characteristic multi-particle entanglement. However, one could imagine

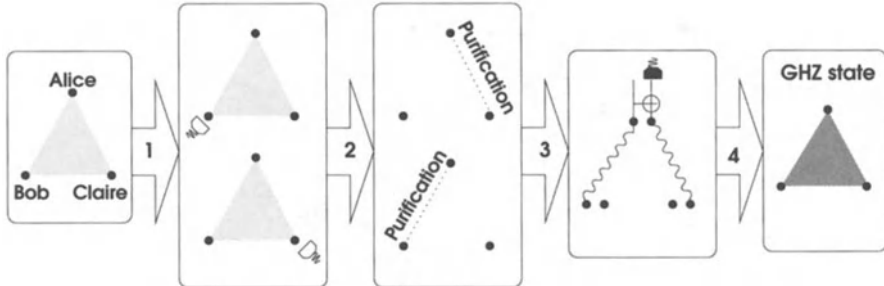


Fig. 8.9. Purification scheme via two-particle purification. The dotted lines represent partial entanglement and the wavy lines represent maximum entanglement. The first measurements (represented by white detector symbols) are in the state $|\chi^\pm\rangle = (|0\rangle \pm |1\rangle)/\sqrt{2}$ and the second measurement (represented by a black detector symbol) is, in the state $|0\rangle$ or $|1\rangle$.

schemes which purify many-particle entanglement via two-particle purification: one of these schemes for three particles (of Alice, Bob, and Claire) uses the fact that we know how to purify two particles. So this scheme converts three-particle states into two-particle states, then purifies these two-particle states, and finally re-converts them to three-particle entangled states. The algorithm for this protocol appears more complicated when described in words, so we provide a figure (Fig. 8.9) to help the reader visualise the entire scheme. This involves the following:

1. Divide the entire ensemble of the state for three particles into two equal sub-ensembles.
2. Bob then projects particles of one sub-ensemble onto

$$|\chi^\pm\rangle = (|0\rangle \pm |1\rangle)/\sqrt{2}$$

and Claire performs the same projection using the other sub-ensemble. When Bob or Claire obtain a successful projection onto $|\chi^-\rangle$, then they instruct Alice to perform the σ_z operation on her particles. If they obtain a successful projection onto $|\chi^+\rangle$, then Alice is instructed to do nothing. The end product of these operations are two sub-ensembles of two-particle entangled states (one pair shared by Alice and Bob, and another pair shared by Alice and Claire).

3. Then Alice and Bob, and separately Alice and Claire perform the two-particle purification protocol in [47, 117] to each of the entangled sub-ensembles of two particles. This results in two maximally entangled ensembles of pairs of particles, shared between Alice and Bob, and between Alice and Claire.
4. Alice now wants to obtain a single GHZ state out of two maximally entangled pairs shared between herself and Bob and Claire. To do this, she chooses one entangled pair from each sub-ensemble and then performs

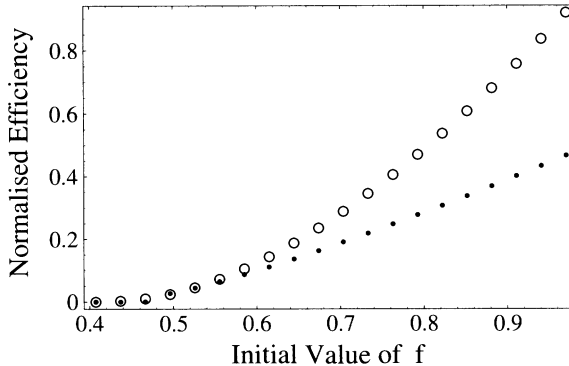


Fig. 8.10. Normalised efficiency of purification of the Werner-type states for three particles against the initial value of fidelity f . The circles are obtained numerically by the purification protocol P1+P2 with a choice of accuracy 10^{-7} . The dots are obtained by the purification scheme via two-particle purification with the same choice of accuracy.

a CNOT operation on her two particles. Then she projects the target particle onto $|0\rangle$ or $|1\rangle$. If Alice obtains a successful projection onto $|1\rangle$, she instructs Claire to perform the σ_x operation on her particle, and otherwise, do nothing. Then we obtain a sub-ensemble containing the maximally entangled GHZ state [300, 303].

We now analyse this indirect scheme and compare it to the direct purification schemes. Any efficient direct three-particle purification scheme should perform better than this indirect method via two particles. We note that we only obtain *one* maximally entangled state of three particles from *two* maximally entangled states of two particles by this scheme (Fig. 8.10, in detail see [391]). For purification of N -particle entangled states, we get one maximally entangled state from $N - 1$ maximally entangled states of two particles. In addition, the number of two-qubit CNOT operations, each of which is difficult in practice to carry out to high accuracy, is greater than in our direct scheme. These “inefficiencies” are the main practical disadvantage of the two-particle scheme.

For two-particle entanglement, an initial fidelity $f > 1/2$ is sufficient for successful purification [47] if we have no knowledge of the initial state. The situation is different if we possess additional information about the state, in which case any entangled state can be purified [50]. However, the sufficiency condition is not as simple for more than three particles. We have found several different criteria, depending on the type of mixed states.

For the Werner-type states of the form $\rho_W = x|\phi^+\rangle\langle\phi^+| + \frac{1-x}{2^N}\mathbf{1}$, and purification by the protocol P1+P2, we obtain numerically the results shown in Table 8.1.

Table 8.1. A: Observed fidelity limit of initial states to be purified for N particles of the Werner-type states by the *direct* protocol P1+P2, B: Theoretical fidelity limit of the *indirect* purification scheme via two-particle purification, and C: the theoretical minimum sufficient fidelity for purification.

N	A	B	C
2	$f \geq 0.5395$	$f > 1/2 = 0.5$	$f > 1/2$
3	$f \geq 0.4073$	$f > 5/12 \approx 0.4167$	unknown
4	$f \geq 0.313$	$f > 3/8 = 0.375$	unknown
5	$f \geq 0.245$	$f > 17/48 \approx 0.3542$	unknown
6	$f \geq 0.20$	$f > 11/32 \approx 0.3438$	unknown

The theoretical fidelity limit for the Werner-type states ρ_W of the purification scheme via two-particle purification is determined by the condition that the fidelity f_r of the reduced two-particle states should satisfy $f_r > 1/2$. For example, for three particles, the Werner state having initial fidelity $f = x + (1 - x)/8$ is reduced to a two-particle state after the measurement of Bob or Claire as follows

$$\rho_r = x |\phi^+\rangle\langle\phi^+| + \frac{1-x}{4} \mathbf{1}. \quad (8.36)$$

The fidelity of the reduced two-particle state is now $f_r = (1 + 6f)/7$. For four particles, we have $f_r = (1 + 4f)/5$, for five particles, $f_r = (7 + 24f)/31$, for six particles, $f_r = (5 + 16f)/21$ and so on. We see from Table 8.1 that the protocol P1+P2 is not optimal for two particles. So it may not be optimal for $N > 2$. However, for more than three particles, our observed fidelity limit is lower than that obtained by the purification scheme via two-particle purification.

For states having no weight of $|\phi^-\rangle\langle\phi^-|$ and equal weight of all other states except $|\phi^+\rangle\langle\phi^+|$, the fidelity limit of purification by the protocol P2 is $f > 2^{-(N-1)}$. The fidelity limit obtained by the purification scheme via two-particle purification is $2/5 = 0.4$ for the three-particle case, $65/23 \approx 0.35846$ for the four-particle case, $125/377 \approx 0.328912$ for five-particle case and so on, i.e. worse than that in our protocols.

As we have seen, the fidelity limit of purifiable initial states depends on the distribution of the weight of other diagonal states. This is a condition of a different character from the case of two particles [47]. For two particles, the distribution of weights of other diagonal elements was basically irrelevant for purification, since any distribution of weights of the other diagonal can be transformed into an even distribution by local random rotations of both particles, without changing the amount of entanglement. This suggests that there may be additional structure for many-particle entangled mixed states, which does not exist for two-particle mixed states.

8.6 Quantum Networks II: Communication over Noisy Channels

H.-J Briegel, W. Dür, S.J. van Enk, J.I. Cirac, P. Zoller

We show how to create maximally entangled EPR pairs between spatially distant atoms, each of them inside a high-Q optical cavity, by sending photons through a general, noisy channel, such as a standard optical fibre. An error correction scheme that uses few auxiliary atoms in each cavity effectively eliminates photon absorption and other transmission errors. For communication over distances much longer than the absorption length or the coherence length of the channel, we describe a novel nested purification protocol, which realises the analogue of a repeater in classical communication.

8.6.1 Introduction

This section continues and generalises the discussion of Sect. 6.2. There, a realisation of a quantum network [278] was proposed, using long-lived states of atoms as the physical basis for storing qubits, and photons as a means for transferring these qubits from one atom to another. To allow for a controlled transfer of the qubit, the atoms are embedded in high finesse optical cavities which are connected by an optical fibre, as shown in Fig. 6.1.

The compound cavity–fibre system, together with the laser pulses constitutes what we abstractly call a *noisy quantum channel*, see Fig. 8.11. When the photons are sent along optical fibres, photon absorption will be a dominant transfer error. Losses will also occur by incoherent scattering on the surface of the cavity mirrors and at the coupling segments between the cavities and the fibre. Another typical transfer error will be caused by imperfectly designed laser pulses for the Raman transition, and an example for a local gate error is spontaneous emission in one of the atoms during the gate operation.

This section shows how high fidelity communication is possible even in the presence of errors due to dissipation and noise, and how one can combat

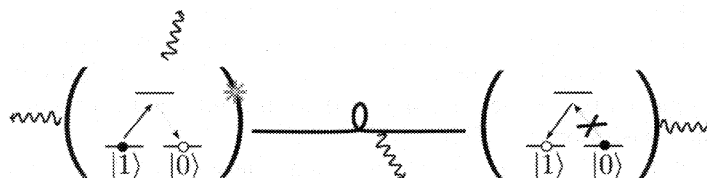


Fig. 8.11. Noisy photon channel: Typical transfer errors include photon absorption, incoherent scattering, and imperfect Raman transitions.

the effects of decoherence. First, we will briefly summarise the arguments of Sect. 6.2, which gives us the opportunity to introduce a notation that is adapted to the language of error correction and quantum information theory. In Sect. 8.6.3 and 8.6.4 we then concentrate on transmission errors that occur during the photon transfer and show how they can be detected and corrected [393]–[395]. For this discussion we assume that local gate operations and measurements can be performed without errors. In Sect. 8.7, we relax this assumption and allow all operations, both local and in the transmission, to be *imperfect*. This reflects the general situation when we have used all means of error correction but cannot exclude the possibility that some errors have escaped our detection and have thus not been corrected, or that the operations and measurements we use are, in some sense, imprecise. In this general context, we study the important problem of ‘long-distance’ communication and the use of quantum repeaters [381, 387].

From a formal perspective it is advantageous to rephrase quantum communication as the problem of creating distant quantum correlations over a channel, instead of directly propagating an unknown qubit through the channel. Once an EPR pair is created, it *can* be employed for teleportation [74], that is real transmission of information, but also for other purposes such as secret key distribution for quantum cryptography [46]. It is worth pointing out that this approach is different from quantum computation in the sense that, until the full EPR is established, there is no genuine information being processed. All one does is to build up nonlocal quantum correlations which may later be used for transmission purposes. In fact, at that later time, the connecting channel need not even exist any more.

The subject of this chapter is therefore how to create an EPR pair between two parties A and B with the aid of a noisy quantum channel of arbitrary length l that connects A and B .

8.6.2 Ideal Communication

Ideally, the scheme in Sect. 6.2 realises the following transmission

$$[\alpha|0\rangle_A + \beta|1\rangle_A]|0\rangle_B \longrightarrow |0\rangle_A [\alpha|0\rangle_B + \beta|1\rangle_B], \quad (8.37)$$

where an unknown superposition of internal states $|0\rangle = |e\rangle$ and $|1\rangle = |g\rangle$ in atom A in the first cavity is transferred to atom B in the second cavity, see again Fig. 8.12. The cavities may be part of a larger network, so we often refer to them as node A and node B , respectively. The selected internal states $|0\rangle$ and $|1\rangle$ of the atoms define, in the language of quantum information theory, the ‘computational basis’ for the qubit.

It is important to realise that the atom A may be entangled to other atoms in the same cavity or at other nodes of the network. In that situation, the coefficients α and β in (8.37) are no longer complex numbers but denote unnormalised states of the other atoms. Thus the transmission (8.37) can be

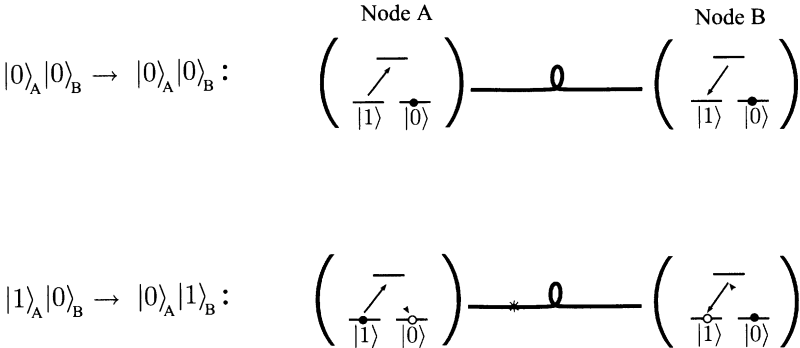


Fig. 8.12. Swapping the state of an atom from node A to node B. When the atom at A is in state $|1\rangle_A$, a sequence of Raman transitions as described in Sect. 6.2 can be used to swap its state onto the atom located at node B via photonic transfer. When atom A is in state $|0\rangle_A$, the Raman pulse does not change the state. A superposition of states $|0\rangle_A$ and $|1\rangle_A$ is thereby transferred to node B according to (8.38).

used to transfer single atomic states, but also to transfer *entanglement*. For instance, starting from single particle states, an EPR pair can be created by a two-step process

$$\begin{aligned} [\alpha|0\rangle_A + \beta|1\rangle_A] |0\rangle_{A_2} |0\rangle_B &\longrightarrow [\alpha|0\rangle_{A_2} |0\rangle_A + \beta|1\rangle_{A_2} |1\rangle_A] |0\rangle_B \\ &\longrightarrow |0\rangle_{A_2} [\alpha|0\rangle_A |0\rangle_B + \beta|1\rangle_A |1\rangle_B]. \end{aligned} \quad (8.38)$$

Here, the first arrow refers to a *local* CNOT operation between two atoms A and A_2 in the first cavity. The second arrow transfers the state of A_2 to B , thereby transferring the entanglement between the atoms A and A_2 to an entanglement between atoms A and B . At the end of this composite transformation, the state of the auxiliary atom A_2 is the same as initially and *factors out*. For $\alpha = \beta$, an ideal EPR pair is created.

8.6.3 Correction of Transfer Errors: The Photonic Channel

In a realistic model, we have to consider the possibility that the transfer of the atomic state from cavity A to B is imperfect. There is a certain probability that the atom in B will not be excited, even though A was excited. This is due to the interaction of the compound atom–cavity–fibre system with the environment which, even if small, in principle always exists. This results in an entanglement of the atomic states in (8.37) with the environment, i.e. the cavity walls, the fibre, and the radiation field of the free space.

In the following, we assume that photons can be absorbed but not created by the channel. This is a very good approximation for optical photons, where

the mean thermal number of photons in the cavities and the fibre is exceedingly small. In this situation, the most general expression for an imperfect transfer operation is of the form

$$\begin{aligned} |0\rangle_A|0\rangle_B|E\rangle &\longrightarrow |0\rangle_A|0\rangle_B|E_0\rangle \\ |1\rangle_A|0\rangle_B|E\rangle &\longrightarrow |0\rangle_A|1\rangle_B|E_1\rangle + |0\rangle_A|0\rangle_B|E_a\rangle, \end{aligned} \quad (8.39)$$

where $|E\rangle, |E_0\rangle, \dots$ denote unnormalised states of the environment. It is expedient to write $|E_0\rangle = \mathcal{T}_0|E\rangle, |E_1\rangle = \mathcal{T}_1|E\rangle, |E_a\rangle = \mathcal{T}_a|E\rangle$, thereby introducing operators that entangle the system with the environment. With this notation, (8.39) can be expressed in the compact form⁸

$$\begin{aligned} |0\rangle_A|0\rangle_B &\longrightarrow |0\rangle_A|0\rangle_B\mathcal{T}_0 \\ |1\rangle_A|0\rangle_B &\longrightarrow |0\rangle_A|1\rangle_B\mathcal{T}_1 + |0\rangle_A|0\rangle_B\mathcal{T}_a, \end{aligned} \quad (8.40)$$

which defines the photonic channel [394].

The optical cavities together with the fibre form a compound optical system with a certain resonant structure that defines its spectrum of quasi modes, its relaxation constants, etc. In the special case when only photon absorption plays a role, the operators in (8.40) have a simple form. For optical frequencies, the state of the environment can be very well approximated by the vacuum state, so one can write $\mathcal{T}_0 = 1, \mathcal{T}_1 = \alpha(\tau) \sim e^{-\kappa\tau}, \mathcal{T}_a = \sum_j \beta_j(\tau)b_j^\dagger$, with $\sum_j |\beta_j(\tau)|^2 \sim 1 - e^{-2\kappa\tau}$ where κ is the damping rate of the total (atom-)cavity-fibre system, and τ is the transfer time. The operators b_j^\dagger, b_j are amplitude operators of the j th oscillator mode of the environment.

More generally, the operators $\mathcal{T}_{0,1,a}$ in (8.40) may describe spontaneous emission processes, photon absorption, as well as transitions to and repumping from other internal states of the atoms. Thus, all complicated physics is hidden in the three operators. In this general (non-stationary) situation, the time dependence of the environmental terms has to be taken into account. The operators $\mathcal{T}_{0,1,a}$ then depend on the initial time when the transfer starts. As a consequence, when iterating the channel (8.40), the temporal ordering of the operators becomes important, e.g. $\mathcal{T}_1(t_1)\mathcal{T}_0(t_0) \neq \mathcal{T}_0(t_1)\mathcal{T}_1(t_0)$.

When using (8.40) to create an EPR pair as in (8.38), we obtain

$$\begin{aligned} [\alpha|0\rangle_A + \beta|1\rangle_A]|0\rangle_B &\longrightarrow [\alpha|0\rangle_A|0\rangle_B\mathcal{T}_0 + \beta|1\rangle_A|1\rangle_B\mathcal{T}_1] \\ &\quad + \beta|1\rangle_A|0\rangle_B\mathcal{T}_a. \end{aligned} \quad (8.41)$$

For $\alpha = \beta$, this expression can be written in the form⁹

⁸ In expressions of this type, it is understood that both the left- and the right-hand sides are applied to a given state of the environment. Using this compact notation keeps the expressions much more transparent when twofold or more complex applications of the channel are studied.

⁹ Throughout this section, normalisation factors are omitted unless they are needed.

$$|\Phi_{AB}^+\rangle [\mathcal{T}_0 + \mathcal{T}_1] + |\Phi_{AB}^-\rangle [\mathcal{T}_0 - \mathcal{T}_1] + (|\Psi_{AB}^+\rangle + |\Psi_{AB}^-\rangle) \mathcal{T}_a, \quad (8.42)$$

where we use the Bell basis

$$|\Phi_{AB}^\pm\rangle = \frac{1}{\sqrt{2}} (|0\rangle_A |0\rangle_B \pm |1\rangle_A |1\rangle_B), \quad |\Psi_{AB}^\pm\rangle = \frac{1}{\sqrt{2}} (|0\rangle_A |1\rangle_B \pm |1\rangle_A |0\rangle_B).$$

The fidelity of the resulting pair (8.42) can be defined by its overlap with the ideal result $|\Phi_{AB}^+\rangle$. This overlap is given by the norm

$$F = \left\| \frac{[\mathcal{T}_0 + \mathcal{T}_1] |E\rangle}{2} \right\|^2 \sim \left| \frac{1 + e^{-\kappa\tau}}{2} \right|^2. \quad (8.43)$$

The estimate of F in the second term demonstrates how the coupling of the modes of the cavity–fibre system to the environment reduces the attainable fidelity of the EPR pair. In particular, F decreases exponentially with the transfer time and the corresponding length of the fibre.

In order to create an EPR pair over a distance comparable to or larger than the absorption length of the photonic channel, we need to find a method to *detect and correct* a photon loss that may occur during the transfer. Loosely speaking, we are seeking to eliminate the absorption term \mathcal{T}_a in (8.42), and to minimise the other term $\mathcal{T}_0 - \mathcal{T}_1$.

In the following, we outline a method that uses either one or two auxiliary atoms in each cavity. This outline just summarises the essential steps. For details, the reader should consult Refs. [393]–[395].

8.6.4 Purification with Finite Means

The main idea is to entangle the atom in the first cavity with auxiliary (backup) atoms, before transmitting the information. This is reminiscent of a redundant coding scheme, with the fundamental difference that our scheme allows one to correct errors to *all orders* in the photo-absorption probability. By measuring a certain joint state of two atoms in the receiver cavity, one is able to *detect* a photon loss while *maintaining* the initial coherence of the atomic state that was sent. Therefore, the transmission can be repeated as often as necessary until no error is detected.

In detail, this requires three steps:

- (1) *Encoding* of the atomic state into a three-particle entangled state

$$\begin{aligned} \alpha |0\rangle_A + \beta |1\rangle_A &\longrightarrow \alpha [|0\rangle_A |0\rangle_{A_2} |0\rangle_{A_3} + |1\rangle_A |1\rangle_{A_2} |1\rangle_{A_3}] \\ &\quad + \beta [|0\rangle_A |0\rangle_{A_2} |1\rangle_{A_3} + |1\rangle_A |1\rangle_{A_2} |0\rangle_{A_3}]. \end{aligned} \quad (8.44)$$

This can be realised by applying two CNOT operations between A_3 and A , and A and A_2 , respectively.

- (2) *Transmission* of a photon *twice* by using (8.40) between atom A_2 and B_2 and then between A_2 and B , applying a local flip operation on A in between.

The result of this operation is a multi-particle entangled state [395] whose explicit form will not be given here.

(3) *Measuring* the states of certain backup atoms in both cavities. Combined with appropriate local unitary transformations, one obtains one of two results.

The effect of this procedure is summarised in the following *absorption-free* (i.e. correcting) channel

$$\begin{aligned} [\alpha|0\rangle_A + \beta|1\rangle_A]|0\rangle_B &\longrightarrow \alpha|0\rangle_A|0\rangle_B\mathcal{S}_0 + \beta|1\rangle_A|1\rangle_B\mathcal{S}_1 \\ &\quad \swarrow \text{error} \\ &[\alpha|0\rangle_A + \beta|1\rangle_A]|0\rangle_B\mathcal{S}_a. \end{aligned} \quad (8.45)$$

Owing to the twofold transmission process, the operators \mathcal{S} appearing in (8.45) are products of the \mathcal{T} operators, e.g. $\mathcal{S}_0 = \mathcal{T}_0\mathcal{T}_1$, $\mathcal{S}_1 = \mathcal{T}_1\mathcal{T}_0$, or in different order. The important feature to notice is that, depending on the results of the measurement in step (3), two outcomes are possible: If an error is detected, the state is projected onto the second line of (8.45) and the transmission can be repeated; if no error is detected, the state is projected onto the first line of (8.45), which completes the channel.

By using (8.45) instead of (8.40) one obtains

$$\begin{aligned} [|0\rangle_A + |1\rangle_A]|0\rangle_B &\longrightarrow |0\rangle_A|0\rangle_B\mathcal{S}_0 + |1\rangle_A|1\rangle_B\mathcal{S}_1 \\ &= |\Phi_{AB}^+\rangle\frac{1}{2}[\mathcal{S}_0 + \mathcal{S}_1] + |\Phi_{AB}^-\rangle\frac{1}{2}[\mathcal{S}_0 - \mathcal{S}_1]. \end{aligned} \quad (8.46)$$

For the simple example considered after (8.40), with $\mathcal{T}_0 = 1$ and $\mathcal{T}_1 = e^{-\kappa\tau}$, we have $\mathcal{S}_0 = e^{-\kappa\tau}$ and $\mathcal{S}_1 = e^{-\kappa\tau}$, thus the second term in (8.46) vanishes. In this situation, an ideal EPR pair is established after a *single* use of the channel (8.45). This corresponds to an average number of phototransmissions of $e^{2\kappa\tau}$.

More generally, a similar result is obtained when the state of the environment does not depend on the temporal ordering of the operators \mathcal{T}_0 and \mathcal{T}_1 . Such a *stationary environment* is defined by $\mathcal{T}_1(t_1)\mathcal{T}_0(t_0)|E\rangle = \mathcal{T}_0(t_1)\mathcal{T}_1(t_0)|E\rangle$, i.e. $\mathcal{S}_0|E\rangle = \mathcal{S}_1|E\rangle$. For any system with a stationary environment, an ideal EPR pair is created by a single application of (8.45).

For the discussion of the general, non-stationary case, let us first rewrite the result (8.46) in the form

$$|\Psi^{(1)}\rangle = |\Phi_{AB}^+\rangle|E_+^{(1)}\rangle + |\Phi_{AB}^-\rangle|E_-^{(1)}\rangle, \quad (8.47)$$

where $|E_\pm^{(1)}\rangle = \frac{1}{2}(\mathcal{S}_0 \pm \mathcal{S}_1)|E\rangle$. The norm (square) of the environment $|E_+^{(1)}\rangle$ determines the fidelity of the pair.

At this point, the key advantage of the absorption-free channel (AFC) comes into play, namely that it corrects errors in the transmission process while maintaining the coherence and possible entanglement of the state it is applied to. This allows an iterative purification protocol [394]. At each purification step, the pair is temporarily entangled with two auxiliary atoms,

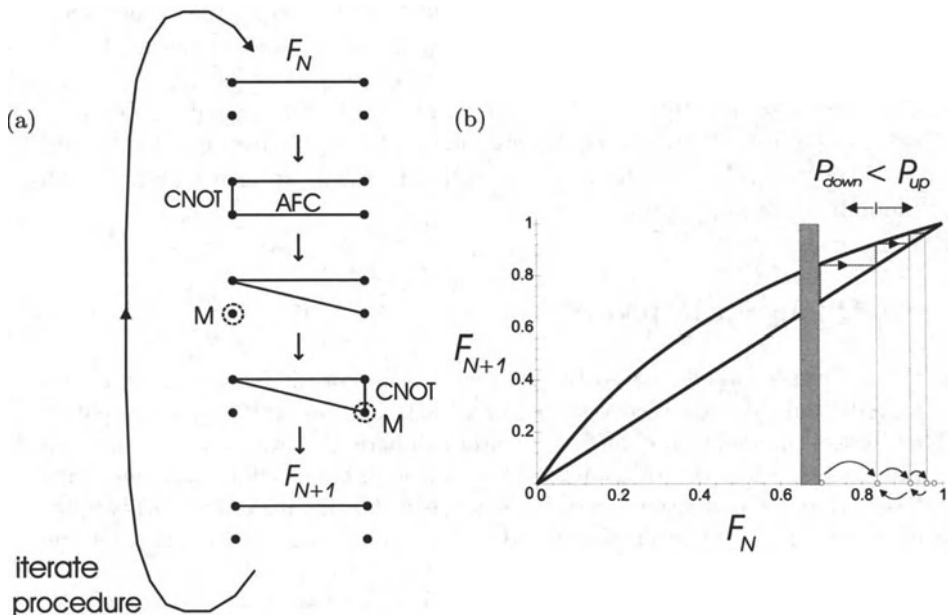


Fig. 8.13. Purification of an EPR pair with finite means. (a) Iterative purification protocol. At each purification step, an EPR pair of the form (8.48) with fidelity F_N is temporarily entangled with two auxiliary atoms. This involves two CNOT operations, the absorption-free channel AFC, and measurements M. Furthermore, there are some Hadamard transformations that are not shown in the figure. The value of the new fidelity F_{N+1} depends on the result of the measurements M, as explained in (b). Note that this scheme operates on the *same set of atoms* at each step, thereby realising a ‘self-purification process’. (b) One-sided random-walk process for fidelity. After each iteration step in (a), the fidelity F_N increases (decreases) with a certain probability P_{up} (P_{down}) that depends on N . If F_N happens to drop below the initial value F_0 , we reset the pair to this value by a single use of the AFC, as in (8.46). This is equivalent to a one-sided random walk process with reflections at a lower barrier at F_0 , as indicated in the figure. On average, the fidelity thereby approaches unity exponentially fast, $F_N \sim 1 - e^{-\text{const} \times N}$.

one at each node, using both local CNOT operations and the AFC. In some sense, this creates an auxiliary EPR pair that is used to purify (8.47). The detailed protocol is shown systematically in Fig. 8.13a.

This protocol transforms (8.47) into a sequence of states of the form

$$|\Psi^{(N)}\rangle = |\Phi_{AB}^+\rangle|E_+^{(N)}\rangle + |\Phi_{AB}^-\rangle|E_-^{(N)}\rangle, \quad (8.48)$$

where either

$$|E_\pm^{(N)}\rangle = \frac{1}{2}(\mathcal{S}_0 \pm \mathcal{S}_1)|E_\pm^{(N-1)}\rangle, \text{ or } |E_\pm^{(N)}\rangle = \frac{1}{2}(\mathcal{S}_0 \mp \mathcal{S}_1)|E_\pm^{(N-1)}\rangle,$$

depending on the result of the measurement. In the first case, which happens with probability $P_{\text{up}} = P_{\text{up}}^{(N)}$, the fidelity of the pair increases. In the second case, which happens with $P_{\text{down}} = 1 - P_{\text{up}}$, the fidelity decreases. One can show that this creates a stochastic process corresponding to a one-sided random-walk process as depicted in Fig. 8.13b. On average, the fidelity $F_N = \langle E_+^{(N)} | E_+^{(N)} \rangle$ thereby converges towards unity exponentially fast with the number of purification steps.

8.7 Quantum Repeaters

With the methods discussed in the previous sections, it is possible to create an EPR pair of high fidelity by sending single photons through a dissipative and noisy channel that connects the atoms. There is, however, a limitation to the method when the transmission time through the channel becomes much larger than its relaxation time, i.e. if $\kappa\tau \gg 1$. As the absorption probability grows exponentially with τ , so will the required number of repetitions for one successful transmission.

Absorption losses are well-known in problems of electric signal transmission through classical channels where, at regularly spaced intervals, repeaters are put in the channel. In classical (digital) communication technique such repeaters are used to both amplify and to restore the signal. The distance between the repeaters is then determined by the damping rate of the fibre and the bit rate of the transmission (dispersion effects).

For quantum communication, we cannot use amplifiers. To build up EPR correlations, single qubits (photons) need to be transmitted and these cannot be amplified [88, 396] without destroying the quantum correlations. All we can do here is to detect whether a photon has been absorbed and, whenever that is the case, repeat the transmission.

For the following discussion, let us assume that the dominant transmission error is given by photon absorption, and that the environment is stationary. This corresponds to a photonic channel (8.40) with $\mathcal{T}_0 = 1$ and $\mathcal{T}_1 = e^{-\kappa\tau} = e^{-l/2l_0}$ where $l_0 = c/2\kappa$ defines the half length of the fibre. The probability for a successful transmission of a qubit from A to B , as indicated in Fig. 8.14(top), is then $p(l) = e^{-l/l_0}$ where l is the length of the fibre. Correspondingly, the average number of required repetitions is

$$n(l) = \frac{1}{p(l)} = e^{l/l_0}. \quad (8.49)$$

It is clear that this leads to unrealistically high numbers for any experiment, if the fibre is much longer than a few half lengths l_0 .

Guided by the idea of repeaters in classical communication, we divide the channel into a certain number N of segments, with connection points (nodes) in between, at which it is measured whether a transmission error

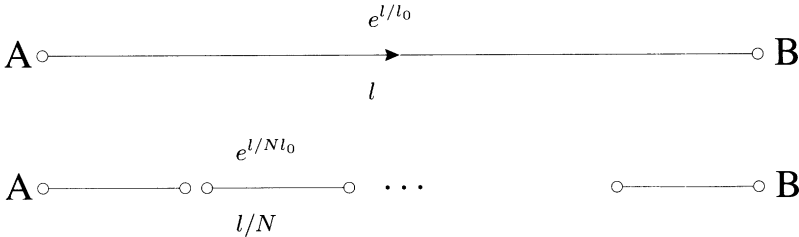


Fig. 8.14. Simple and compound fibre for transmission of single qubits from A to B . As with classical repeaters, to transmit single qubits over long distances, we divide the fibre (channel) into several segments, at the end of which transmission errors are measured.

has occurred (see Fig. 8.14(bottom)). This can be done e.g. with the method explained in Sect. 5.2 by using a few extra ions in a cavity. If an absorption error is detected, the transmission across that segment is repeated. Then a photon is sent through the subsequent segment, and so on. Thereby, ideally, the state of the atom at A can be swapped from one connection point to the next, until one reaches atom B . The average total number of repetitions on each segment is $n(l/N) = e^{l/l_0 N}$. Correspondingly, the total number of transmissions required for successfully sending the qubit across the *compound fibre* is

$$n_{\text{com}} = \frac{N}{p(l/N)} = Ne^{l/Nl_0}. \quad (8.50)$$

This is to be compared with (8.49). The compound fibre is thus preferable to the simple fibre if

$$Ne^{l/Nl_0} < e^{l/l_0}. \quad (8.51)$$

The optimum number of segments is given by the value of N that minimises the left-hand side of above equation, which is $N_{\min} = l/l_0$. The minimum number of transmissions along the compound fibre is thus given by (8.50) with $N = N_{\min}$, that is

$$n_{\min} = N_{\min} e^{l/N_{\min} l_0} = l/l_0 e^1. \quad (8.52)$$

This situation is realised when the connection points are placed along the fibre with a spacing corresponding to the half length l_0 .

Up to this point we have assumed that local operations can be performed without errors. There are, in fact, schemes [397] which allow error detection and correction for local 2-bit operations. However, even with these methods, there is the possibility of errors that escape detection, since the detection mechanism itself uses 1-bit operations and measurements which may not be perfect. This has two effects: (i) the local operations at every checkpoint in

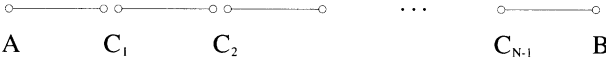


Fig. 8.15. Connection of a sequence of N EPR pairs, see text.

Fig. 8.14(bottom) will introduce some noise into the transmission process; (ii) the fidelity of transmission across every segment is already limited to some maximum value F_{\max} . This can be seen from the fact that both the absorption free channel (8.45) and the purification protocol of Fig. 8.13a involve local operations that introduce some noise and thereby limit the maximum attainable fidelity. Both effects accumulate (exponentially) with the number of checkpoints and eventually spoil the fidelity of the transmission completely.

To make this point clearer, we consider the following equivalent problem. We first create N elementary EPR pairs of fidelity $F_1 < F_{\max}$ between the nodes $A \& C_1$, $C_1 \& C_2$, \dots $C_{N-1} \& B$, as in Fig. 8.15. We then connect these pairs by making Bell measurements at the nodes C_i and classically communicating the results between the nodes as in the schemes for teleportation [74] and entanglement swapping [74, 398]. This will result in a single EPR pair shared between the endpoints A and B in Fig. 8.15. Unfortunately, with every connection the fidelity of the resulting pair will decrease, since the connection process involves imperfect operations that introduce noise. Furthermore, even for perfect connections, the fidelity decreases: Connecting e.g. two Werner states of fidelity F_1 by a Bell measurement, one obtains a new Werner state of fidelity

$$F_2 = \frac{1}{4} \left\{ 1 + 3 \left(\frac{4F_1 - 1}{3} \right)^2 \right\}, \quad (8.53)$$

so that $F_2 \sim F_1^2$ for $F_1 \sim 1$. Both effects accumulate with every connection and lead to an exponential decrease of the fidelity F_N with N of the final pair shared between $A \& B$. Eventually, the value of F_N drops below a certain threshold value $F_{\min} \geq 1/2$ below which it cannot be purified any more. That means, it will not be possible to increase the fidelity by purification [47, 49].

By dividing the channel into shorter segments, it seems, we have thus eliminated the effect of an exponentially increasing number of required transmissions, at the cost of introducing an exponentially decreasing fidelity!

A possibility to circumvent this limitation is to connect a smaller number $L \ll N$ of pairs so that $F_L > F_{\min}$ and purification becomes possible. The idea is to connect the resulting pairs, purify again, and continue in the same vein. The way in which such alternating sequences of connections and purifications is done has to be properly designed so that the number of required resources does not grow exponentially with N and thus with l .

In the remainder of this section we describe a *nested purification protocol* [381] which consists of connecting and purifying the pairs simultaneously in

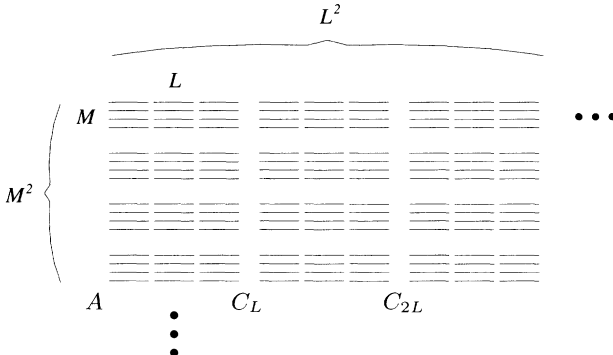


Fig. 8.16. Nested purification with an array of elementary EPR pairs.

the following sense (see Fig. 8.16). For simplicity, assume that $N = L^n$ for some integer n . On the first level, we simultaneously connect the pairs (initial fidelity F_1) at all the connection points except at $C_L, C_{2L}, \dots, C_{N-L}$. As a result, we have N/L pairs of length L (and fidelity F_L) between A & C_L , C_L & C_{2L} and so on. To purify these pairs, we need a certain number M of copies that we construct in parallel fashion. For keeping track of the resources, it is convenient to arrange them in form of an array of elementary pairs as is done in Fig. 8.16 for $L = 3$ and $M = 4$. We then use these copies on the segments A & C_L , C_L & C_{2L} etc., to purify and (re-)obtain one pair of fidelity F_1 on each segment. This last condition determines the (average) number of copies M that we need, which will depend on the initial fidelity, the degradation of the fidelity under connections, and the efficiency of the purification protocol. The total number of elementary pairs we used up to this point is LM . [In Fig. 8.16, this means that each group of $L \times M = 3 \times 4$ pairs has now been replaced by one single pair of the initial fidelity.] On the second level, we connect L of these larger pairs at every connection point C_{kL} ($k = 1, 2, \dots$) except at $C_{L^2}, C_{2L^2}, \dots, C_{N-L^2}$. As a result, we have N/L^2 pairs of length L^2 between A & C_{L^2} , C_{L^2} & C_{2L^2} , and so on of fidelity F_L . Again, we need M parallel copies of these long pairs to repurify up to a fidelity $\geq F_1$. The total number of elementary pairs involved up to this point is $(LM)^2$. [Now, the whole array of $3^2 \times 4^2$ pairs in Fig. 8.16 has been replaced by a single pair of fidelity F_1 .] We iterate the procedure to higher and higher levels, until we reach the n -th level. As a result, we have obtained a final pair between A & B of length N and fidelity F_1 . In this way, the total number R of elementary pairs will be $(LM)^n$, where M^n alone gives the number of required ‘parallel channels’ in Fig. 8.16. We can re-express this result in the form

$$R = N^{\log_L M + 1}, \quad (8.54)$$

which shows that the resources grow *polynomially* with the distance N .

The idea of nested purification is related to the idea of concatenated coding [399] which has been used in the context of fault-tolerant quantum computing [400]. That scheme allows one, in principle, to transmit a qubit over arbitrarily long distances with a polynomial overhead in the resources. It requires one, however, to encode a single qubit into an entangled state of a large number of qubits which is sent through the channel, and to operate on this code repeatedly during the transmission process. In contrast, in the nested purification scheme, we are not sending an arbitrary qubit through the channel, but creating EPR correlations across the whole channel simultaneously. While creating the correlations, there is no real quantum information being processed (although the EPR pair may subsequently be used for communication via teleportation). As a result, we obtain fidelity requirements on the local operations which are in the few-percent region. In the case of fault-tolerant quantum computing, this number is of the order of 10^{-5} [399].

The array in Fig. 8.16 represents an ensemble of identical (elementary) EPR pairs with which the purification is performed. Alternatively, one can do the purification with the aid of a single auxiliary pair at each level (see [381, 387]). In a sense, the vertical dimension of the diagram in Fig. 8.16 is thereby translated into a temporal axis (number of repetitions). In this case, it is the total *time* needed to create the EPR pair between *A* and *B* that scales polynomially in (8.54), whereas the number of backup atoms needed at each connection point grows only logarithmically with $N = l/l_0$. The resulting scheme of a quantum repeater is illustrated schematically in Fig. 8.17. Every connection point in the channel consists of a simple “quantum processor” that stores a small number of atoms on which it performs the gate operations and measurements required for purification. Some of the atoms are used to repeatedly build up EPR pairs between neighbouring connection

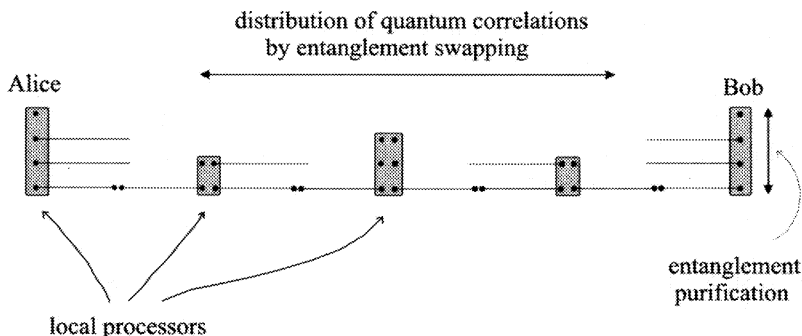


Fig. 8.17. Scheme for the quantum repeater. At every connection point, a small “quantum processor” (consisting of a few qubits only) is used to execute the protocols of entanglement purification and entanglement swapping. The distribution of high-fidelity entanglement across the compound channel is then coordinated by a global protocol called nested entanglement purification [381].

points (here $L=2$), for example by using the methods described in Sect. 8.6. These repeatedly created pairs are used for entanglement purification. More distant pairs are then created by entanglement swapping. To (re-)purify these more distant pairs, one auxiliary atom is needed for storage at each level. The total number that each processor has to store, thus grows only logarithmically with l [381, 387].

In contrast to the case in classical communication, the quantum repeater is not a local amplifier, but it involves both the local checkpoints and global (nested) purification protocol. We have just reported here that our scheme tolerates errors for local operations and measurements that are in the percent region. For more details, the reader should consult Refs. [381, 387].

References

1. R.P. Feynman, R.B. Leighton, and M. Sands, *The Feynman Lectures of Physics, Vol. III, Quantum Mechanics*, Addison-Wesley, Reading (1965).
2. G.I. Taylor, Proc. Camb. Phil. Soc. **15**, 114 (1909).
3. G. Möllenstedt and C. Jönsson, Z. Phys. **155**, 472 (1959); A. Tonomura, J. Endo, T. Matsuda, and T. Kawasaki, Am. J. Phys. **57**, 117 (1989).
4. A. Zeilinger, R. Gähler, C.G. Shull, W. Treimer, and W. Mampe, Rev. Mod. Phys. **60**, 1067 (1988).
5. O. Carnal and J. Mlynek, Phys. Rev. Lett. **66**, 2689 (1991).
6. S.L. Braunstein, A. Mann, and M. Revzen, Phys. Rev. Lett. **68**, 3259 (1992).
7. A. Zeilinger, Am. J. Phys. **49**, 882 (1981).
8. M.P. Silverman, *More than One Mystery: Explorations in Quantum Interference*, Springer, Berlin (1995).
9. E. Schrödinger, "Die gegenwärtige Situation in der Quantenmechanik", Naturwissenschaften, **23**, 807; 823; 844 (1935). English translation, "The Present Situation in Quantum Mechanics", Proc. of the American Philosophical Society, **124**, 323 (1980); reprinted in *Quantum Theory and Measurement* edited by J.A. Wheeler and W.H. Zurek, Princeton, 152 (1983).
10. M.A. Horne and A. Zeilinger, in: *Proceedings of the Symposium Foundations of Modern Physics*, P. Lahti, P. Mittelstaedt (Eds.), World Scientific, Singapore 435 (1985); M.A. Horne and A. Zeilinger, in: *Microphysical Reality and Quantum Formalism*, A. van der Merwe, et al. (Eds.), Kluwer, Dordrecht, 401 (1988).
11. J.S. Bell, Phys. World **3**, 33 (1990).
12. J.F. Clauser, M.A. Horne, A. Shimony, and R.A. Holt, Phys. Rev. Lett. **23**, 880 (1969).
13. D. Greenberger, M.A. Horne, A. Zeilinger, *Going beyond Bell's Theorem, in "Bell's Theorem, Quantum Theory, and Conceptions of the Universe"*, M. Kafatos (Ed.), Kluwer, Dordrecht, 69 (1989).
14. N.D. Mermin, Phys. Today **43**, No. 6, 9 (1990); D.M. Greenberger, M.A. Horne, A. Shimony, and A. Zeilinger, Am. J. Phys. **58**, 1131 (1990).
15. D. Bohm, *Quantum Theory*, Prentice-Hall, Englewood Cliffs, 614 (1951).
16. P.G. Kwiat, H. Weinfurter, T. Herzog, and A. Zeilinger, Phys. Rev. Lett. **74**, 4763 (1995).
17. K.F. Weizsäcker, Z. Phys. **40**, 114 (1931).
18. D. Bouwmeester, J.-W. Pan, M. Daniell, H. Weinfurter, and A. Zeilinger, Phys. Rev. Lett. **82**, 1345 (1999).
19. D. Bruss, A. Ekert, F. Huelga, J.-W. Pan, and A. Zeilinger, Phil. Trans. R. Soc. (London) A **355**, 2259 (1997).
20. N. Bohr, "Discussions with Einstein on Epistemological Problems in Atomic Physics" in *Albert Einstein: Philosopher-Scientist*, Edited by P.A. Schilpp, The Library of Living Philosophers, Evanston, 200 (1949).

21. A. Einstein, B. Podolsky, and N. Rosen, Phys. Rev. **47**, 777 (1935).
22. N. Bohr, Phys. Rev. **48**, 696 (1935).
23. J.S. Bell, *On the Einstein-Podolsky-Rosen paradox*, Physics **1**, 195 (1964), reprinted in J.S. Bell, *Speakable and Unspeakable in Quantum Mechanics*, Cambridge U.P., Cambridge (1987).
24. S.J. Freedman and J.S. Clauser, Phys. Rev. Lett. **28**, 938 (1972); A. Aspect, J. Dalibard, and G. Roger, Phys. Rev. Lett. **47**, 1804 (1982); W. Tittel, J. Brendel, H. Zbinden, and N. Gisin, Phys. Rev. Lett. **81**, 3563 (1998); G. Weihs, T. Jennewein, C. Simon, H. Weinfurter, and A. Zeilinger, Phys. Rev. Lett. **81**, 5039 (1998).
25. A. Aspect, P. Grangier, and G. Roger, Phys. Rev. Lett. **47**, 460 (1981); **49**, 91 (1982); A. Aspect, J. Dalibard, and G. Roger, ibid. **49**, 1804 (1982).
26. P.G. Kwiat, K. Mattle, H. Weinfurter, A. Zeilinger, A.V. Sergienko, and Y.H. Shih, Phys. Rev. Lett. **75**, 4337 (1995).
27. P.M. Pearle, Phys. Rev. D **2**, 1418 (1970); J.F. Clauser, A. Shimony, Rep. Prog. Phys. **41**, 1881 (1978).
28. E.P. Wigner, Am. J. Phys. 38, 1005 (1970).
29. D. Kahn, *The Codebreakers: The Story of Secret Writing*, Macmillan, New York (1967).
30. A.J. Menezes, P.C. van Oorschot, and S.A. Vanstone, *Handbook of Applied Cryptography*, CRC Press (1996).
31. B. Schneier, *Applied cryptography: protocols, algorithms, and source code in C*, John Wiley & Sons (1994).
32. D. Welsh, *Codes and Cryptography*, Clarendon Press, Oxford, (1988).
33. C.E. Shannon, Bell Syst. Tech. J. **28**, 656 (1949).
34. W. Diffie, and M.E. Hellman, IEEE Trans. Inf. Theory, **IT-22**, 644 (1976).
35. R. Rivest, A. Shamir, and L. Adleman, *On Digital Signatures and Public-Key Cryptosystems*, MIT Laboratory for Computer Science, Technical Report, MIT/LCS/TR-212 (January 1979).
36. P. Shor, (1994) *Proc. of 35th Annual Symposium on the Foundations of Computer Science*, (IEEE Computer Society, Los Alamitos), p. 124 (Extended Abstract). Full version of this paper appears in S. I. A. M. Journal on Computing, **26** (1997), 1484 and is also available at quant-ph/9508027.
37. S. Wiesner, *SIGACT News*, **15**, 78 (1983); original manuscript written circa 1970.
38. C.H. Bennett and G. Brassard, in "Proc. IEEE Int. Conference on Computers, Systems and Signal Processing", IEEE, New York, (1984).
39. J.F. Clauser and M.A. Horne, Phys. Rev. D **10**, 526 (1974).
40. B. Huttner and A. Ekert, J. Mod. Opt., **41**, 2455 (1994).
41. P.D. Townsend, Nature **385**, 47 (1997).
42. C.H. Bennett, F. Bessette, G. Brassard, L. Salvail, and J. Smolin, J. Cryptol. **5**, 3 (1992).
43. A. Muller, J. Breguet, and N. Gisin, Europhys. Lett. **23**, 383 (1993).
44. A.K. Ekert, J.G. Rarity, P.R. Tapster, and G.M. Palma, Phys. Rev. Lett. **69** 1293 (1992).
45. C.H. Bennett, Phys. Rev. Lett. **68**, 3121 (1992).
46. A.K. Ekert, Phys. Rev. Lett. **67**, 661 (1991).
47. D. Deutsch, A. Ekert, R. Jozsa, C. Macchiavello, S. Popescu, and A. Sanpera, Phys. Rev. Lett. **77**, 2818 (1996); C. Macchiavello, Phys. Lett. A **246**, 385 (1998).
48. Q.A. Turchette, C.J. Hood, W. Lange, H. Mabuchi, and H.J. Kimble, Phys. Rev. Lett. **75**, 4710 (1995).

49. Bennett, C. H., Brassard, G., Popescu, S., Schumacher, B., Smolin, J. A., Wootters, W. K. Purification of noisy entanglement and faithful teleportation via noisy channels. *Phys. Rev. Lett.* **76**, 722-725 (1996).
50. M. Horodecki, P. Horodecki, and R. Horodecki, *Phys. Rev. Lett.* **78** 574 (1997).
51. G. Brassard and L. Salvail, *Eurocrypt '93, Lofthus, Norway* (1993).
52. B.A. Slutsky, R. Rao, P.-C. Sun and Y. Fainman, *Phys. Rev. A* **57**, 2383 (1998).
53. J.I. Cirac and N. Gisin, *Phys. Lett. A* **229**, 1 (1997)
54. C.A. Fuchs, N. Gisin, R.B. Griffiths, C.-S. Niu, and A. Peres, *Phys. Rev. A* **56**, 1163 (1997).
55. H. Bechmann-Pasquinucci and N. Gisin, *Phys. Rev. A* **59**, 4238 (1999).
56. N. Lütkenhaus, *Phys. Rev. A* **59**, 3301 (1999).
57. C.H. Bennett, G. Brassard, C. Crépeau, and U. Maurer, *1994 IEEE International Symposium on Information Theory*, Trondheim, Norway, June (1994).
58. A. Peres, *Quantum Theory: Concepts and Methods*, Kluwer Academic Publishers, (1995).
59. E. Biham, M. Boyer, G. Brassard, J. van de Graaf, and T. Mor, *Security of Quantum Key Distribution against all Collective attacks*, quant-ph/9801022 (1998).
60. D. Mayers, *Unconditional security in Quantum Cryptography*, quant-ph/9802025 (1998).
61. M.N. Wegman, J.L. Carter, *Journal of Computer and System Sciences* **22**, 265-279 (1981).
62. G. Ribordy, J.D. Gautier, H. Zbinden, and N. Gisin, *Applied Optics* **37**, 2272 (1998).
63. R.Y. Chiao and Y.S. Wu, *Phys. Rev. Lett.* **57**, 933 (1986).
64. B.C. Jacobs and J.D. Franson, *Opt. Lett.* **21**, 1854 (1996).
65. W.T. Buttler, R.J. Hughes, P.G. Kwiat, S.K. Lamoreaux, G.G. Luther, G.L. Morgan, J.E. Nordholt, C.G. Peterson, and C.M. Simmons, Los Alamos preprint, quant-ph/9805071.
66. P.D. Townsend, C. Marand, S.J.D. Phoenix, K.J. Blow, and S.M. Barnett, *Phil. Trans. Roy. Soc. London A* **354**, 805 (1996).
67. R.J. Hughes, G.G. Luther, G.L. Morgan, C.G. Peterson, C.G. and C. Simmons, C. *Quantum cryptography over underground optical fibres*, Advances in Cryptology - Proceedings of Crypto'96, Springer, Berlin, Heidelberg (1996).
68. G. Ribordy, J.-D. Gautier, N. Gisin, O. Guinnard, and H. Zbinden, *Electronics Letters* **34**, 2116-2117 (1998).
69. J.D. Franson, *Phys. Rev. Lett.* **62**, 2205 (1989).
70. J.G. Rarity, P.C.M. Owens, and P.R. Tapster, *Phys. Rev. Lett.* **73**, 1923 (1994).
71. W. Tittel, J. Brendel, B. Gisin, T. Herzog, H. Zbinden and N. Gisin, *Phys. Rev. A* **57**, 3229 (1998); W. Tittel, J. Brendel, H. Zbinden and N. Gisin, *Phys. Rev. Lett.* **81**, 3563 (1998).
72. G. Weihs, T. Jennewein, C. Simon, H. Weinfurter, and A. Zeilinger, *Phys. Rev. Lett.* **81**, 5039 (1998).
73. C.H. Bennett and S.J. Wiesner, *Phys. Rev. Lett.*, **69**, 2881 (1992).
74. C.H. Bennett, G. Brassard, C. Crépeau, R. Jozsa, A. Peres, and W.K. Wootters, *Phys. Rev. Lett.* **70**, 1895 (1993).
75. K. Mattle, H. Weinfurter, P.G. Kwiat, and A. Zeilinger, *Phys. Rev. Lett.* **76**, 4656 (1996).
76. D. Bouwmeester, J.-W. Pan, K. Mattle, M. Eible, H. Weinfurter, and A. Zeilinger, Experimental quantum teleportation. *Nature* **390**, 575-579 (1997).
77. S. Popescu, LANL E-print quant-ph 9501020.

78. D. Boschi, S. Branca, F. De Martini, L. Hardy, and S. Popescu, Phys. Rev. Lett. **80**, 1121 (1998).
79. L. Vaidman, Phys. Rev. A **49**, 1473 (1994).
80. S.L. Braunstein and H.J. Kimble, Phys. Rev. Lett. **80**, 869 (1998).
81. A. Furusawa, J.L. Sørensen, S.L. Braunstein, C.A. Fuchs, H.J. Kimble, and E.S. Polzik, Science Oct23 1998 pp 706-709.
82. Comment by F. De Martini, and Reply by A. Zeilinger, Physics World **11**, nr.3, 23-24 (March 1998).
83. Comment by S.L. Braunstein and H.J. Kimble, and Reply by D. Bouwmeester, J.-W. Pan, M. Daniell, H. Weinfurter, M. Zukowski, and A. Zeilinger, Nature (London) **394**, 840-841 (1998).
84. D. Bouwmeester, J.-W. Pan, H. Weinfurter, and A. Zeilinger, High-fidelity teleportation of qubits, J. Mod. Opt. **47**, 279 (2000).
85. M. Zukowski, A. Zeilinger, M.A. Horne, and A. Ekert, Phys. Rev. Lett. **71**, 4287 (1993).
86. J.-W. Pan, D. Bouwmeester, H. Weinfurter, and A. Zeilinger, Experimental entanglement swapping: Entangling photons that never interacted. Phys. Rev. Lett. **80**, 3891-3894 (1998).
87. S. Bose, V. Vedral, and P.L. Knight, *A multiparticle generalisation of entanglement swapping* Phys. Rev. A **57**, 822 (1998).
88. W.K. Wootters and W.H. Zurek, Nature (London) **299**, 802, (1982).
89. D.N. Klyshko, Sov. Phys. JETP **28**, 522 (1969).
90. D.C. Burnham and D.L. Weinberg, Phys. Rev. Lett. **25**, 84 (1970).
91. J.D. Franson and K.A. Potocki, Phys. Rev. A **37**, 2511 (1988).
92. J. Brendel, E. Mohler, and W. Martienssen, Europhys. Lett. **20**, 575 (1992); P.G. Kwiat, A.M. Steinberg and R.Y. Chiao, Phys. Rev. A **47**, R2472 (1993).
93. J. Brendel, N. Gisin, W. Tittel and H. Zbinden, Phys. Rev. Lett. **82**, 2594 (1999).
94. J.G. Rarity and P.R. Tapster, Phys. Rev. Lett. **64**, 2495 (1990).
95. R. Loudon, *Coherence and Quantum Optics VI*, ed. Eberly, J.H. and Mandel, L. Plenum New York, 703 (1990).
96. A. Zeilinger, H.J. Bernstein, and M.A. Horne, J. Mod. Optics, **41**, 2375, (1994).
97. H. Weinfurter, Europhys. Lett. **25**, 559 (1994).
98. S.L. Braunstein and A. Mann, Phys. Rev. A **51**, R1727 (1995).
99. M. Michler, K. Mattle, H. Weinfurter, and A. Zeilinger, Phys. Rev. A **53**, R1209 (1996).
100. A. Zeilinger, *Proc. of the Nobel Symp. 104* "Modern Studies of Basic Quantum Concepts and Phenomena" E.B. Karlsson and E. Brändes (Eds.), Physica Scripta, T76, 203 (1998).
101. M. Zukowski, A. Zeilinger and H. Weinfurter in *Fundamental Problems in Quantum Theory* vol. 755 Annals of the New York Academy of Sciences (Greenberger and Zeilinger Eds.) p. 91 (1995).
102. J. Kim, S. Takeuchi, Y. Yamamoto, and H.H. Hogue, Appl. Phys. Lett. **74**, 902 (1999).
103. E. Hagley, X. Maître, G. Nogues, C. Wunderlich, M. Brune, J.M. Raimond, and S. Haroche, Generation of Einstein-Podolsky-Rosen pairs of atoms. Phys. Rev. Lett. **79**, 1-5 (1997).
104. H.-J. Briegel, W. Dür, J.I. Cirac, and P. Zoller, Phys. Rev. Lett. **81**, 5932 (1998).
105. M. Zukowski, Phys. Lett. A 157, 198 (1991).
106. R. Loudon, *The Quantum Theory of Light, second edition*. Clarendon Press, Oxford, (1983).

107. A. Yariv, *Quantum Electronics, third edition*. John Wiley& Sons (1989).
108. D.F. Walls and G.J. Milburn, *Quantum Optics, second edition*. Springer, Berlin, Heidelberg (1994).
109. P.W. Milonni, *The Quantum Vacuum* Academic Press, San Diego, 1994.
110. Z.Y. Ou, S.F. Pereira, H.J. Kimble, and K.C. Peng, Rhys. Rev. Lett. **68**, 3663 (1992).
111. Z.Y. Ou, S.F. Pereira, and H.J. Kimble, Appl. Phys. B **55**, 265 (1992).
112. H.J. Kimble, in *Fundamental Systems in Quantum Optics, Les Houches, 1990*, eds. J. Dalibard, J.M. Raimond, J. Zinn-Justin (Elsevier Science Publishers, Amsterdam, 1992), pp. 549-674.
113. Ling-An Wu, H.J. Kimble, J.L. Hall, and Huifa Wu, Phys. Rev. Lett. **57**, 2520 (1986).
114. See, for example, S.J. Freedman and J.S. Clauser, Phys. Rev. Lett. **28**, 938 (1972).
115. M. Lamehi-Rachti and W. Mittig, Phys. Rev. D **14**, 2543 (1976).
116. E. Biham, B. Huttner and T. Mor, Phys. Rev. A **54**, 2651 (1996).
117. C.H. Bennett, H.J. Bernstein, S. Popescu, and B. Schumacher, Phys. Rev. A **53**, 2046 (1996).
118. S. Bose, V. Vedral, and P.L. Knight, Phys. Rev. A **60**, 194 (1999).
119. A. Zeilinger, M.A. Horne, H. Weinfurter, and M. Zukowski, Phys. Rev. Lett. **78**, 3031 (1997).
120. L. Grover, *Proc. 28 Annual ACM Symposium on the Theory of Computing*, ACM Press New York, 212 (1996).
121. G. Brassard, Science **275**, 627 (1997).
122. R. Rivest, A. Shamir, and L. Adleman, *On Digital Signatures and Public-Key Cryptosystems*, MIT Laboratory for Computer Science, Technical Report, MIT/LCS/TR-212 (January 1979).
123. R. Feynman, Int. J. Theor. Phys. **21**, 467, (1982).
124. D. Deutsch, Proc. R. Soc. London A **400**, 97 (1985).
125. D. Deutsch, Proc. R. Soc. London A: **425**, 73, (1989).
126. S.F. Huelga, C. Macchiavello, T. Pellizzari, A.K. Ekert, M.B. Plenio, and J.I. Cirac, Phys. Rev. Lett. **79**, 3865 (1997).
127. D. Deutsch, *The Fabric of Reality* (Allen Lane, Penguin Press, London).
128. D. Deutsch and A. Ekert, Phys. World **11**, 47 (March 1998).
129. A. Barenco, C.H. Bennett, R. Cleve, D. DiVincenzo, N. Margolus, P. Shor, T. Sleator, J. Smolin, and H. Weinfurter, Phys. Rev. A **52**, 3457 (1995).
130. D. Deutsch, A. Barenco, and A. Ekert, Proc. Roy. Soc. Lond. A **449**, 669 (1995).
131. C.H. Papadimitriou, *Computational Complexity* (Addison-Wesley, Reading, MA, 1994).
132. M. Garey, and D. Johnson, *Computers and Intractability: A Guide to the Theory of NP Completeness* (W. H. Freeman and Co., 1979).
133. R. Jozsa, Entanglement and Quantum Computation in *The Geometric Universe*, 369, eds. S. Huggett, L. Mason, K.P. Tod, S.T. Tsou and N.M.J. Woodhouse (Oxford University Press, 1998).
134. A. Ekert and R. Jozsa, Phil. Trans. Roy. Soc. London Ser A, **356**, 1769 (1998).
135. A.S. Holevo, Probl. Inf. Transm **9**, 177 (1973).
136. C. Fuchs and A. Peres, Phys. Rev. A. **53**, 2038 (1996).
137. T. Cover and J. Thomas, *Elements of Information Theory*, John Wiley and Sons (1991).
138. D. Deutsch and R. Jozsa, Proc. Roy. Soc. Lond. A **439**, 553 (1992).
139. R. Cleve, A. Ekert, C. Macchiavello, and M. Mosca, Proc. Roy. Soc. London Ser A, **454**, 339 (1998).

140. E. Bernstein and U. Vazirani, *Proc. 25th Annual ACM Symposium on the Theory of Computing*, (ACM Press, New York), p. 11-20 (1993) (Extended Abstract). Full version of this paper appears in S. I. A. M. Journal on Computing, **26**, 1411 (1997).
141. D. Simon, (1994) *Proc. of 35th Annual Symposium on the Foundations of Computer Science*, (IEEE Computer Society, Los Alamitos), p. 116 (Extended Abstract). Full version of this paper appears in S. I. A. M. Journal on Computing, **26**, 1474 (1997).
142. G.H. Hardy and E.M. Wright *An Introduction to the Theory of Numbers* (4th edition, Clarendon, Oxford, 1965).
143. M.R. Schroeder, *Number Theory in Science and Communication* (2nd enlarged edition, Springer, New York, 1990).
144. A. Ekert and R. Jozsa, Rev. Mod. Phys. **68**, 733 (1996).
145. D.K. Maslen and D.N. Rockmore, “Generalised FFT’s – A Survey of Some Recent Results”, in *Proc. DIMACS Workshop on Groups and Computation – II* (1995).
146. R. Jozsa, Proc. Roy. Soc. London Ser A, **454**, 323 (1998).
147. G. Brassard and P. Hoyer, “An exact polynomial-time algorithm for Simon’s problem”, *Proc. 5th Israeli Symposium on Theory of Computing and Systems (ISTCS 97)*, 12 (1997), also available at quant-ph/9704027.
148. A. Kitaev, Russian Math. Surveys **52**, 1191 (1997), also available at quant-ph/9511026.
149. R. Beals, *Proc. 29th Annual ACM Symposium on the Theory of Computing – STOC* (ACM Press, New York), 48 (1997).
150. L. Grover, Phys. Rev. Lett. **78**, 325 (1997).
151. M. Boyer, G. Brassard, P. Hoyer, and A. Tapp, *Proc. of fourth workshop on Physics and Computation – PhysComp’96*, 36-43 (1996).
152. L. Grover, “A Framework for Fast Quantum Algorithms”, *Proc. 30th ACM Symposium on Theory of Computation (STOC’98)*, 53 (1998), also available at quant-ph/9711043.
153. G. Brassard, P. Hoyer, and A. Tapp, “Quantum Counting”, *Proc. 25th ICALP*, Vol 1443, Lecture Notes in Computer Science, 820 (Springer, 1998), also available at quant-ph/9805082.
154. L. Grover, Phys. Rev. Lett. **80**, 4325 (1997).
155. C.H. Bennett, E. Bernstein, G. Brassard, and U. Vazirani, S. I. A. M. Journal on Computing, **26**, 1510 (1997).
156. J.I. Cirac and P. Zoller, Phys. Rev. Lett. **74**, 4091 (1995).
157. J.F. Poyatos, J.I. Cirac, and P. Zoller, Phys. Rev. Lett. **81**, 1322 (1998).
158. C. Monroe, D.M. Meekhof, B.E. King, W.M. Itano, and D. J. Wineland, Phys. Rev. Lett. **75**, 4714 (1995).
159. E.T. Jaynes and F.W. Cummings, Proc. IEEE **51**, 89 (1963).
160. *Cavity Quantum Electrodynamics, Advances in atomic, molecular and optical physics, Supplement 2*, P. Berman editor, Academic Press (1994).
161. S. Haroche, in *Fundamental systems in quantum optics, les Houches summer school session LIII*, J. Dalibard, J.M. Raimond and J. Zinn-Justin eds, North Holland, Amsterdam (1992).
162. D.G. Hulet and D. Kleppner, Phys. Rev. Lett. **51**, 1430 (1983).
163. P. Nussenzvzeig, F. Bernardot, M. Brune, J. Hare, J.M. Raimond, S. Haroche and W. Gawlik, Phys. Rev. A **48**, 3991 (1993).
164. M. Brune, P. Nussenzveig, F. Schmidt-Kaler, F. Bernardot, A. Maali, J.M. Raimond, and S. Haroche, Phys. Rev. Lett. **72**, 3339 (1994).
165. M. Brune, F. Schmidt-Kaler, A. Maali, J. Dreyer, E. Hagley, J.M. Raimond, and S. Haroche, Phys. Rev. Lett. **76**, 1800 (1996).

166. M. Brune, E. Hagley, J. Dreyer, X. Maître, A. Maali, C. Wunderlich, J.M. Raimond, and S. Haroche, Phys. Rev. Lett., **77**, 4887 (1996).
167. X. Maître, E. Hagley, G. Nogues, C. Wunderlich, P. Goy, M. Brune, J.M. Raimond and S. Haroche, Phys. Rev. Lett. **79**, 769 (1997).
168. E. Hagley, X. Maître, G. Nogues, C. Wunderlich, M. Brune, J.M. Raimond and S. Haroche, Phys. Rev. Lett. **79**, 1 (1997).
169. G. Nogues, A. Rauschenbeutel, S. Osnaghi, M. Brune, J.M. Raimond and S. Haroche, Nature **400**, 239 (1999).
170. G. Raithel, C. Wagner, H. Walther, L.M. Narducci and M.O. Scully, in *Cavity Quantum Electrodynamics*, P. Berman ed. 57, Academic, New York (1994).
171. J.H. Eberly, N.B. Narozhny and J.J. Sanchez-Mondragon, Phys. Rev. Lett. **44**, 1323 (1980).
172. R.J. Thompson, G. Rempe and H.J. Kimble, Phys. Rev. Lett. **68**, 1132 (1992).
173. F. Bernardot, P. Nussenzveig, M. Brune, J.M. Raimond and S. Haroche , Euro. Phys. Lett. **17**, 33 (1992).
174. P. Domokos, J.M. Raimond, M. Brune and S. Haroche, Phys. Rev. A **52**, 3554 (1995).
175. J.I. Cirac and P. Zoller, Phys. Rev. A **50**, R2799 (1994).
176. D.M. Greenberger, M.A. Horne, A. Shimony, and A. Zeilinger, Am.J.Phys **58**, 1131 (1990). N.D. Mermin, Physics Today (June 9, 1990).
177. S. Haroche in *Fundamental problems in quantum theory*, D. Greenberger and A. Zeilinger Eds, Ann. N.Y. Acad. Sci. **755**, 73 (1995).
178. E. Schrödinger, *Naturwissenschaften* **23**, 807, 823, 844 (1935). Reprinted in english in J.A. Wheeler and W.H. Zurek, *Quantum theory of measurement*, Princeton University Press (1983).
179. W.H. Zurek, Phys. Rev. D **24**, 1516 (1981).
180. W.H. Zurek, Phys. Rev. D **26**, 1862 (1982).
181. A.O. Caldeira and A.J. Leggett Physica A, **121**, 587 (1983).
182. E. Joos and H.D. Zeh, Z.Phys.B **59**, 223 (1985).
183. W.H. Zurek, Physics Today **44**, 10 p.36 (1991).
184. R. Omnès, *The Interpretation of Quantum Mechanics*, Princeton University Press (1994).
185. D.F. Walls and G.J. Milburn, Phys. Rev. A **31**, 2403.
186. L. Davidovich, M. Brune, J.M. Raimond and S. Haroche, Phys. Rev. A **53**, 1295 (1996).
187. M.O. Scully and H. Walther, Phys. Rev. A **39**, 5299 (1989).
188. J.M Raimond, M. Brune and S. Haroche, Phys. Rev. Lett. **79**, 1964 (1997).
189. C.A. Blockley, D.F. Walls, and H. Risken, Europhys. Lett. **17**, 509 (1992).
190. J.I. Cirac, R. Blatt, A.S. Parkins, and P. Zoller, Phys. Rev. Lett. **70**, 762 (1993).
191. J.I. Cirac, R. Blatt, A.S. Parkins, and P. Zoller, Phys. Rev. A **49**, 1202 (1994).
192. J.I. Cirac, R. Blatt, and P. Zoller, Phys. Rev. A **49**, R3174 (1994).
193. Proc.5th Symp.Freq.Standards and Metrology, ed. J.C. Bergquist, (World Scientific, 1996).
194. D.J. Berkeland, J.D. Miller, J.C. Bergquist, W.M. Itano, and D.J. Wineland, Phys. Rev. Lett. **80**, 2089 (1998).
195. R. Blatt, in *Atomic Physics* **14**, 219, ed. D.J. Wineland, C. Wieman, S.J. Smith, AIP New York (1995).
196. W. Paul, O. Osberghaus, and E. Fischer, Forschungsberichte des Wirtschafts- und Verkehrsministerium Nordrhein-Westfalen **415** (1958).
197. P.K. Ghosh, Ion traps, Clarendon, Oxford (1995).
198. D.J. Wineland, and H. Dehmelt, Bull. Am. Phys. Soc. **20**, 637 (1975).

199. D.J. Wineland, R.E. Drullinger, and F.L. Walls, Phys. Rev. Lett. **40**, 1639 (1978).
200. A. Steane, Appl. Phys. B **64**, 623 (1997), see Table 1 in which a list of candidate ions is given together with relevant experimental parameters.
201. <http://www.blrdoc.gov/timefreq/ion/index.htm>
202. <http://horology.jpl.nasa.gov/research.html>
203. <http://mste.laser.physik.uni-muenchen.de/lg/worktop.html>
204. <http://p23.lanl.gov/Quantum/quantum.html>
205. http://dipmza.physik.uni-mainz.de/www_werth/calcium/calcium.html
206. <http://www-phys.rrz.uni-hamburg.de/home/vms/groupa/index.html>
207. <http://heart-c704.uibk.ac.at/>
208. D.J. Wineland, W.M. Itano, J.C. Bergquist, and R.G. Hulet, Phys. Rev. A **36**, 2220 (1987).
209. J.I. Cirac, A.S. Parkins, R. Blatt, and P. Zoller, Phys. Rev. Lett. **70**, 556 (1993).
210. S. Stenholm, Rev. Mod. Phys. **58**, 699 (1986).
211. C. Monroe, D.M. Meekhof, B.E. King, S.R. Jeffers, W.M. Itano, D.J. Wineland, and P. Gould, Phys. Rev. Lett. **74**, 4011 (1995).
212. H.C. Nägerl, W. Bechter, J. Eschner, F. Schmidt-Kaler, and R. Blatt, Appl. Phys. B **66**, 603 (1998).
213. H.C. Nägerl, D. Leibfried, H. Rohde, G. Thalhammer, J. Eschner, F. Schmidt-Kaler, and R. Blatt, Phys. Rev. A **60**, 145 (1999).
214. F. Diedrich, J.C. Bergquist, W.M. Itano, and D.J. Wineland, Phys. Rev. Lett. **62**, 403 (1989).
215. Ch. Roos, Th. Zeiger, H. Rohde, H.C. Nägerl, J. Eschner, D. Leibfried, F. Schmidt-Kaler, and R. Blatt, Phys. Rev. Lett. **83**, 4713 (1999).
216. B.E. King, C.S. Wood, C.J. Myatt, Q.A. Turchette, D. Leibfried, W.M. Itano, C. Monroe, and D.J. Wineland, Phys. Rev. Lett. **81**, 1525 (1998).
217. H. Dehmelt, Bull. Am. Phys. Soc. **20** 60 (1975).
218. D.J. Wineland, C. Monroe, W.M. Itano, D. Leibfried, B. King, and D.M. Meekhof, Journal of Research of the National Institute of Standards and Technology **103**, 259 (1998).
219. D. Leibfried, D.M. Meekhof, B.E. King, C. Monroe, W.M. Itano, and D.J. Wineland, Phys. Rev. Lett **77**, 4281 (1996).
220. D.M. Meekhof, C. Monroe, B.E. King, W.M. Itano, and D.J. Wineland, Phys. Rev. Lett. **76**, 1796 (1996).
221. C. Monroe, D.M. Meekhof, B.E. King, and D.J. Wineland, Science **272**, 1131 (1996).
222. J.F. Poyatos, J.I. Cirac, and P. Zoller, Phys. Rev. Lett. **77**, 4728 (1996).
223. C. Monroe, D.M. Meekhof, B.E. King, W.M. Itano, and D.J. Wineland, Phys. Rev. Lett. **75**, 4714 (1995).
224. L.G. Lutterbach and L. Davidovich, Phys. Rev. Lett. **78**, 2547 (1997).
225. M.B. Plenio and P.L. Knight Phys. Rev. A **53**, 2986 (1996).
226. J.I. Cirac, A.S. Parkins, R. Blatt, and P. Zoller, Adv. At. Molec. Opt. Physics **37**, 238 (1996).
227. D.P. DiVincenzo, Phys. Rev. A **51**, 1015 (1995).
228. D.J. Wineland, C. Monroe, W.M. Itano, D. Leibfried, B. King, and D.M. Meekhof, Rev. Mod. Phys. (1998).
229. G. Morigi, J. Eschner, J.I. Cirac, and P. Zoller, Phys. Rev. A **59**, 3797 (1999).
230. E. Peik, J. Abel, T. Becker, J. von Zanthier, and H. Walther, Phys. Rev. A **60**, 439 (1999).
231. I. Waki, S. Kassner, G. Birk, and H. Walther, Phys. Rev. Lett. **68**, 2007 (1992); G. Birk, S. Kassner, H. Walther, Nature 357, 310 (1992).

232. D.F.V. James, *Appl. Phys. B* **66**, 181 (1998).
233. C. Monroe, D. Leibfried, B.E. King, D.M. Meekhof, W.M. Itano, and D.J. Wineland, *Phys. Rev. A* **55**, R2489 (1997)
234. W. Nagourney, J. Sandberg, and H. Dehmelt, *Phys. Rev. Lett.* **56**, 2797 (1986); Th. Sauter, W. Neuhauser, R. Blatt, and P.E. Toschek, *Phys. Rev. Lett.* **57**, 1696 (1986); J.C. Bergquist, R. Hulet, W.M. Itano, and D.J. Wineland, *Phys. Rev. Lett.* **57**, 1699 (1986).
235. P.J. Hore, *Nuclear Magnetic Resonance*, Oxford University Press, Oxford (1995).
236. R.R. Ernst, G. Bodenhausen, and A. Wokaun, *Principles of Nuclear Magnetic Resonance in One and Two Dimensions*, Oxford University Press, Oxford (1987).
237. D.G. Cory, A.F. Fahmy, and T.F. Havel, *Proceedings of the Fourth Workshop on Physics and Computation, Nov. 22–24, 1996*, New England Complex Systems Institute, Cambridge, MA (1996).
238. D.G. Cory, A.F. Fahmy, and T.F. Havel, *Proc. Natl. Acad. Sci. USA* **94**, 1634 (1997).
239. N.A. Gershenfeld and I.L. Chuang, *Science* **275**, 350 (1997).
240. A. Abragam, *Principles of Nuclear Magnetism*, Clarendon Press, Oxford (1961).
241. C.P. Slichter, *Principles of Magnetic Resonance* 3rd ed. Springer, Berlin, Heidelberg (1990).
242. M. Goldman, *Quantum Description of High-Resolution NMR in Liquids*, Clarendon Press, Oxford (1988).
243. J.A. Jones and M. Mosca, *J. Chem. Phys.* **109**, 1648 (1998).
244. A. Barenco, C.H. Bennett, R. Cleve, D.P. DiVincenzo, N. Margolus, P. Shor, T. Sleator, J.A. Smolin, and H. Weinfurter, *Phys. Rev. A*, **52**, 3457 (1995).
245. J.A. Jones, R.H. Hansen, and M. Mosca, *J. Magn. Reson.* **135**, 353 (1998).
246. L.M.K. Vandersypen, C.S. Yannoni, M.H. Sherwood, and I.L. Chuang, *Phys. Rev. Lett.* **83**, 3085 (1999).
247. E. Knill, I. Chuang, and R. Laflamme, *Phys. Rev. A*, **57**, 3348 (1998).
248. T.F. Havel, S.S. Somaroo, C.-H. Tseng, and D.G. Cory, LANL E-print quant-ph/9812026.
249. R. Cleve, A. Ekert, C. Macchiavello, and M. Mosca, *Proc. R. Soc. Lond. A* **454**, 339 (1998).
250. I.L. Chuang, L.M.K. Vandersypen, X.L. Zhou, D.W. Leung, and S. Lloyd, *Nature*, **393**, 143 (1998).
251. I.L. Chuang, N. Gershenfeld, and M. Kubinec, *Phys. Rev. Lett.* **80**, 3408 (1998).
252. J.A. Jones, M. Mosca, and R.H. Hansen, *Nature*, **393**, 344 (1998).
253. L.K. Grover, *Science*, **280**, 228 (1998).
254. J.A. Jones and M. Mosca, *Phys. Rev. Lett.* **83**, 1050 (1999).
255. R. Laflamme, E. Knill, W.H. Zurek, P. Catasti, and S.V.S. Mariappan, *Phil. Trans. Roy. Soc. Lond A*, **356**, 1941 (1998).
256. R.J. Nelson, D.G. Cory, S. Lloyd, LANL E-print quant-ph/9905028.
257. D.G. Cory, M.D. Price, W. Maas, E. Knill, R. Laflamme, W.H. Zurek, T.F. Havel, and S.S. Somaroo, *Phys. Rev. Lett.* **81**, 2152 (1998).
258. D. Leung, L. Vandersypen, X. Zhou, M. Sherwood, C. Yannoni, M. Kubinec, and I. Chuang, *Phys. Rev. A* **60**, 1924 (1999).
259. M.A. Nielsen, E. Knill, and R. Laflamme, *Nature*, **396**, 52 (1998).
260. N. Linden, H. Barjat, and R. Freeman, *Chem. Phys. Lett.* **296**, 61 (1998).
261. R. Marx, A. F. Fahmy, J. M. Myers, W. Bermel, and S. J. Glaser, LANL E-print quant-ph/9905087.

262. W.S. Warren, *Science*, **277**, 1688 (1997).
263. G. Navon, Y.-Q. Song, T. Rööm, S. Appelt, R.E. Taylor, and A. Pines, *Science*, **271**, 1848 (1996).
264. L. J. Schulman and U. Vazirani, LANL E-print quant-ph/9804060.
265. R. Freeman, *Spin Choreography*, Spektrum, Oxford, (1997).
266. N. Linden, H. Barjat, R.J. Carbojo, and R. Freeman, *Chem. Phys. Lett.* **305**, 28 (1999).
267. D.W. Leung, I.L. Chuang, F. Yamaguchi, and Y. Yamamoto, LANL E-print quant-ph/9904100.
268. J.A. Jones and E. Knill, *J. Magn. Reson.* in press, LANL E-print quant-ph/9905008.
269. N. Linden, Ē. Kupče, and R. Freeman, LANL E-print quant-ph/9907003.
270. P.T. Callaghan, *Principles of Nuclear Magnetic Resonance Microscopy*, Clarendon Press, Oxford (1991).
271. B.E. Kane, *Nature* **393**, 133 (1998).
272. S.L. Braunstein, C.M. Caves, R. Jozsa, N. Linden, S. Popescu, and R. Schack, *Phys. Rev. Lett.* **83**, 1054 (1999).
273. R. Schack and C. M. Caves, LANL E-print quant-ph/9903101.
274. T. Pellizzari *et al.*, *Phys. Rev. Lett.* **75**, 3788 (1995).
275. C. Monroe *et al.*, *Phys. Rev. Lett.* **75**, 4714 (1995).
276. Q. Turchette *et al.*, *Phys. Rev. Lett.* **75**, 4710 (1995).
277. K. Mattele *et al.*, *Phys. Rev. Lett.* **76**, 4656 (1996).
278. J. I. Cirac, P. Zoller, H.J. Kimble, and H. Mabuchi, *Phys. Rev. Lett.* **78**, 3221 (1997).
279. C.H. Bennett, *Physics Today* **24**, (October 1995) and references cited; A.K. Ekert, *Phys. Rev. Lett.* **67**, 661 (1991); W. Tittel *et al.*, quant-ph/9707042; W.T. Buttler *et al.*, quant-ph/9801006.
280. C.H. Bennett *et al.*, *Phys. Rev. Lett.* **70**, 1895 (1993); D. Bouwmeester *et al.*, *Nature* **390**, 575 (1997); D. Boschi *et al.*, *Phys. Rev. Lett.* **80**, 1121 (1998).
281. L.K. Grover, quant-ph/9704012.
282. A.K. Ekert *et al.*, quant-ph/9803017.
283. C.K. Law and J.H. Eberly, *Phys. Rev. Lett.* **76**, 1055 (1996).
284. H.J. Carmichael, *Phys. Rev. Lett.* **70**, 2273 (1993).
285. For a review see P. Zoller and C.W. Gardiner in *Quantum Fluctuations*, Les Houches, ed. E. Giacobino *et al.*, Elsevier, NY, in press.
286. C.W. Gardiner, *Phys. Rev. Lett.* **70**, 2269 (1993).
287. P.W. Shor, *Phys. Rev. A* **52**, R2493 (1995); A.M. Steane, *Phys. Rev. Lett.* **77**, 793 (1996); J.I. Cirac, T. Pellizzari and P. Zoller, *Science* **273**, 1207 (1996); P. Shor, *Fault-tolerant quantum computation*, quant-ph/9605011; D. DiVincenzo and P.W. Shor, *Phys. Rev. Lett.* **77**, 3260 (1996).
288. C.H. Bennett *et al.*, *Phys. Rev. Lett.* **76**, 722 (1996); D. Deutsch *et al.*, *Phys. Rev. Lett.* **77**, 2818 (1996); N. Gisin, *Phys. Lett. A* **210**, 151 (1996).
289. D.M. Greenberger, M.A. Horne, A. Zeilinger, A. Going beyond Bell's theorem, in *Bell's Theorem, Quantum Theory, and Conceptions of the Universe*, edited by M. Kafatos, (Kluwer, Dordrecht, 1989) pp. 73-76.
290. D.M. Greenberger, M.A. Horne, A. Shimony, A. Zeilinger, Bell's theorem without inequalities. *Am. J. Phys.* **58**, 1131 (1990).
291. D. Bouwmeester, J.-W.. Pan, M. Daniell, H. Weinfurter, and A. Zeilinger, Observation of three-photon Greenberger-Horne-Zeilinger entanglement. *Phys. Rev. Lett.* **82**, 1345 (1999).
292. D.M. Greenberger, M.A. Horne, A. Zeilinger, Multiparticle interferometry and the superposition principle. *Physics Today*, 22, August 1993.
293. N.D. Mermin, *Am. J. Phys.* **58**, 731 (1990).

294. N.D. Mermin, What's wrong with these elements of reality? *Physics Today*, 9, June 1990.
295. S.J. Freedman and J.S. Clauser, Experimental test of local hidden-variable theories. *Phys. Rev. Lett.* **28**, 938-941 (1972).
296. A. Aspect, J. Dalibard, and G. Roger, Experimental test of Bell's inequalities using time-varying analysers. *Phys. Rev. Lett.* **47**, 1804-1807 (1982).
297. G. Weihs, T. Jennewein, C. Simon, H. Weinfurter, and A. Zeilinger, Violation of Bell's inequality under strict Einstein locality conditions. *Phys. Rev. Lett.* **81**, 5039-5043 (1998).
298. L. Hardy, Nonlocality for two particles without inequalities for almost all entangled states. *Phys. Rev. Lett.* **71**, 1665-1668 (1993).
299. D. Boschi, S. Branca, F. De Martini, and L. Hardy, Ladder proof of nonlocality without inequalities: Theoretical and experimental results. *Phys. Rev. Lett.* **79**, 2755 (1997).
300. A. Zeilinger, M.A. Horne, H. Weinfurter, and M. Zukowski, Three particle entanglements from two entangled pairs. *Phys. Rev. Lett.* **78**, 3031-3034 (1997).
301. S. Haroche, Ann. N. Y. Acad. Sci. **755**, 73 (1995); J.I. Cirac, P. Zoller, *Phys. Rev. A* **50**, R2799 (1994).
302. S. Lloyd, *Phys. Rev. A* **57**, R1473 (1998); R. Laflamme, E. Knill, W.H. Zurek, P. Catasti, S.V.S. Mariappan, *Phil. Trans. R. Soc. Lond. A* **356**, 1941 (1998).
303. S. Bose, V. Vedral, P.L. Knight, *Phys. Rev. A* **57**, 822 (1998).
304. M. Zukowski, A. Zeilinger, H. Weinfurter, Entangling photons radiated by independent pulsed source. *Ann. NY Acad. Sci.* **755**, 91-102 (1995).
305. M.A. Horne, *Fortschr. Phys.* **46**, 6 (1998).
306. G. Krenn, A. Zeilinger, *Phys. Rev. A* **54**, 1793 (1996).
307. Z.Y. Ou and L. Mandel, Violation of Bell's inequality and classical probability in a two-photon correlation experiment. *Phys. Rev. Lett.* **61**, 50-53 (1988).
308. Y.H. Shih and C.O. Alley, New type of Einstein-Podolsky-Rosen-Bohm experiment using pairs of light quanta produced by optical parametric down conversion. *Phys. Rev. Lett.* **61**, 2921-2924 (1988).
309. P. Kwiat, P.E. Eberhard, A.M. Steinberger, and R.Y. Chiao, Proposal for a loophole-free Bell inequality experiment. *Phys. Rev. A* **49**, 3209-3220 (1994).
310. L. De Caro and A. Garuccio, Reliability of Bell-inequality measurements using polarisation correlations in parametric-down-conversion photons. *Phys. Rev. A* **50**, R2803-R2805 (1994).
311. S. Popescu, L. Hardy, and M. Zukowski, Revisiting Bell's theorem for a class of down-conversion experiments. *Phys. Rev. A* **56**, R4353-4357 (1997).
312. M. Zukowski, Violations of local realism in multiphoton interference experiments. *quant-ph/9811013*.
313. J.-W. Pan, D. Bouwmeester, M. Daniell, H. Weinfurter, and A. Zeilinger, Experimental test of quantum nonlocality in three-photon Greenberger-Horne-Zeilinger entanglement, *Nature* **403**, 515 (2000).
314. N.D. Mermin, Extreme quantum entanglement in a superposition of macroscopically distinct states. *Phys. Rev. Lett.* **65**, 1838-1841 (1990).
315. S.M. Roy and V. Singh, Tests of signal locality and Einstein-Bell locality for multiparticle systems. *Phys. Rev. Lett.* **67**, 2761-2764 (1991).
316. M. Zukowski and D. Kaszlikowski, Critical visibility for N -particle Greenberger-Horne-Zeilinger correlations to violate local realism. *Phys. Rev. A* **56**, R1682-1685 (1997).
317. The original reference is E. Schmidt, *Zur Theorie der linearen und nicht linearen Integralgleichungen*, *Math. Annalen* **63**, 433 (1907), in the context of quantum theory see H. Everett III, in *The Many-World Interpretation of*

- Quantum Mechanics*, ed. B.S. DeWitt and N. Graham, Princeton University Press, Princeton, 3 (1973), and H. Everett III, Rev. Mod. Phys. **29**, 454 (1957). A graduate level textbook by A. Peres, *Quantum Theory: Concepts and Methods*, Kluwer, Dordrecht, (1993), Chapt. 5 includes a brief description of the Schmidt decomposition; A. Ekert and P.L. Knight, Am. J. Phys., **63**, 415 (1995).
318. A. Peres, "Higher order Schmidt Decompositions", lanl-gov e-print server no. 9504006, 1995.
 319. J. von Neumann, "Mathematische Grundlagen der Quantenmechanik" (Springer, Berlin, 1932; English Translation, Princeton University Press, Princeton, 1955).
 320. M. Horodecki, P. Horodecki, and R. Horodecki, *Mixed-state entanglement and distillation: is there a "bound" entanglement in nature?*, lanl.gov e-print quant-ph/9801069.
 321. V. Vedral, M.B. Plenio, M.A. Rippin, and P.L. Knight, Phys. Rev. Lett. **78**, 2275 (1997).
 322. V. Vedral and M. B. Plenio, Phys. Rev. A **57**, 1619 (1998).
 323. C.H. Bennett, D.P. DiVincenzo, J.A. Smolin, and W.K. Wootters, Phys. Rev. A **54**, 3824 (1996).
 324. W.K. Wootters, *Entanglement of Formation of an Arbitrary State of Two Qubits*, lanl e-print server quant-ph/9709029, (1997); S. Hill and W.K. Wootters, Phys. Rev. Lett. **78**, 5022 (1997).
 325. T. Rockafeller, *Convex Analysis*, Princeton University Press, New Jersey, (1970).
 326. N. Gisin, Phys. Lett. A **210**, 151 (1996), and references therein; A. Peres, Phys. Rev. A **54**, 2685 (1996); M. Horodecki, P. Horodecki, R. Horodecki, Phys. Lett. A **223**, 1 (1996).
 327. V. Vedral, M.B. Plenio, K. Jacobs, and P.L. Knight, Phys. Rev. A **56**, 4452 (1997).
 328. W.K. Wootters, Phys. Rev. D **23**, 357 (1981).
 329. T.M. Cover and J.A. Thomas, *Elements of Information Theory*, Wiley-Interscience,(1991).
 330. F. Hiai and D. Petz, Comm. Math. Phys. **143**, 99 (1991).
 331. M. Hayashi, *Asymptotic Attainment for Quantum Relative Entropy*, lanl e-print server: quant-ph/9704040 (1997).
 332. W.H. Zurek, Physics Today, 36 (October 1991).
 333. G.M. Palma, K.-A. Suominen, and A.K. Ekert, Proc. R. Soc. London A. **452**, 567 (1996).
 334. D. DiVincenzo, Phys. Rev. A, **50**, 1015 (1995).
 335. W. Unruh, Phys. Rev. A, **51**, 992 (1995).
 336. D. Loss and D. DiVincenzo, Phys. Rev. A, **57**, 120 (1998).
 337. A. Barenco et.al, Phys. Rev. Lett. **74**, 4083 (1995).
 338. C. Cohen-Tannoudji, J. Dupont-Roc, and Grynberg, *Atom Photon Interaction*, John Wiley (1992).
 339. M. Gross and S. Haroche, Phys. Rep. **93**, 301 (1982).
 340. A. Crubellier, S. Liberman, D. Pavolini, and A. Pillet, J. Phys. B, **18**, 3811 (1985).
 341. P. Zanardi and M. Rasetti, Phys. Rev. Lett. **79**, 3306 (1997).
 342. D.G. Cory, M.D. Price, T.F. Havel, Physica D **120**, 82 (1998).
 343. N.A. Gershenfeld and I.L. Chuang, Science, **275**, 350 (1997).
 344. P.L. Knight, M.B. Plenio and V. Vedral, Phil. Trans. Roc. Soc. Lond. A, **355**, 2381 (1997).
 345. M.B. Plenio and P.L. Knight, Phys. Rev. A, **53**, 2986 (1996).

346. M.B. Plenio and P.L. Knight, Proc. R. Soc. Lond. A, **453**, 2017 (1997).
347. M.B. Plenio and P.L. Knight, *New Developments on Fundamental Problems in Quantum Physics*, edited by M. Ferrero and A. van der Merwe, Kluwer, Dordrecht, 311 (1997).
348. A. Garg, Phys. Rev. Lett. **77**, 964 (1996).
349. R.J. Hughes, D.F.V. James, E.H. Knill, R. Laflamme, and A.G. Petschek, Phys. Rev. Lett. **77**, 3240 (1996).
350. P.W. Shor, in *Proceedings of the 35th Annual Symposium on the Foundations of Computer Science, Los Alamitos*, CA IEEE Computer Society Press, New York, 124 (1994).
351. V. Vedral, A. Barenco, and A. Ekert, Phys. Rev. A, **54**, 147 (1996).
352. D. Deutsch, (1993) talk presented at the Rank Prize Funds Mini-Symposium on Quantum Communication and Cryptography, Broadway, England; A. Berthiaume, D. Deutsch and R. Jozsa, in *Proceedings of Workshop on Physics and Computation — PhysComp94*, IEEE Computer Society Press, Dallas, Texas, (1994).
353. A. Barenco, A. Berthiaume, D. Deutsch, A. Ekert, R. Jozsa and C. Macchiavello, SIAM J. Comput. **26**, 1541 (1997).
354. Ash, *Information Theory*, Dover (1996).
355. A. Ekert and C. Macchiavello, Phys. Rev. Lett. **77**, 2585 (1996).
356. R. Laflamme, C. Miquel, J.P. Paz and W.H. Zurek, Phys. Rev. Lett. **77**, 198 (1996).
357. A. Steane, Error correcting codes in quantum theory, Phys. Rev. Lett. **77**, 793 (1995).
358. A. Steane, Multiple particle interference and quantum error correction, Proc. R. Soc. Lond. A, **452**, 2551 (1995).
359. J. Preskill, Reliable quantum computers, Proc. Roy. Soc. Lond. A, **454**, 469 (1998).
360. D. Gottesman, Class of quantum error-correcting codes saturating the quantum Hamming bound, Phys. Rev. A, **54**, 1862 (1996).
361. A.R. Calderbank, E.M. Rains, N.J.A. Sloane and P.W. Shor, Quantum error correction and orthogonal geometry, Phys. Rev. Lett. **78** 405 (1997).
362. A.R. Calderbank, E.M. Rains, P.W. Shor and N.J.A. Sloane, Quantum error correction via codes over $GF(4)$, IEEE Trans. Information Theory **44** 1369 (1998).
363. P.W. Shor, Scheme for reducing decoherence in quantum computer memory, Phys. Rev. A, **52**, R2493 (1995).
364. A.R. Calderbank and P.W. Shor, Good quantum error-correcting codes exist, Phys. Rev. A, **54**, 1098 (1996).
365. E. Knill and R. Laflamme, A theory of quantum error correcting codes, Phys. Rev. A, **55**, 900 (1997).
366. E. Knill and R. Laflamme, Concatenated quantum codes, LANL eprint quant-ph/9608012.
367. P.W. Shor, Fault-tolerant quantum computation, in *Proc. 37th Symp. on Foundations of Computer Science*, (Los Alamitos, CA: IEEE Computer Society Press), pp15-65 (1996).
368. A.M. Steane, Space, time, parallelism and noise requirements for reliable quantum computing, Fortschr. Phys. **46**, 443 (1998). (LANL eprint quant-ph/9708021).
369. D. Aharonov and M. Ben-Or, Fault-Tolerant Quantum Computation With Constant Error Rate, LANL eprint quant-ph/9906129.

370. E. Knill, R. Laflamme and W.H. Zurek, Resilient quantum computation: Error Models and Thresholds, Proc. Roy. Soc. Lond A **454**, 365 (1998); Science **279**, 342 (1998). (LANL eprint quant-ph/9702058).
371. A.M. Steane, Active stabilisation, quantum computation and quantum state synthesis, Phys. Rev. Lett. **78**, 2251 (1997).
372. A.M. Steane, Efficient fault-tolerant quantum computing, Nature, vol. **399**, 124-126 (May 1999). (LANL eprint quant-ph/9809054).
373. D. Gottesman, A theory of fault-tolerant quantum computation, Phys. Rev. A **57**, 127 (1998). (LANL eprint quant-ph/9702029).
374. W.H. Itano et al., Phys. Rev. A, **47**, 3554 (1993).
375. W.J. Wineland et al., Phys. Rev. A, **46**, R6797 (1992).
376. D. J. Wineland et al., Phys. Rev. A, **50**, 67 (1994).
377. J.J. Bollinger et al., Phys. Rev. A, **54**, R4649 (1996).
378. C.W. Gardiner, *Quantum Noise*, Springer-Verlag, Berlin (1991).
379. S.F. Huelga, C. Macchiavello, T. Pellizzari, A.K. Ekert, M.B. Plenio and J.I. Cirac, Phys. Rev. Lett. **79**, 3865 (1997).
380. A. Barenco, A. Berthiaume, D. Deutsch, A. Ekert, R. Jozsa and C. Macchiavello, SIAM J. Comput. **26**, 1541 (1997).
381. H.-J. Briegel, W. Dür, J.I. Cirac, and P. Zoller, Phys. Rev. Lett. **81**, 5932 (1998).
382. N. Gisin, Phys. Lett. A **210**, 151 (1996).
383. M. Horodecki, P. Horodecki, and R. Horodecki, Phys. Rev. Lett. **80**, 5239 (1998); Phys. Rev. Lett. **82**, 1056 (1999).
384. E.M. Rains, Phys. Rev. A **60**, 173 (1999).
385. A. Kent, N. Linden, and S. Massar, Los Alamos preprint quant-ph/9802022.
386. G. Giedke, H.-J. Briegel, J.I. Cirac, and P. Zoller, Phys. Rev. A **59**, 2641 (1999).
387. W. Dür, H.-J. Briegel, J.I. Cirac, and P. Zoller, Phys. Rev. A **59**, 169 (1999); ibid. **60**, 729 (1999).
388. B. Huttner, J.D. Gautier, A. Muller, H. Zbinden and N. Gisin, Phys. Rev. A, **54**, 3783 (1996).
389. M. Horodecki P. Horodecki and M. Horodecki. Violating bell inequality by mixed spin 1/2 states: necessary and sufficient condition. Phys. Lett. A, **200**, 340 (1995).
390. C. Macchiavello, Phys. Lett. A **246**, 385 (1998).
391. M. Murao, M.B. Plenio, S. Popescu, V. Vedral and P.L. Knight, Phys. Rev. A **57**, R4075 (1998).
392. N. Linden S. Popescu, Fortsch. Phys. **46**, 567 (1998).
393. S.J. van Enk, J.I. Cirac, and P. Zoller, Phys. Rev. Lett., **78**, 4293 (1997).
394. S.J. van Enk, J.I. Cirac, and P. Zoller, Science, **279**, 205 (1998).
395. J.I. Cirac, et al, Physica Scripta, Proceedings of the Nobel Symposium 104, Modern Studies of Basic Quantum Concepts and Phenomena, Uppsala, Sweden, June 13-17 (1997).
396. R.J. Glauber, In *Frontiers in Quantum Optics*, (eds. E.R. Pike and S. Sarkar), 534, Adam Hilger, Bristol (1986).
397. S.J. van Enk, J.I. Cirac, and P. Zoller, Phys. Rev. Lett. **79**, 5178 (1997).
398. M. Zukowski et al., Phys. Rev. Lett. **71**, 4287 (1993); see also S. Bose et al., Phys. Rev. A, **57**, 822 (1998); J.-W. Pan et al., Phys. Rev. Lett. **80**, 3891 (1998).
399. E. Knill and R. Laflamme, quant/ph-9608012. See also A. Yu. Kitaev, Russ. Math. Surv. **52**, 1191 (1997); D. Aharonov and M. Ben-Or, quant-ph/9611025; C. Zalka, quant-ph/ 9612028.

400. P. Shor, quant-ph/9605011; A.M. Steane, Phys. Rev. Lett. **78**, 2252 (1997). D. Gottesman, Phys. Rev. A **57**, 127 (1998); For a review see, for example, J. Preskill, in *Introduction to Quantum Computation*, ed. by H.K. Lo, S. Popescu and T.P. Spiller.

Index

- Abelian group 117
- amplitude error 91, 240
- annihilation operator 80
- antisymmetry 60
- atom–atom entanglement 140
- authentication 21, 41
- balanced function 109
- beamsplitter 4, 61
- Bell
 - state 50
 - theorem 25
- Bell’s Inequality 12
- Bell-state
 - analyser 60
 - measurement 51, 76, 78
- bosonic symmetry 60
- breathing mode 170
- Bures metric 217
- Caratheodory’s theorem 217
- cavity QED 135
- centre-of-mass
 - mode 169
 - motion 128, 154
- circular Rydberg atom 135
- classical error correction 234
- Clauser–Horne–Shimony–Holt (CHSH) inequality 34
- clear operation 180
- codevector 236
- coherent
 - attack 40
 - field 138
 - state of motion 154
 - superposition 1, 94
- coincidence rate 64
- collective
 - attack 40
 - interaction 224
- collinear phase matching 82
- compensator 59
- complete measurement 212
- complexity 112
- composite system 210
- compound fibre 289
- concatenated coding 292
- conditional phase shift 160
- confinement frequency 129
- continuous quantum variables 77
- control qubit 11
- convex analysis 217
- correlation coefficient 33
- Coulomb repulsion 131
- creation operator 80
- cryptography 15
- Cytosine 178
- Data Encryption Standard 18, 99
- decoherence 145, 186, 222, 256
- decoupled subspace 225
- detection efficiency 162, 175
- Deutsch’s
 - algorithm 109
 - problem 181
- Diffie–Hellman key exchange 19
- digitisation of noise 242
- discrete Fourier transform 115
- dissipation 226
- Doppler
 - cooling 149
 - effect 127
- double-slit experiment 1
- eavesdropper 18, 34
- eavesdropping 29
- Einstein locality 199
- Einstein–Podolsky–Rosen (EPR) paradox 12, 24
- electron shelving 153
- element of reality 25, 200
- entangled
 - entanglement 204
 - light fields 81

- photons 46, 53, 201
- state 9
- entanglement 7
 - based quantum cryptography 24
 - fidelity 266
 - of creation 215
 - of formation 215
 - purification 89, 262
 - swapping 72, 85, 290
- environment 26
- EPR
 - pair 51, 283
 - source 78
- erasure technique 203
- error
 - correction 37
 - operator 243
 - syndrome 236, 243
- Euclid's algorithm 120
- exponential
 - separation 111, 112
 - speedup 105
- factorisation 100, 114, 227
- Faraday
 - mirror 45
 - rotator 45
- fast Fourier transform 116
- fault tolerance 250
- fault-tolerant quantum computation 241
- fermionic symmetry 60
- fidelity 71, 233, 272, 285, 290
 - limit of purification 280
- field quantization 138
- Fourier transform 115
- Franson–interferometer 55
- frequency standard 253
- GHZ argument 206
- Greenberger–Horne–Zeilinger (GHZ) state 8, 91, 197
- ground-state cooling 152
- Grover's search algorithm 98, 121, 184
- Hadamard transformation 3, 4, 61, 277
- Hamiltonian circuit problem 125
- Hamming
 - bound 234
 - distance 234
- Heisenberg uncertainty relation 78
- high-Q cavity 135, 192
- homodyne detection 83
- hydrogenic ions 149
- incoherent
 - attack 38
 - mixture 3, 262
- indistinguishability 9, 67
- infrared photon 27
- interactive error correction 37
- interference
 - filter 67
 - pattern 1
- interferometer 96
- inversion about the mean 123
- Jaynes–Cummings Hamiltonian 134
- key 16
 - distribution 17
- Lamb–Dicke
 - limit 128
 - parameter 129, 147
 - regime 168
- laser cooling 127, 167
- linear Paul trap 126, 164
- local
 - filtering 269
 - measurement 212
 - operation 108, 269
 - realism 199
- locality hypothesis 13
- loopholes 209
- Mach–Zehnder interferometer 5, 30, 44, 55
- master equation 226, 255
- Mathieu equations 165
- maximally
 - entangled state 90, 211, 256, 275
 - mixed state 188
- measure of entanglement 211, 214
- mesoscopic field 145
- micromaser 138
- micromotion 166
- microwave resonator 135
- minimum uncertainty 81
- mixed state 211
- momentum entanglement 57, 75
- multi-particle entanglement 275
- nested purification 291
- no-cloning theorem 22, 52, 263
- noise 248

- noisy quantum channel 25, 197, 261, 271, 281
- non-collinear 58
- non-locality 13, 58
- NP problems 124
- nuclear magnetic resonance (NMR) 177
- number state 158
- one-time pad 17
- optical parametric oscillator 83
- oracle 110
- parallel
 - computation 97
 - universes 96
- parametric
 - amplification 82
 - down-conversion 47, 53
- parity check 235
- Paul trap 147
- perfect correlations 199
- periodic
 - function 114
 - state 115
- periodicity 114
- phase
 - encoding 30, 44
 - error 237, 240
 - matching 54
 - modulator 45
 - shifter 6
- photon polarisation 27
- photonic channel 283, 288
- polarisation
 - encoding 43
 - entanglement 75
- polynomial time 126
- polynomial-time algorithm 105
- post selection 213
- prime number theorem 120
- probability 3
 - amplitude 4
- projection
 - measurement 52
 - operator 10
- public key cryptography 19
- pure state 211
- purification 213, 277, 290
- quadrature field amplitudes 80
- quadrupole potential 164
- quantized radiation field 79
- quantum
 - algorithm 98, 104
 - channel 26
 - codeword 245
 - controlled NOT 11, 160, 163, 228, 263
 - counting 184
 - cryptography 19, 271
 - data bus 173
 - dense coding 50, 62
 - entanglement 107
 - eraser 10
 - error correction 237
 - gates 126
 - Hamming bound 238, 249
 - harmonic oscillator 79, 129, 134
 - information 109
 - interference 96
 - jump 154, 194
 - key distribution 22
 - logic 160
 - logic gate 100, 163
 - memory 99, 139
 - money 22
 - network 192, 281
 - noise 197
 - non-demolition measurement 143
 - parallel computation 106, 114
 - privacy amplification 26, 35, 271
 - register 97, 171
 - relative entropy 216
 - repeater 288
 - Sanov's theorem 219
 - searching algorithm 121
 - superposition 1, 145
 - telephone exchange 88
 - teleportation 51, 67, 74, 77
 - trajectory 194
 - unitarity 4
 - qubit 3, 94, 179
- Rabi
 - flopping 127
 - frequency 128
 - oscillation 138, 156
- Raman transition 151, 193
- Ramsey
 - fringes 140
 - interferometry 253
 - spectroscopy 252
- random choice 28, 31
- Rarity-Tapster experiment 57
- raw key 29
- reduced entropy 211

- relativised separation 112
- Rivest–Shamir–Adleman (RSA) encryption 20, 99
- scalar (J -) coupling 178
- Schmidt decomposition 210, 269
- Schrödinger
 - cat state 146, 159
 - kitten 145
 - scytale 15
 - secular motion 166
 - security criteria 34
 - separable 213
 - seven qubit code 239
 - Shannon’s
 - coding theorem 37
 - information theory 108
 - shift-invariant 118
 - shifting operator 118
 - Shor’s factorisation algorithm 114, 119
 - shot noise limit 254
 - sideband cooling 150, 167
 - sifted key 29
 - silica fibre 27
 - Simon’s algorithm 114, 118
 - single-particle interference 95
 - single-qubit quantum gate 129
 - singlet-spin state 24, 269
 - spin–spin coupling 178
 - spontaneous emission 227
 - spontaneous parametric down-conversion 54
 - squeezed
 - light 80
 - vacuum 159
 - stabiliser 243
 - statistical mixture 145
 - Stern–Gerlach apparatus 263
 - strong coupling regime 135
 - subradiance 226
 - superradiance 226
 - susceptibility 53
 - symmetric sub-space 232, 257
 - symmetrisation 232
 - syndrome extraction 245
 - target qubit 11
 - three-level system 193
 - three-qubit code 237
 - time entanglement 54
 - time–energy entanglement 47
 - trapped ions 126, 148
 - Turing principle 103
 - two-level
 - atom 134
 - system 134
 - two-qubit quantum gate 130, 174
 - type-I phase matching 54
 - type-II
 - parametric down-conversion 10, 75
 - phase matching 58
 - universal quantum computer 100
 - vacuum Rabi oscillation 138
 - velocity-selective optical pumping 136
 - Vernam cipher 17
 - vibrational
 - ground state 130, 169
 - motion 151, 156
 - von Neumann entropy 211
 - walkoff 58
 - Werner state 276, 290
 - Wigner function 158
 - Zeeman interaction 178



Location: <http://www.springer.de/phys/>

**You are one click away
from a world of physics information!**

**Come and visit Springer's
Physics Online Library**

Books

- Search the Springer website catalogue
- Subscribe to our free alerting service for new books
- Look through the book series profiles

You want to order?

Email to: orders@springer.de

Journals

- Get abstracts, ToC's free of charge to everyone
- Use our powerful search engine LINK Search
- Subscribe to our free alerting service LINK Alert
- Read full-text articles (available only to subscribers of the paper version of a journal)

You want to subscribe?

Email to: subscriptions@springer.de

Electronic Media

- Get more information on our software and CD-ROMs
- Email to: helpdesk-em@springer.de

You have a question on
an electronic product?

.....● Bookmark now:

**http://
www.springer.de/phys/**

Springer · Customer Service
Haberstr. 7 · D-69126 Heidelberg, Germany
Tel: +49 6221 345200 · Fax: +49 6221 300186
d&p - 6437a/MNT/SF - Gha.



Springer